Nonlinear Parameter Estimation for Multiple Site-Type Polyolefin Catalysts Using an Integrated Microstructure Deconvolution Methodology

by

Mohammad A. Al-Saleh

A thesis
presented to the University of Waterloo
in fulfillment of the
thesis requirement for the degree of
Doctor of Philosophy
in
Chemical Engineering

Waterloo, Ontario, Canada, 2011

AUTHOR'S DECLARATION

I hereby declare that I am the sole author of this thesis. This is a true copy of the thesis, including any required final revisions, as accepted by my examiners.

I understand that my thesis may be made electronically available to the public.

Abstract

The microstructure of polyolefins determines their macroscopic properties. Consequently, it is essential to predict how polymerization conditions will affect polyolefin microstructure. The most important microstructural distributions of ethylene/α-olefin copolymers made with coordination catalysts are their molecular weight (MWD), chemical composition (CCD), and comonomer sequence length (CSLD). Several mathematical models have been developed to predict these microstructural distributions; reliable techniques to estimate parameters for these models, however, are still poorly developed, especially for catalysts that have multiple site types, such as heterogeneous Ziegler-Natta complexes.

Most commercial polyolefins are made with heterogeneous Ziegler-Natta catalysts, which make polyolefins with broad MWD, CCD, and CSLD. This behavior is attributed to the presence of several active site types, leading to a final product that can be seen as a blend of polymers made on the different catalyst site types.

The main objective of this project is to develop a methodology to estimate the most important parameters needed to describe the microstructure of ethylene/α-olefin copolymers made with these multiple site-type catalysts. To accomplish this objective, we developed the Integrated Deconvolution Estimation Model (IDEM). IDEM estimates ethylene/α-olefin reactivity ratios for each site type in two-steps. In the first step, the copolymer MWD, measured by high-temperature gel permeation chromatography, is deconvoluted into several Flory's most probable distributions to determine the number of site types and the weight fractions of copolymer made on each of them. In the second estimation step, the model uses the MWD deconvolution information to fit the copolymer triad distributions measured by ^{13}C NMR and estimate the reactivity ratios per site type. This is the first time that MWD and triad distribution information is integrated to estimate the reactivity ratio per site type of multiple site-type catalysts used to make ethylene/α-olefin copolymers.

IDEM was applied to two sets of ethylene-*co*-1-butene copolymers made with a commercial $TiCl_4/MgCl_2$ Ziegler-Natta catalyst, covering a wide range of 1-butene fractions. In the first set of samples (EBH), hydrogen was used as a chain transfer agent, whereas it was absent in the second set (EB). Comparison of the reactivity ratio estimates for the sets of samples permitted the quantification

of the hydrogen effect on the reactivity ratios of the different site types present in the $TiCl_4/MgCl_2$ Ziegler-Natta catalyst used in this thesis.

Since ^{13}C NMR it is an essential analytical step in IDEM, triad distributions for the EB and EBH copolymers were measured in two different laboratories (Department of Chemistry at the University of Waterloo, and Dow Chemical Research Center at Freeport, Texas). IDEM was applied to both set of triad measurements to find out the effect of interlaboratory ^{13}C NMR analysis on reactivity ratio estimation.

Acknowledgements

An accumulative learning process shapes our characters and enhances our knowledge, but most importantly is the wisdom which is the key to success and excellence. Our parents are the most crucial factors in igniting our passion and desire to explore the world. Initially they direct us to make sound judgment of our observations. As we grow older we start to search for greater achievements to reach self-satisfaction and serve humanity.

I owe my success to my mother Dr. Khairiya Al-Zaid and my father Abdulla Al-Saleh. I also owe my success to my little family my wife Dr. Amal Sadeq and two daughters Jasmine and Haneen. They are the ones who carried the heaviest burden during the last few years and to that I am very thankful. I thank my sisters Suha Al-Saleh and Dr. Noha Al-Saleh for the support they always provided and special thanks to my youngest and sweetest sister Dr. Dhoha Al-Saleh.

I thank my supervisors Prof Joao B.P. Soares and Prof Thomas A. Duever for their guidance, advice and support.

I thank my friends in the Process Control and Simulation Center and the Polymer Laboratories of the Institute for Polymer Research at the University of Waterloo. Also special thanks to Dow Chemical Research Center at Freeport, Texas and to my scholarship provider the Petroleum Research and Studies Center, Kuwait Institute for Scientific Research.

Dedication

.

To my mother,

Dr. Khairiya Al-Zaid

Table of Contents

List of Figures

List of Tables

Chapter 1
Introduction

Polyolefin molecular architectures are designed according to customer needs and demands. Therefore, it is essential to determine the process conditions and catalytic behavior that gives the polymer the characteristics it needs to meet the market requirements.

In this thesis, experimental microstructural data from ethylene/α-olefin copolymer samples made with a commercial heterogeneous Ziegler-Natta multiple site-type catalyst was used to estimate the polymer mass fraction and reactivity ratios for each site type using copolymer average composition, molecular weight distribution and comonomer sequence length distribution. Each site type was assumed to produce polymer having different microstructural distributions; therefore, the whole polymer was treated as a blend of polymer chains having distinct average properties.

Chapter 2 presents a literature review on coordination polymerization mechanisms, polyolefin characterization, and parameter estimation for olefin polymerization models. Chapter 3 introduces the parameter estimation methodology developed in this thesis, called Integrated Deconvolution Estimation Model (IDEM) and shows that it can be used to discriminate between different probabilistic polymerization models very effectively, including simulated data with noise. Chapter 4 presents the experimental procedure used to synthesize the two sets of copolymer samples, with and without hydrogen (EBH and EB samples, respectively), that are used later to validate IDEM experimentally. Also included in Chapter 4 are the descriptions of the analytical techniques used to characterize the microstructures of the EB and EBH copolymers. Chapter 5 discusses the application of IDEM to the EBH copolymers, including a series of case studies designed to find the conditions that led to the "best" reactivity ratio estimates and triad distribution fit. Chapter 6 extends the application of IDEM to the EB copolymers and compares the resulting reactivity ratios with those obtained in Chapter 5, to investigate how the presence of hydrogen during polymerization affect these parameters. Chapter 7 introduces a new set of triad estimates for the EBH and EB copolymers, using ^{13}C NMR results measured at Dow Chemical, and compares them with the results obtained by ^{13}C NMR at the University of Waterloo, to evaluate how triad distributions measured by different laboratories influence IDEM performance. Chapter 8 provides the results from a hierarchical design of the replicate samples. The hierarchical design describes the sources and magnitudes of errors in the data. It takes a lot of time and effort and

that explains why most of researchers do not include such evaluations in their research. Finally, Chapter 9 details the contributions and recommendations of this research.

Chapter 2
Literature Review

2.1 Coordination Polymerization

Coordination polymerization is the mechanism for polymerization of olefins with Ziegler-Natta, metallocene, and late transition metal catalysts. We will first explain the polymerization mechanism with these catalysts, then discuss the general characteristics of multiple site-type and single site-type catalysts commonly used to make polyolefins.

2.1.1 Polymerization Mechanism

The active site in coordination polymerization catalysts is a transition metal surrounded by ligands. In most cases, the active site is produced by the activation of a complex, called the pre-catalyst or catalyst precursor, with an alkylaluminum or alkylalumoxane compound, called the cocatalyst or activator.

Figure 2.1 illustrates the catalyst activation mechanism; *A* is the transition metal (most commonly, Ti or Zr), *L* is a ligand, *X* is a halogen atom (commonly Cl), AlR_3 is the alkylaluminum cocatalyst, and *R* is an alkyl group (methyl, ethyl).

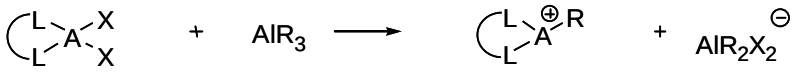

Figure 2.1 Catalyst activation by reaction of pre-catalyst and cocatalyst (Soares et al., 2007).

Polymerization with coordination catalysts proceeds via two main steps: monomer coordination to the active site and insertion into the growing polymer chain, as illustrated in Figure 2.2. In the case of copolymerization, there is a competition between the comonomers to coordinate to the active sites and be inserted into the growing polymer chain. Different rates of comonomer coordination and insertion determine the final chemical composition of the copolymer chain (Soares et al., 2007).

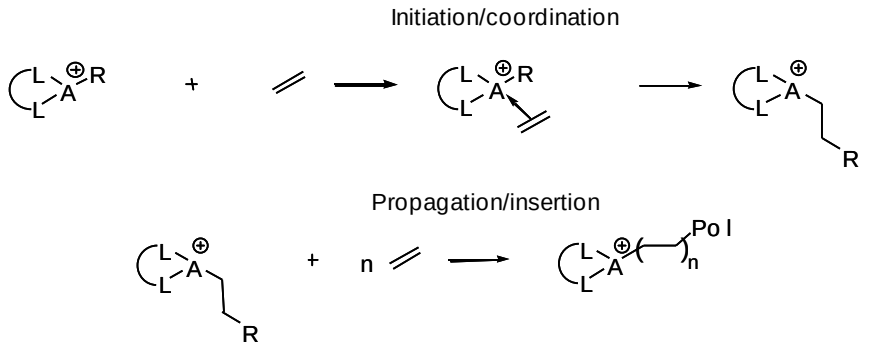

Figure 2.2 Monomer coordination and insertion (Soares et al., 2007).

Several chain transfer mechanisms are operative in coordination polymerization: a) β-hydride elimination, b) β-methyl elimination (when propylene is used), c) transfer to monomer, d) transfer to chain transfer agent -commonly hydrogen - or other small molecules, and e) transfer to cocatalyst. The type of termination reaction determines the terminal chemical group in the polymer chain. The first three types produce unsaturated chain ends, while the last two types produce saturated chain ends. These five chain transfer mechanisms are illustrated in Figure 2.3.

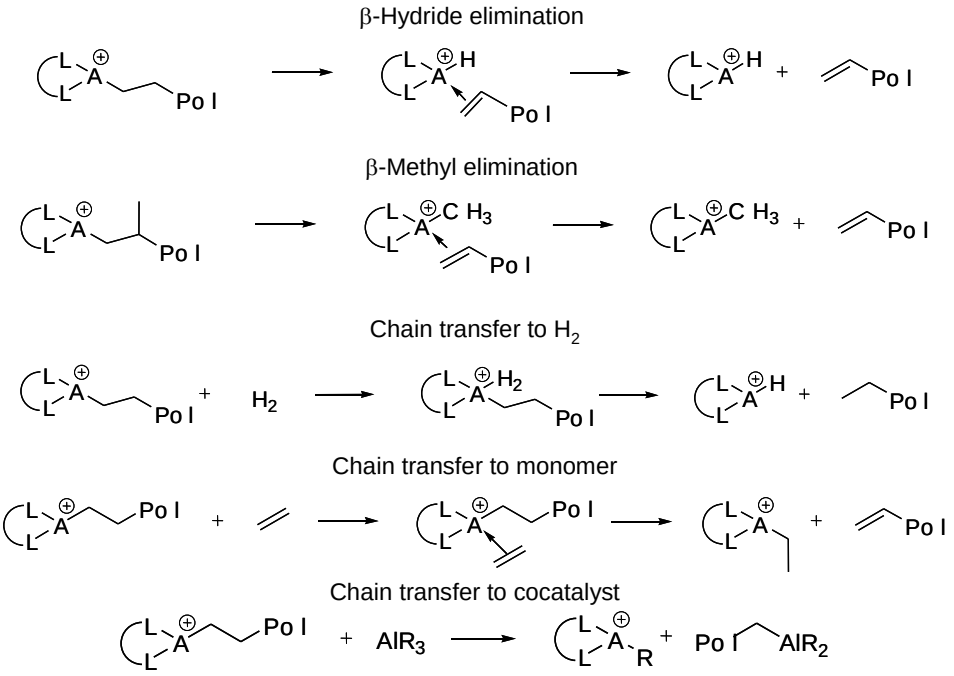

Figure 2.3 Chain transfer mechanisms (Soares et al., 2007).

Reaction of the active site with polar impurities deactivates the catalyst. Due to the cationic nature of the active sites, nucleophilic groups with a lone pair of electrons, such as substances containing oxygen, nitrogen or sulfur, can coordinate with the active sites, causing irreversible catalyst deactivation. Bimolecular catalyst deactivation may also happen when two active sites form a stable complex that is inactive for monomer polymerization. This type of bimolecular intermediate is favored at high catalyst concentrations and may be reversible. Figure 2.4 illustrates the chemical equations for this catalyst deactivation mechanism.

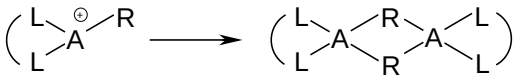

Figure 2.4 Catalyst deactivation by bimolecular reactions (Soares et al., 2007).

2.1.2 Single Site-Type Catalysts

Metallocene catalysts became relevant in the early 1980s, when Kaminsky and others found out that they were very active for olefin polymerization when activated with methylaluminoxane (MAO) instead of trimethylaluminum (TMA), commonly used for Ziegler-Natta catalysts (Bubeck, 2002). Several metallocenes are very active catalysts for olefin polymerization. More importantly, they can make polyolefins with a degree of microstructural control not possible by conventional heterogeneous Ziegler-Natta and Phillips catalysts. (Epacher et al., 2000). Commercialization of metallocene polyolefins started soon after Kaminsky's discovery, mainly because polymerization processes designed for Ziegler-Natta catalysts could be easily adapted to work with metallocenes. The polymers produced with metallocene catalysts have narrower MWDs and CCDs than those produced by multiple-site-type Phillips or Ziegler-Natta catalysts. Their narrow MWD and CCD provide metallocene polyolefins with special properties such as high strength (Kaminsky et al., 2007).

Metallocenes are complexes of a transition metal - in most case an early transition metal - and cyclopentadienyl or cyclopentadienyl-derivative ligands. Figure 2.5 shows the structures of two metallocene catalysts.

a) 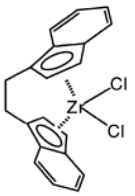

b) 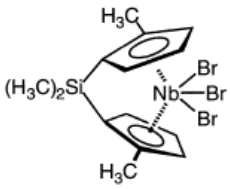

Figure 2.5 Typical metallocene catalysts, a) dichloro[1,2-di(η^5-inden-1-yl)ethane]zirconium b) tribromo[2,2'-(dimethylsilanediyl)-di(η^5-cyclopentadienyl)niobium (Salzer, 1999).

The MWD and CCD of polymers made with single-site-type catalysts under uniform polymerization conditions follow Flory's and Stockmayer's distributions, respectively. They can also be used as model compounds for multiple site-type catalysts, if we assume that each site type on a Ziegler-Natta catalyst behaves as a single-site-type catalysts, as will be discussed later in this chapter.

Two molecular weight averages are commonly used to quantify the breadth of the MWD: the number (M_n) and the weight (M_w) average molecular weight. Polymers made with a single-site-type catalyst follow the relation,

$$M_w = 2 \times M_n \tag{2.1}$$

The polydispersity index (*PDI*) of a polymer is given by the ratio of these two averages,

$$PDI = \frac{M_w}{M_n} \tag{2.2}$$

Therefore, the *PDI* of polyolefins made with single site-type catalyst is equal to two (Soares, 2004).

Metallocenes are not the subject of this research project, which focuses on polyolefins made with multiple-site-type catalysts such as Ziegler-Natta catalysts, and therefore will not be discussed any further.

2.1.3 Multiple Site-Type Catalysts

In 1950s Hogan and Banks at the Phillips Petroleum Company discovered a catalyst containing chromium oxide (commonly known as Phillips catalysts) that produced highly crystalline polyethylene at moderate temperatures and pressures (Whiteley, 2002; Bergstra, 2004). Phillips catalysts are widely used for the production of high-density polyethylene (HDPE), but they cannot be used to make ethylene/1-butene copolymers with high 1-butene incorporation required in this research.

Ziegler-Natta catalysts were also discovered in the early 1950s. The work on olefin polymerization catalysis done by Karl Ziegler in Germany and by Giulio Natta in Italy had such a great impact on the role of macromolecular chemistry as an academic discipline and on the development of the commodity polymer industry that both scientist were awarded the Nobel Prize in Chemistry in 1963. The original $TiCl_3$ complexes developed by Ziegler and Natta had low activities and stereoselectivities. Natta's work focused on the relationship between the crystal structure of titanium trichloride ($TiCl_3$) and the overall activity and selectivity of these catalysts (Cerruti, 1999). In 1968, the discovery that $TiCl_4$ supported on $MgCl_2$ improved the activity and the stereoselectivity of Ziegler-Natta catalysts was a breakthrough that led to improvements on the properties of polyolefins and significant cuts in production costs (Kashiwa, 2004). The structure of typical Ziegler-Natta and Philips catalysts are compared in Figure 2.6. Vanadium-based, homogeneous Ziegler-Natta catalysts are also used industrially to produce ethylene/propylene/diene (EPDM) terpolymers (Kim and Choi, 1991).

Table 2.1 compares the general characteristics of Ziegler-Natta and Phillips catalysts.

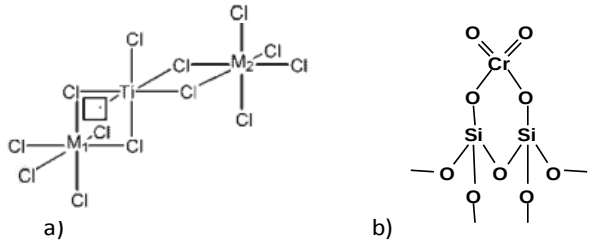

Figure 2.6 Typical a) Ziegler-Natta, M_1 and M_2: Mg or Ti (Liu et al., 2003), and b) Phillips catalysts (Hamielec and Soares, 1996).

Table 2.1 Examples of multiple-site-type catalysts and their general characteristics.

Catalyst	Transition Metal	Characteristics
Ziegler-Natta	Ti	▪ Broad molecular weight distribution (*PDI* = 4-6) ▪ Aluminum alkyl cocatalyst required ▪ Hydrogen is used for molecular weight control
Phillips	Cr	▪ Very broad molecular weight distribution (*PDI* > 6) ▪ Cocatalyst not required ▪ Reactor temperature is used for molecular weight control

One of the important characteristics of Ziegler-Natta catalysts is that they produce polymer with broad microstructural distributions because they have more than one type of active site, each one making polymer with different average properties. Polymers made with multiple site-type catalysts have much broader molecular weight distribution (MWD) and chemical composition distribution (CCD) than those made with single site-type catalysts. Each type of active site present on Ziegler-Natta catalysts are usually assumed to produce polymers that follow different Flory's and Stockmayer's distributions (Soares et al., 1996).

The MWD of a linear polyolefin made with a single site-type catalyst under uniform and time-invariant polymerization conditions is given by Flory's most probable distribution. Flory's equation, in log scale, is given by,

$$W_{\log MW} = 2.3026 \times MW^2 \, \tau_{MW}^2 \, e^{-MW \, \tau_{MW}} \tag{2.3}$$

where MW is the molecular weight of polymer chain and τ_{MW} is the reciprocal of the number average molecular weight,

$$\tau_{MW} = \frac{1}{M_n} \tag{2.4}$$

On the other hand, the MWD of a polymer made with a multiple site-type catalyst can be represented as a weighted superposition of two or more Flory's distributions (Soares, 2007; Thompson et al., 2007; Soares et al., 1996; Hamielec et al., 1996). The weighted sum of Flory's most probable distributions for a multiplesite-type catalyst in log scale is given by,

$$W_{\log MW} = 2.3026 \times MW^2 \sum_{i=1}^{ns} w_i \, \tau_{MW,i}^2 \, e^{-MW \, \tau_{MW,i}} \tag{2.5}$$

where w_i is the weight fraction of polymer made on site *i*, and *ns* is the total number of site types in the catalyst.

During the MWD deconvolution procedure, the minimum number of Flory's distributions required to describe the MWD of a polymer sample is determined. This modeling technique has been used extensively to describe the MWD of polyolefins made with multiple site-type catalysts and reported in many publications in the literature (Soares, 2007; Thompson et al., 2007; Soares et al., 1996; Hamielec et al., 1996).

The model parameters $\tau_{MW,j}$ and w_j are obtained by minimizing the value of an objective function such as,

$$\chi^2 = \sum_{i=1}^{n_{GPC}} [W_{\log MW}^{GPC} - \sum_{j=1}^{ns} w_j (2.3026 MW_i^{\,2} \tau_{MW,j}^2 e^{-MW_i \tau_{MW,j}})]^2 \tag{2.6}$$

where $W_{\log MW}^{GPC}$ is the sample MWD measured by GPC, and n_{GPC} is the number of sampling points taken by GPC.

Figure 2.7 illustrates the use of the MWD deconvolution of a polyethylene sample made with a mixture of two metallocene catalysts (Kim et al., 1999), which can serve as a model for actual Ziegler-Natta catalysts, albeit generally more than two site types are required to describe Ziegler-Natta catalysts. The MWDs of the polymers made with both metallocenes in Figure 2.7 obey Flory's most probable

distribution. During the MWD deconvolution procedure, the differences between the GPC-measured MWD and the predicted MWD are minimized by varying w_1, $\tau_{MW,j}$, and $\tau_{MW,j}$ ($w_2 = 1 - w_1$).

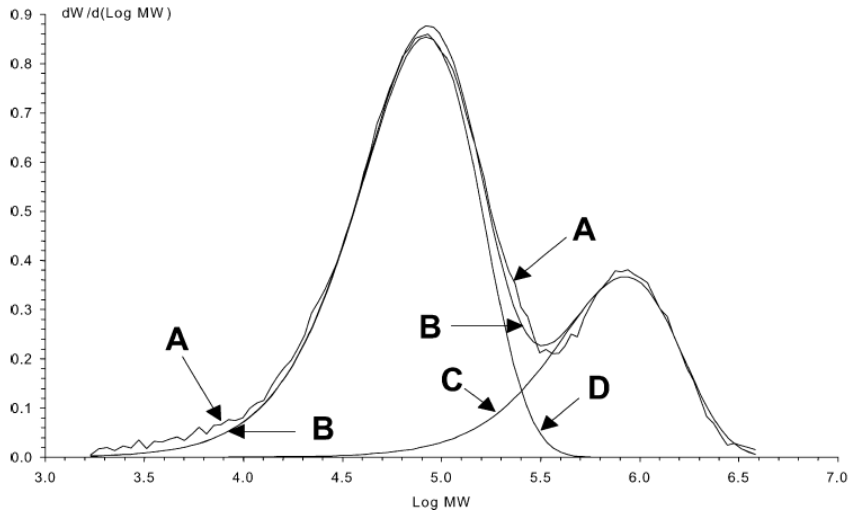

Figure 2.7 Molecular weight distribution (MWD) of polyethylene made with a two metallocene catalysts. A: Experimental MWD; B: Superposition of curves C and D; C and D: Flory's most probable distribution for polymer made on each metallocene (Kim et al., 1999).

2.2 Polyolefin Microstructure

The composition and lengths of copolymer molecules in a sample made with a coordination catalyst are not identical, even if the copolymer is formed during a very small time interval; there always exists a distribution of chain lengths and compositions for all synthetic polymers (Stockmayer, 1945). Therefore, polymers do not have a single value for molecular weight and chemical composition, but instead a distribution of these values characterized by their MWDs and CCDs. Assuming that all active sites in the catalyst behave the same way (as for single-site type catalysts such as metallocenes), the shapes of these distributions can be predicted precisely with theoretical distributions derived by Flory and Stockmayer (Soares, 2004).

Several factors may contribute to CCD heterogeneity. The more pervasive one is the statistical nature of polymerization which forces the composition of any synthetic copolymer chain to be always distributed around a certain average value. For multiple site-type catalysts, such as heterogeneous Ziegler–Natta

catalysts, each active site type has a distinct set of polymerization kinetics constants and produces polymer chains with different average microstructures. Therefore, the polymers synthesized with these catalysts are mixtures of chains with different average chain lengths and comonomer compositions, as illustrated in Figure 2.8 (Anantawaraskul et al., 2005).

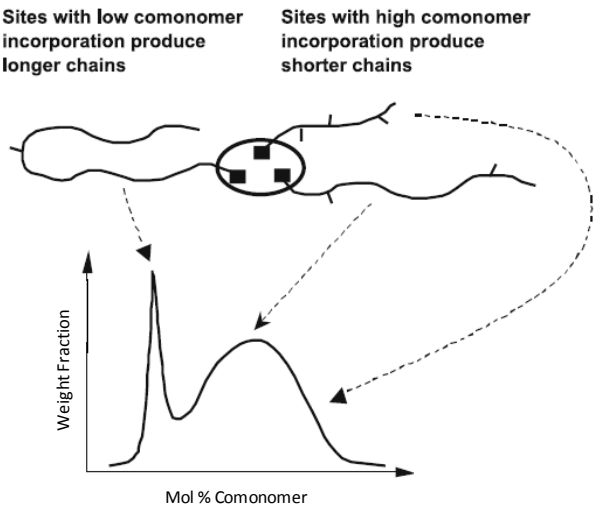

Figure 2.8 Copolymers produced by Ziegler–Natta catalysts exhibiting a broad chemical composition distribution (Anantawaraskul et al., 2005).

The final properties of polymers are determined by their chain microstructures. For example, increasing the average molecular weight of polyethylene improves its tensile strength, impact toughness, creep resistance, and wear resistance. On the other hand, the density, stiffness and strength of polymers are controlled by short-chain branching (SCB) and long-chain branching (LCB). The presence of SCBs reduces the strength, whereas LCBs increase it (Askeland and Phule, 2003).

Polyethylene resins are classified in three main types: low-density polyethylene (LDPE), linear low-density polyethylene (LLDPE), and high-density polyethylene (HDPE). A comprehensive classification, based on their microstructural characteristics is presented in Figure 2.9. For the same comonomer molar fraction, the density and melting points of an ethylene/α-olefin copolymer generally decrease in the order propylene > 1-butene > 1-hexene > 1-octene (Soares, 2007).

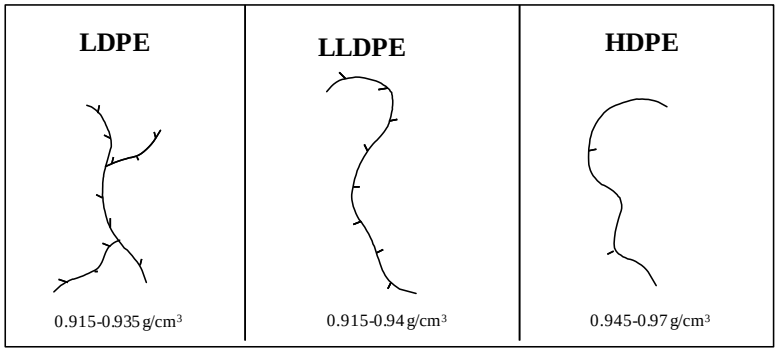

Figure 2.9 Classification of polyethylenes according to branching structure and density (Soares, 2007).

LLDPE is weaker than HDPE because it has a higher SCB frequency. Addition of SCBs to polyethylene chains decreases their crystallinity, and the longer their length, the stronger their effect (Ohshima and Tanigaki, 2000). Qualitative relationships between molecular properties and polyolefin properties are listed in Table 2.2.

Table 2.2 Relationship between molecular structure and properties of polyethylene. The symbol "o" denotes that a relation exists between property and molecular structure (Ohshima and Tanigaki, 2000).

Molecular structure	Molecular weight (M_w)	Molecular weight distribution	Average Branching Degree	Branching distribution
Transparency	o	o	o	o
Tensile Strength	o	o	o	o
Impact strength	o	o	o	o
Rigidity			o	o
Heat resistance			o	o
Cold resistance	o	o	o	o
Chemical resistance	o	o	o	o

2.3 Polymer Analysis and Characterization

Gel permeation chromatography (GPC) and carbon-13 nuclear magnetic resonance spectroscopy (^{13}C NMR) are essential analytical tools in characterizing the microstructure of polyolefins. GPC is used to determine the molecular weight distribution (MWD) of polymer samples, whereas the average chemical composition (monomer and comonomer fractions) and the comonomer sequence length distribution are measured by ^{13}C NMR. This section will also include a brief description on crystallization elution fractionation (CEF), which is a new characterization technique used in the analysis of the chemical composition distribution.

2.3.1 Gel Permeation Chromatography

High-temperature gel permeation chromatography (GPC), also called high-temperature size exclusion chromatography (SEC), is the technique used to measure the MWD of polyolefins. A typical gel permeation chromatographer consists of a pump to move the mobile phase (generally trichlorobenzene – TCB) through a series of columns, a sample carrousel used to inject polymer sample solutions into the mobile phase, a set of columns to fractionate the polymer chains according to their sizes in solution (which can be correlated to their molecular weights via a calibration curve), and at least one detector to measure the concentration of polymer eluting from the last column in the series. These components are kept at high temperature (generally 140-145^{o}C) inside a well-insulated oven because of the low solubility of most polyolefins. A block diagram of a GPC apparatus is shown in Figure 2.10.

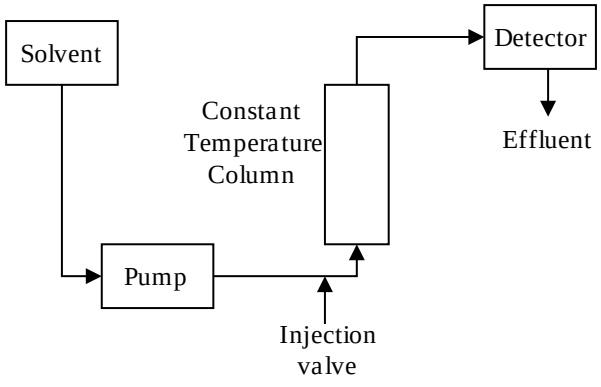

Figure 2.10 Block diagram of a gel permeation chromatographer.

The columns are at the heart of GPC analysis. They are filled with packing having different pore sizes that promote the fractionation of the polymer chains by the mechanism of size exclusion: short chains have a small volume in solution and can penetrate most of the pores of the support, while long chains can diffuse only into the larger pores in the support. Consequently, chains with lower molecular weights will take longer time to exit the column set than chains with higher molecular weights (Soares, 2004).

Thus, GPC separates polymer chains by their sizes in solution or, in more technical terms, by their hydrodynamic volumes. The hydrodynamic volume of polymers is a function of their molecular weight, temperature, concentration, solvent and polymer type. The column effluent is monitored by detectors which respond to the weight concentration of the polymer in the flowing eluant. The most common GPC detector is a differential refractometer, although infrared detectors are becoming increasingly more common due to their more stable baselines and higher signal-to-noise ratios. A series of commercially available anionically polymerized polystyrene standards is particularly suited for calibration of GPC columns. A calibration curve needs to be constructed in order to convert raw data (elution times) into molecular weight distribution (Rudin, 1999).

The concentrations measured by the on-line mass detector generate a distribution of elution times or elution volumes. This distribution can be converted into a MWD using a calibration curve, which is a mathematical relation between the molecular weight of a polymer standard and the time it requires to exit the GPC columns at a given set of analytical conditions. Figure 2.11 shows a generic molecular weight calibration curve. The total exclusion limit defines the highest molecular weight that can be analyzed with a given column set: polymers with molecular weights over this limit will be excluded from all the pores and elute at the same time from the column. Similarly, the total permeation limit determines the lowest molecular weight the technique is capable to detect: chains with lower molecular weights will permeate through all the pores and be eluted at the same time without any fractionation taking place (Soares, 2004).

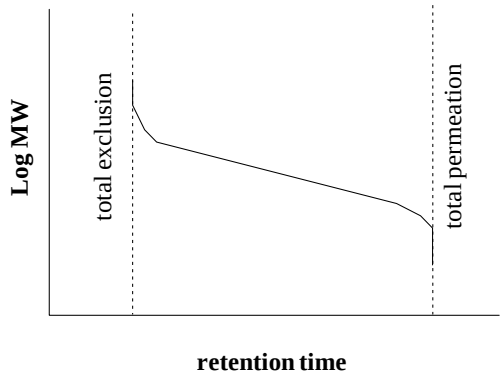

Figure 2.11 A generic GPC calibration curve.

The universal calibration curve is based on the theory that polymer molecules are separated in GPC based on their hydrodynamic volume. This is illustrated in Figure 2.12, as the calibration curves for polyethylene and polystyrene, expressed as hydrodynamic volume versus elution volume, coincide (Barlow et al., 1977). The universal calibration allows GPC to be calibrated for polymers for which it is difficult to obtain narrow molecular weight distribution standards.

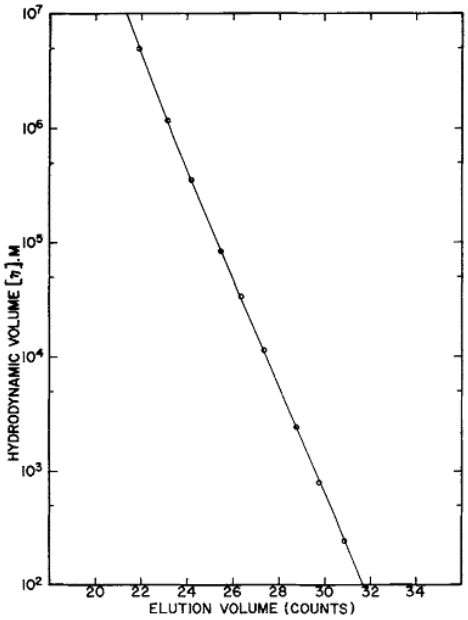

Figure 2.12 Universal GPC calibration curve illustrating that the calibration curves for polyethylene and polystyrene are the same: universal calibration polyethylene (continuous line); polystyrene (o) (Barlow et al., 1977).

2.3.2 Carbon 13-Nuclear Magnetic Resonance

2.3.2.1 Background and General Concepts

Carbon-13 nuclear magnetic resonance (^{13}C NMR) spectroscopy records the interaction of radiofrequency electromagnetic radiation with the nuclei of molecules. When an atomic nucleus with magnetic moment is placed in a magnetic field, it tends to align with the applied field. By determining the energy transition levels for all of the atoms in a molecule, it is possible to identify the carbon atoms in an organic molecule. It is a fundamental technique for determining the chemical structure of copolymers such as branching type, chain end structure, and chemical composition (Blumich et al., 2005; Atta-ur-Rahman et al., 1996).

2.3.2.2 Nomenclature

The nomenclature used to identify different carbon structures in branched polyethylene is well developed. A pair of Greek letters is used to represent the distance of a carbon atom to the branch points in either direction of the copolymer backbone: α, β, γ, δ and δ^+ for branches placed 1, 2, 3, 4, and longer than 4 carbon atoms away from the reference carbon atom. The carbon atoms located at the side-chain branches are identified by iB_n, where *i* indicates the position of the carbon atom in the branch, with the methyl carbon (at the end of the branch) in position 1, and the optional subscript *n* indicating the size of the branch. Saturated chain end carbons in the main chain are designated by 1s, 2s, and 3s, starting with methyl carbon at the chain end as position 1. This nomenclature is illustrated in Figure 2.13 (Sahoo et al., 2003).

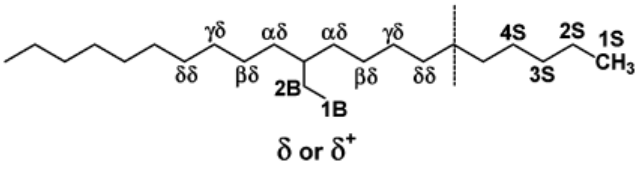

Figure 2.13 Nomenclature for poly(ethylene-*co*-1-butene) substructure (Sahoo et al., 2003).

The carbon chemical shifts of some monomers at high field are influenced by the structure of the adjacent monomer units. Therefore, the simple two letter labeling presented above may become ambiguous and the *n*-ad (triad and/or tetrad) sequence must also be indicated. Some possible tetrad

sequences for poly(ethylene-*co*-1-butene) copolymers are shown in Figure 2.14, where E refers to ethylene and B to 1-butene units in the copolymer chain (Sahoo et al., 2003).

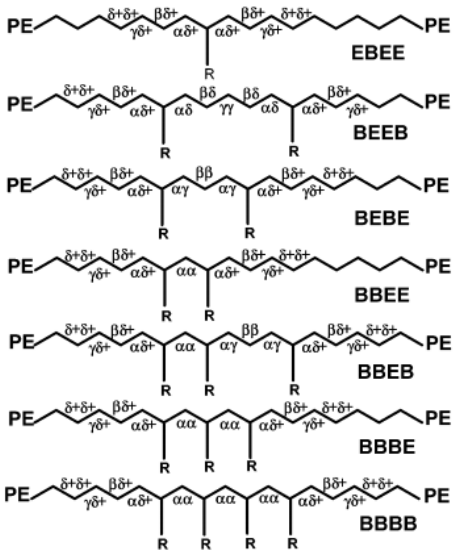

Figure 2.14 Monomer and comonomer sequences for poly(ethylene-*co*-1-butene) (Sahoo et al., 2003).

Figure 2.15 presents 188.6 MHz ^{13}C NMR spectrum of a commercial poly(ethylene-*co*-1-butene) copolymer sample synthesized by Aldrich using a metallocene catalyst (Sahoo et al., 2003), obtained at 120^{o}C to optimize sensitivity and resolution (Liu et al., 2001). This temperature ensures segmental mobility of the copolymer chains which increases dramatically with the increase in temperature, resulting in better resolution. More detailed diagrams and spectra of olefin copolymers can be found in the literature (Bovey et al., 1996; Pooter et al., 1991; Randall, 1989).

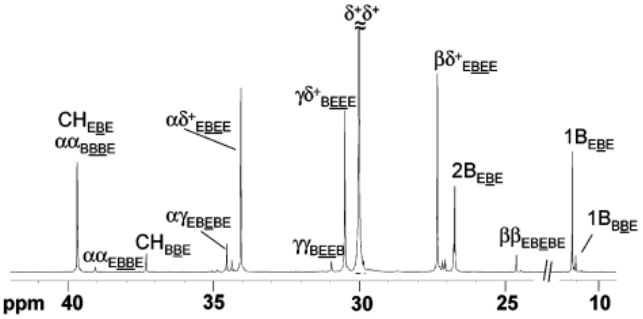

Figure 2.15 ^{13}C NMR spectra of poly(ethylene-*co*-1-butene), containing 12% 1-butene (Sahoo et al., 2003).

2.3.2.3 Triad and Tetrad Determination

The ^{13}C NMR spectrum for ethylene-*co*-1-butene copolymers is divided into regions. Resonance broadening in the , , and regions arisising from the chemical shift differences produced by long range structural differences prevents the use of relative peak heights in these regions. There is also overlap between methine (>CH) and branch methylene (CH_2) resonances with the polymer backbone methylene resonance. Thus a quantitative treatment based on collective assignments is needed to avoid errors from overlap.

The seven regions shown in Table 2.3 are used for quantitative determination of composition and comonomer sequence length of ethylene-*co*-1-butene copolymers. Regions A to G are liked below to their respective triads. The relationships are used to describe the intensity of each region as a function of only triads. The chemical shifts for each region are for copolymer samples prepared in 1,1,2,2-terachloroethane (TCE). Some of these regions may have to be combined if a good baseline is not achieved between regions during spectral integration. The actual method will depend on the particular copolymer sample being examined and its ethylene to 1-butene ratio.

Table 2.3 Intensity expressions for ethylene-1-butene copolymers (Randall, 1989).

Region	Chemical shift (ppm)	Carbon assignment	Intensity expression
A	37.0-40.0	αα Methylene, $(Methine)_{EBE}$	$T_A = k$ (BBB + (1/2) [BBE+EBB] + EBE)
B	37.4	$(Methine)_{EBB+BBE}$	$T_B = k$ (EBB + BBE)
C	33.5-35.5	αγ, $\alpha\delta^+$, $(Methine)_{BBB}$	$T_C = k$ (2BEB + [BEE+EEB] +BBB)
D	29.5-31.5	γγ, γ δ^+, δ^+ δ^+	$T_D = k$ (2EEE + (1/2)[BEE+EEB])
E	26.0-28.0	β δ^+, $2B_2$	$T_E = k$ ([BEE+EEB] + EBE + [EBB+BBE] + BBB)
F	24.0-25.0	ββ	$T_F = k$ (BEB)
G	10.5-11.5	Methyl	$T_G = k$ (EBE + [EBB+BBE] + BBB)

k – NMR instrumental constant

Seven equations are available to solve for six triads (Randall, 1989). For copolymers with very low 1-butene content, shorter relaxation times are observed and it is preferable to use region G. Solving the

equations for regions A to F gives the following classic expressions published by Randall in his 1989 seminal paper,

$$k\,(\mathrm{EEE}) = (1/2)\,T_D - (1/4)\,T_E + (1/4)\,T_A + (1/8)\,T_B \quad (2.7)$$

$$k\,(\mathrm{BEE{+}EEB}) = T_E - T_A - (1/2)\,T_B \quad (2.8)$$

$$k\,(\mathrm{BEB}) = T_F \quad (2.9)$$

$$k\,(\mathrm{EBE}) = 2T_F + T_E - T_B - T_C \quad (2.10)$$

$$k\,(\mathrm{EBB{+}BBE}) = T_B \quad (2.11)$$

$$k\,(\mathrm{BBB}) = T_C - 2T_F - T_E + T_A + (1/2)\,T_B \quad (2.12)$$

Difficulties may arise when the above set of equations is used to calculate the triad distribution of copolymers with low 1-butene content, particularly if good baseline separation is not achieved between the different regions during spectral integration. Equation (2.12) shows that *k*(BBB) depends on five different experimental measurements, a higher margin of error is expected for triads with lowest fractions. In this case, the expression for T_G may be used because the spin-lattice relaxation time decreases for the methyl resonances when 1-butene content in the copolymer is fairly low. Introducing the seventh region G leads to the following set if equations for the triad distribution (Randall, 1989) of samples that have small 1-butene incorporation,

$$k\,(\mathrm{EEE}) = (1/2)\,T_D - (1/4)\,T_E + (1/4)\,T_G \quad (2.13)$$

$$k\,(\mathrm{BEE{+}EEB}) = T_E - T_G \quad (2.14)$$

$$k\,(\mathrm{BEB}) = T_F \quad (2.15)$$

$$k\,(\mathrm{EBE}) = T_C - T_A - (1/2)\,T_B \quad (2.16)$$

$$k\,(\mathrm{EBB{+}BBE}) = T_B \quad (2.17)$$

$$k\,(\mathrm{BBB}) = 2T_A - T_C \quad (2.18)$$

Normalization of Equations (2.7) to (2.12) or (2.13) to (2.18) removes the NMR constant, *k*, and gives the triad fractions. Although the triad distribution is satisfactory for the complete characterization of a copolymer sample, the higher order tetrad distribution is considered of interest from a statistical point of

view. Only few of the tetrad distributions can be determined directly from the ^{13}C NMR spectral data. The following relationships between triads and tetrads result in quantitative identification of the complete set (Hsieh and Randall, 1982),

$$[EEEE] + [BEEE]/2 = [EEE] \quad (2.19)$$

$$[BEEE] + 2[BEEB] = [BEE] \quad (2.20)$$

$$[EBEE] + [EBEB] = 2[EBE] \quad (2.21)$$

$$[BBEE] + [BBEB] = [BBE] \quad (2.22)$$

$$[EBEB] + [BBEB] = 2[BEB] \quad (2.23)$$

$$[EBEE] + [BBEE] = [BEE] \quad (2.24)$$

$$[BBBE] + 2[EBBE] = [BBE] \quad (2.25)$$

$$[BBBE] + 2[BBBB] = 2[BBB] \quad (2.26)$$

Three tetrads can be directly quantified from the ^{13}C NMR spectra because their respective peaks are clear: EBBE, EBEE and BEEB. The spectral peaks are dependent on the 1-butene concentration. The EBBE tetrad falls in region A at 38.97-39.30 ppm, EBEE in region C at 34.01-34.04 ppm, and BEEB in region D at 30.93-30.92 ppm (Hsieh and Randall, 1982). To solve Equations (2.19) to (2.26) for the unknown tetrad, it is necessary to divide the above equations in three groups. The first group contains Equations (2.19) and (2.20). Since we have three unknowns we need to identify one tetrad to solve for the other two. Since BEEB is the most resolved tetrad in this group, it is determined directly from the ^{13}C NMR spectra, and EEEE and BEEE are calculated. The second group, comprised of Equations (2.21) to (2.24), also requires the identification of one tetrad and EBEE is the most suitable choice. In the final group, Equations (2.25) and (2.26), EBBE must be measured so that BBBB and BBBE can be calculated.

2.3.3 Crystallization Elution Fractionation

Crystallization elution fractionation (CEF) is a new characterization technique used to analyze CCDs of semicrystalline polymers. Before we discuss CEF advantages and operation concepts we must briefly

introduce temperature rising elution fractionation (TREF), which is an older technique also used to analyze the CCDs of semicrystalline polymers.

TREF operates in two full temperature cycles, crystallization and elution, to analyze copolymer composition distribution. First, the sample is dissolved in a solvent at high temperature, then the solution is introduced into a column containing an inert support, such as glass beads. This is followed by a crystallization step at a slow cooling rate. The polymer chains crystallize from lower to higher comonomer content (i.e., more crystalline chains crystallize first). TREF requires a second temperature cycle to physically separate those fractions. This is done by flowing solvent through the column while the temperature is increased. Fractions of higher crystallinity (less branch content) are dissolved in the eluant as the temperature rises. The polymer concentration eluting from the column is monitored with an infrared detector to generate the TREF curve (Monrabal et al., 2007; Soares et al., 2005; Wild, 1990). A calibration curve, relating elution temperature to comonomer content, is then used to obtain the copolymer CCD.

The TREF analysis of a blend of three different components is represented schematically in Figure 2.16.a. The sample is loaded into the column in the first step, then the crystallization cycle starts, followed by the elution cycle where solvent is flown through the column at increasing temperatures, eluting the fractions that were deposited during the crystallization cycle (Monrabal et al., 2007; 2009).

Crystallization elution fractionation differs from TREF because the crystallization cycle takes place under constant solvent flow that prevents the different polymer fractions from being deposited on top of each other, thus significantly minimizing cocrystallization effects and enhancing resolution. The second temperature cycle in CEF is similar to that in TREF. CEF operation is illustrated in Figure 2.16.b (Monrabal et al., 2007; 2009).

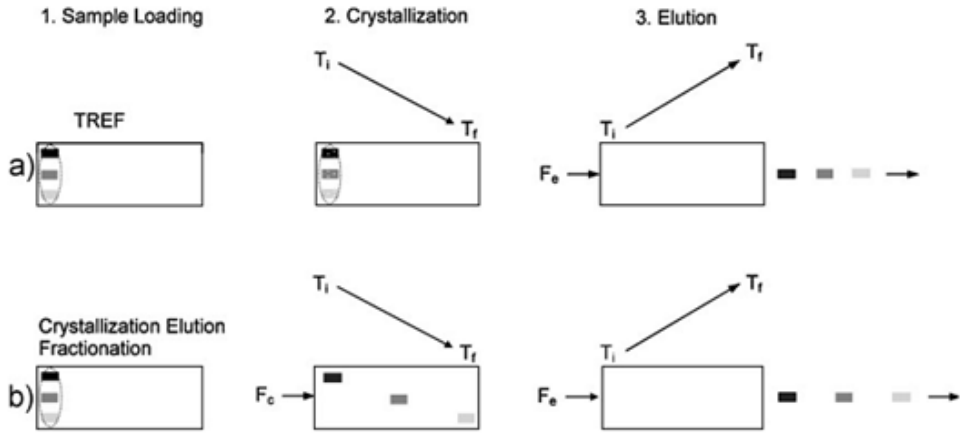

Figure 2.16 Comparison between TREF and CEF operation: a) TREF, b) CEF (Monrabal et al., 2009).

2.4 Optimization-Parameter Point Estimate

In parameter estimation, it is important to distinguish between linear-in-the parameters models and non-linear-in-the parameters models. Polymerization models are generally nonlinear and therefore linear regression methods cannot be used. Tidwell and Mortimer suggested that a good estimation procedure should include the following features (Tidwell and Mortimer, 1970):

a. The method should give unbiased estimates of all parameters (i.e. the mean of the sampling distribution is equal to the parameter).
b. The method should utilize all, or nearly all, the information resident in the data with regard to the parameters to be estimated.
c. The parameter values calculated by the method should not depend upon arbitrary factors (such as the starting point of the calculation).
d. The method should give a valid measure of the errors of the resulting estimates.
e. The method should be reasonably easy to use.

The objective of the parameter estimation step is to obtain a set of parameter values that are robust and have the least possible variability. There are several criteria available for multiresponse parameter estimation such as least squares and the determinant criteria. Knowing that multiple local optima may exist when dealing with a nonlinear system requires a robust optimization method. The criteria for

multiresponse parameter estimation are all based on the same assumptions about the model and the error structure, as stated below;

a. The model structure is correct.
b. The errors from trial to trial are independent of one another and within a trial they are assumed to be normally distributed with a mean of zero and constant covariance matrix.
c. The measurement error is additive.
d. The measurement error is homoscedastic, that is the statistical distribution have the same variance and is not dependant on the dependent or independent variables.
e. The random errors in the dependent variable are normally distributed.

The general model structure for the multiple response Nonlinear Least Squares (NLLS) method can be written as,

$$y_{ij} = f_j(\underline{x}_i, \underline{\theta}) + \varepsilon_{ij}, \qquad j = 1,2,...,m \text{ and } i = 1,2,...,n \tag{2.27}$$

where *m*: the number of responses, *n* is the number of trials, $\underline{x}_i$ is $1 \times k$ vector of independent variables $(x_{i1}, x_{i2}, \cdots, x_{ik})$, f_j is the model function for the *j*th response depending on some or all of the experimental settings $\underline{x}_i$ and some or all of the parameters $\underline{\theta}$, y_{ij} is the measured value of the *j*th response for the *i*th case, $\underline{\theta}$ is $p \times 1$ vector of unknown parameters $(\theta_1, \theta_2, ..., \theta_p)$, and ε_{ij} is the residual.

The objective in this case is to minimize the square difference between the fitted values and the measured values. The least square estimates are obtained by selecting the values of $(\underline{\theta})$ that minimize the squared residuals,

$$S(\underline{\theta}) = \sum_{j=1}^{m} \sum_{i=1}^{n} (y_{ij} - f_j(\underline{x}_i, \underline{\theta}))^2 \tag{2.28}$$

Minimization of the objective function ($\underline{\theta}$) in the posed nonlinear parameter estimation problem is an iterative numerical problem. In principle, any minimization method can be used to solve this problem including Newton's, Simplex and Simulated Annealing methods (Draper and Smith, 1998). Simulated Annealing is preferred for a function with numerous local minima. Although it requires a larger number of function evaluations to find the optimum solution, it is more likely to find the global optimum even for ill-conditioned functions because it relies on random evaluations of the objective function to make transitions out of local minima possible.

The determinant criterion is another popular method introduced by Box and Draper (1965) and is used to estimate parameters for multiresponse data. The general model for *m* responses measured in each of *n* experimental runs is represented by,

$$Y_{ij} = f_j(\underline{x}_i, \underline{\theta}) + z_{ij} \qquad , i, jth \text{ element} \tag{2.29}$$

where z_{ij} is the random variable associated with the measured value of the *j*th response for the *i*th case (Bates and Watts, 2007). The objective function to be minimized in this case is the determinant of the estimated measurement error covariance matrix,

$$\phi(\underline{\theta}) = \left|\underline{Z}'\,\underline{Z}\right| \tag{2.30}$$

where $\underline{Z} = [Y_{ij} - f_j(\underline{x}_i, \underline{\theta})]$ i,j^{th} element.

Optimization methods that could be used in this case include Newton, Simplex and Simulated Annealing.

The following are some advantages of the determinant criteria (Box and Tiao, 1973):

a. The expectation function can be linear or nonlinear.
b. The parameters can be common to more than one response.
c. The design variables can be common to more than one response.
d. The responses used can be rescaled or a linear combination of responses can be used.

2.5 Parameter Estimation for Ethylene/α-Olefin Copolymerization with Coordination Catalysts

Cheng (1989, 1990, 1991, 1993) published several articles over the past two decades concerning ^{13}C NMR analysis of polyolefins and developed statistical models for multiple-site-type polymerization catalysts.

Copolymerization kinetics are generally described with zeroth-order (Bernoullian), first-order (terminal) or second-order Markovian (penultimate) models. The probability of monomer addition in the Bernoullian model is influenced only by the type of catalytic site and monomer type; the chemical nature of the chain end does not affect the monomer insertion onto the growing chain. In the terminal model, site type, monomer type, and the chemical nature of the last monomer added to the chain are assumed to influence monomer propagation. Finally, in the penultimate model, in addition to site type and monomer type, the chemical nature of the two last inserted monomer units will determine monomer propagation (Cheng, 1991).

The terminal model usually provides a better description of triad distributions than the Bernoullian model and is the most commonly used model for olefin copolymerization with coordination catalysts. The penultimate model is considered to add unnecessary complexity to the parameter estimation procedure and is very seldom used for polyolefins (Randall, 1977).

Cheng developed a general methodology for the treatment of ^{13}C NMR data of ethylene-propylene copolymers. He estimated weight fractions and reaction probabilities for each site type assuming two or three site types using ^{13}C NMR data measured from polymer fractions (Cheng, 1989). Cheng also used a similar approach to study ethylene/1-butene copolymers. The triad data of fractionated ethylene/1-butene copolymers were taken from literature (Kuroda et al., 1987). The fractionation was done by successively extracting the sample with diisopropyl ether at 20^{o}C (Fraction 1), n-hexane at 20^{o}C (Fraction 2), n-hexane at its boiling point (Fraction 3), and cyclohexane at its boiling point (Fraction 4). The residual polymer (cyclohexane insolubles) was designated Fraction 5. Two fractions (two sets of triad sequences) were fitted at a time (Fraction 1 and Fraction 2), (Fraction 2 and Fraction 3), (Fraction 3 and Fraction 4) and (Fraction 4 and Fraction 5). The weight fractions and only the reaction probabilities can be estimated using the triad data of fractionated copolymer sample. The author claims that the procedure of using triad data with pairwise fractions produced more reliable results for the two site case (Cheng, 1990). The author also examined the ^{13}C NMR spectral assignments for ethtylene-1-

hexene copolymers. Cheng developed a scheme to extract the information on sequence distribution from spectral intensities. Previously, the author based his studies on Bernoullian models whereas in this case the author used Terminal model. The model fit used the reaction probabilities rather than the reactivity ratios as the model parameters. The author concluded that the data fit to one-component first-order Markovian models and the addition of 3-4% of second component improved the fit slightly (Cheng, 1991). Cheng also described a methodology to determine the reactivity ratios for separate components from ^{13}C NMR and comonomer feed ratio data. He used the theoretical probability expressions for Bernoullian copolymers containing two and three site types to determine the estimates. The theoretical and observed intensities of the triads for five samples were compared and minimized by varying the reaction probabilities. The monomer and comonomer feed concentrations and the NMR data were analyzed simultaneously to give the reactivity ratios and the component weight fractions estimates (Cheng, 1993).

Even though Cheng et al. systematically analyzed a variety of olefin copolymers using different statistical models, their methodology suffered from several limitations: 1) their optimization method was not the best suited for multiresponse problems; 2) they did assess the errors associated with the data of the experiments; 3) all comonomer sequence distributions were used during data fit, not taking into account near linear dependencies that may lead to poor parameter estimation; and 4) mass fractions of polymers made on different site types were determined only from ^{13}C NMR data. We hope to eliminate all these shortcomings in our methodology.

Kou et al. (2005) developed models to simulate gas-phase ethylene/hexene copolymerization. The models were able to predict ethylene consumption rate, gas composition drift during the experimental runs, number-and weight-average molecular weight, short chain branching levels, and triad sequence distributions of copolymer removed from the reactor at the end of each run. A single-site-type model was first developed, but failed to accurately predict the molecular weight data and its distribution. A two-site-type model was built to improve model predictions. Model fits and model verification results for triad fractions with low frequencies (HHH, HEH, and EHH) were poor. The authors suggest that this was possibly due to the use of an inadequate mechanism or perhaps due to unreliable measurements.

Chapter 3[1]
Methodology Validation

3.1 Introduction

In this chapter we discuss our methodology and describe, the Integrated Deconvolution Estimation Model (IDEM), which estimates reactivity ratios of a multiple-site-type catalyst using MWD and CSLD data. In the first step, the MWD is deconvoluted into several Flory's distributions to estimate the number of site types and the polymer weight fractions made on each of them. In the second step, this information is combined with the triad or tetrad data that characterize the CSLD of the polymer to estimate the reactivity ratios for each site type. To test whether this parameter estimation approach was effective, we simulated the MWDs, triad and tetrad distributions of model polymers made with a model three-site-type catalyst under different polymerization conditions. These simulated data were used as "experimental" data to test if the optimization method could retrieve the correct reactivity ratios used to generate the triad and tetrad data. Finally, we added random noise to the triad and tetrad data to simulate experimental error, and to evaluate whether IDEM also worked under these more realistic conditions.

3.2 Model Development

3.2.1 Generation of Simulated Data

A 3 site-type terminal model was used to generate the MWD, triad and tetrad distributions for nine simulated copolymer samples (A-1 to A-9) made with different comonomer molar fractions in the reactor under steady state conditions (Table 3.1). The weight fractions of polymer produced by the three site types (w_1, w_2, and w_3) were calculated using the propagation and termination rate constants for each site type, as shown in Appendix A. The reactivity ratios for monomers *A* (ethylene) and *B* (α-olefin) used to generate the model polymers are given in Table 3.2. Notice that $r_{A,1} \times r_{B,1} = 1$, that is, we assumed that site type 1 produces ideal (random) copolymer, whereas, $r_{A,2} \times r_{B,2} = 1.2$ and $r_{A,3} \times r_{B,3} =$

[1] * *This is the pre-peer reviewed version of the following article*: M.A. Al-Saleh, J.B.P. Soares, T.A. Duever. The Integrated deconvolution estimation model. A parameter estimation methodology for ethylene/α-olefin copolymers made with multiple-site-type catalysts. *Macromolecular Reaction Engineering*, **2010**, 4, 578-590.

2.5; therefore sites 2 and 3 produce copolymer with non ideal comonomer distribution, with a tendency to not have a significant effect on the form longer ethylene (*A*) blocks.

These values are within the range commonly encountered for the copolymerization of ethylene and α-olefins, but their absolute values should proposed parameter estimation methodology.

Table 3.1 Weight fractions of copolymer made on each site type.

Sample	w_1	w_2	w_3	M_n	M_w	PDI	f_A	F_A
A-1	0.1759	0.4518	0.3724	81 959	477 131	5.82	0.9	0.9578
A-2	0.1401	0.4741	0.3858	55 949	317 595	5.68	0.8	0.9154
A-3	0.1230	0.4869	0.3901	42 580	217 823	5.12	0.7	0.8668
A-4	0.1149	0.4953	0.3898	33 376	153 115	4.59	0.6	0.8085
A-5	0.1125	0.5010	0.3866	26 409	109 819	4.16	0.5	0.7366
A-6	0.1142	0.5045	0.3813	20 962	80 150	3.82	0.4	0.6463
A-7	0.1198	0.5052	0.3750	16 670	59 486	3.57	0.3	0.5316
A-8	0.1288	0.5014	0.3698	13 300	44 991	3.38	0.2	0.3859
A-9	0.1409	0.4890	0.3701	10 696	34 913	3.26	0.1	0.2056

M_n – number average molecular weight; M_w – weight average molecular weight; PDI – polydispersity index; f_A – monomer molar fraction in the reactor; F_A – monomer fraction in the copolymer.

Table 3.2 Reactivity ratios for the model catalyst.

Site-type	r_A	r_B	$r_A \times r_B$
1	1	1	1
2	3	0.4	1.2
3	5	0.5	2.5

3.2.2 Molecular Weight Distribution Deconvolution

This section describes the deconvolution method used to determine the minimum number of Flory's distributions required for MWD representation. This modeling technique has been used extensively to describe the MWD of polyolefins made with multiple-site-type catalysts, and is briefly reviewed in Appendix A (Hamielec et al., 1996; Soares et al., 1996; Soares, 2001; Soares, 2007).

To illustrate the MWD deconvolution methodology, we will apply it to model copolymer A-5; the parameters used to model the MWD of this sample are shown in Table 3.3. Similar results would be obtained for the other model copolymers in Table 1, but it MWD deconvolution is not the main objective of this manuscript.

Table 3.3 Parameters for model copolymer A-5.

Site type	w	M_n	M_w	PDI
1	0.1125	5 972	11 943	2.0
2	0.5010	33 271	66 541	2.0
3	0.3866	97 190	194 380	2.0
All	1.00	26 409	109 819	4.16

The MWD deconvolution procedure starts by assuming a given number (i) of active site types. The optimum values for w_i and $M_{n,i}$ are found by minimizing the sum of squares of the differences between experimental and predicted MWDs (χ^2 in Equation A.17). The process is then repeated by adding more site types, until the fit cannot be improved any further. Table 3.4 and Figure 3.1 shows how χ^2 decreases as the number of site types is increased from 1 to 4; adding 4 or more sites will not result in a better MWD representation. The MWD deconvolution into three site types for model copolymer A-5 is shown in Figure 3.2.

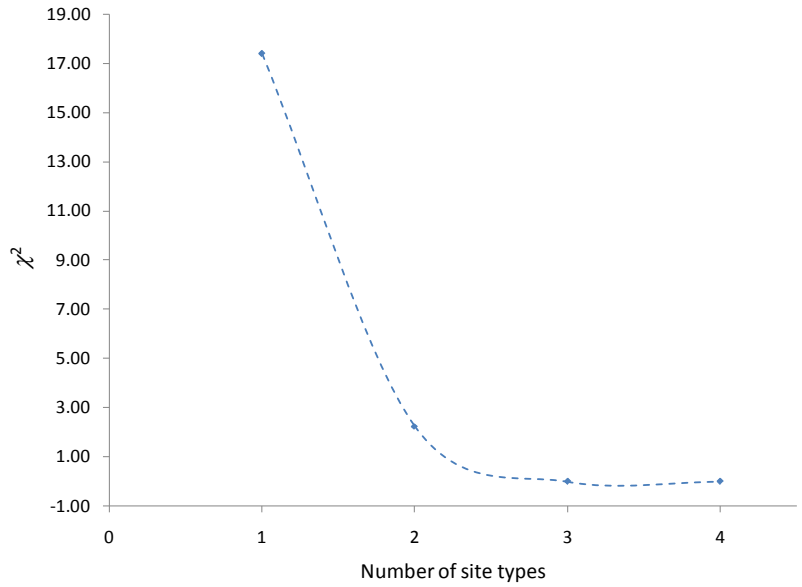

Figure 3.1 Influence of the number of site types on the value of χ^2.

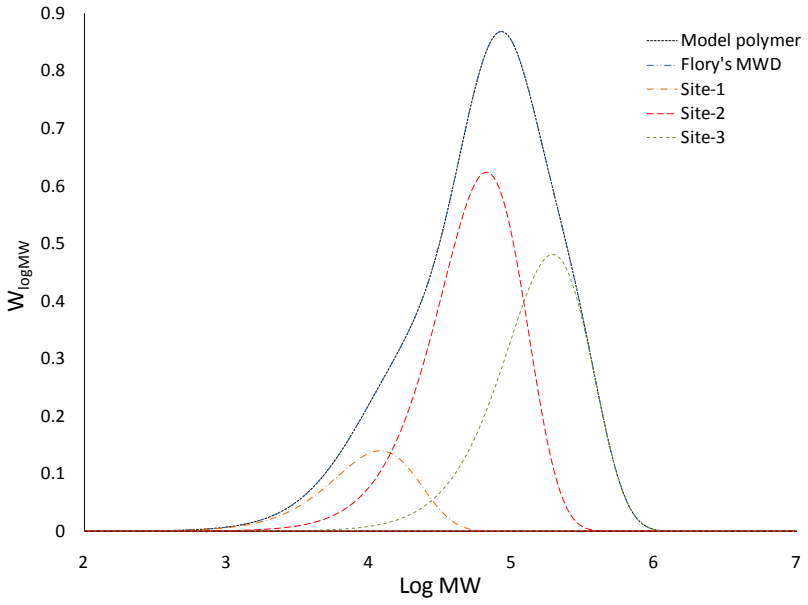

Figure 3.2 MWD deconvolution with three site types for model copolymer A-5 (χ^2=3.7×10^{-10}).

The parameters estimated for the three-site-type model agree well with those used to generate the model copolymer (Table 3.3), as expected. It has been shown (Alghyamah and Soares, 2009) that, even if noise is added to the MWD, the "right" parameters can still be recovered with this procedure.

Table 3.4 MWD deconvolution parameters for model with 1 to 4 site types.

Number of Site Types	Site type	w	M_n	M_w	PDI	χ^2
1	1	1.00000	47 331	94 662	2.00	17.41
	All	1.00000	47 331	94 662	2.00	
2	1	0.42000	21 415	42 830	2.00	2.25
	2	0.58000	78 373	156 746	2.00	
	All	1.00000	36 949	108730	2.94	
3	1	0.11245	5 972	11 943	2.00	$3.7 \quad 10^{-10}$
	2	0.50098	33 271	66 541	2.00	
	3	0.38656	97 190	194 381	2.00	
	All	1.00000	26 409	109 819	4.16	
4	1	0.11233	5 969	11 939	2.00	$5.3 \quad 10^{-6}$
	2	0.50010	33 237	66 474	2.00	
	3	0.29444	95 157	190 314	2.00	
	4	0.09313	103 244	206 489	2.00	
	All	1.00000	26 413	109 851	4.16	

3.2.3 Triad and Tetrad Distributions

The terminal model equations used to predict the triad and the tetrad distributions are given in Table 3.5, and the reaction probability equations are shown in Table 3.6. These expressions have been derived before by Cheng, Bovey and Mirau (Cheng, H.N., 1989; Cheng, H.N., 1990; Cheng, N.H., 1991; Cheng, N.H., 1993; Bovey et al., 1996).

Table 3.5 Triad and tetrad distribution expressions using the terminal model.

Triads		Tetrads	
AAA	$\sum_{i=1}^{N} w_i F_{A,i} P_{AA,i}^{2}$	AAAA	$\sum_{i=1}^{N} w_i F_{A,i} P_{AA,i}^{3}$
AAB	$\sum_{i=1}^{N} w_i P_{AA,i} (F_{A,i} P_{AB,i} + F_{B,i} P_{BA,i})$	AAAB	$\sum_{i=1}^{N} w_i P_{AA,i}^{2} (F_{A,i} P_{AB,i} + F_{B,i} P_{BA,i})$
BAB	$\sum_{i=1}^{N} w_i F_{B,i} P_{BA,i} P_{AB,i}$	BAAB	$\sum_{i=1}^{N} w_i F_{B,i} P_{BA,i} P_{AA,i} P_{AB,i}$
ABA	$\sum_{i=1}^{N} w_i F_{A,i} P_{AB,i} P_{BA,i}$	ABAA	$2 \cdot \sum_{i=1}^{N} w_i F_{A,i} P_{AB,i} P_{BA,i} P_{AA,i}$
BBA	$\sum_{i=1}^{N} w_i P_{BB,i} (F_{B,i} P_{BA,i} + F_{A,i} P_{AB,i})$	BBAA	$\sum_{i=1}^{N} w_i P_{AA,i} P_{BB,i} (F_{B,i} P_{BA,i} + F_{A,i} P_{AB,i})$
BBB	$\sum_{i=1}^{N} w_i F_{B,i} P_{BB,i}^{2}$	ABAB	$\sum_{i=1}^{N} w_i P_{AB,i} P_{BA,i} (F_{A,i} P_{AB,i} + F_{B,i} P_{BA,i})$
		BBAB	$2 \cdot \sum_{i=1}^{N} w_i F_{B,i} P_{BB,i} P_{BA,i} P_{AB,i}$
		ABBA	$\sum_{i=1}^{N} w_i F_{A,i} P_{AB,i} P_{BB,i} P_{BA,i}$
		BBBA	$\sum_{i=1}^{N} w_i P_{BB,i}^{2} (F_{B,i} P_{BA,i} + F_{A,i} P_{AB,i})$
		BBBB	$\sum_{i=1}^{N} w_i F_{B,i} P_{BB,i}^{3}$

$P_{xy,i}$ – propagation probability for a copolymer ending with monomer x and propagating with monomer y on site type i; $F_{x,i}$ –fraction of comonomer x in copolymer made on site type i; w_i – mass fraction of polymer made on site type i; N – number of site types (N = 3 in the present simulations).

Table 3.6 Reaction probabilities and copolymer composition equation.

	Terminal Model
Propagation Probabilities	$P_{BA,i} = \dfrac{1}{1 + r_{B,i}\dfrac{f_B}{f_A}}$
	$P_{AB,i} = \dfrac{1}{1 + r_{A,i}\dfrac{f_A}{f_B}}$
Copolymer Composition Equation (Mayo-Lewis Equation)	$F_{A,i} = \dfrac{r_{A,i}\, f_A^{\,2} + f_A\, f_B}{r_{A,i}\, f_A^{\,2} + 2\, f_A\, f_B + r_{B,i}\, f_B^{\,2}}$

The triad and tetrad distributions shown in Tables 3.7 and 3.8 were calculated using the expressions in Table 3.5. Figure 3.3 shows the effect of changing the molar fraction of monomer *A* in the reactor (f_A) on the triad distribution of the model copolymer.

Table 3.7 Triad distribution for the model copolymers.

Sample	f_A	BBB	BBA	ABA	BAB	AAB	AAA
A-1	0.9	0.02	0.53	3.66	0.23	7.40	88.15
A-2	0.8	0.17	1.90	6.40	0.79	13.12	77.63
A-3	0.7	0.57	4.10	8.65	1.66	18.08	66.94
A-4	0.6	1.48	7.27	10.41	2.90	22.28	55.66
A-5	0.5	3.32	11.55	11.47	4.58	25.32	43.76
A-6	0.4	6.95	16.89	11.53	6.75	26.46	31.42
A-7	0.3	13.94	22.69	10.21	9.25	24.61	19.30
A-8	0.2	27.34	26.88	7.19	11.37	18.53	8.70
A-9	0.1	52.80	23.77	2.87	10.69	8.12	1.74

Table 3.8 Tetrad distribution for the model copolymers.

Sample	f_A	BBBB	BBBA	ABBA	BBAB	ABAB	BBAA	ABAA	BAAB	AAAB	AAAA
A-1	0.9	0.002	0.042	0.245	0.038	0.424	0.494	6.903	0.213	6.971	84.668
A-2	0.8	0.028	0.278	0.809	0.245	1.335	1.651	11.465	0.677	11.763	71.750
A-3	0.7	0.138	0.867	1.614	0.737	2.583	3.358	14.725	1.327	15.429	59.221
A-4	0.6	0.463	2.027	2.622	1.676	4.125	5.594	16.688	2.162	17.958	46.686
A-5	0.5	1.292	4.066	3.742	3.304	5.864	8.245	17.073	3.158	19.001	34.255
A-6	0.4	3.269	7.361	4.763	5.956	7.539	10.932	15.527	4.208	18.043	22.403
A-7	0.3	7.870	12.142	5.274	9.944	8.551	12.746	11.866	5.007	14.597	12.004
A-8	0.2	18.522	17.629	4.623	14.919	7.813	11.957	6.573	4.892	8.747	4.326
A-9	0.1	43.218	19.173	2.297	17.247	4.142	6.519	1.602	2.864	2.394	0.545

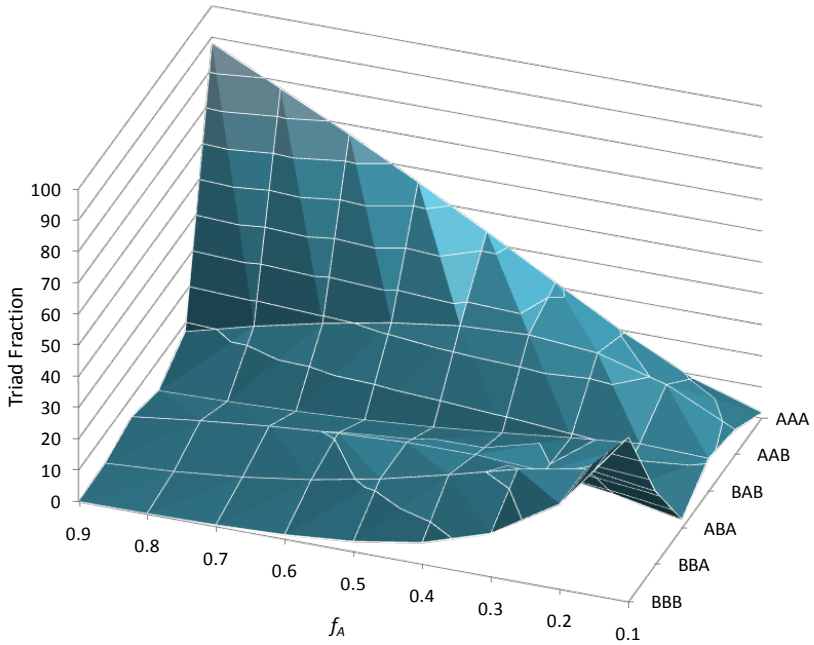

Figure 3.3 Effect of changing the molar fraction of monomer A (f_A) in the reactor on the triad distribution of the model copolymers.

3.2.4 Data Fitting and Optimization Method

IDEM uses the data in Table 3.1, and Table 3.7 or Table 3.8, to estimate the reactivity ratios of each site type in the catalyst with the determinant criterion, a popular method introduced by Box and Draper (Box and Draper, 1965). The general model for *m* responses measured in *n* experimental runs is represented by

$$Y_{ij} = f_j(\underline{x}_i, \underline{\theta}) + z_{ij} \text{ , } i, j\text{th element} \qquad (3.1)$$

where z_{ij} is the random error associated with the measured value of the *j*th response for the *i*th case (Polic et al., 2004). In our particular case, Y_{ij} is the matrix of triad, or tetrad, intensities, x_i are the molar fractions of monomer *A* (f_A) and comonomer *B* (f_B) in the reactor, and θ are the estimated reactivity ratios.

The objective function to be minimized is the determinant of the estimated measurement error covariance matrix

$$\phi(\underline{\theta}) = \left|\underline{Z}'\,\underline{Z}\right| \qquad (3.2)$$

Some of the advantages of the determinant criterion are: 1) the expectation function can be linear or not, 2) the parameters can be common to more than one response, 3) the design variables can be common to more than one response, and 4) the responses used can be rescaled, or a linear combination of responses can be used (Box and Tiao, 1973; Burke et al., 1996).

Our estimation problem is nonlinear; we used the Simplex method to search for the minimum value of the objective function to obtain the point estimates for the reactivity ratios per site type.

3.3 Results and Discussion

3.3.1 IDEM Validation using Error-Free Data

IDEM was initially tested using the error-free triad and tetrad data presented in Tables 3.7 and 3.8. To find out whether IDEM was able to discriminate between different statistical polymerization models, we compared fitting results assuming Bernoulian and terminal model statistics, since we know that the terminal model was used to generate the triad and tetrad distributions.

Table 3.9 lists the values estimated for the reactivity ratios when all of the 6, or only 4, triads were used in the terminal and Bernoullian models. We realize that reactivity ratios cannot be determined experimentally with an accuracy of four decimal places; these values, however, are reported in Table 3.9 to illustrate how close the estimates are to the values shown in Table 3.2.

Table 3.9 Reactivity ratio estimates using terminal and Bernoullian models with 4 and 6 triads (Error free).

	Model		6 triads (T)		4 triads (T)		6 triads (B)		4 triads (B)	
Site-type	r_A	r_B	r_A	r_B	r_A	r_B	r_A	r_B	r_A	r_B
1	1.0000	1.000	0.9589	1.0236	1.0257	1.0058	1.0840	0.9225	1.0633	0.9404
2	3.0000	0.4000	3.0001	0.4070	2.9642	0.4041	3.6194	0.2763	3.5333	0.2830
3	5.0000	0.5000	5.0055	0.4862	5.0280	0.4930	3.5191	0.2842	3.6501	0.2740
$\phi(\underline{\theta})$			1.09	10^{-33}	2.51×10^{-11}		4.25	10^{-18}	0.2351	

T – terminal model; B – Bernoullian model.

The value of the objective function, $\phi(\underline{\theta})$, is always lower when the terminal model is used, indicating that, had we not known *a priori* that the terminal model was used to generate the triad data, we still would have selected it as the preferred model. For the same statistical model, $\phi(\underline{\theta})$ values are higher when 4 triads are used but, interestingly, the prediction of the triad intensities is better, as can be seen in Table 3.10 and 3.11.

Table 3.10 Percentage absolute deviations between predicted and simulated triad values when all triads are used.

	ΔBBB%	ΔBBA%	ΔABA%	ΔBAB%	ΔAAB%	ΔAAA%
A-1	8.14	4.62	1.86	6.65	1.76	0.27
A-2	4.51	2.03	0.39	3.21	0.29	0.17
A-3	1.94	0.60	0.01	1.29	0.09	0.06
A-4	0.31	0.15	0.15	0.11	0.22	0.12
A-5	0.66	0.01	0.25	0.10	0.26	0.15
A-6	0.18	0.31	0.37	0.63	0.19	0.64
A-7	0.46	0.07	0.11	0.23	0.20	0.21
A-8	0.30	0.08	0.37	0.19	0.17	0.23
A-9	0.00	0.03	0.20	0.17	0.22	0.74
Average	1.83	0.88	0.41	1.40	0.38	0.29

Near linear dependency may occur among the errors, the expected values of the responses, and the experimental data, when dealing with multiresponse data. The determinant criterion overcomes the difficulties associated with the near linear dependency among the errors. The dependencies in expected values of the responses and the experimental data "the sum of all sequence distributions of each sample = 1" may lead to high correlations among estimated model parameter, producing unstable estimates which add difficulties to the parameter estimation process (Box et al., 1973; Burke et al., 1994). Near linear dependency was avoided during parameter estimation by using only four triads (ABA and BAB were excluded). As a consequence, the triad distribution predicted with the estimated reactivity ratios were closer to the "experimental" data than all triads were included, as can be verified by comparison of Tables 3.10 and 3.11, and for model copolymer A-1 in Figure 3.4.

Table 3.11 Percentage absolute deviations between predicted and simulated triad values, excluding ABA and BAB from the parameter estimation procedure.

	ΔBBB%	ΔBBA%	ΔABA%	ΔBAB%	ΔAAB%	ΔAAA%
A-1	1.13	0.50	0.13	1.05	0.23	0.03
A-2	0.34	0.39	0.31	1.68	0.15	0.08
A-3	1.33	0.72	0.14	1.60	0.00	0.11
A-4	1.79	0.79	0.03	1.42	0.09	0.19
A-5	0.65	0.23	0.01	0.60	0.10	0.12
A-6	0.87	0.31	0.11	0.76	0.10	0.48
A-7	0.11	0.16	0.14	0.40	0.03	0.50
A-8	0.19	0.03	0.20	0.07	0.19	0.20
A-9	0.01	0.03	0.12	0.02	0.04	0.13
Average	0.71	0.35	0.13	0.84	0.10	0.20

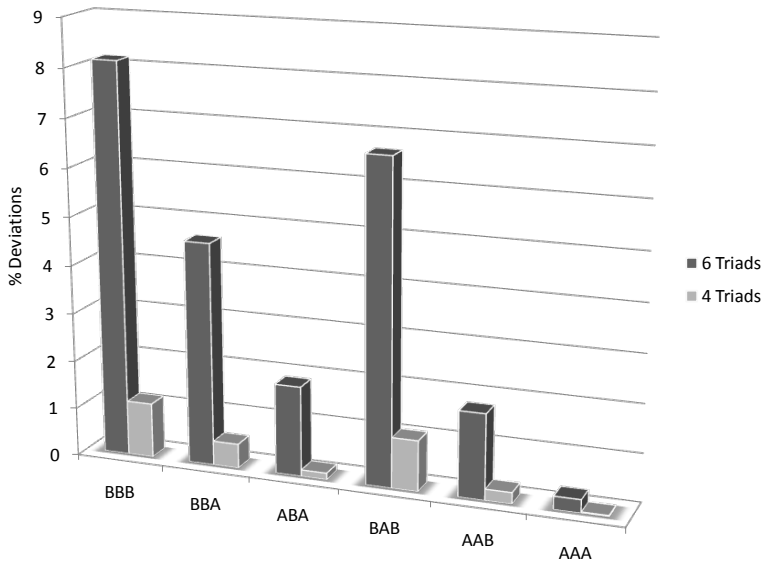

Figure 3.4 Absolute percent deviations for the triad distribution of model copolymer A-1 using 6 or 4 triads.

When the parameter estimation was repeated using 6 or 4 triads assuming that all site types followed a Bernoullian model ($r_A \times r_B = 1.0$), the percentage deviations between predicted and simulated triad

distributions were significantly worse, as shown in Table 3.12 for 6 triads, proving that IDEM can select the correct model used to generate the triad distribution.

Table 3.12 Percentage absolute deviations between predicted and simulated when all triads are used.

	ΔBBB%	ΔBBA%	ΔABA%	ΔBAB%	ΔAAB%	ΔAAA%
A-1	26.89	19.79	1.07	7.59	0.11	0.09
A-2	30.37	21.57	3.82	5.92	1.32	0.11
A-3	33.34	22.29	6.98	4.15	2.40	0.20
A-4	35.45	21.85	10.92	2.04	3.60	0.42
A-5	35.48	19.64	16.02	1.23	5.11	0.59
A-6	35.96	16.72	22.92	4.22	7.16	1.59
A-7	33.75	11.19	32.72	8.96	10.10	3.05
A-8	30.00	2.05	48.75	15.81	15.48	6.66
A-9	21.46	15.48	78.29	28.31	26.11	14.57
Average	31.41	16.73	24.61	8.69	7.93	3.03

When tetrads are used, IDEM performs even better, estimating the reactivity ratios shown in Table 3.13, which are essentially the same values used to generate the tetrad sequences. The percentage deviations between predicted and simulated tetrads are excellent as shown in Table 3.14 and Table 3.15. As observed for the triads, when the near linear dependency is removed by excluding 4 tetrads (BBBB, BBBA, BBAB, and ABAB), a better fit of the model data is obtained. Figure 3.5 depicts this observation for model copolymer A-1.

Table 3.13 Reactivity ratio estimates using terminal and Bernoulian modes with 4 and 6 triads (Error free).

	Model		10 tetrads (T)		6 tetrads (T)		10 tetrads (B)		6 tetrads (B)	
Site-type	r_A	r_B	r_A	r_B	r_A	r_B	r_A	r_B	r_A	r_B
1	1.0000	1.000	1.0000	0.9999	1.0029	0.9972	0.9693	1.0317	1.0413	0.9604
2	3.0000	0.4000	3.0002	0.4197	2.9963	0.3978	3.2014	0.3124	3.5065	0.2852
3	5.0000	0.5000	5.0001	0.4999	5.0288	0.5048	5.3111	0.1883	3.7861	0.2641
$\phi(\underline{\theta})$			2.94×10^{-50}		1.91×10^{-31}		7.34×10^{-38}		3.96×10^{-14}	

T – terminal model; B – Bernoulian model.

Table 3.14 Percentage absolute deviations between predicted and simulated tetrad values when all tetrads are used.

	ΔBBBB%	ΔBBBA%	ΔABBA%	ΔBBAB%	ΔABAB%	ΔBBAA%	ΔABAA%	ΔBAAB%	ΔAAAB%	ΔAAAA%
A-1	4.71	2.95	2.29	2.37	1.38	2.34	0.49	1.44	0.56	0.12
A-2	1.48	1.74	1.24	0.69	0.39	1.40	0.40	0.24	0.17	0.05
A-3	0.25	1.07	0.81	0.29	1.10	1.12	0.52	0.76	0.12	0.13
A-4	0.12	0.91	0.58	0.70	1.50	1.09	0.65	0.92	0.04	0.25
A-5	1.73	1.89	0.60	0.38	1.45	1.32	1.01	0.60	0.13	0.17
A-6	1.64	1.60	0.02	0.09	2.15	1.14	1.34	0.86	0.06	0.56
A-7	2.97	1.83	0.44	0.91	1.86	0.67	1.93	0.47	0.66	0.83
A-8	2.75	0.94	1.79	0.04	3.10	0.05	2.79	1.10	0.94	0.70
A-9	1.62	0.44	3.30	1.04	4.13	0.87	3.53	1.49	1.17	0.84
Average	1.92	1.49	1.23	0.72	1.90	1.11	1.41	0.88	0.43	0.41

Table 3.15 Percentage absolute deviations between predicted and simulated tetrad values when tetrads BBBB, BBBA, BBAB, and ABAB were excluded from the parameter estimation procedure.

	ΔBBBB%	ΔBBBA%	ΔABBA%	ΔBBAB%	ΔABAB%	ΔBBAA%	ΔABAA%	ΔBAAB%	ΔAAAB%	ΔAAAA%
A-1	0.28	1.03	0.83	1.07	1.09	0.82	0.44	1.06	0.43	0.09
A-2	0.67	0.46	0.32	0.66	0.45	0.29	0.26	0.46	0.25	0.11
A-3	2.15	1.41	0.73	1.78	0.88	0.67	0.16	0.87	0.15	0.24
A-4	2.84	1.72	0.75	2.25	0.95	0.66	0.02	0.93	0.00	0.44
A-5	1.22	0.69	0.34	1.10	0.50	0.21	0.06	0.49	0.02	0.48
A-6	1.40	0.72	0.35	1.36	0.70	0.05	0.01	0.58	0.25	1.03
A-7	0.05	0.04	0.04	0.06	0.32	0.05	0.02	0.10	0.09	0.13
A-8	0.19	0.03	0.12	0.07	0.04	0.04	0.16	0.13	0.03	0.30
A-9	0.04	0.01	0.08	0.03	0.16	0.09	0.04	0.04	0.19	0.51
Average	0.98	0.68	0.40	0.93	0.57	0.32	0.13	0.52	0.16	0.37

As expected, when Bernoullian statistics were assumed for all site types, the tetrad distribution could not be adequately represented with the values found for the reactivity ratios as shown in Table 3.13. These results are not reproduced here to avoid unnecessary repetition.

From these results we can conclude that IDEM can discriminate between Bernoulian and terminal models used to generate the triad and tetrad data. When tetrad data is available, the parameter estimation is more accurate, as well as when some of the triads or tetrads are excluded from the parameter estimation procedure to avoid near linear dependency.

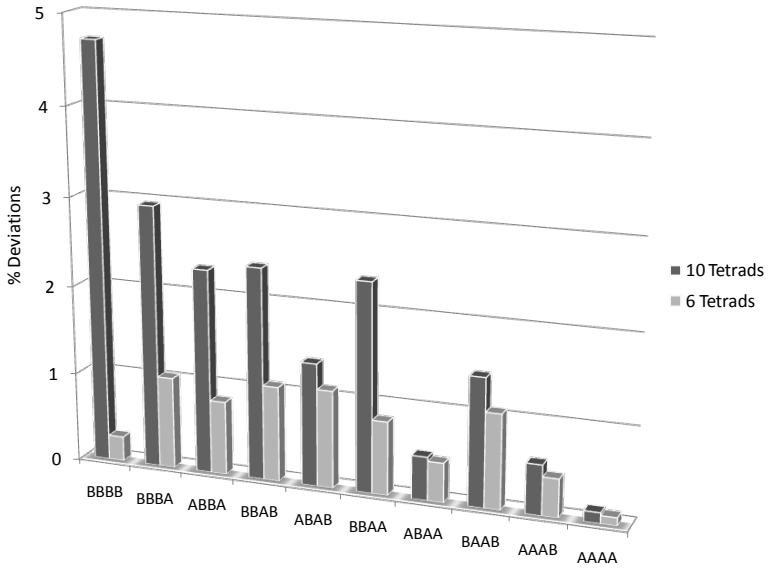

Figure 3.5 Absolute percent deviations for the tetrad distribution of model copolymer A-1 using 10 or 6 tetrads.

3.3.2 IDEM Validation using Data with Random Noise

Comonomer sequence length distributions measured by ^{13}C NMR will be subject to experimental errors; it is important to evaluate whether these errors may affect the parameter estimation methodology proposed herein. In order simulate this effect, we added random noise to our model data and repeated the parameter estimation described in the previous section. We used a routine that generates normally distributed numbers within the range of -1 to +1. Errors were made to vary from ±1%, for the most intense triad frequency, to ±5%, for the least intense, since weaker triads will experience lower signal-to-noise ratios. Other error magnitudes, including the use of the same value for all triads and tetrads were also used. Since they did not affect significantly the outcome of the proposed parameter estimation methodology, they are not reported herein. We will report only simulations with terminal model for these parameter estimations for conciseness. We have already established that the Bernoulian model is inadequate to describe error-free data and the same was observed for data containing the noise levels we are considering.

Repeating the IDEM procedure with the data containing random errors shown in Table 3.16 and Table 3.17, we find that the reactivity ratio estimates agree well with the reactivity ratios used to generate the

data (Table 3.18). The reactivity ratio estimates are very similar for both cases, but as described previously, a better triad prediction is obtained when only 4 triads are considered during the data estimation procedure.

Table 3.16 Random error coefficients (±) used for the 6 and 4 triad data.

	BBB	BBA	ABA	BAB	AAB	AAA
A-1	0.05	0.04	0.03	0.04	0.02	0.01
A-2	0.05	0.04	0.03	0.04	0.02	0.01
A-3	0.05	0.03	0.03	0.04	0.02	0.01
A-4	0.05	0.03	0.03	0.04	0.02	0.01
A-5	0.05	0.03	0.03	0.04	0.02	0.01
A-6	0.05	0.03	0.04	0.05	0.02	0.01
A-7	0.04	0.02	0.05	0.05	0.01	0.03
A-8	0.01	0.01	0.05	0.03	0.02	0.04
A-9	0.01	0.02	0.04	0.03	0.03	0.05

Table 3.17 Random error coefficients (±) used for the 10 and 6 tetrad data.

	BBBB	BBBA	ABBA	BBAB	ABAB	BBAA	ABAA	BAAB	AAAB	AAAA
A-1	0.05	0.05	0.04	0.05	0.03	0.03	0.02	0.04	0.02	0.01
A-2	0.05	0.04	0.03	0.04	0.03	0.03	0.02	0.03	0.02	0.01
A-3	0.05	0.04	0.03	0.04	0.03	0.03	0.02	0.03	0.02	0.01
A-4	0.05	0.04	0.04	0.04	0.03	0.03	0.02	0.04	0.02	0.01
A-5	0.05	0.04	0.04	0.04	0.03	0.03	0.02	0.04	0.02	0.01
A-6	0.05	0.03	0.04	0.04	0.03	0.03	0.02	0.04	0.02	0.01
A-7	0.04	0.02	0.05	0.03	0.04	0.02	0.02	0.05	0.01	0.02
A-8	0.01	0.01	0.05	0.02	0.04	0.03	0.04	0.05	0.03	0.05
A-9	0.01	0.02	0.04	0.02	0.03	0.03	0.04	0.04	0.04	0.05

Figure 3.6 compares the triad predictions for the error-free and random-noise cases using 6 triads. Evidently, IDEM was able to “filter out” the simulated experimental errors and produce good point estimates for the reactivity ratios for all samples in this case.

Table 3.18 Reactivity ratio estimates with terminal model using 6 or 4 triads (Data with error).

	Model		6 triads		4 triads	
Site-type	r_A	r_B	r_A	r_B	r_A	r_B
1	1.0000	1.000	1.0009	1.0307	1.0258	0.9855
2	3.0000	0.4000	2.9726	0.4061	2.9780	0.4036
3	5.0000	0.5000	5.0477	0.4874	5.1147	0.4952
$\phi(\underline{\theta})$			3.91×10^{-9}		1.87×10^{-5}	

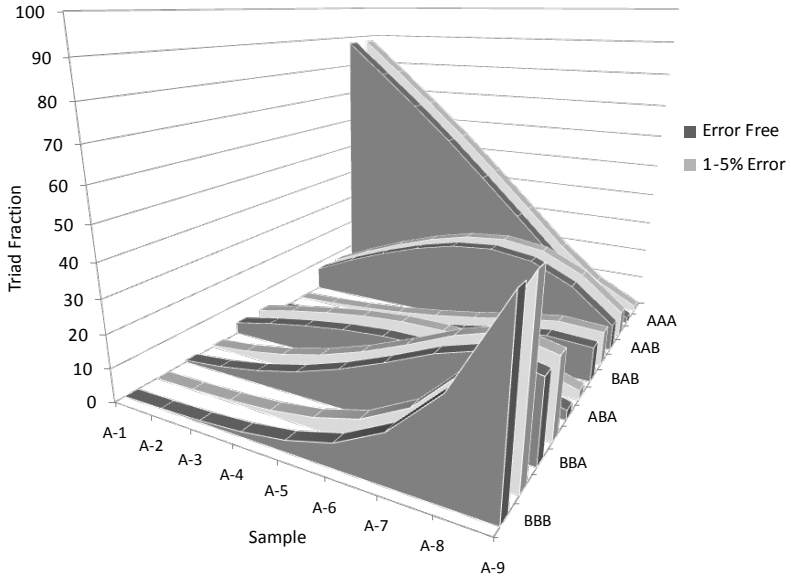

Figure 3.6 Triad distribution for samples A-1 to A-9 using 6 triads (error-free and ±1-5% error).

Figure 3.7 compares the triad percent deviations with and without added error for model copolymer A-1. Even though the deviations for the error-free data are smaller, the predictions for the data with simulated experimental error are also satisfactory.

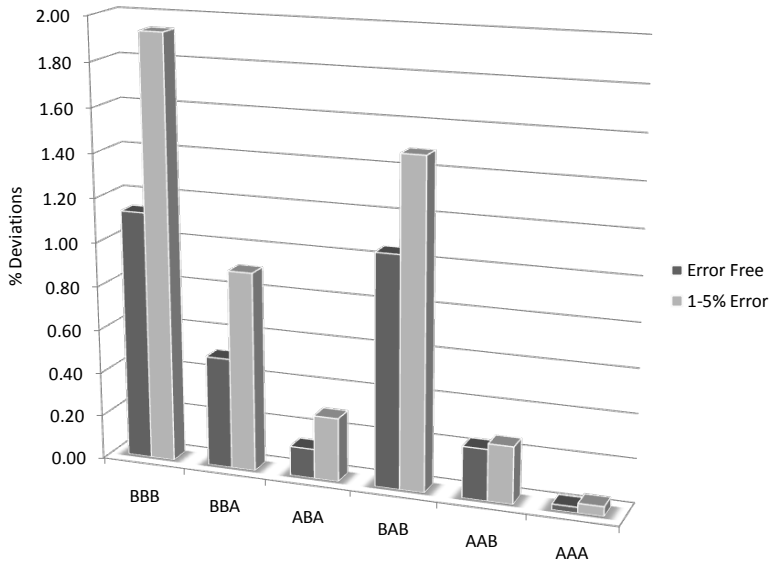

Figure 3.7 Absolute percent deviations for model copolymer A-1 using four triads (error free and ±1-5% error).

When this procedure is repeated for the tetrad distribution, even better reactivity ratio estimates are obtained, as shown in Table 3.19. Once again, IDEM was able to produce good point estimates with acceptable percentage deviations for the tetrads, as shown in Table 3.20.

Table 3.19 Reactivity ration estimates using 10 and 6 tetrads (Data with error).

	Model		10 tetrads		6 tetrads	
Site-type	r_A	r_B	r_A	r_B	r_A	r_B
1	1.0000	1.000	1.0039	0.9969	1.0063	1.0315
2	3.0000	0.4000	3.0113	0.3994	2.9932	0.4041
3	5.0000	0.5000	4.9923	0.5254	4.9846	0.5007
$\phi(\underline{\theta})$			2.47×10^{-32}		2.62×10^{-11}	

Table 3.20 Percentage Absolute deviations between predicted and simulated tetrads with ±1-5% error when all tetrads were used.

	ΔBBBB%	ΔBBBA%	ΔABBA%	ΔBBAB%	ΔABAB%	ΔBBAA%	ΔABAA%	ΔBAAB%	ΔAAAB%	ΔAAAA%
A-1	0.28	1.99	1.44	1.33	0.84	1.51	0.32	0.87	0.37	0.08
A-2	0.41	0.80	0.42	0.50	0.75	0.63	0.44	0.65	0.27	0.11
A-3	0.48	0.13	0.01	1.49	1.24	0.37	0.44	1.07	0.15	0.22
A-4	0.79	0.04	0.13	1.87	1.40	0.42	0.43	1.10	0.00	0.36
A-5	1.15	1.01	0.05	0.68	1.07	0.81	0.65	0.64	0.02	0.28
A-6	1.15	0.82	0.30	0.95	1.45	0.80	0.85	0.75	0.11	0.62
A-7	2.33	1.07	0.40	0.31	0.67	0.45	1.20	0.18	0.46	0.88
A-8	2.20	0.46	1.23	0.14	1.44	0.11	1.96	0.68	0.86	1.11
A-9	1.17	0.46	1.89	0.69	1.88	0.86	2.64	1.10	1.50	1.98
Average	1.11	0.75	0.65	0.88	1.19	0.66	0.99	0.78	0.42	0.63

Similarly to Figure 3.7, Figure 3.8 shows that the fit for the tetrads in the presence of simulated experimental error is acceptable for model copolymer A-1.

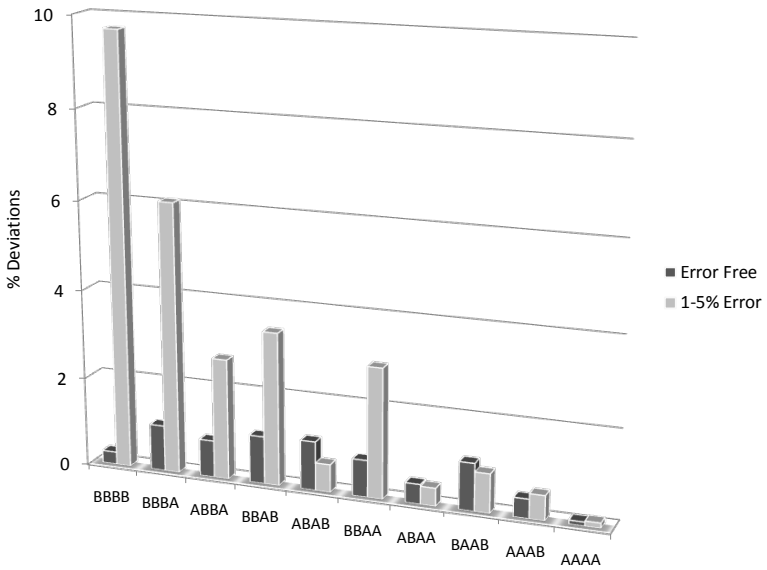

Figure 3.8 Absolute percent deviations for copolymer sample A-1 using six tetrads (error free and ±1-5% error).

In conclusion, IDEM performed well using triad or tetrad distributions even when random errors of ±1% to ±5% were added to the data. These are very encouraging results, since they indicate that the IDEM is able to accommodate the experimental errors that will be present with the ^{13}C NMR analyses of the polyolefin samples that will be investigated in next step of this research project.

3.4 Conclusions

We have developed a parameter estimation method, IDEM, that can be used to estimate the reactivity ratios of multiple-site-type catalysts, such as Ziegler-Natta and Phillips catalysts. The method combines MWD deconvolution to determine the number of active site types in the catalyst, with the analysis of comonomer sequence length (triad, tetrads, or higher) distributions.

IDEM can discriminate well between Bernoulian and terminal models, and obtain excellent estimates for the reactivity ratios for each site type, even in the presence of simulated experimental error.

As expected, when tetrads were used instead of triads, the point estimates for the reactivity ratios improve. We have also shown that by eliminating some of the comonomer sequences from the parameter estimation procedure we avoided near linear dependency problems and improved the point estimates.

The next step of this research is to apply this integrated methodology to a series of copolymer samples made with a Ziegler-Natta catalyst and characterized by GPC and ^{13}C NMR to apply the deconvolution methodology on their MWDs, triad and tetrad distributions.

Chapter 4
Polymerization and Polymer Characterization Experimental Procedures

4.1 Copolymer Sample Synthesis

Two sets of ethylene-*co*-1-butene copolymer samples were synthesized in a stainless steel autoclave reactor operated in semi-batch mode. More details on the polymerization procedure will be given below.

These samples were characterized by gel permeation chromatography (GPC) to determine their molecular weight distributions (MWD) and ^{13}C NMR to measure their comonomer sequence length distributions and average composition. The chemical composition distributions (CCD) of some samples were also measured by crystallization elution fractionation (CEF). This microstructure characterization data was used to estimate the weight fractions of copolymer made on each catalyst site type and their respective reactivity ratios.

4.1.1 Materials

All materials used in the polymerizations are listed in Table 4.1.

Table 4.1 Materials used for synthesizing ethylene-*co*-1-butene copolymer samples.

Material	Formula	Grade	Supplier
Ethylene	$CH_2=CH_2$	Polymer (3.0 PL-G)	PRAXAIR
1-Butene	$CH_2=CHCH_2CH_3$	2.1-Research	PRAXAIR
Hydrogen	H_2	Ultraplus-6.0	PRAXAIR
Nitrogen	N_2	5.0 UHP	PRAXAIR
Hexane	$CH_3(CH_2)_4CH_3$	HPLC Grade	EMD
Triethylaluminum	$Al(C_2H_5)_3$	1.0 M in hexanes	SIGMA-ALDRICH
Ethanol	CH_3CH_2OH	Denatured	VWR
Ziegler-Natta	$TiCl_4/MgCl_2$		MITSUI Chemicals

The solvent, hexane, was purified prior to use by placing it over dry molecular sieves to absorb residual water. Then, a continuous flow of nitrogen was bubbled through the liquid for 20 minutes before each polymerization run to purge residual oxygen out of the hexane. After nitrogen purging, hexane was transferred to the reactor. Ethylene was flown through molecular sieves (de moisturizing) and CuO on Alumina (Deoxygenation) beds. The $TiCl_4/MgCl_2$ Ziegler-Natta catalyst used in this research was a commercial catalyst from Mitsui Chemicals Inc.

4.1.2 Polymerization Procedure

All copolymer samples were synthesized in a 300 mL Parr autoclave reactor operated in semi-batch mode. The polymerization reactor set up is illustrated in Figure 4.1.

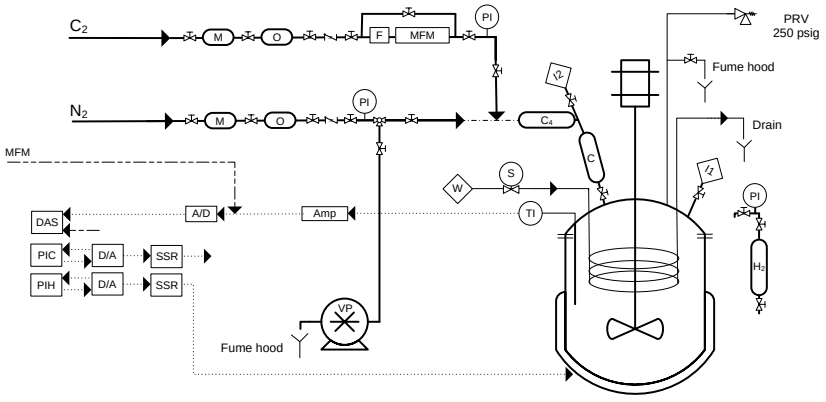

C_2	:	Ethylene supply from manifold	PI	:	Pressure gauge
N_2	:	Nitrogen supply from manifold	TI	:	J-type thermocouple
C_4	:	1-butene bomb	Amp	:	Signal amplifier
C	:	Catalyst killer bomb	A/D	:	Analog to digital conversion board
H_2	:	Hydrogen bomb	D/A	:	Digital to analog conversion board
M	:	Molecular sieves-de moisturizing	DAS	:	Data acquisition system
O	:	Deoxygenation bed (CuO on alumina)	PIC	:	Proportional-Integral loop for cooling
F	:	7 µm inlet filter	PIH	:	Proportional-Integral loop for heating
MFM	:	Mass flow meter	SSR	:	Solid state relay
I_1	:	Injection port 1	PRV	:	Pressure release valve
I_2	:	Injection port 2	VP	:	Vacuum pump
W	:	Cold water supply	Drain	:	Open drain for spent cooling water
S	:	Solenoid valve	Fume hood	:	Vent to fume hood

Figure 4.1 Semi-batch polymerization reactor system for ethylene-*co*-1-butene copolymer.

After assembling the reactor impeller and body, the reactor was purged with vacuum and nitrogen three times, heated to 125^{o}C, and finally cooled down to 35^{o}C. While cooling, the nitrogen pressure was kept at 10 psig with the vent open to create a flow of dry nitrogen through the reactor. The injection points were also purged for 5 minutes with nitrogen using a narrow cannula.

Once the reactor was purged and cooled down to 35^{o}C, 150 mL hexane was transferred into the reactor from the transfer flask. The catalyst and co-catalyst were weighed in the glove box in 20 mL vials and sealed with Teflon-lined rubber septa. Each reaction consumed one vial of the catalyst powder (8.5 mg, Ziegler Natta catalyst) and co-catalyst (0.8 g, triethylaluminum). The triethylaluminum was transferred from the vial through the injection port 1, as shown in Figure 4.1, followed by the catalyst transfer, while keeping the agitator at a speed of 100 rpm. If hydrogen was used, it was transferred to the hydrogen bomb and connected to the reactor through injection port 1. The hydrogen bomb was fitted with a pressure gauge to ensure the hydrogen pressure into the reactor was 14 psig. The 1-butene was weighed after transfer from the 1-butene cylinder into the 1-butene bomb, then fitted as illustrated in Figure 4.1 with a coupling connection. The 1-butene molar fraction dissolved in the diluent was varied from 0.3 to 0.57 for the set of copolymer samples made with no hydrogen and from 0.34 to 0.77 for the samples made with hydrogen (Table 4.2). The 1-butene molar fractions in the diluent phase were calculated using a Matlab script developed by John McCoy (private communication). The model uses the Peng-Robinson equation of state to predict the vapor-liquid equilibrium in the reactor, as described in Appendix B. It was assumed that the 1-butene molar fraction in the diluent was approximately the same at the active sites, that is, intraparticle mass transfer resistances were ignored during parameter estimation.

Before the beginning of the polymerization, the reactor temperature was raised to 60^{o}C, while checking all valve positions and sealing the injection ports. The reactor stirring was increased to 500 rpm to ensure good mixing and temperature control. Next, the 1-butene bomb connected to the reactor was pressurized with ethylene and then the ethylene/1-butene mixture were fed into the reactor at constant pressure while maitaining the temperature at 60^{o}C to start the polymerization.

Table 4.2 Molar fraction of 1-butene in the reactor.

Sample	1-Bu (g)	f_B	Sample	1-Bu (g)	f_B
EBH-1	3.0	0.342	**EB-1**	3.0	0.295
EBH-2	5.0	0.485	**EB-2**	4.0	0.358
EBH-3	6.0	0.532	**EB-3**	4.5	0.386
EBH-4	7.0	0.571	**EB-4**	5.0	0.411
EBH-5	8.0	0.605	**EB-5**	5.5	0.434
EBH-6	9.0	0.634	**EB-6**	6.0	0.456
EBH-7	10.0	0.659	**EB-7**	7.0	0.494
EBH-8	13.0	0.719	**EB-8**	8.0	0.527
EBH-9	17.0	0.774	**EB-9**	9.5	0.570

EBH – Samples made with hydrogen; EB – Samples made without hydrogen.

The ethylene pressure into the reactor was set by adjusting the regulator on the gas cylinder. The ethylene feed pressure was 100 psig for the polymerizations without hydrogen and 114 psig for all runs with hydrogen (hydrogen pressure at 14 psig). An in-line mass flow meter monitored the ethylene flow rate. A J-type thermocouple placed between the cooling coil and the reactor vessel wall supplied the temperature feedback. The temperature control was maintained by a proportional-integral controller using on/off control of an external electric band heater and cold tap water (around 10^{o}C) (Kim, 1998).

After 20 minutes of polymerization, the reactor feed was closed and the reactor operation ended. The heating jacket was removed and the vent was opened. After being depressurized, the reactor was opened and washed with ethanol to kill the remaining catalyst. Then, the polymer product was transferd to a beaker filled with 200 mL of ethanol, stirred for around 6 hours, and then filtered using a Buchner funnel and Erlenmeyer flask. The resulting polymer cake and filter paper were dried overnight in a vacuum oven.

4.2 Copolymer Characterization

4.2.1 Gel Permeation Chromatography

Gel permeation chromatography was used to determine the molecular weight distribution of the poly(ethylene-*co*-1-butene) samples. The analyses were performed on a high temperature GPC Polymer

Char instrument. During GPC analysis, the mobile phase was 1,2,4-trichlorobenzene (TCB), flown at a rate of 1.0 mL/min. The GPC was equipped with three linear columns (PLgel Olexis, 13 µm gel particles, 300 mm × 7.5 mm) in series, located in a constant temperature oven kept at 140°C. The columns were calibrated with polystyrene standards to generate the calibration curve. A typical sample preparation method consists in dissolving 10 mg of polymer in 9 mL of TCB inside the sample vial. The GPC volume injection is typically 200 µL. The GPC chromatographer is equipped with three detectors: a concentration IR detector, a light scattering detector for absolute molecular weight determination, and a viscometer. The resulting chromatograms were evaluated using the universal calibration curve and the Polymer Char software package for determining the molecular weight distribution of the sample.

4.2.2 Carbon 13 Nuclear Magnetic Resonance

A Bruker 500 MHz high resolution ^{13}C NMR spectrometer was used to determine the average chemical composition, triad and tetrad distributions of the copolymer samples. A mass of 0.1 g of each sample was dissolved in 1,1,2,2-terachloroethane (TCE) in NMR tubes and homogenized by heating the tube in a heating block at 120°C for about 12 hours before the test. Typical operation conditions were: pulse angle 90°, 2000 scannings per sample, acquisition time of about 6 seconds, spin-lattice relaxation time of 10 seconds, and spectrometer reference frequency of 125 MHz. The operation temperature for the ^{13}C NMR analysis was set at 120°C. The peak assignments calculations were done using Equations (2.7) to (2.26), according to the methodology described in Chapter 2, Sub-Section 2.3.2.3.

4.2.3 Crystallization Elution Fractionation

The samples were analyzed with the crystallization elution fractionation (CEF) Polymer Char instrument to measure their chemical composition distributions. About 10.5 mg of each sample was dissolved in 8 mL of TCB using 10 mL vial at 160°C for 60 minutes with gentle shaking in the autosampler. The test was carried out at a concentration of 1.3 mg/mL. The crystallization flow rate was 0.04 mL/min. After the crystallization ended, the temperature was kept constant at 35°C for eight minutes to ensure full dissolution of the components previously crystallized in the column. Then the elution flow began at 1.0 mL/min to elute the sample resin separated into the column at a rate of 3°C/min up to 140°C.

Chapter 5
Copolymer Samples made with Hydrogen

5.1 Introduction

The IDEM approach described in Chapter 3 is applied in this chapter to ethylene-*co*-1-butene copolymers synthesized in an autoclave reactor in the presence of hydrogen (EBH samples). The copolymer samples were made with different comonomer molar fractions under steady state-conditions. Different assumptions were tested to obtain the model that best fitted the experimental data.

First, the MWD deconvolution results will be presented. Then, six case studies will be discussed: 1) a four site-type model where all parameters are allowed to vary, 2) a four site-type model with $r_{B,4} = 0$, 3) a four site-type model where site type 4 was consider to be a homopolymer site (no 1-butene incorporation), 4) a four site-type model considering both triads and tetrads, 5) a four site-type model considering only triads and ignoring the results from the MWD deconvolution, and 6) a four site-type model using the triads and the MWD deconvolution simultaneously. These different approaches were used to find the combination that led to the best fit for the comonomer sequence length and average chemical composition experimental data.

Cases 1 to 4 were performed by applying a sequential method described in Chapter 3, in which the mass fraction of polymer made on each site type was first estimated from MWD deconvolution, and then used to fit the comonomer sequence length distribution. The objective function for the MWD deconvolution, defined in Chapter 2 (Section 2.1.3), is repeated here for convenience,

$$\chi^2 = \sum_{i=1}^{n_{GPC}} [W_{\log MW}^{GPC} - \sum_{j=1}^{ns} w_j (2.3026 MW_i^{\,2} \tau_{MW,j}^2 e^{-MW_i \tau_{MW,j}})]^2 \qquad (5.1)$$

where $W_{\log MW}^{GPC}$ is the sample MWD measured by GPC, and n_{GPC} is the number of sampling points taken during GPC analysis.

The objective function used to fit the triads and tetrads, also introduced in Chapter 3 (Section 3.2.4), is repeated for convenience below.

$$\phi(\underline{\theta}) = \left|\underline{Z}'\underline{Z}\right| \tag{5.2}$$

Case study 5 also used the objective function described by Equation (5.2).

Finally, case study 6 used a method in which the MWD and triad of all samples were fitted simultaneously, using an objective function formed by the summation of Equations (5.1) and (5.2). In this case, all parameters were updated with the same optimization routine and the objective function is represented by Equation (5.3),

$$\psi = \sum_{l=1}^{S}\sum_{i=1}^{n_{GPC}}[W_{\log MW}^{GPC} - \sum_{j=1}^{ns} w_j (2.3026 MW_i^2 \tau_{MW,j}^2 e^{-MW_i \tau_{MW,j}})]^2 + \quad \left|\underline{Z}'\underline{Z}\right| \tag{5.3}$$

where S is the number of samples.

5.2 Molecular Weight Distribution Deconvolution

The molecular weight distributions measured by GPC for the nine copolymer samples (EBH-1 to EBH-9) were deconvoluted using the procedure described in Chapter 3. Sample EBH-5 will be used to illustrate the deconvolution process; the procedure adopted for the other samples is analogous. Table 5.1 shows values estimated for the weight fractions of polymer made by each site type (w_i), their average molecular weights (M_n and M_w) and polydispersities (PDI) for sample EBH-5.

Table 5.1 MWD deconvolution parameters for copolymer EBH-5.

Site type	w	M_n	M_w	PDI
1	0.102	10 000	20 000	2.00
2	0.365	29 000	58 000	2.00
3	0.360	76 000	153 000	2.00
4	0.172	221 000	441 000	2.00
All	1.000	35 000	154 000	4.42

In reaching this decision, we followed the methodology explained in Chapter 3, by progressively increasing the number of site types representing the polymerization system to find the best MWD fit, as shown by the decreasing value of χ^2, given in Equation (5.1), in Figure 5.1. Similar patterns were observed for the other 8 copolymer samples in this set. The polymerization system for all EBH copolymer samples is best described with four site types, as the addition of a 5th site type does not significantly improve the fit.

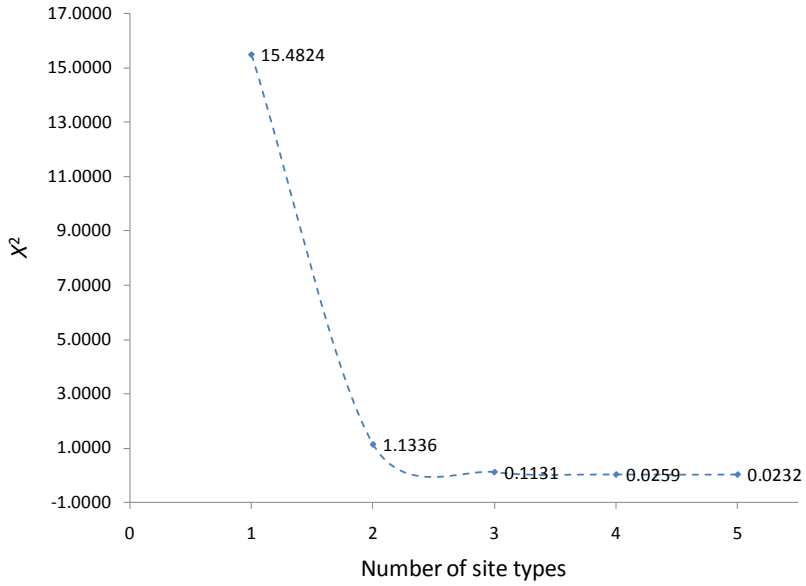

Figure 5.1 Influence of the number of site types on the value of χ^2 for sample EBH-5.

The MWD deconvolution for EBH-5 using two site types is clearly inadequate, as shown in Figure 5.2. When the number of site types is increased to three, the fit is improved (Figure 5.3), but still not satisfactory. The fit is clearly much better with four site types (Figure 5.4), but is not improved appreciably with the addition of a 5th site type (Figure 5.5).

Table 5.2 shows how the MWD deconvolution parameter estimates varies with increasing the number of site types for sample EBH-5 using the MWD deconvolution procedure outlined above.

The GPC-measured MWDs, MWD deconvolution results, and parameter estimates from MWD deconvolution for copolymer samples EBH-1 to EBH-9 are shown in Appendix C.1.

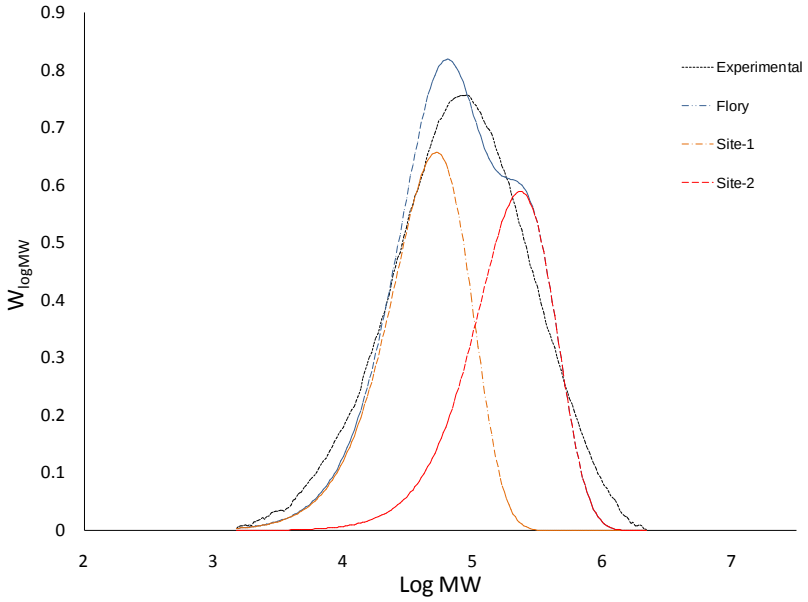

Figure 5.2 MWD deconvolution with two site types for copolymer EBH-5 (χ^2=1.1336).

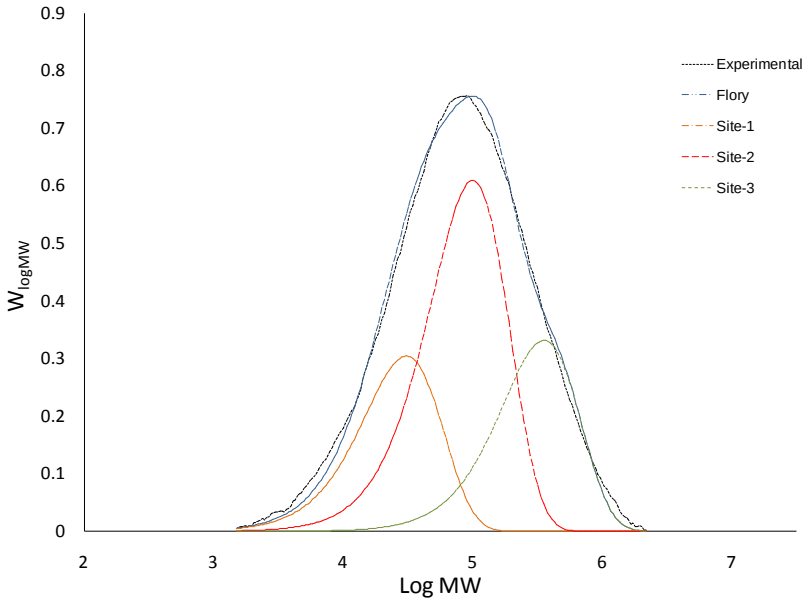

Figure 5.3 MWD deconvolution with three site types for copolymer EBH-5 (χ^2=0.1131).

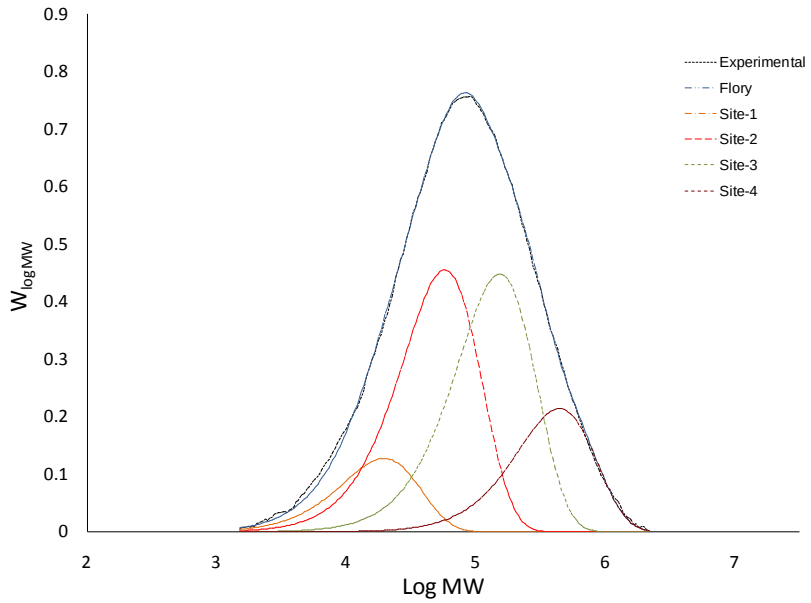

Figure 5.4 MWD deconvolution with four site types for copolymer EBH-5 (χ^2=0.0259).

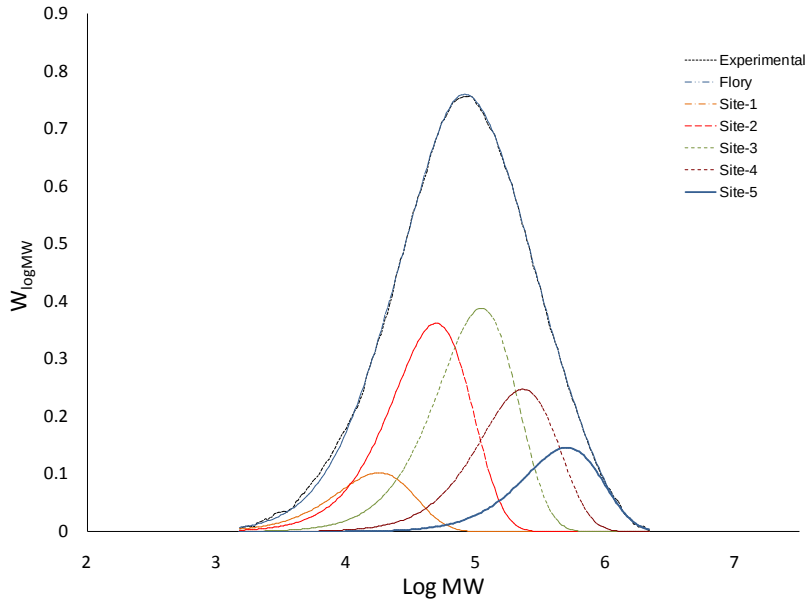

Figure 5.5 MWD deconvolution with five site types for copolymer EBH-5 (χ^2=0.0232).

Table 5.2 MWD deconvolution parameters for EBH-5 with 1 to 5 site types.

Number of Site Types	Site type	w	M_n	M_w	PDI	χ^2
1	1	1.000	50 000	100 000	2.00	15.4824
	All	1.000	50 000	100 000	2.00	
2	1	0.527	26 000	52 000	2.00	1.1336
	2	0.473	116 000	232 000	2.00	
	All	1.000	41 000	137 000	3.33	
3	1	0.245	15 000	31 000	2.00	0.1131
	2	0.489	50 000	100 000	2.00	
	3	0.266	176 000	353 000	2.00	
	All	1.000	37 000	150 000	4.10	
4	1	0.102	10 000	20 000	2.00	0.0259
	2	0.365	29 000	58 000	2.00	
	3	0.360	76 000	153 000	2.00	
	4	0.172	221 000	441 000	2.00	
	All	1.000	35 000	154 000	4.42	
5	1	0.082	9 000	18 000	2.00	0.0232
	2	0.291	25 000	49 000	2.00	
	3	0.311	55 000	110 000	2.00	
	4	0.199	115 000	231 000	2.00	
	5	0.117	252 000	503 000	2.00	
	All	1.000	35 000	155 000	4.46	

The estimated values for the weight fraction of copolymers made on each site type for the nine EBH copolymer samples are presented in Table 5.3. The molecular weight averages of polymer made on each site type increase steadily from site type 1 to 4. Those parameters are required in the estimation process for the reactivity ratios using the sequential method described in Chapter 3.

Table 5.3 Weight fractions of copolymer made on each site type for ethylene-*co*-1-butene copolymer samples made in the presence of hydrogen.

Sample	w_1	w_2	w_3	w_4	M_n	M_w	*PDI*	f_A	F_A
EBH-1	0.081	0.324	0.375	0.219	46 000	213 000	4.64	0.658	0.990
EBH-2	0.105	0.362	0.371	0.162	42 000	178 000	4.26	0.515	0.984
EBH-3	0.106	0.355	0.365	0.174	38 000	174 000	4.59	0.468	0.980
EBH-4	0.150	0.387	0.331	0.132	36 000	164 000	4.63	0.429	0.975
EBH-5	0.102	0.365	0.360	0.172	35 000	154 000	4.42	0.395	0.962
EBH-6	0.118	0.361	0.363	0.159	32 000	144 000	4.48	0.366	0.954
EBH-7	0.108	0.335	0.373	0.185	24 000	128 000	5.31	0.341	0.950
EBH-8	0.130	0.438	0.321	0.112	32 000	125 000	3.87	0.281	0.933
EBH-9	0.086	0.311	0.413	0.189	17 000	92 000	5.54	0.226	0.919

5.3 Triad and Tetrad Distribution Deconvolution

5.3.1 Triad and Tetrad Data

The EBH ethylene-*co*-1-butene copolymer samples were analyzed with ^{13}C NMR to determine their triad and tetrad distributions. The triad and tetrad calculations were performed using Equations (2.7) to (2.26), following the methodology described in Chapter 2. The triad distributions for the EBH samples are shown in Table 5.4 and the tetrad distributions in Table 5.5. Only three of the tetrads (ABBA, ABAA and BAAB) are used in the IDEM as they are the selected independent measurement from the ^{13}C NMR spectra in this study. The ^{13}C NMR spectra for the nine samples are shown in Appendix D.1.

Table 5.4 Triad distributions for the EBH copolymers.

Sample	f_A	F_A	BBB	BBA	ABA	BAB	AAB	AAA
EBH-1	0.658	0.990	0.12	0.06	0.85	0.12	1.47	97.39
EBH-2	0.515	0.984	0.12	0.14	1.22	0.15	2.58	95.79
EBH-3	0.468	0.980	0.04	0.21	1.88	0.08	3.32	94.48
EBH-4	0.429	0.975	0.27	0.28	1.87	0.11	4.03	93.43
EBH-5	0.395	0.962	0.35	0.66	2.69	0.29	5.86	90.14
EBH-6	0.366	0.954	0.50	0.65	3.45	0.50	6.82	88.08
EBH-7	0.341	0.950	0.82	0.75	3.44	0.61	6.48	87.90
EBH-8	0.281	0.933	0.96	1.06	4.46	0.72	9.46	83.34
EBH-9	0.226	0.919	1.01	1.46	5.59	1.13	10.50	80.31

Table 5.5 Tetrad distributions for the EBH copolymers.

Sample	f_A	BBBB	BBBA	ABBA	BBAB	ABAB	BBAA	ABAA	BAAB	BAAA	AAAA
EBH-1	0.658	0.11	0.02	0.02	0.06	0.23	0.00	1.47	0.12	1.23	96.75
EBH-2	0.515	0.11	0.02	0.06	0.00	0.00	0.14	2.45	0.08	2.43	94.72
EBH-3	0.468	0.03	0.02	0.10	0.21	0.44	0.00	3.31	0.17	2.97	92.76
EBH-4	0.429	0.23	0.09	0.09	0.21	0.02	0.31	3.72	0.45	3.12	91.76
EBH-5	0.395	0.20	0.29	0.18	0.33	0.26	0.73	5.12	0.29	5.27	87.33
EBH-6	0.366	0.47	0.07	0.29	0.00	1.02	0.95	5.86	1.04	4.73	85.58
EBH-7	0.341	0.77	0.11	0.32	0.38	0.84	0.45	6.03	1.18	4.12	85.81
EBH-8	0.281	0.77	0.38	0.34	0.41	1.02	1.57	7.85	1.02	7.37	79.27
EBH-9	0.226	0.75	0.53	0.46	0.03	2.22	1.54	8.95	1.39	7.71	76.41

5.3.2 Model Fit Using 4 Site Types and the Triad Distribution

In this section, the reactivity ratios of the four site types will be estimated using the second step of the IDEM procedure for the nine EBH copolymers. The estimates of the weight fractions of copolymer made on each site type obtained from MWD deconvolution are used to fit the triad distributions as independent variables.

Table 5.6 shows the reactivity ratios predicted using 6 or 4 triads. The 4 triad method is used to avoid near linear dependency, as discussed in Chapter 3. Eliminating the BBB and BAB distributions (the weakest signals in the spectra) resulted in different estimates, especially for r_B. The results show that the reactivity ratios for 1-butene (r_B) decreases from site type 1 to 4. This is in agreement with the trend commonly observed with heterogeneous Ziegler-Natta ethyelne/α-olefin copolymers, where the α-olefin comonomer fraction decreases with increasing molecular weight.

Table 5.6 Reactivity ratio estimates using 6 and 4 triads.

	6 triads			**4 triads**		
Site-type	r_A	r_B	$r_A \times r_B$	r_A	r_B	$r_A \times r_B$
1	29.8601	0.0954	2.85	28.3916	0.0964	2.74
2	48.9719	0.0569	2.79	49.6352	0.0758	3.76
3	79.4151	0.0223	1.77	79.5149	0.0353	2.81
4	117.5388	0.0023	0.27	116.3613	0.0069	0.80
$\phi(\underline{\theta})$	1.3×10^{-9}			1.4×10^{-5}		

r_A – ethylene reactivity ratio; r_B – 1-butene reactivity ratio.

Figure 5.6 shows the average percentage absolute deviations for the triads of the EBH copolymers using 6 or 4 triads (BBB and BAB excluded). Since the BBB and BAB were not considered during the model fit with 4 triads, higher deviations with respect to those two triads are observed when compared to the results obtained when all the 6 triads were used. However, when 6 triads were used for parameter estimation, much higher deviations were observed for the BBA, ABA, AAB and AAA triads, which are present in higher intensity in the ^{13}C NMR spectra of the EBH samples. More importantly, the average deviations for the 3 most intense triads (AAA, AAB, and ABA) are all below 20% when only 4 triads are used for the model fit.

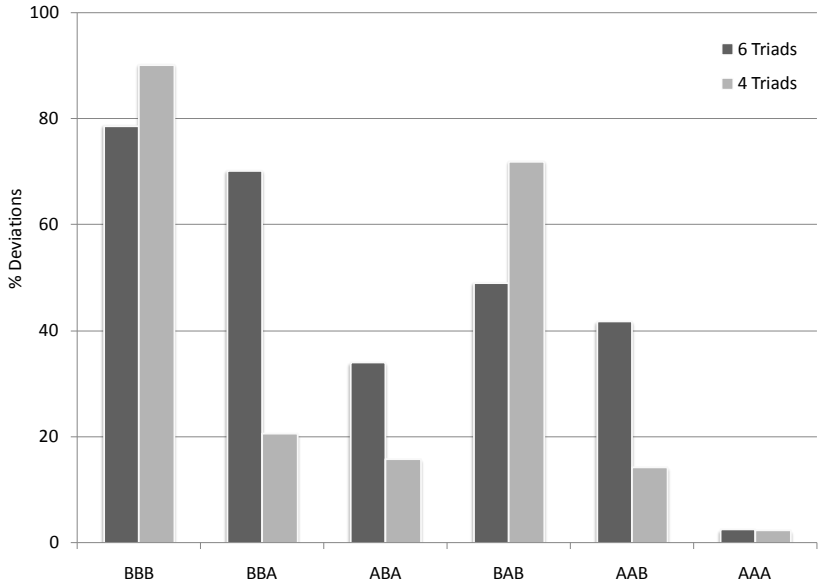

Figure 5.6 Comparison of the absolute average percentage deviations for the triad distribution when 4 or 6 triads were used during parameter estimation.

Tables showing the percentage absolute deviations for the triad distributions each EBH sample can be found in Appendix E.1.

5.3.3 Model Fit Using 4 Site Types, $r_{B,4} = 0$

Table 5.6 shows that the comnomer reactivity ratio for site 4 ($r_{B,4}$) is very small. This results was expected, since site 4 makes polymers with the highest molecular weight averages and, in heterogeneous Ziegler-Natta catalyst, high molecular weight is associated with low α-olefin incorporation. In fact, one may speculate that the highest molecular weight site may not be able to incorporate comonomer to any extent, that is, $r_{B,4} = 0$. Therefore, the triad data was refitted under the constraint that $r_{B,4} = 0$ to test whether this assumption would improve the model fit. The resulting reactivity ratios are shown in Table 5.7.

Table 5.7 Reactivity ratio estimates using 6 or 4 triads, with $r_{B,4} = 0$.

	6 triads			4 triads		
Site-type	r_A	r_B	$r_A \times r_B$	r_A	r_B	$r_A \times r_B$
1	28.7426	0.1390	4.00	29.8897	0.0951	2.84
2	49.248	0.0610	3.00	49.9723	0.0742	3.71
3	79.7619	0.0400	3.19	79.8677	0.0305	2.44
4	116.0735	0.000	0.00	107.912	0.000	0.00
$\phi(\underline{\theta})$	5.88×10^{-7}			2.45×10^{-5}		

Figure 5.7 shows the average percentage absolute deviations for the EBH sample triads under the condition $r_{B,4} = 0$. The reactivity ratio estimates obtained when $r_{B,4}$ was set to zero or allowed to vary (compare with results in Table 5.6) are close, especially for r_A, but the overall percentage deviations for the current approach increased slightly.

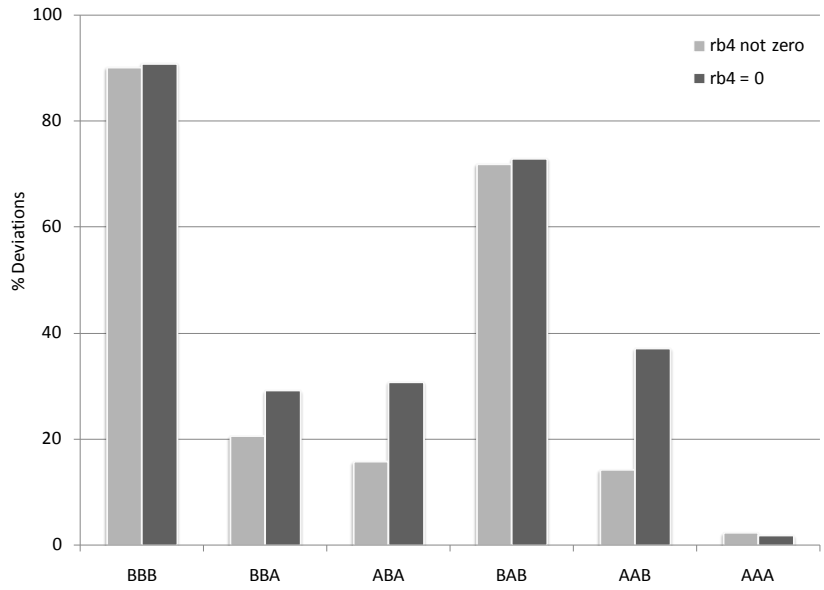

Figure 5.7 Comparison of the absolute average percentage deviations for the triad distribution when $r_{B,4} = 0$ and when it is allowed to vary (using 4 triads).

Therefore, it does not seem that making the assumption $r_{B,4} = 0$ benefits model fitting for this series of copolymers.

5.3.4 Model Fit Using 4 Site Types, 4th Site Homopolymer

This case study assumes that one of the site types produces only polyethylene homopolymer (the 4th site, responsible for the chain with the highest molecular weight averages). This assumption is akin to setting $r_{B,4} = 0$, but was implemented in a different way to further access the possibility that the highest molecular weight site was incapable of incorporating 1-butene. The weight fractions for polymer made by the 4th site type (listed in Table 5.3) were removed and the weight fractions for the polymer made in the remaining site types 1 to 3 were renormalized as shown in Table 5.8. The triad fractions shown in Table 5.4 were also modified to account for the subtraction of the homopolymer site (4th site type, making only AAA triads), as shown in Table 5.9. These new results were then used to estimate the reactivity ratios, which are shown in Table 5.10. Once again, the reactivity ratios estimated using this procedure are very similar to the ones obtained in Sections 5.3.2 and 5.3.3.

Table 5.8 Weight fractions from MWD deconvolution, renormalized after subtraction of the 4th site type (homopolymer site).

Sample	w_1	w_2	w_3
EBH-1	0.104	0.416	0.481
EBH-2	0.125	0.433	0.442
EBH-3	0.128	0.430	0.442
EBH-4	0.173	0.446	0.381
EBH-5	0.124	0.441	0.435
EBH-6	0.140	0.429	0.431
EBH-7	0.132	0.411	0.457
EBH-8	0.146	0.493	0.361
EBH-9	0.106	0.384	0.510

Table 5.9 Triad distribution renormalized after subtraction of the 4th site type (homopolymer site).

Sample	BBB	BBA	ABA	BAB	AAB	AAA	AAA from 4th Site
EBH-1	0.12	0.06	0.85	0.12	1.47	76.02	21.37
EBH-2	0.12	0.14	1.22	0.15	2.58	80.26	15.53
EBH-3	0.04	0.21	1.88	0.08	3.32	78.02	16.46
EBH-4	0.27	0.28	1.87	0.11	4.03	81.09	12.33
EBH-5	0.35	0.66	2.69	0.29	5.86	74.62	15.52
EBH-6	0.50	0.65	3.45	0.50	6.82	74.06	14.01
EBH-7	0.82	0.75	3.44	0.61	6.48	71.66	16.23
EBH-8	0.96	1.06	4.46	0.72	9.46	74.02	9.32
EBH-9	1.03	1.46	5.59	1.13	10.54	65.11	15.20

Table 5.10 Reactivity ratio estimates using 6 and 4 triads, with 4th site type removed.

	6 triads			4 triads		
Site-type	r_A	r_B	$r_A \times r_B$	r_A	r_B	$r_A \times r_B$
1	29.9999	0.1184	3.55	29.0805	0.0971	2.82
2	49.2814	0.0550	2.71	49.5608	0.0552	2.74
3	77.6391	0.0190	1.48	69.1281	0.0196	1.36
$\phi(\underline{\theta})$	9.45×10^{-5}			0.0116		

Figure 5.8 compares the absolute average percentage deviations for the three last case studies. It is clear that, with respect to the BBA, ABA and AAB triads, the model fit is best when the four site-type model is used without forcing any parameter to a certain value. Therefore, it can be concluded that assuming a homopolymer site, either by setting $r_{B,4} = 0$ or by subtraction of the AAA triads generated by the homopolymerization site, do not improve the data fit and that the 4 site-model without any assumption regarding the reactivity ratios is the most adequate approach to model the triad distributions for the EBH copolymers.

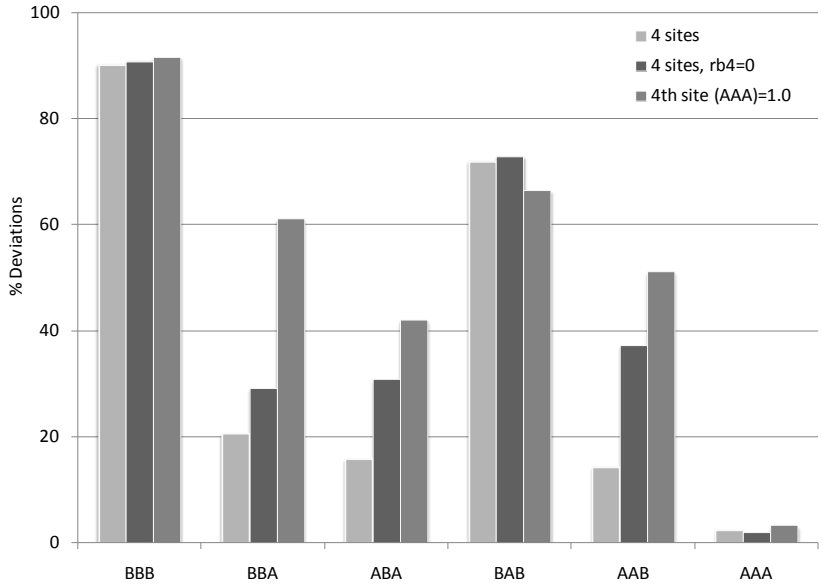

Figure 5.8 Comparison of the absolute average percentage deviation for the triad distribution of the EBH copolymers using a 4 site model without simplifying assumptions, with $r_{B,4}$=0, and with $(AAA)_4$ = 1.0.

5.3.5 Model Fit Using 4 Site Types, Triad and (Partial) Tetrad Distributions

In this case study, the six triads and three tetrads (ABBA, ABAA and BAAB) were used to estimate the reactivity ratios. The (ABBA, ABAA and BAAB) were selected as their respective NMR peaks were clear which make these 3 tetrads prediction more reliable. The use of a higher order *n*-ad distribution could be useful in fitting statistical models as more observations are available to describe the polymerization system. This attempt is performed to explore the model results and evaluate if this test is a better way to fit the data.

Table 5.11 shows the reactivity ratio estimates following this approach. Those values are close to the ones provided by the triad deconvolution using only 6 or 4 triads, although the value of the objective function, $\phi(\underline{\theta})$, is lower. As observed before, the estimates for r_A are less affected than for r_B.

Figure 5.9 shows the absolute average percentage deviations using the 6 or 4 triads and 3 tetrads. Comparing Figure 5.9 with Figure 5.6 where only triads were used, it is apparent that both procedures

led to similar results. It seems that the addition of the tetrads had very little impact on parameter estimation and model fit.

Since the experimental determination of higher comonomer sequences is difficult due to peak superposition and weaker signals, and due to the fact that considering them does not seem to enhance the model fit, their use will not be further considered in this thesis.

Table 5.11 Reactivity ratio estimates using triads and tetrads.

	6 triads + 3 Tetrads			**4 triads + 3 Tetrads**		
Site-type	r_A	r_B	$r_A \times r_B$	r_A	r_B	$r_A \times r_B$
1	26.5571	0.1457	3.87	29.8577	0.1036	3.09
2	47.1503	0.0821	3.87	49.9875	0.0558	2.79
3	76.1082	0.0208	1.58	73.108	0.0213	1.56
4	91.445	0.0088	0.81	107.8166	0.0011	0.12
$\phi(\underline{\theta})$	2.99×10^{-14}			3.65×10^{-9}		

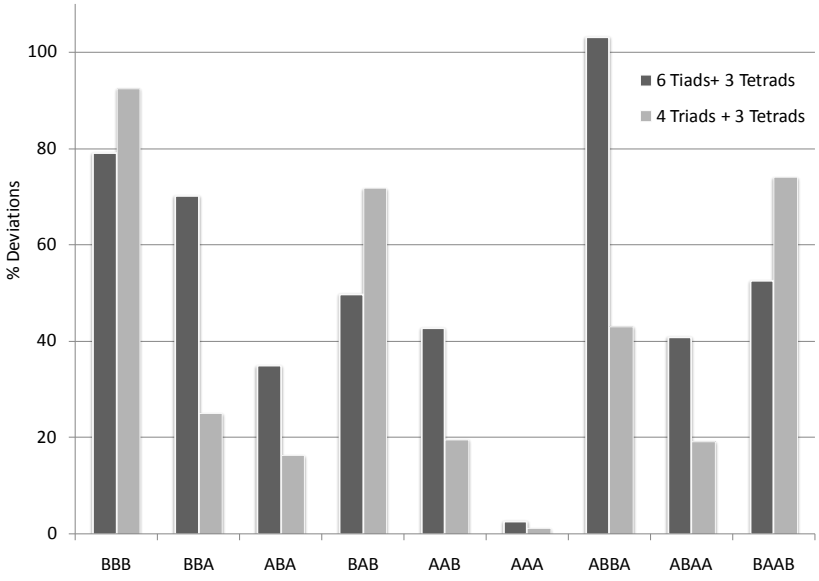

Figure 5.9 Absolute average percentage deviations for triad and tetrad distributions.

5.3.6 Model Fit Using only the Triad Distribution – No MWD Deconvolution

In all the previous case studies, weight fractions of polymer made on each site type arising from MWD deconvolutions were used to fit the triad or the triad and tetrad distributions. In order to test if a better fit for the triad distributions would be obtained without this restriction, the weight fractions were also allowed to vary in the present case study. This approach required the estimation of a significantly larger number of parameters per site type and was not successful, as it produced high value for the objective function reflecting that the model was unable to fit the data or predict the desired parameter estimates. Table 5.12 and Table 5.13 show that this test failed to meet our objectives.

Table 5.12 Weight fraction estimates of copolymer made on each site type for the EBH copolymers from triad deconvolution. Estimates shown between brackets are from the MWD deconvolution.

	EBH-1	**EBH-2**	**EBH-3**	**EBH-4**	**EBH-5**	**EBH-6**	**EBH-7**	**EBH-8**	**EBH-9**
w_1	0.178	0.244	0.2811	0.250	0.157	0.236	0.209	0.270	0.244
	[0.081]	[0.105]	[0.106]	[0.150]	[0.102]	[0.118]	[0.108]	[0.130]	[0.086]
w_2	0.279	0.261	0.343	0.298	0.262	0.266	0.216	0.309	0.264
	[0.324]	[0.362]	[0.355]	[0.387]	[0.365]	[0.361]	[0.335]	[0.438]	[0.311]
w_3	0.184	0.299	0.165	0.239	0.289	0.165	0.162	0.143	0.153
	[0.375]	[0.371]	[0.365]	[0.331]	[0.360]	[0.363]	[0.373]	[0.321]	[0.413]
w_4	0.359	0.196	0.212	0.213	0.292	0.332	0.413	0.278	0.339
	[0.219]	[0.162]	[0.174]	[0.132]	[0.172]	[0.159]	[0.185]	[0.112]	[0.189]

Table 5.13 Reactivity ratio estimates using only the triad distribution.

4 triads			
Site-type	r_A	r_B	$r_A \times r_B$
1	11.496	0.0262	0.30
2	11.8317	0.122	1.44
3	13.724	0.1758	2.41
4	13.8833	3.33E-04	0.00
$\phi(\underline{\theta})$		$2.27E\times10^{3}$	

5.3.7 Model Fit Using 4 Site Types and the Triad Distribution Simultaneously

In the simultaneous IDEM, the MWD and the triad distributions are fitted simultaneously, as part of the same optimization routine, using Equation (5.3) as the objective function. Parameter estimates for the simultaneous IDEM are shown in Table 5.14 and 5.15 (values between brackets are for the sequential IDEM approach). The reactivity ratio estimates for the simultaneous IDEM are close to the ones predicted earlier in Section 5.3.2, Table 5.6, using the sequential IDEM approach. Figure 5.10 compares absolute average percentage deviations for the present case study with the previously described sequential method. The results of both tests are very similar but the objective function is higher using the simultaneous method.

Table 5.14 Weight fractions and number-average molecular weight estimates using simultaneous IDEM, between brackets the results from the sequential method.

Sample	w_1	w_2	w_3	w_4	M_{n1}	M_{n2}	M_{n3}	M_{n4}
EBH-1	0.080	0.400	0.304	0.216	8 000	28 000	75 000	198 000
	[0.081]	[0.324]	[0.375]	[0.219]	[11 000]	[34 000]	[96 000]	[267 000]
EBH-2	0.081	0.405	0.342	0.172	9 000	32 000	79 000	212 000
	[0.105]	[0.362]	[0.371]	[0.162]	[12 000]	[33 000]	[93 000]	[253 000]
EBH-3	0.085	0.400	0.318	0.198	14 000	31 000	77 000	207 000
	[0.106]	[0.355]	[0.365]	[0.174]	[11 000]	[31 000]	[88 000]	[245 000]
EBH-4	0.099	0.400	0.314	0.187	10 000	30 000	77 000	213 000
	[0.150]	[0.387]	[0.331]	[0.132]	[12 000]	[35 000]	[92 000]	[276 000]
EBH-5	0.082	0.407	0.326	0.186	15 000	30 000	76 000	220 000
	[0.102]	[0.365]	[0.360]	[0.172]	[10 000]	[29 000]	[76 000]	[221 000]
EBH-6	0.100	0.429	0.310	0.161	14 000	28 000	78 000	212 000
	[0.118]	[0.361]	[0.363]	[0.159]	[9 000]	[28 000]	[76 000]	[207 000]
EBH-7	0.146	0.401	0.312	0.141	9 000	29 000	71 000	199 000
	[0.108]	[0.335]	[0.373]	[0.185]	[6 000]	[21 000]	[59 000]	[186 000]
EBH-8	0.118	0.458	0.324	0.100	13 000	28 000	79 000	218 000
	[0.130]	[0.438]	[0.321]	[0.112]	[12 000]	[29 000]	[77 000]	[212 000]
EBH-9	0.129	0.462	0.301	0.108	10 000	27 000	75 000	210 000
	[0.148]	[0.437]	[0.325]	[0.090]	[11 000]	[30 000]	[76 000]	[212 000]

Table 5.15 Reactivity ratio estimates using simultaneous and sequential IDEM.

	Simultaneous			Sequential		
Site-type	r_A	r_B	$r_A \times r_B$	r_A	r_B	$r_A \times r_B$
1	29.2916	0.0969	2.84	28.3916	0.0964	2.74
2	49.3836	0.0506	2.50	49.6352	0.0758	3.76
3	82.2713	0.0215	1.77	79.5149	0.0353	2.81
4	105.9521	0.0052	0.55	116.3613	0.0069	0.80
ψ	3.96			0.22		

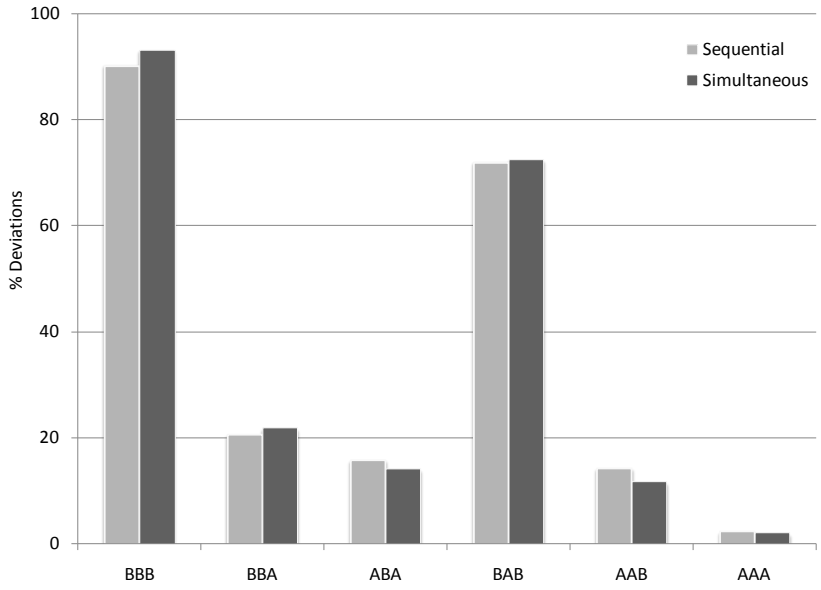

Figure 5.10 Comparison of the absolute average percentage deviations for the triad distribution using 4 sites by the simultaneous and sequential methods (4 triads).

These results reveal that both the simultaneous and sequential IDEM produce very similar reactivity ratio estimates and led to analogous fit of the triad distributions. Since the use of the sequential IDEM

method is the simplest of the two, for practical reasons it should be preferred to the simultaneous approach.

5.4 Crystallization Elution Fractionation

The EBH samples were also analyzed with CEF to measure their chemical composition distributions. Figure 5.11 compare the CEF profiles of samples EBH-3 and EBH-7, having 2 mol% and 5 mol% of 1-butene, respectively. As the 1-butene fraction in the copolymer increases, the fraction of polymer that elutes at lower temperatures increases, indicating higher 1-butene incorporation in the copolymer chains. Similarly, the fraction of polymer soluble at room temperature increases as more 1-butene is added to the reactor during polymerization. Interestingly, the high temperature peak, containing very little 1-butene, is always present, even when the average 1-butene incorporation is 5 mol%. These CEF results are in complete agreement with the reactivity ratios estimated for the EBH copolymers. Site 4, having the lowest r_B and highest r_A values almost does not copolymerize 1-butene and is responsible for making most of the polymer at the high CEF peak temperature. Interestingly, as the 1-butene content in the copolymer is increased from 2% to 5%, the high crystallinity peak moves slightly to a lower temperature, indicating that site 4 is capable of incorporating 1-butene, even if slightly. This observation also agrees with our findings that setting $r_{B,4} = 0$ or $(AAA)_4 = 1$ did not improve the model fit. It is also apparent that one of the sites (site type 1) has a higher reactivity towards 1-butene and is responsible for making part of the polymer that remains soluble at room temperature. The other two site types, having intermediate reactivity ratios, produce most of the chains in the intermediate crystallizability region that varies from the high to the low (soluble region) CEF temperature peaks.

Appendix D.2 presents CEF results for all SBH samples.

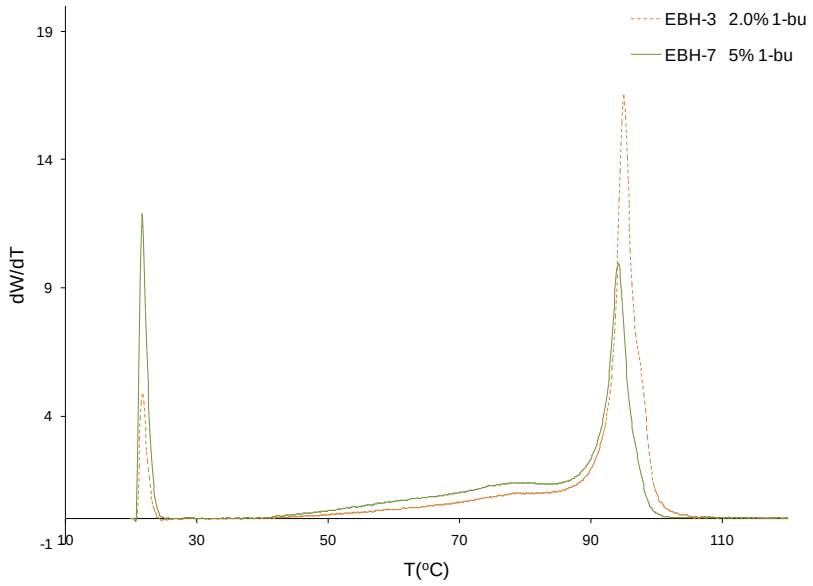

Figure 5.11 CEF analysis of poly(ethylene-*co*-1-butene), EBH-3, EBH-7.

5.5 Conclusions

In this chapter, IDEM was applied to model ethylene-*co*-1-butene samples synthesized in the presence of hydrogen. IDEM was applied to estimate: 1) the minimum number of site types required to model MWD, 2) weight fraction of copolymer made on each site type, and 3) reactivity ratios for each site type. In the standard sequential IDEM approach, the copolymer MWD are first deconvoluted into several Flory's most probable distributions to determine the number of site types and the weight fraction of copolymer made on each of them. Then, the triad (tetrad or higher n-ad) distribution of the copolymer is fitted by determining the reactivity ratios for each site type using the mass fractions estimated by MWD deconvolution.

Six case studies were explored to find the best approach for parameter estimate: 1) the standard sequential IDEM with 4 site types using either 4 or 6 triads, 2) a 4 site model with $r_{B,4} = 0$, 3) a 4 site model with $(AAA)_4 = 1$, 4) a 4 site model that also considered 3 tetrads in addition to the triads, 5) a 4 site triad deconvolution model that ignored the MWD deconvolution results, and 6) a simultaneous IDEM 4 site type model.

It was found that the sequential IDEM with 4 site types was the best choice to represent the EBH copolymer set, since it was the easiest to use and led to reactivity ratio estimated that represented reasonably well the most important triads in the copolymer.

Looking closely to all these case studies we conclude that the addition of the tetrads to the IDEM did not provide significant improvements. It is better to focus on shorter distributions and work on improving the model fit. The elimination of the 4^{th} site or forcing that site to certain value did not also provide improvement in respect with the model fit. It is better not to restrict the model capability to predict the best optimal estimates. Therefore, the four-site-type model using only four triads is the best scenario to predict the reactivity ratios.

Chapter 6
Copolymer Samples Made without Hydrogen

6.1 Introduction

In this chapter, IDEM was used to model ethylene-*co*-1-butene copolymers synthesized without hydrogen (EB). The main objectives of this study were to investigate whether IDEM could also be used to describe the comonomer sequence length distributions of polymers made in the absence of hydrogen and, more importantly, how hydrogen influences the reactivity ratios of ethylene/1-butene copolymers made with heterogeneous Ziegler-Natta catalysts. The EB samples had different 1-butene fractions and were made under steady-state polymerization conditions, as described in Chapter 4.

First, the results from the MWD deconvolution will be presented. Then, the mass fractions for polymer made on each site type, estimated from the MWD deconvolution, will be used to fit the comonomer sequence length distribution in the second step of the IDEM procedure, as explained in Chapter 3 and already applied in Chapter 5 to the EBH samples. The several case studies presented in Chapter 5 for the EBH copolymers will not be duplicated herein to avoid unnecessary repetition. Instead, only two "best" case scenarios will be discussed: a four site-type model will be used to fit 3 triads, and a four site-type model will be used to fit 3 triads and the average fraction of ethylene in the copolymer. Differently from the EBH samples, during the preliminary model fit it was found out that 3 triads led to a better description of the comonomer sequence length distribution of the EB samples than the 4 triads used in Chapter 5.

The triad deconvolution objective function is given by Equation (6.1). This equation is the same as the one used earlier in Chapter 3 and Chapter 5.

$$\phi(\underline{\theta}) = \left|\underline{Z}'\underline{Z}\right| \tag{6.1}$$

In this chapter, we also decided to fit the average ethylene fraction in the copolymer simultaneously with the triad distribution. The modified objective function for this case is given by Equation (6.2),

$$\omega = \phi(\underline{\theta}) + \left|\underline{ZF_A}'\underline{ZF_A}\right| \tag{6.2}$$

where, $ZF_A = F_{A,Obs} - F_{A,Fit}$, $F_{A,Obs}$ is the average ethylene fraction in the copolymer measured by ^{13}C NMR and $F_{A,Fit}$ is the model predicted average ethylene fraction in the copolymer.

6.2 Molecular Weight Distribution Deconvolution

The MWD of copolymers EB-1 to EB-9 were analyzed with high-temperature GPC. Their MWDs were deconvoluted using the methodology described in Chapter 3. The MWD deconvolution results for EB-1 to EB-9 are shown in Appendix C.2.

The estimates for the weight fractions of copolymer made on each site type and their molecular weight averages for copolymers EB-1 to EB-9 are presented in Table 6.1. The molecular weight averages per site type will not be used further, but the mass fractions will be applied to estimate the reactivity ratios per site type. By convention, site 1 makes polymer with the lowest molecular weight, while site 4 makes chains with the highest molecular weight, as also adopted in Chapter 5.

Table 6.1 Weight fractions of copolymer made on each site type and their respective molecular weight averages chemical compositions.

Sample	w_1	w_2	w_3	w_4	M_n	M_w	*PDI*	f_A	F_A
EB-1	0.151	0.306	0.365	0.178	117 000	712 000	6.11	0.705	0.988
EB-2	0.170	0.348	0.350	0.133	94 000	546 000	5.82	0.642	0.977
EB-3	0.202	0.343	0.321	0.134	96 000	548 000	5.71	0.614	0.974
EB-4	0.230	0.345	0.318	0.108	76 000	470 000	6.16	0.589	0.967
EB-5	0.234	0.363	0.313	0.090	77 000	436 000	5.69	0.566	0.954
EB-6	0.228	0.364	0.311	0.098	61 000	368 000	6.03	0.544	0.939
EB-7	0.197	0.356	0.320	0.128	55 000	297 000	5.43	0.506	0.927
EB-8	0.204	0.383	0.316	0.098	50 000	305 000	6.17	0.473	0.912
EB-9	0.135	0.402	0.312	0.151	30 000	173 000	5.83	0.430	0.878

6.3 Triad Distribution Deconvolution

6.3.1 Triad Data

The triad distributions for the EB copolymers were calculated from their ^{13}C NMR spectra and are shown in Tables 6.2. These distributions were calculated according to Equations (2.7) to (2.18), following the procedure outlined in Chapter 2. The ^{13}C NMR spectra for the nine samples, EB-1 to EB-9, are shown in Appendix D.3.

Table 6.2 Triad distribution for the EB copolymers.

Sample	f_A	F_A	BBB	BBA	ABA	BAB	AAB	AAA
EB-1	0.705	0.988	0.16	0.05	1.02	0.04	1.85	96.88
EB-2	0.642	0.977	0.43	0.07	1.11	0.27	4.43	93.70
EB-3	0.614	0.974	0.88	0.05	1.13	0.24	4.13	93.57
EB-4	0.589	0.967	1.13	0.72	1.59	0.27	2.87	93.41
EB-5	0.566	0.954	1.41	0.71	2.54	0.55	4.38	90.42
EB-6	0.544	0.939	2.06	0.95	2.68	0.52	6.94	86.85
EB-7	0.506	0.927	2.48	1.56	3.85	0.74	5.29	86.08
EB-8	0.473	0.912	2.35	1.72	5.24	1.10	7.98	81.61
EB-9	0.430	0.878	2.76	3.54	6.63	1.87	10.04	75.16

6.3.2 Model Fit Using 4 Site Types

The MWD deconvolution study indicates that four site types are required to describe the MWDs of the nine samples under investigation. Similarly to the procedure followed in Chapter 5, it was assumed that each site type is characterized not only for making polymer with varying average molecular weights but also with different chemical compositions due to their distinct reactivity ratios. The estimates of the copolymer weight fractions made on each site type obtained by MWD deconvolution were used during the triad deconvolution as input variables.

Table 6.3 compares the reactivity ratio estimates using two approaches. In the first, the same procedure adopted for case study 1 in Chapter 5 was followed, with the exception that only triads ABA, AAB and AAA were used to fit the data, as they produced the best possible fit. Avoiding the weak fractions

improved the model fit (in Chapter 5, triad BBA was also used during parameter estimation). In the seconds, the average copolymer composition was also added to the objective function was an attempt to improve data fitting.

The reactivity ratios for 1-butene (r_B) decrease from site 1 to 4, while the molecular weight averages increase from site 1 to 4 (see Appendix C.2 for all resins). This is in agreement with the MWD deconvolution results (site 1 makes polymer with the lowest, and site 4 with the highest, molecular weight).

Table 6.3 Reactivity ratio estimates using only triads and triads with average copolymer composition (F_A).

	3 triads			**3 triads+F_A**		
Site-type	r_A	r_B	$r_A \times r_B$	r_A	r_B	$r_A \times r_B$
1	17.9995	0.9517	17.13	18.6904	0.9096	17.00
2	19.9996	0.894	17.88	18.3441	0.8919	16.36
3	27.5316	0.8313	22.89	28.9567	0.8430	24.41
4	32.7702	0.4066	13.32	25.1834	0.5324	13.41
	$\phi(\underline{\theta})$ = 0.032			ω =0.0290		

r_A – ethylene reactivity ratio; r_B – 1-butene reactivity ratio.

Figure 6.1 compares the absolute average percentage deviations for the triad distribution of all samples using only the 3 triads and the 3 triads and F_A. As mentioned above, only the ABA, AAB and AAA triads were used during parameter estimation, while the deviations for the other triads were calculated from the reactivity ratio estimates. The absolute averages percentage deviations for BBA were very high about 800% and are not shown in Figure 6.1 to permit a more clear comparison for the other 5 triads. This explains the need to use 3 triads instead of 4 triads. The large average percentage deviations observed for the BBA triads is due their very small frequencies (near zero) for the first three copolymer samples, as can be observed in the triad distribution results shown in Appendix E.2. Notice that when only the triads were considered, a slight improvement on the data fit with respect to the ABA, AAB and AAA triads was observed but, in general, the absolute average percentage deviations for the triads for both case studies are very similar. As expected, when the copolymer composition is used with the triads, the F_A fit is slightly improved, as shown in Figure 6.2. Since the precise knowledge of the

average copolymer composition is generally desirable when modeling a copolymer microstructure, and considering that the inclusion of F_A during parameter estimation is not complex or costly from a computational time point of view, neither does it influence the prediction of the triad distribution significantly, the use of the four site-model with 3 triads and average copolymer composition seems to be the best approach for this set of copolymers.

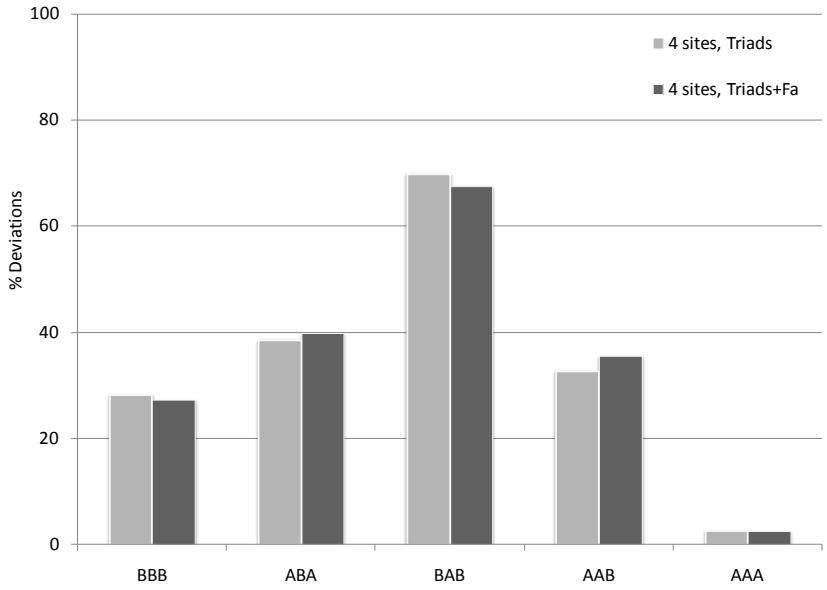

Figure 6.1 Comparison of the absolute average percentage deviations for the triad distribution when triads and triads with average copolymer composition were used during parameter estimation.

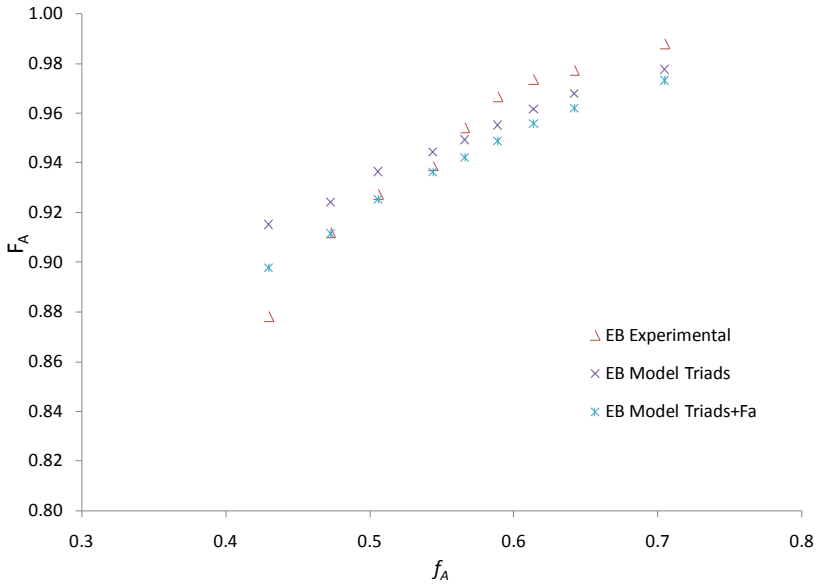

Figure 6.2 Average fraction of ethylene in copolymer (F_A) as a function of molar fraction of ethylene in the polymerization reactor (f_A) for the EB samples.

Tables with the absolute percentage deviations for the triad distribution of all EB samples are shown in Appendix E.2.

6.4 Comparison of EB and EBH Copolymers

When the reactivity ratio estimates for the EB copolymers (using 3 triads and F_A) are compared with those for the EBH results (4 triads) it becomes clear that hydrogen increases the reactivity ratios for ethylene (r_A) in all site types, while decreasing the reactivity ratios for 1-butene (r_B), as shown in Table 6.4. As a consequence, the EB samples have a higher average 1-butene fraction than the EBH samples, when made at the same ethylene/1-butene ratio in the reactor, as shown in Figure 6.3.

Table 6.4 Reactivity ratio estimates using for the EB and EBH samples using triads.

	EB			EBH		
Site-type	r_A	r_B	$r_A \times r_B$	r_A	r_B	$r_A \times r_B$
1	18.6904	0.9096	17.00	28.3916	0.0964	2.74
2	18.3441	0.8919	16.36	49.6352	0.0758	3.76
3	28.9567	0.8430	24.41	79.5149	0.0353	2.81
4	25.1834	0.5324	13.41	116.3613	0.0069	0.80

It is observed form Table 6.4 that the reactivity ratios of the high molecular weight sites seem to be more affected by hydrogen addition than those of the lower molecular weight sites. To our knowledge this is first time this phenomenon is observed. It seems that the sites that incorporate less comonomer (high molecular weight sites) are more affected by the presence of hydrogen than the lower molecular weight sites. Perhaps, they "slow down" after 1-butene insertion, enhancing the chance of transfer to hydrogen.

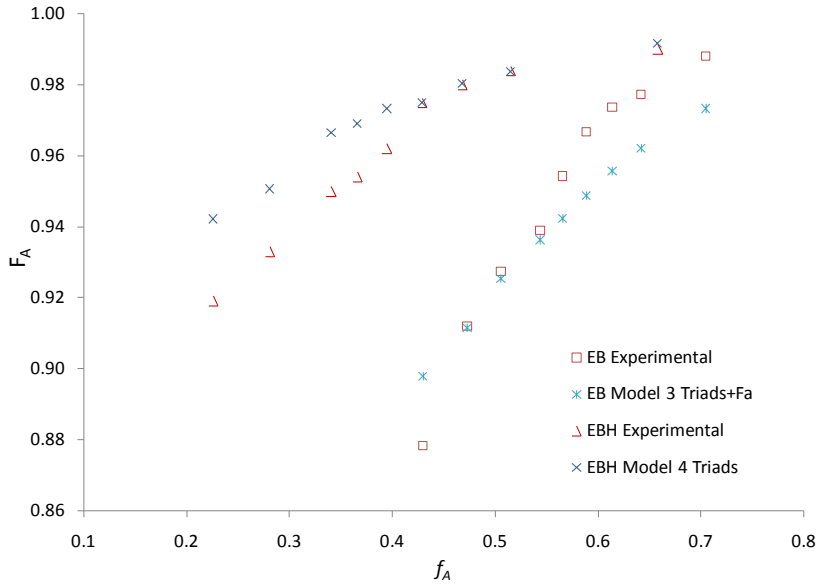

Figure 6.3 Average fraction of ethylene in copolymer (F_A) as a function of molar fraction of ethylene in the polymerization reactor (f_A) for the EB and EBH samples.

6.5 Conclusions

The case studies were discussed to explore the polymerization system using 4 site model. It was illustrated in this chapter that the IDEM works for the samples made without hydrogen.

For the data presented in this chapter, the IDEM provided a better fit when the objective function was modified to include the average fraction of the ethylene in the copolymer. Therefore, using 3 triads with the copolymer composition was the best choice to represent the polymerization system since it provided a satisfactory objective function values and acceptable triad fit.

Also, the IDEM showed its capability to predict the effect of hydrogen presence in the polymerization system. This was demonstrated by the new parameter estimate values for the EB samples.

Chapter 7
Effect of Interlaboratory ^{13}C NMR Analysis on IDEM Performance

7.1 Introduction

As discussed in the previous chapters, ^{13}C NMR spectroscopy is used to measure the triad distributions that are required in the second parameter estimation step with IDEM. Since quantifying the triad distribution by ^{13}C NMR is a crucial step in our estimation methodology, it is important to find out how interlaboratory differences in this technique would affect parameter estimation and model predictions. Therefore, the triad distributions for the EB and EBH samples were graciously reanalyzed at the Dow Chemical Research Center at Freeport, Texas, using a high temperature cryoprobe that has been reported to dramatically increase ^{13}C NMR sensitivity for polyolefins analysis. The newly developed high temperature 10 mm cryoprobes increases the signal-to-noise ratio to values that are 3 to 4 times higher than that of conventional probes, such as the one used at the University of Waterloo. The efficiency of the NMR probe is increased by cooling the radio frequency (RF) coil with cryogenic liquids or gases, leading to a reduction in the RF coil resistance and improving the probe performance (Zhou et al., 2009).

This chapter discusses IDEM estimations using Dow ^{13}C NMR data and compares these results with those obtained using the NMR spectrometer available in the Department of Chemistry at the University of Waterloo.

7.2 Copolymer Samples Made with Hydrogen

7.2.1 Triad Data

The triad distributions for the EBH samples analyzed by Dow Chemical are shown in Table 7.1. The results are close to the ones reported in Chapter 5, but some triads differ more than others. Figure 7.1 shows the triad distributions for the EBH samples analyzed by Dow Chemical and at the University of Waterloo (UW) as a function of the monomer molar fraction into the reactor. Even though the results obtained in both laboratories follow the same trends, Dow's measurements for the BBB triads are consistently lower, a result that is also repeated for other 1-butene-rich triads.

Table 7.1 Triad distribution for the EBH copolymer samples analyzed at Dow Chemical.

Sample	f_A	F_A	BBB	BBA	ABA	BAB	AAB	AAA
EBH-1	0.658	0.989	0.00	0.20	0.90	0.00	1.90	97.00
EBH-2	0.515	0.981	0.00	0.20	1.60	0.10	3.30	94.70
EBH-3	0.468	0.976	0.00	0.30	2.10	0.10	4.30	93.30
EBH-4	0.429	0.972	0.20	0.50	2.10	0.00	4.70	92.50
EBH-5	0.395	0.956	0.00	0.90	3.50	0.60	6.60	88.40
EBH-6	0.366	0.951	0.00	1.00	3.90	0.80	7.20	87.20
EBH-7	0.341	0.946	0.00	1.20	4.20	0.90	7.70	86.10
EBH-8	0.281	0.943	0.20	1.00	4.50	0.70	8.60	85.00
EBH-9	0.226	0.915	0.00	2.10	6.40	1.70	11.50	78.30

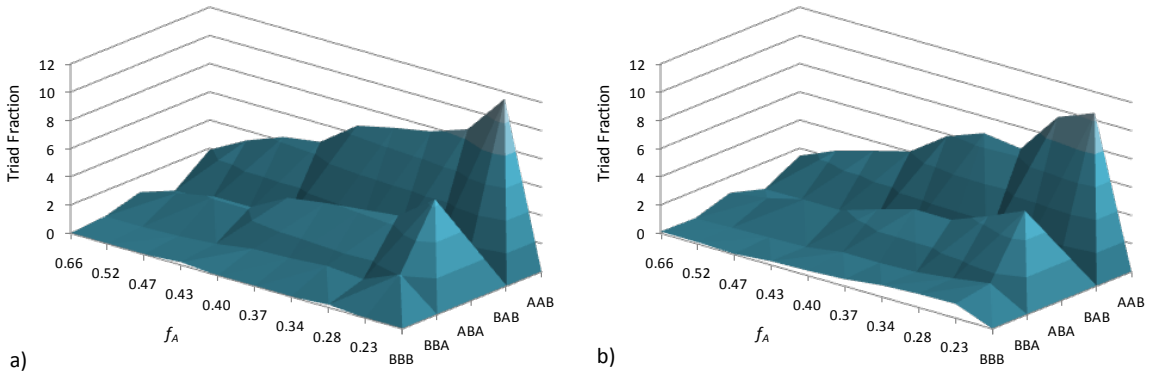

Figure 7.1 Triad Distribution as a function of monomer molar feed fraction in the polymerization reactor for the EBH samples: a): Dow Chemical results, b) University of Waterloo results.

Table 7.2 shows the percentage deviations between the UW and Dow triad data, using the UW data as the reference values, according to Equation 7.1.

$$\%\ Deviations\ UW\ \&\ Dow = \frac{(UW\ Triad - Dow\ Triad)}{UW\ Triad} \times 100 \qquad (7.1)$$

The highest deviations are observed for the weaker triads, which correspond to the 1-butene-rich sequences BBB, BBA and BAB. Assuming that the cryoprobe used at Dow does indeed increase ^{13}C

NMR sensitivity, it may be assumed that the measurements done at UW overestimated the fraction 1-butene-rich triads, perhaps by overestimating the area of noisy small ^{13}C NMR peaks assigned to these triads. The consequence of these differences on the reactivity ratio estimates will be discussed below.

Table 7.2 Percentage deviations between the triad fractions measured at the University of Waterloo and Dow Chemical.

Sample	ΔBBB%	ΔBBA%	ΔABA%	ΔBAB%	ΔAAB%	ΔAAA%
EBH-1	100.00	-233.33	-5.88	100.00	-29.25	0.40
EBH-2	100.00	-42.86	-31.15	33.33	-27.91	1.14
EBH-3	100.00	-42.86	-11.70	-25.00	-29.52	1.25
EBH-4	25.93	-78.57	-12.30	100.00	-16.63	1.00
EBH-5	100.00	-36.36	-30.11	-106.90	-12.63	1.93
EBH-6	100.00	-53.85	-13.04	-60.00	-5.57	1.00
EBH-7	100.00	-60.00	-22.09	-47.54	-18.83	2.05
EBH-8	79.17	5.66	-0.90	2.78	9.09	-1.99
EBH-9	100.00	-43.84	-14.49	-50.44	-9.52	2.50

7.2.2 Model Fit Using Dow Triad Distributions

Table 7.3 shows IDEM reactivity ratios estimated using 6 or 4 triads reported by Dow in Table 7.1, with the weight fractions presented in Table 5.3. Similarly to the results shown in Section 5.3.2, the reactivity ratios for 1-butene (r_B) decrease from site type 1 to 4, in agreement with the trends commonly observed with heterogeneous Ziegler-Natta ethylene/α-olefin copolymers, as the α-olefin comonomer fraction decreases with increasing molecular weight.

Table 7.3 Reactivity ratio estimates using 6 and 4 triads with Dow Chemical ^{13}C NMR data.

	6 triads			4 triads		
Site-type	r_A	r_B	$r_A \times r_B$	r_A	r_B	$r_A \times r_B$
1	16.0903	0.1013	1.63	28.7474	0.1500	4.31
2	48.4934	0.0628	3.05	38.0227	0.0551	2.10
3	76.3814	0.0193	1.47	78.1060	0.0397	3.10
4	118.4638	0.0021	0.24	118.9036	0.0054	0.64
$\phi(\underline{\theta})$	2.28×10^{-4}			0.7481		

r_A – ethylene reactivity ratio; r_B – 1-butene reactivity ratio.

Figure 7.2 shows the average percentage absolute deviations for the EBH samples using 6 and 4 triads (BBB and BAB excluded). The percentage absolute deviations tables for each sample are shown in Appendix F. As observed before for the UW results, using only 4 triads led to a better triad distribution prediction than using all the 6 triads, as discussed before in Chapter 5.

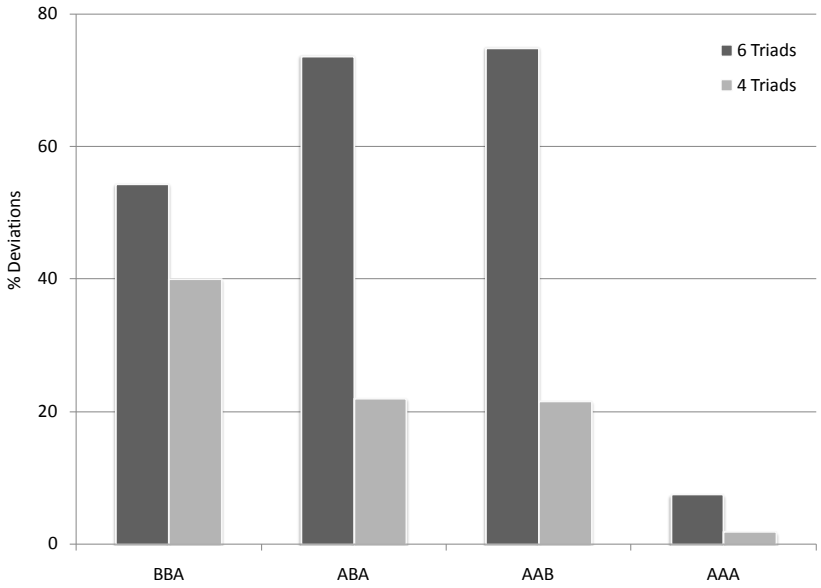

Figure 7.2 Comparison of the absolute average percentage deviations for the Dow Chemical triad distribution when 4 or 6 triads were used during parameter estimation.

Figure 7.3 shows the model predictions for the average ethylene fraction in the copolymer, F_A. As for the triad distribution, a better fit is obtained when only 4 triads are used to estimate the reactivity ratios.

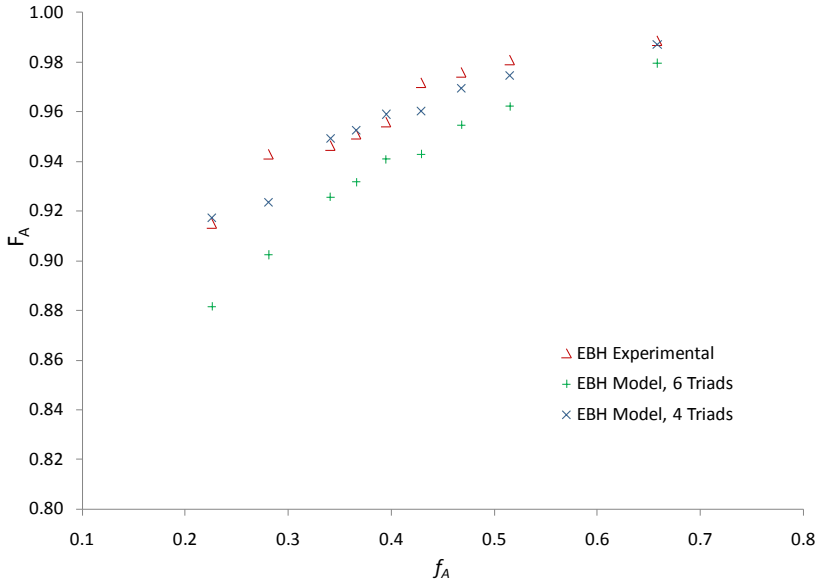

Figure 7.3 Average ethylene fraction in the copolymer (F_A) as a function of molar fraction of ethylene in the polymerization reactor (f_A) for the EBH samples, using 6 or 4 triads measured by Dow Chemical.

7.2.3 Interlaboratory Comparison: EBH Copolymers

The reactivity ratios estimated by IDEM using the triad distributions measured by ^{13}C NMR analysis at Dow Chemical or UW are compared in Table 7.4. The agreement between the two laboratories is surprisingly good, especially considering that no effort was made to standardize data collection and analysis procedures. This indicates that IDEM is a robust parameter estimation method for the reactivity ratios of the different site types present on heterogeneous Ziegler-Natta catalysts.

Table 7.4 Reactivity ratio estimates using Dow Chemical and UW triad distributions.

EBH	Dow			UW		
Site-type	r_A	r_B	$r_A \times r_B$	r_A	r_B	$r_A \times r_B$
1	28.7474	0.1500	4.31	28.3916	0.0964	2.74
2	38.0227	0.0551	2.10	49.6352	0.0758	3.76
3	78.1060	0.0397	3.10	79.5149	0.0353	2.81
4	118.9036	0.0054	0.64	116.3613	0.0069	0.80

Figure 7.4 shows that the average ethylene fraction in the copolymer can be better represented using the reactivity ratio estimates from Dow Chemical triad distributions. Notice that the measured average fractions of ethylene in the copolymer from both laboratories are close.

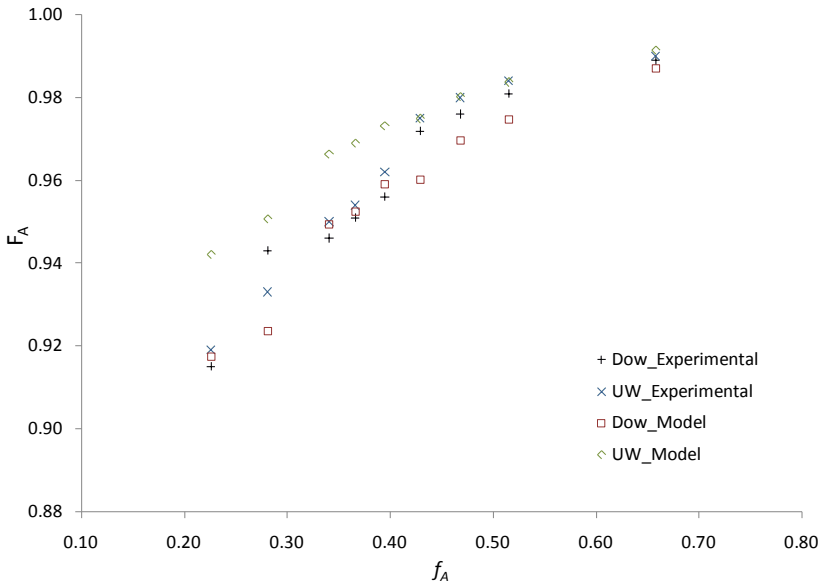

Figure 7.4 Average fraction of ethylene in copolymer (F_A) as a function of molar fraction of ethylene in the polymerization reactor (f_A) for the EBH samples using Dow Chemical and UW triad data.

7.3 Copolymer Samples Made without Hydrogen

7.3.1 Triad Data

In this section we apply the IDEM to model the ethylene-*co*-1-butene copolymers synthesized without hydrogen (EB) and described in Chapter 6. The triad distribution data for the EB samples measured at Dow Chemical is shown in Table 7.5 and Figure 7.5 compares these results with the ones measured at the University of Waterloo. As noticed for the EBH samples, Dow's results systematically underpredict the 1-butene-rich triad fractions (or UW's results systematically overpredict them), likely for the same reasons already presented above for the EBH samples.

Table 7.5 Triad distribution for the EB copolymer samples.

Sample	f_A	F_A	BBB	BBA	ABA	BAB	AAB	AAA
EB-1	0.705	0.985	0.00	0.20	1.20	0.00	2.60	95.90
EB-2	0.642	0.980	0.10	0.30	1.60	0.00	3.40	94.70
EB-3	0.614	0.978	0.00	0.20	1.90	0.00	4.00	93.80
EB-4	0.589	0.977	0.00	0.40	1.90	0.10	4.00	93.60
EB-5	0.566	0.962	0.20	0.60	2.90	0.00	6.30	89.90
EB-6	0.544	0.945	0.00	1.00	4.50	0.80	8.50	85.20
EB-7	0.506	0.936	0.00	1.50	4.90	1.00	9.50	83.20
EB-8	0.473	0.919	0.00	1.80	6.30	1.60	11.20	79.20
EB-9	0.430	0.889	0.00	2.90	8.10	2.50	14.20	72.30

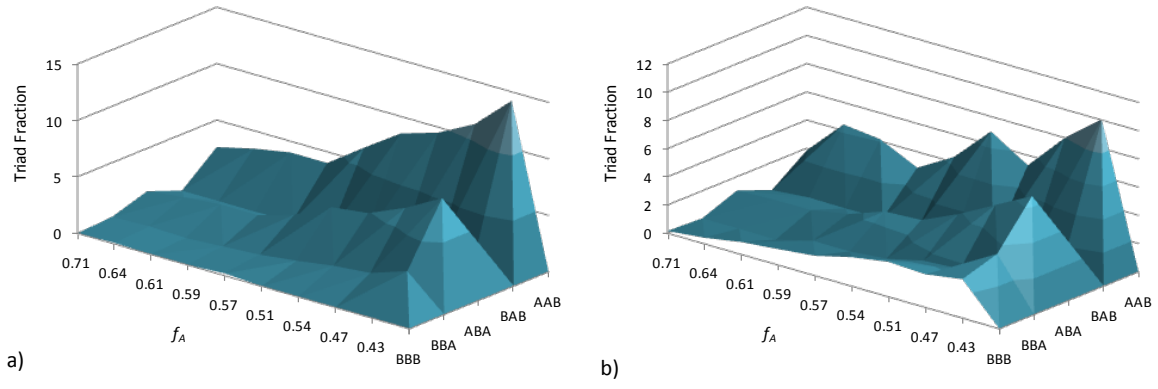

Figure 7.5 Triad Distribution as a function of monomer molar feed fraction in the polymerization reactor for the EB samples: a): Dow Chemical results, b) University of Waterloo results.

The triad distributions deviations between the triads measured at UW and Dow are shown in Table 7.6. Similarly to the EBH samples, most of the differences are found in for BBB, BBA and BAB triads, which correspond to the less intense peaks in the ^{13}C NMR spectra and are more likely to be influenced by changes in signal-to-noise ratio.

Table 7.6 Percentage differences between the triad fractions measured at the University of Waterloo and Dow Chemical.

Sample	ΔBBB%	ΔBBA%	ΔABA%	ΔBAB%	ΔAAB%	ΔAAA%
EB-1	100.00	-300.00	-17.65	100.00	-40.54	1.01
EB-2	76.74	-328.57	-44.14	100.00	23.25	-1.07
EB-3	100.00	-300.00	-68.14	100.00	3.15	-0.25
EB-4	100.00	44.44	-19.50	62.96	-39.37	-0.20
EB-5	85.82	15.49	-14.17	100.00	-43.84	0.58
EB-6	100.00	-5.26	-67.91	-53.85	-22.48	1.90
EB-7	100.00	3.85	-27.27	-35.14	-79.58	3.35
EB-8	100.00	-4.65	-20.23	-45.45	-40.35	2.95
EB-9	100.00	18.08	-22.17	-33.69	-41.43	3.81

7.3.2 Model Fit Using Dow Triad Distributions

To estimate the reactivity ratios for the four site type model, the weight fractions of copolymer made on each site type shown in Table 6.1 were used with the triad distributions measured by Dow Chemical (Table 7.5). The reactivity ratio estimates using 6, or 4 (BBB and BAB excluded) or 3 triads (BBB, BBA and BAB excluded) are shown in Table 7.7. The decision to present the 3 triads scenario was due to the fact it produced lower triad deviations as will be shown in this section. This BBB, BBA and BAB are the weakest triads. Therefore they have the highest associated errors.

Table 7.7 Reactivity ratio estimates using 6, 4 or 3 triads measured by Dow Chemical.

	6 triads			4 triads			3 triads		
Site-type	r_A	r_B	$r_A \times r_B$	r_A	r_B	$r_A \times r_B$	r_A	r_B	$r_A \times r_B$
1	17.9521	0.8113	14.56	18.0000	0.9991	17.98	17.9055	0.9911	17.75
2	19.8858	0.0407	0.81	14.4729	0.0230	0.33	19.6129	0.0224	0.44
3	28.8787	0.0092	0.27	25.5572	0.0048	0.12	27.9960	0.0128	0.36
4	32.9482	0.0026	0.09	23.3362	0.0028	0.07	31.8641	0.0012	0.04
$\phi(\underline{\theta})$	9.96×10^{-4}			0.0092			0.0045		

r_A – ethylene reactivity ratio; r_B – 1-butene reactivity ratio.

Figure 7.6 shows the average percentage absolute deviations for the EB samples using 6, 4 or 3 triads. Lower average percentage deviations are observed when using the 3 triads. This is due to eliminating the weaker triad distributions which inherently carries higher associated errors. Tables with the absolute percentage deviations for all EB samples can be found in Appendix F.

Looking at the model fit for the average ethylene fraction in the copolymer, F_A we notice that using the 3 triads provide acceptable fit as shown in Figure 7.7. The 3 triad scenario provides the lowest triad deviations and acceptable fit for the average ethylene fraction in the copolymer. Hence we suggest the use of the four-site-type model with 3 triads.

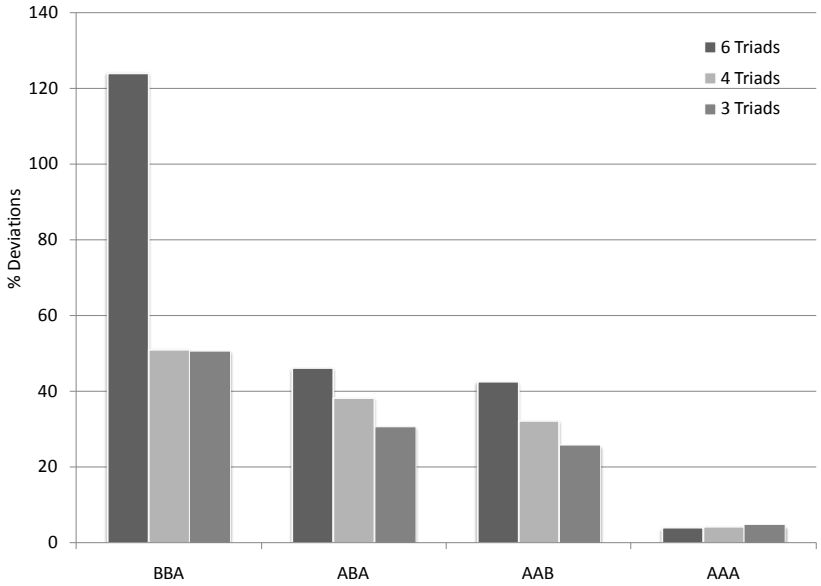

Figure 7.6 Comparison of the absolute average percentage deviations for the triad distribution when 3, 4 or 6 triads were used during parameter estimation using Dow Chemical ^{13}C NMR data**.**

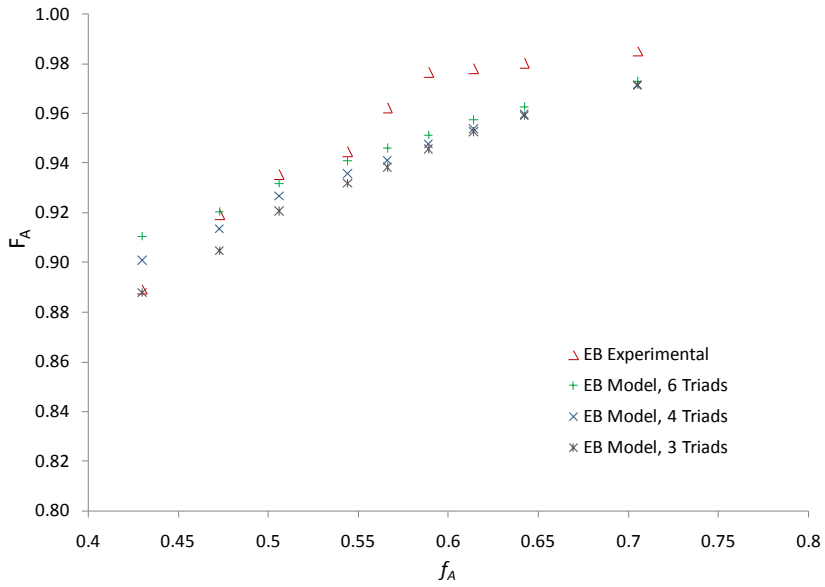

Figure 7.7 Average ethylene fraction in the copolymer (F_A) as a function of molar fraction of ethylene in the polymerization reactor (f_A) for the EB samples measured at Dow Chemical.

7.3.3 Interlaboratory Comparison: EB Copolymers

Table 7.8 compares the reactivity ratios estimated using UW and Dow ^{13}C NMR analysis when only 3 triads were included (excluding BBB, BBA and BAB). As observed for the EBH samples, the agreement between the two sets of estimates is acceptable, particularly keeping in mind that no effort was made towards achieving standard ^{13}C NMR procedures. In fact, the main objective of this comparison was to find out whether the triad data measured with two different NMR instruments, operated at different conditions in distinct laboratories would still lead to comparable IDEM reactivity ratio estimates. Table 7.8 shows that these estimates are close, with the major differences being observed for the r_B values, which is not surprising considering that Dow Chemical systematically measured lower fractions for the 1-butene-rich triads.

Table 7.8 Reactivity ratio estimates using Dow Chemical and UW triad distributions.

EB	**Dow**			**UW**		
Site-type	r_A	r_B	$r_A \times r_B$	r_A	r_B	$r_A \times r_B$
1	17.9055	0.9911	17.75	18.6904	0.9096	17.00
2	19.6129	0.0224	0.44	18.3441	0.8919	16.36
3	27.9960	0.0128	0.36	28.9567	0.8430	24.41
4	31.8641	0.0012	0.04	25.1834	0.5324	13.41

Figure 7.8 compares the average ethylene fraction in the copolymer as a function of the molar fraction of ethylene in the reactor using UW's and Dow's data. After analysing the triad data and studying the model fit and parameter estimates, we suggest that Dow Chemical Research Center ^{13}C NMR and the University of Water analysis are more equivalent as any of them did not produce perfect fit.

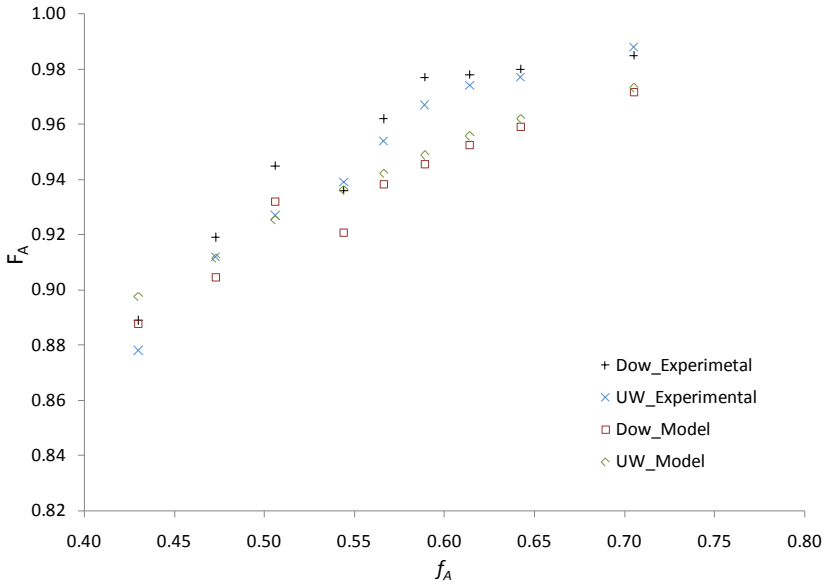

Figure 7.8 Average fraction of ethylene in the copolymer (F_A) as a function of molar fraction of ethylene in the polymerization reactor (f_A) for the EB samples using Dow Chemical and UW triad data**.**

7.4 Conclusions

In this chapter IDEM was applied to estimate the reactivity ratios of the EBH and EB samples studied in Chapters 5 and 6 using triad distributions measured by Dow Chemical to find out how robust the parameter estimation was when ^{13}C NMR data from different laboratories were used. No attempt was made to standardize data acquisition or analysis between the UW and Dow laboratories.

The triad distributions measured at Dow systematically underpredicted the fractions of the 1-butene-rich triads (BBB, BAB, BBA) in the EB and EBH copolymers or, alternatively, the UW results systematically overpredicted these triad fractions. Dow's use of a cryoprobe has been claimed to enhance ^{13}C NMR resolution and this may, explain in part some of the observed differences. It may be that the lower signal-to-noise ratio obtained in the UW measurement led us to overpredict the areas under the weaker peaks corresponding to the 1-butene-rich triads.

Despite of these differences, the values estimated for r_A and r_B for each site type are reasonably close, especially the values for r_A, as expected, since the measures for the ethylene-rich-triads from both UW

and Dow were much closer than those for the 1-butene-rich triads. The agreement is, in fact, very good, considering that no attempt was made to standardize the operation conditions of both laboratories.

Chapter 8
A Hierarchical Design of Replicates

8.1 Background and Problem Definition

The analytical data from high temperature gel permeation chromatography (GPC) or carbon 13 nuclear magnetic resonance (^{13}C NMR) are subject to variability. The variability in the measurements such as the weight-average molecular weight or the triad and tetrad distributions exists from several sources of errors, including non-uniform conditions in the polymerization reactor, experimental, and instrumental errors. Typically, the errors quoted by researchers come from instrument operating manuals which likely neglect all other sources of error.

We tried to quantify the sources and magnitudes of errors in the data discussed in this thesis through a series of replicate polymerization experiments and polymer analyses using a nested or hierarchical measurement design (Manson et al., 2003; D'Agnillo et al., 1999; Dube and Penlidis, 1996).

In our methodology, we used a 4 × 2 × 3 hierarchical experiment design in which ethylene and 1-butene copolymerizations were performed four times under identical conditions, and two polymer samples were drawn at the end of each polymerization. These eight samples were analyzed by GPC and ^{13}C NMR three times, totalizing 48 GPC and ^{13}C NMR analyses. Figure 8.1 illustrates the hierarchical design followed in this investigation

Figure 8.1 A 4 × 2 × 3 hierarchical design of poly(ethylene-*co*-1-butene) replicate samples, P: Polymerization batch, S: Samples of each batch, T: Tests of the copolymer samples.

The lowest level of the experimental design is for the test (T), or analytical error, represented by the variance σ_t^2. The second level yields sampling (S) error, between the copolymer samples drawn from

the same polymerization, represented by the variance σ_s^2. The highest level of the experiment allows us to determine σ_s^2 , the variance between different polymerizations (P) conducted under same conditions.

Next we describe the analysis of a general P × S × T hierarchical design. In our study we have the polymerizations P = 4 carried under identical conditions, S = 2 samples of each of the copolymers produced from same batch, and T = 3 test analyses performed on each sample.
Each of the measurement can be represented by the following model,

$$y_{pst} = \mu + a_p + b_{s(p)} + c_{t(ps)} \tag{8.1}$$

where p = 1,.., P; s = 1,.., S; t = 1,.., T. In Equation (8.1), $b_{s(p)}$ means the s^{th} level of factor B is nested within the p^{th} level of factor A.

All the terms in the model are random effects, meaning that:

$a_p : N(0, \sigma_p^2)$; between polymerization error.

$b_{s(p)} : N(0, \sigma_s^2)$; sampling error.

$c_{t(ps)} : N(0, \sigma_t^2)$; analytical error.

The total variability is decomposed into the parts assignable to the various sources by calculating a sum of squares for each level of nesting. Each nested sum of squares is calculated as a sum of squared differences between the average response for a factor-level combination and the average of responses at the previous levels of nesting (Box et al., 2005; Montgomery, 2001), as given by the expressions,

$$SS_A = ST \sum_{p=1}^{P} (\bar{y}_{p..} - \bar{y}_{...})^2 = \frac{1}{ST} \sum_{p=1}^{P} y_{p..}^2 - SS_M ; \; y_{p..} = \sum_s \sum_t y_{pst} \tag{8.2}$$

$$SS_M = \frac{1}{PST} \left(\sum_p \sum_s \sum_t y_{pst} \right)^2 \tag{8.3}$$

$$SS_{B(A)} = T\sum_{p=1}^{P}\sum_{s=1}^{S}(\bar{y}_{ps.} - \bar{y}_{p..})^2 = \frac{1}{T}\sum_{p}\sum_{s} y_{ps.}^2 - \frac{1}{ST}\sum_{p} y_{p..}^2;\ y_{ps.} = \sum_{t} y_{pst} \tag{8.4}$$

$$Total\ SS = \sum_{p}\sum_{s}\sum_{t}(y_{pst} - \bar{y}_{...})^2 = \sum_{p}\sum_{s}\sum_{t} y_{pst}^2 - SS_M \tag{8.5}$$

$$SS_{C(AB)} = Total\ SS - SS_A - SS_{B(A)} \tag{8.6}$$

Table 8.1 shows the degrees of freedom (df), calculated sum of squares (SS), mean squares (MS), and the expected values of mean squares (E(MS)), assembled into an analysis of variance (ANOVA) table.

Table 8.1 Sums of squares assembled into ANOVA table.

Source of variation	df	SS	MS	E(MS)
Factor A	$P-1$	SS_A	$SS_A/(P-1)$	$\sigma_t^2 + T\sigma_s^2 + ST\sigma_p^2$
Factor B	$P(S-1)$	$SS_{B(A)}$	$SS_{B(A)}/(P(S-1))$	$\sigma_t^2 + T\sigma_s^2$
Factor C	$PS(T-1)$	$SS_{C(AB)}$	$SS_{C(AB)}/(PS(T-1))$	σ_t^2
Total	$PST-1$	$Total\ SS$		

The last column of the E(MS) indicates which variance components or combination of variance components are being estimated by the calculated mean squares. Inspection of the E(MS) indicates that a series of sequential F-tests are approperiate for assessing the significance of the variance components.

To test the significance of the contribution to variability due to different polymerizations the following expressions are used

$$H_o : \sigma_p^2 = 0 \qquad H_1 : \sigma_p^2 > 0$$

$$F_{Observed} = \frac{MS_A}{MS_B} : f_{P-1,P(S-1),\alpha} \tag{8.7}$$

Similarly, to test the significance of the contribution to variability due to sampling,

$$H_o : \sigma_s^2 = 0 \qquad H_1 : \sigma_s^2 > 0$$

$$F_{Observed} = \frac{MS_B}{MS_C} : f_{P(S-1),PS(T-1),\alpha} \tag{8.8}$$

Estimation of the individual variance components follows the structure of the E(MS). Equations (8.9) and (8.10) shows how to estimate the variance attributed to different polymerizations (s_p^2) and sampling (s_s^2):

$$s_p^2 = \frac{MS_A - MS_B}{ST} \tag{8.9}$$

$$s_s^2 = \frac{MS_B - MS_C}{T} \tag{8.10}$$

D'Agnillo et al. presented the results from a hierarchical experiment design to analyze the molecular weight distributions of replicate ethylene polymerizations using homogeneous metallocene/methylalumoxane catalysts. Their study showed significant differences in the molecular weight of polyethylene replicate samples, as well as differences between samples from the same polymerization. The authors concluded those could be attributed to imperfect reactor mixing and batch-to-batch variations between the polymerizations (D'Agnillo et al., 1999).

8.2 Experimental Results and Data Analysis

8.2.1 Copolymer Synthesis

Poly(ethylene-*co*-1-butene) replicate samples were synthesized using a Ziegler-Natta $TiCl_4/MgCl_2$ catalyst in a 300 mL slurry stainless steel autoclave reactor, at 60 ^oC, hydrogen pressure of 14 psig, and ethylene pressure of 114 psig for 20 minutes, following the procedure detailed in Chapter 4. The molar fractions of monomer and comonomer in the reactor were f_A = 0.2 and f_B = 0.8, respectively. Those

samples were synthesized with highest possible amount of comonomer into the reactor to enhance the ^{13}C NMR peaks corresponding to the 1-butene-rich triads. Those polymerizations are difficult to reproduce since the polymer particles produced are sticky and tend to cause reactor fouling, which may lead to poor reactor temperature control.

8.2.2 Copolymer Characterization

The weight-average molecular weight (M_w) of the poly(ethylene-*co*-1-butene) copolymer samples were measured by high temperature GPC (Polymer Char), as described in Chapter 4, Triad and tetrad distributions were measured by ^{13}C NMR, following the procedure detailed in Chapter 4 and equations presented in Chapter 2. These polymer analysis results are summarized in Table 8.2.

Table 8.2 Characterization results from the GPC and ^{13}C NMR.

Poly (p)	Sample (s)	Test (t)	M_w	BBB	ABB	ABA	BAB	BAA	AAA	ABBA	ABAA	BAAB
A	1	1	76 563	2.40	2.66	7.14	2.05	14.82	70.93	1.03	12.62	2.03
		2	72 367	3.38	2.70	6.65	2.12	13.45	71.70	1.03	12.36	1.92
		3	69 962	2.85	2.61	6.68	2.01	14.41	71.44	1.08	12.71	2.15
	2	1	75 982	2.10	2.26	6.62	1.86	13.17	74.00	0.84	11.44	1.64
		2	70 371	1.03	2.42	8.43	2.18	14.58	71.37	1.07	12.57	1.50
		3	96 509	2.24	2.36	6.73	1.81	13.68	73.19	0.96	11.45	1.67
B	1	1	63 726	2.86	2.23	5.75	1.54	12.84	74.77	0.80	11.28	1.93
		2	90 295	2.48	2.12	6.30	1.57	12.74	74.78	0.82	11.38	2.12
		3	86 574	2.17	2.16	6.41	1.58	13.41	74.27	0.75	11.72	1.80
	2	1	91 826	2.33	2.03	6.22	1.50	13.01	74.91	0.71	10.95	2.19
		2	93 044	3.79	2.13	5.27	1.33	12.37	75.11	0.82	10.40	2.44
		3	89 189	3.10	2.14	5.14	1.26	13.05	75.32	0.76	9.95	1.87
C	1	1	67 975	1.12	2.08	7.53	1.63	15.00	72.64	0.82	12.31	1.84
		2	72 456	0.98	2.23	8.28	2.09	14.18	72.25	0.76	12.55	1.69
		3	73 836	1.42	2.54	7.90	1.96	15.38	70.81	0.83	12.11	1.68
	2	1	68 909	2.17	2.63	7.72	2.03	14.34	71.11	1.15	12.63	1.94
		2	82 919	1.25	2.60	8.51	2.08	15.18	70.38	1.01	12.94	2.09
		3	70 267	3.08	2.87	6.49	1.97	14.38	71.20	0.98	12.55	2.44
D	1	1	74 273	1.69	2.65	8.57	2.41	14.28	70.40	1.05	12.51	2.15
		2	80 941	2.89	2.83	6.45	1.89	14.41	71.54	0.96	12.05	1.94
		3	84 822	3.45	2.66	5.97	1.71	14.67	71.53	1.15	11.72	2.11
	2	1	83 343	1.40	3.15	8.51	2.33	16.34	68.27	1.12	13.26	2.31
		2	87 699	1.21	2.97	9.32	2.38	16.17	67.96	1.18	13.94	2.08
		3	88 517	1.16	3.33	8.75	2.52	16.35	67.90	1.28	13.52	1.95

8.2.3 Hierarchical Design Results

The weight-average molecular weight (M_w) is the measured value for the GPC. The calculations of the 4 × 2 × 3 hierarchical design for M_w are included in Appendix G.1. Based on the data shown in Table 8.2 for M_w, the ANOVA results shown in Table 8.3 was prepared.

Table 8.3 ANOVA table for the weight-average molecular weight.

Source	SS	df	MS	F_{obs}	Variance Estimate (s_i^2)
Poly, P	634 580 332	3	211 526 777	2.376	20 415 398
Sample, S	356 137 552	4	89 034 388	1.379	8 151 469
Test, T	1 033 279 711	16	64 579 982		64 579 982
Total	2 023 997 595	23			

The observed F-value of 2.376, which tests the significance of the variability due to different polymerizations, is compared with the F-distribution having 3 and 4 degrees of freedom (F-value of 6.590 for P-value of 0.05). The comparison indicates that we accept the null hypothesis and suggests that there are no differences in the M_w values among different polymerization runs. There is only a 5% chance that the ratio could be 2.376 or higher. Similarly, there are no significant differences between sample to sample within the same polymerization run, as the F-value for 4 and 16 degrees of freedom is 3.010 for P-value of 0.05.

Table 8.4 shows the ANOVA table for the BBB calculated from the ^{13}C NMR spectra. By comparing the F-observed value with the F-distribution, we suggest that there is no significant difference between polymerizations, but a significant difference between sample to sample. This might be the result of having non homogeneous sample or due to some fluctuation in reactor conditions.

Table 8.4 ANOVA table for the BBB sequence.

Source	SS	df	MS	F_{obs}	Variance Estimate (s_i^2)
Poly, P	4.184	3	1.395	0.824	0.0000
Sample, S	6.774	4	1.694	4.461	0.4380
Test, T	6.074	16	0.380		0.3796
Total	17.033	23			

Table 8.5 shows the ANOVA table for ABB. By looking at the F-observed values we can say that there is no significant difference between polymerization and there is significant variability from sample to sample.

Table 8.5 ANOVA table for the ABB sequence.

Source	SS	df	MS	F_{obs}	Variance Estimate (s_i^2)
Poly, P	1.909	3	0.636	3.623	0.0768
Sample, S	0.703	4	0.176	10.423	0.0529
Test, T	0.270	16	0.017		0.0169
Total	2.882	23			

ABA results shown in Table 8.6 suggest that there are no significant differences between polymerizations. The F-value for sample is not sufficient to evaluate the differences. Therefore, we observe the P-value for sample to sample (0.078) and conclude that sample to sample variability exists, rejecting the null hypothesis.

Table 8.6 ANOVA table for the ABA sequence.

Source	SS	df	MS	F_{obs}	Variance Estimate (s_i^2)
Poly, P	15.920	3	5.307	3.411	0.6252
Sample, S	6.223	4	1.556	2.571	0.3169
Test, T	9.680	16	0.605		0.6050
Total	31.824	23			

Table 8.7 for the BAB shows there are significant polymerization to polymerization variation. The P-value for the sample is 0.067 which leads to conclude that there is significant variability between sample to sample.

Table 8.7 ANOVA table for the BAB sequence.

Source	SS	df	MS	F_{obs}	Variance Estimate (s_i^2)
Poly, P	1.785	3	0.595	6.786	0.0846
Sample, S	0.351	4	0.088	2.725	0.0185
Test, T	0.515	16	0.032		0.0322
Total	2.651	23			

The P-value for the BAA for the polymerization in Table 8.8 is 0.078 which suggests there are differences between polymerizations. The F-observed value of the sample in Table 8.8 is higher that the F-distribution which means there are differences between the samples.

Table 8.8 ANOVA table for the BAA sequence.

Source	SS	df	MS	F_{obs}	Variance Estimate (s_i^2)
Poly, P	20.213	3	6.738	4.981	0.8975
Sample, S	5.411	4	1.353	5.627	0.3708
Test, T	3.847	16	0.240		0.2404
Total	29.471	23			

Table 8.9 shows the ANOVA table for the AAA and suggests that there are significant variability in polymerization and sampling. Knowing that the P-value for the polymerization is 0.061.

Table 8.9 ANOVA table for the AAA sequence.

Source	SS	df	MS	F_{obs}	Variance Estimate (s_i^2)
Poly, P	86.034	3	28.678	5.795	3.9549
Sample, S	19.793	4	4.948	10.741	1.4959
Test, T	7.371	16	0.461		0.4607
Total	113.198	23			

The tetrad distribution results are shown in Table 8.10, 8.11 and 8.12 for ABBA, ABAA and BAAB, respectively. The tetrad distributions results suggest there are no significant differences between polymerizations and significant variability exists between samples.

Table 8.10 ANOVA table for the ABBA sequence.

Source	SS	df	MS	F_{obs}	Variance Estimate (s_i^2)
Poly, P	0.382	3	0.127	3.941	0.0159
Sample, S	0.129	4	0.032	6.154	0.0090
Test, T	0.084	16	0.005		0.0053
Total	0.596	23			

Table 8.11 ANOVA table for the ABAA sequence.

Source	SS	df	MS	F_{obs}	Variance Estimate (s_i^2)
Poly, P	12.282	3	4.094	2.772	0.4362
Sample, S	5.907	4	1.477	10.488	0.4453
Test, T	2.253	16	0.141		0.1408
Total	20.441	23			

Table 8.12 ANOVA table for the BAAB sequence.

Source	SS	df	MS	F_{obs}	Variance Estimate (s_i^2)
Poly, P	0.275	3	0.092	0.599	0.0000
Sample, S	0.612	4	0.153	4.963	0.0408
Test, T	0.494	16	0.031		0.0308
Total	1.381	23			

For more details of the calculation process please refer to Appendix G.1. The ^{13}C NMR spectra of the (ethylene-*co*-1-butene) copolymer replicate samples are presented in Appendix G.2.

8.3 Conclusions

It is important to evaluate the quality and reproducibility of the experimental data. Developing a hierarchical design takes a lot of time and effort and that explains why most of researchers do not include such evaluations in their research.

In this chapter we synthesized poly(ethylene-*co*-1-butene) replicate samples and used a 4 × 2 × 3 hierarchical experiment to study the sources and magnitudes of errors in the measured data from the GPC and ^{13}C NMR.

The weight-average molecular weight results showed that the polymerization and sampling were reproducible. This shows that measuring the weight-average molecular weight by the GPC is not associated with large uncertainties.

In most of the triads and all tetrads results the polymerization was reproducible. For the A centered triads we found that there are differences between polymerizations and sampling. Those differences in the polymerization and sampling results could be justified due to the uncertainty encountered during the NMR analysis.

Chapter 9
Contributions and Recommendations

The main contribution of this thesis is the development of the first systematic and robust methodology to estimate reactivity ratios per site type for ethylene/α-olefin copolymers made with multiple site-type catalysts, called IDEM: Integrated Deconvolution Estimation Model. IDEM is a sequential procedure that for the first time combines MWD and triad/tetrad deconvolution to obtain the number of site types, mass fraction of polymer made on each site type and their respective reactivity ratios.

IDEM was applied to two sets of ethylene-*co*-1-butene copolymer samples made with an industrial $TiCl_4/MgCl_2$ catalyst in the presence and absence of hydrogen. Optimum conditions for parameter estimation were developed and the effect of the presence of hydrogen on the reactivity ratio per site type was quantified for the first time for these copolymers.

The effect of measuring the triad distribution in different laboratories with different ^{13}C NMR procedures on the reactivity ratio estimates was also compared for the first time in this thesis, showing that, despite the lack of standardization between the two laboratories, a reasonable agreement was met for the reactivity ratios of ethylene and 1-butene with and without hydrogen during the polymerization. This finding is an important new contribution and attests that IDEM is a robust parameter estimation methodology for these complex copolymers.

Another contribution is the replicate samples that were synthesized to study the quality and reproducibility of the experimental data. Most experimenters avoid evaluating those factors. The hierarchical experiment design applied in this research measured and identified the variability sources in the experimental data.

Therefore, the microstructure characterization data and the values of the parameter estimates that characterize each site type for the Ziegler-Natta catalyst and the hierarchical design analysis provided us with a better understanding on the nature of site types of heterogeneous Ziegler-Natta catalysts used for ethylene and 1-butene copolymerization.

Several recommendations can be made to improve the use and further developments of the methodology developed in this thesis. The most important are discussed below.

One of the major limitations encountered during parameter estimation was due to the fact that the concentration of 1-butene could not be increased to higher values, limiting the observability of the model parameters, especially r_B. This limitation is due to two main reasons: first, most heterogeneous Ziegler-Natta catalysts are not capable to incorporate high fractions of 1-butene, particularly by the high molecular weight sites; second, when the 1-butene average fraction in the copolymer increases, the particles become stickier, leading to particle agglomeration, reactor fouling, and loss of reactor temperature control. Both limitations can be partially solved by applying IDEM to ethylene-propylene copolymers. Ziegler-Natta catalysts can be used to make highly crystalline (non sticky) isotactic polypropylene particles, which will decrease in crystallinity when ethylene is added to the copolymer. Therefore, at least for the case of ethylene-propylene samples, it should be possible to make copolymers (with high crystallinities that will not foul the reactor) that are both rich in ethylene and propylene, thus considerably extending the range of copolymer compositions that could be tested by IDEM. A similar problem will still arise when the ethylene/propylene ratio in the copolymer approached one and the polymer particles become increasingly less crystalline and more sticky, but at least this approach would allow us to sample a wider range of copolymer compositions and likely permit a more accurate estimate for both r_A and r_B for each site type in the catalyst.

Evidently, the suggestion proposed in the paragraph above does not solve the problem of how to improve the estimates for ethylene/butene or ethylene/higher α-olefin copolymers, as no heterogeneous Ziegler-Natta catalyst exists that can make crystalline polybutene, polyhexene, etc. For these copolymers, a possible solution would be to operate the reactor in the gas phase, instead of using slurry polymerization. A lower particle crystallinity limit will still occur in this case, but the absence of a diluent that swells and may even extract the chains with high 1-butene content from the polymer particles, may also help extend the range of feasible 1-butene content in the copolymer that can be investigated without significant reactor fouling.

Another interesting possibility is extend IDEM by combining CCD measurements (as measured by TREF or CEF) to MWD and triad/tetrad information. As discussed in Chapter 5, the CCDs measured by CEF follow well the trends observed by ^{13}C NMR analysis and open another window into the

microstructure of these copolymers. The simultaneous deconvolution of MWD, CCD and triad/tetrad distributions (let's call it IDEM^{+}) is likely to lead to better estimates for the reactivity ratios of ethylene/α-olefin copolymers made with multiple site-type Ziegler-Natta catalysts.

Appendix A

The model used to generate copolymers A-1 to A-9 has been described in details in the literature (Hamielec et al., 1996; Soares et al., 1996; Soares, 2001; Soares, 2007). For the sake of completeness, only a summary of the equations will be discussed here. The polymerization kinetic parameters and reactivity ratios used to simulate the model copolymers are shown in Table A.1. We assumed that the catalyst had three site types: site type 1 has the highest tendency to incorporate α-olefins (*B*), following Bernoulian statistics ($r_A \times r_B = 1.0$), and also makes polymer chains with the lowest average molecular weights, as generally observed in Ziegler-Natta catalysts; the other two site types make copolymer with longer ethylene (*A*) sequences and higher molecular weight averages.

Table A.1 Model parameters for a 3-site-type catalyst.

Parameter	Site-1	Site-2	Site-3
x	0.3	0.45	0.25
$k_{p,AA}$, (L.mol^{-1}.s^{-1})	1000	1000	1500
$k_{p,BB}$, (L.mol^{-1}.s^{-1})	100	200	300
$k_{\beta,A}$, (L.mol^{-1}.s^{-1})	0.15	0.1	0.05
$k_{\beta,B}$, (L.mol^{-1}.s^{-1})	1.3	1.0	0.5
$k_{H,A}$, (L.mol^{-1}.s^{-1})	1.5	1.1	0.6
$k_{H,B}$, (L.mol^{-1}.s^{-1})	1.5	1.1	0.6
$k_{t,AA}$, (L.mol^{-1}.s^{-1})	0.01	0.015	0.005
$k_{t,AB}$, (L.mol^{-1}.s^{-1})	0.1	0.08	0.05
$k_{t,BA}$, (L.mol^{-1}.s^{-1})	0.01	0.008	0.005
$k_{t,BB}$, (L.mol^{-1}.s^{-1})	1.1	1.0	0.5
r_A	1.0	3.0	5.0
r_B	1.0	0.4	0.5
$r_A r_B$	1.0	1.2	2.5

x_i: molar fraction of site type i in the catalyst; $k_{p,AA,i}$: propagation rate constant for ethylene with ethylene-terminated chain for site type i; $k_{p,BB,i}$: propagation rate constant for α-olefin with α-olefin-terminated chain for site type i; $k_{\beta,A,i}$: β-hydride elimination constant for ethylene-terminated chain for site type i; $k_{\beta B,i}$: β-hydride elimination constant for α-olefin-terminated chain for site type i; $k_{H,A,i}$: transfer to hydrogen constant for ethylene-terminated chain for site type i; $k_{H,B,i}$: transfer to hydrogen constant for α-olefin-terminated chain for site type i; $k_{t,AA,i}$: transfer to ethylene with ethylene-terminated chain for site type i; $k_{t,AB,i}$: transfer to ethylene with α-olefin-terminated chain for site type i; $k_{t,BA,i}$: transfer to α-olefin with ethylene-terminated chain for site type i; $k_{t,BB,i}$: transfer to α-olefin with α-olefin-terminated chain for site type i; $r_{A,i}$: reactivity ratio for ethylene for site type i; $r_{B,i}$: reactivity ratio for α-olefin for site type i.

The cross propagation constants, $k_{p,AB,i}$ and $k_{p,BA,i}$ are calculated from the values of the reactivity ratios for each site type

$$r_{A,i} = \frac{k_{p,AA,i}}{k_{p,AB,i}} \Rightarrow k_{p,AB,i} = \frac{k_{p,AA,i}}{r_{A,i}} \tag{A.1}$$

$$r_{B,i} = \frac{k_{p,BB,i}}{k_{p,BA,i}} \Rightarrow k_{p,BA,i} = \frac{k_{p,BB,i}}{r_{B,i}} \tag{A.2}$$

The fraction of living chains terminated with ethylene is calculated using the long chain approximation

$$\phi_{A,i} = \frac{k_{p,BA,i} f_A}{k_{p,AB,i}(1 - f_A) + k_{p,BA,i} f_A} \tag{A.3}$$

$$\phi_{B,i} = 1 - \phi_{A,i} \tag{A.4}$$

where f_A is the molar fraction of ethylene in the reactor

$$f_A = \frac{[A]}{[A]+[B]} \tag{A.5}$$

and [*A*] and [*B*] are the concentrations of ethylene and α-olefin, in the reactor, respectively. Pseudo-kinetic constants for copolymerization can be calculated with the expression

$$\hat{k}_{p,i} = k_{p,AA,i}\phi_{A,i} f_A + k_{p,AB,i}\phi_{A,i}(1-f_A) + k_{p,BA,i}(1-\phi_{A,i})\, f_A + k_{p,BB,i}(1-\phi_{A,i})(1-f_A) \tag{A.6}$$

Finally, the mass fraction of polymer made on each site type can be found using the equation

$$w_i = \frac{R_{p,i}}{\sum R_{p,j}} = \frac{\hat{k}_{p,i}([A]+[B])x_i[C^*]}{\sum \hat{k}_{p,j}([A]+[B])x_j[C^*]} = \frac{\hat{k}_{p,i}x_i}{\sum \hat{k}_{p,j}x_j} \tag{A.7}$$

where [C^*] is the concentration of catalyst in the reactor and $R_{p,i}$ is the rate of propagation for site type *i*. The MWD of the polymer made with a multiple-site-type catalyst can be represented as a weighted superposition of two or more Flory's distributions (Soares, 2001; Soares, 2007) as shown below in log scale

$$W_{\log MW} = 2.3026 \times MW^2 \sum_{i=1}^{N} w_i\, \tau_{MW,i}^2\, e^{-MW\,\tau_{MW,i}} \tag{A.8}$$

where *MW* is the molecular weight of polymer chain, $\tau_{MW,i}$ is the reciprocal of the number average molecular weight ($\tau_{MW,i} = M_{n,i}^{-1}$) for site type *i*, and *N* is the total number of site types in the catalyst. The value of $M_{n,i}$ is related to the polymerization conditions and polymerization kinetic constants for site type *i* according to the equation

$$M_{n,i} = \overline{MW_i}\,\frac{R_{p,i}}{R_{t,i}} \tag{A.9}$$

In Equation (A.9), $R_{t,i}$ is the rate of chain transfer for site type *i* and $\overline{MW_i}$ is the average molar mass of the copolymer made by site type *i*. The latter parameter is defined as

$$\overline{MW_i} = F_{A,i}MW_A + (1-F_{A,i})MW_B \tag{A.10}$$

where MW_A and MW_B are the molar masses of ethylene and α-olefin comonomer, respectively, and $F_{A,i}$ is the fraction of ethylene in the copolymer, calculated with the Mayo-Lewis equation,

$$F_{A,i} = \frac{r_{A,i} f_A^{\,2} + f_A(1-f_A)}{r_{A,i} f_A^{\,2} + 2 f_A(1-f_A) + r_{b,i}(1-f_A)^2} \tag{A.11}$$

Finally, the rate of chain transfer can be decomposed into the contributions of its several elementary steps as,

β-Hydride elimination $$R_{\beta,i} = [k_{\beta,A,i}\phi_{A,i} + k_{\beta,B,i}(1-\phi_{A,i})]x_i[C^*] = \hat{k}_{\beta,i}x_i[C^*] \quad \text{(A.12)}$$

Transfer to hydrogen $$R_{H,i} = [k_{H,A,i}\phi_{A,i} + k_{H,B,i}(1-\phi_{A,i})][H_2]x_i[C^*] = \hat{k}_{H,i}[H_2]x_i[C^*] \quad \text{(A.13)}$$

Transfer to monomer $$\begin{aligned} R_{t,i} = & \begin{bmatrix} k_{t,AA,i}\phi_{A,i}f_A + k_{t,AB,i}\phi_{A,i}(1-f_A) \\ + k_{t,BA,i}(1-\phi_{A,i})f_A + k_{t,BB,i}(1-\phi_{A,i})(1-f_A) \end{bmatrix} \\ & \times([A]+[B])x_i[C^*] \\ = & \hat{k}_{t,i}([A]+[B])x_i[C^*] \end{aligned} \quad \text{(A.14)}$$

where $\hat{k}_{\beta,i}$, $\hat{k}_{H,i}$, and $\hat{k}_{t,i}$ are pseudo-kinetic constants for β-hydride elimination, transfer to hydrogen and transfer to monomer, respectively.

Therefore, Equation (A.9) becomes,

$$M_{n,i} = [F_{A,i}MW_A + (1-F_{A,i})MW_B]\frac{\hat{k}_{p,i}([A]+[B])}{\hat{k}_{\beta,i} + \hat{k}_{H,i}[H_2] + \hat{k}_{t,i}([A]+[B])} \quad \text{(A.15)}$$

or,

$$M_{n,i} = \frac{[F_{A,i}MW_A + (1-F_{A,i})MW_B]}{\frac{\hat{k}_{\beta,i} + \hat{k}_{H,i}[H_2]}{\hat{k}_{p,i}([A]+[B])} + \frac{\hat{k}_{t,i}}{\hat{k}_{p,i}}} \quad \text{(A.16)}$$

Equation (A.16) can be used to calculate the $M_{n,i}$ for polymer made on each site type on the catalyst as a function of polymerization conditions and kinetic parameters and then can be used to find the MWD of the polymer using Equations (A.8) and (A.7). For our simulations, we assumed that [H_2] = 0. In principle, H_2 concentration should not influence reactivity ratios and copolymer composition.

Equation (A.17) is the objective function used to determine the minimum number of Flory's distributions required to describe the MWD of a polymer sample. This modeling technique has been used extensively to describe the MWD of polyolefin made with Ziegler Natta and Phillips catalysts (Hamielec et al., 1996; Soares et al., 1996; Soares, 2001).

$$\chi^2 = \sum_{i=1}^{n_{GPC}}[W_{\log MW}^{GPC} - \sum_{j=1}^{ns} w_j(2.3026MW_i^{\,2}\tau_{MW,j}^2 e^{-MW_i\tau_{MW,j}})]^2 \quad \text{(A.17)}$$

where $W_{\log MW}^{GPC}$ is the sample MWD measured by GPC, and n_{GPC} is the number of sampling points taken by GPC.

Appendix B

The vapor-liquid equilibria of the reactor mixture were calculated using Peng-Robinson equation of state (Peng and Robinson, 1976).

The Peng-Robinson equation of state for single component is as follows:

$$P = \frac{RT}{v-b} - \frac{a(T)}{v(v+b)+b(v-b)} \tag{B.1}$$

where, R is the gas constant, T is absolute temperature, a is attraction parameter, b is van der Walls covolume and v is molar volume. Equation (B.1) can be re-written as following:

$$Z^3 - (1-B)Z^2 + (A - 3B^2 - 2B)Z - (AB - B^2 - B^3) = 0 \tag{B.2}$$

The constants A and B are defined by,

$$A = \frac{a\,P}{R^2\,P^2} \tag{B.3}$$

$$B = \frac{b\,P}{RT} \tag{B.4}$$

The compressibility factor Z is given by,

$$Z = \frac{P\,v}{RT} \tag{B.5}$$

At critical point equation (B.1) employs,

$$a(T_C) = 0.45724\,\frac{R^2\,T_C^2}{P_C} \tag{B.6}$$

$$b(T_C) = 0.07780\,\frac{R\,T_C}{P_C} \tag{B.7}$$

$$Z_C = 0.307 \tag{B.8}$$

At other temperatures (B.1) uses the following,

$$a(T) = a(T_C).\alpha(T_r, \omega) \tag{B.9}$$

$$b(T) = b(T_C) \tag{B.10}$$

$\alpha(T_r, \omega)$ is a dimensionless function of reduced temperature and acentric factor. It equals unity at

critical temperature. For all substances the relationship between T_r (reduced temperature) and α (scaling factor in equation B.9) can be linearized by the following expressions:

$$\alpha^{1/2} = 1 + \kappa\ (1 - T_r^{1/2}) \tag{B.11}$$

and κ is a constant characteristics of a substance,

$$\kappa = 0.37464 + 1.54226\ \omega\ -\ 0.26992\ \omega^2 \tag{B.12}$$

The van der Waals mixing rules define the mixture parameters in equations (B.2) as follows:

$$a = \sum_i \sum_j x_i x_j a_{ij} \tag{B.13}$$

$$b = \sum_i x_i b_i \tag{B.14}$$

and,

$$a_{ij} = (1 - \delta_{ij})\, a_i^{1/2} a_j^{1/2} \tag{B.15}$$

where, x_i and x_j are the molar fractions of component i and j and δ_{ij} is an interaction coefficient.

Appendix C

C.1 MWD Deconvolution of EBH Samples

Experimental MWDs measured by GPC and their MWD deconvolutions for EBH-1 to EBH-9 are shown along with their MWD deconvolution parameter estimates.

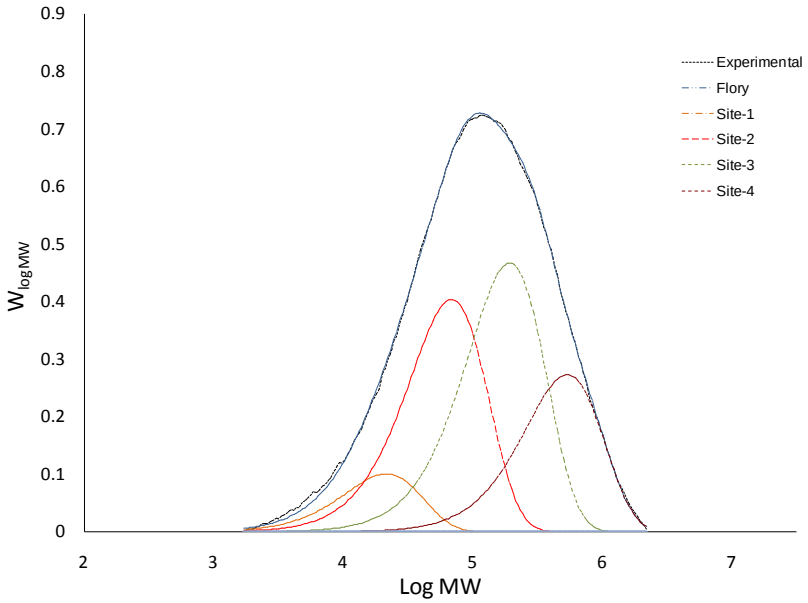

Figure C.1 MWD deconvolution for EBH-1 (χ^2=0.0146).

Table C.1 Parameter estimates from MWD deconvolution for EBH-1.

Site type	*w*	M_n	M_w	*PDI*
1	0.081	11 000	21 000	2.00
2	0.324	34 000	68 000	2.00
3	0.375	96 000	192 000	2.00
4	0.219	267 000	533 000	2.00
All	1.000	46 000	213 000	4.64

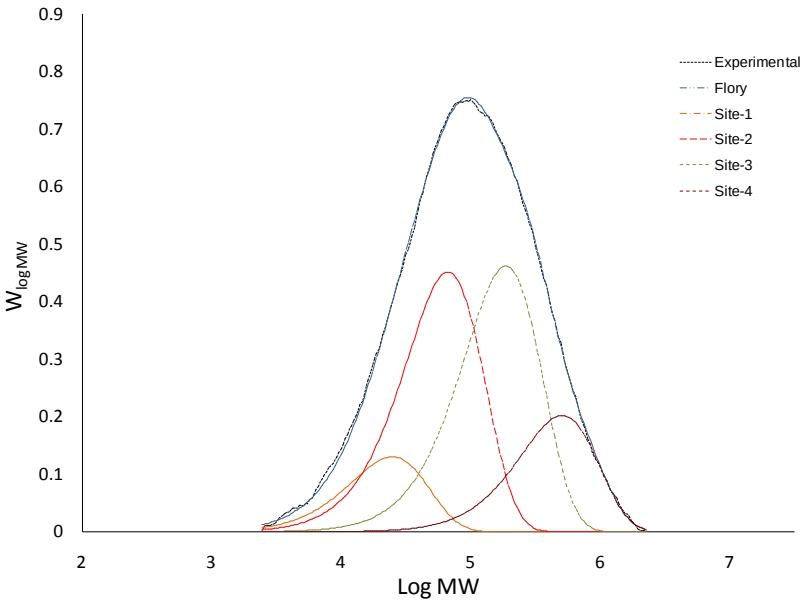

Figure C.2 MWD deconvolution for EBH-2 (χ^2= 0.0268).

Table C.2 Parameter estimates from MWD deconvolution for EBH-2.

Site type	*w*	M_n	M_w	*PDI*
1	0.105	12 000	25 000	2.00
2	0.362	33 000	67 000	2.00
3	0.371	93 000	186 000	2.00
4	0.162	253 000	505 000	2.00
All	1.000	42 000	178 000	4.26

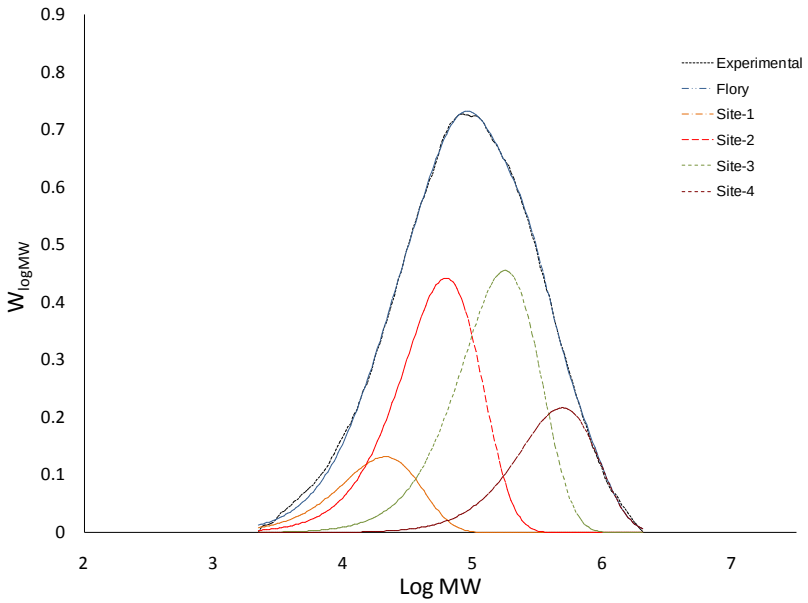

Figure C.3 MWD deconvolution for EBH-3 (χ^2= 0.0265).

Table C.3 Parameter estimates from MWD deconvolution for EBH-3.

Site type	*w*	M_n	M_w	*PDI*
1	0.106	11 000	21 000	2.00
2	0.355	31 000	62 000	2.00
3	0.365	88 000	177 000	2.00
4	0.174	245 000	489 000	2.00
All	1.000	38 000	174 000	4.59

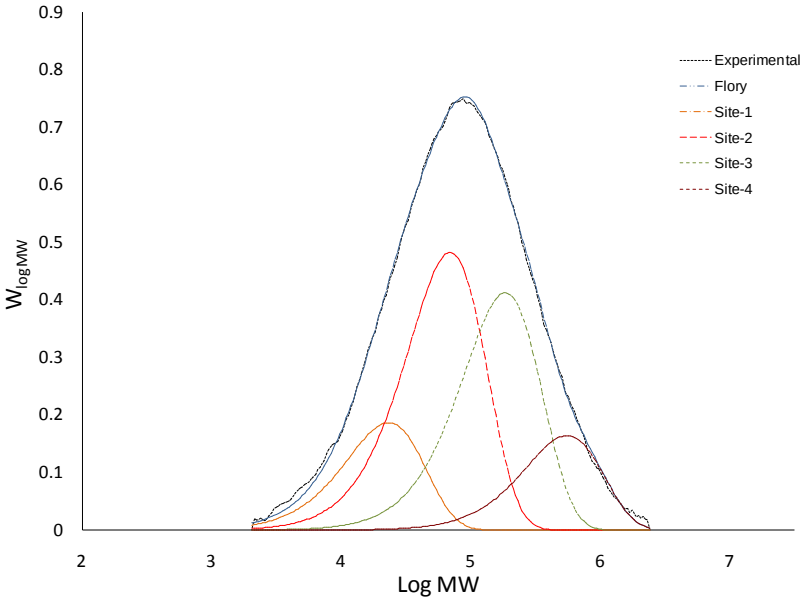

Figure C.4 MWD deconvolution for EBH-4 (χ^2= 0.0272).

Table C.4 Parameter estimates from MWD deconvolution for EBH-4.

Site type	*w*	M_n	M_w	*PDI*
1	0.150	12 000	23 000	2.00
2	0.387	35 000	69 000	2.00
3	0.331	92 000	184 000	2.00
4	0.132	276 000	551 000	2.00
All	1.000	36 000	164 000	4.63

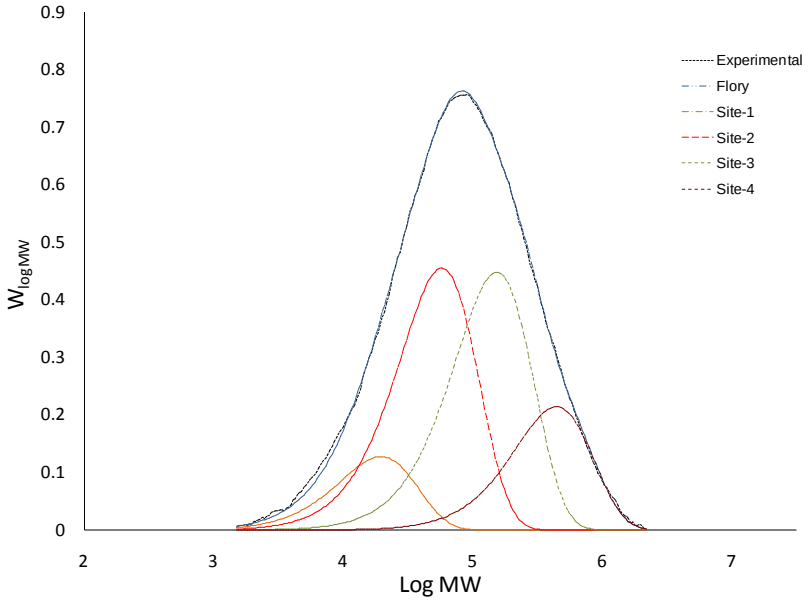

Figure C.5 MWD deconvolution for EBH-5 (χ^2= 0.0259).

Table C.5 Parameter estimates from MWD deconvolution for EBH-5.

Site type	*w*	M_n	M_w	*PDI*
1	0.102	10 000	20 000	2.00
2	0.365	29 000	58 000	2.00
3	0.360	76 000	153 000	2.00
4	0.172	221 000	441 000	2.00
All	1.000	35 000	154 000	4.42

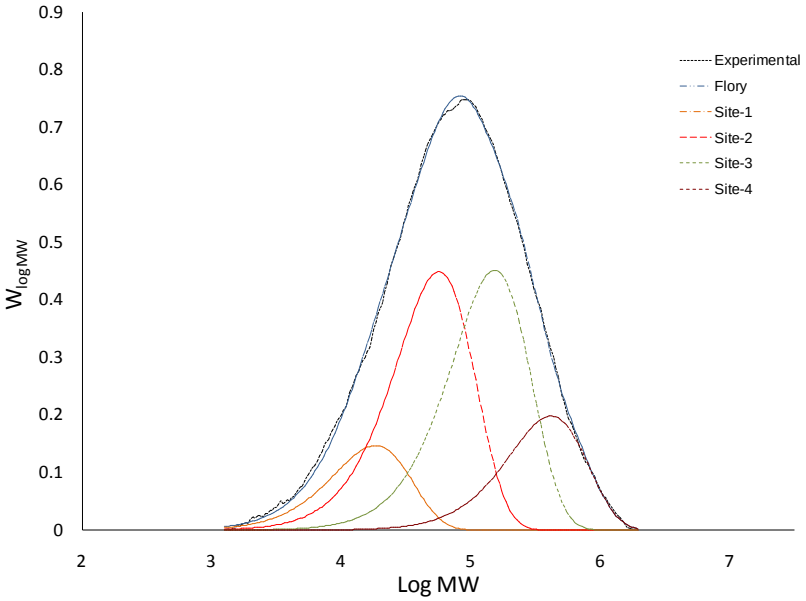

Figure C.6 MWD deconvolution for EBH-6 (χ^2= 0.0269).

Table C.6 Parameter estimates from MWD deconvolution for EBH-6.

Site type	*w*	M_n	M_w	*PDI*
1	0.118	9 000	18 000	2.00
2	0.361	28 000	57 000	2.00
3	0.363	76 000	152 000	2.00
4	0.159	207 000	415 000	2.00
All	1.000	32 000	144 000	4.48

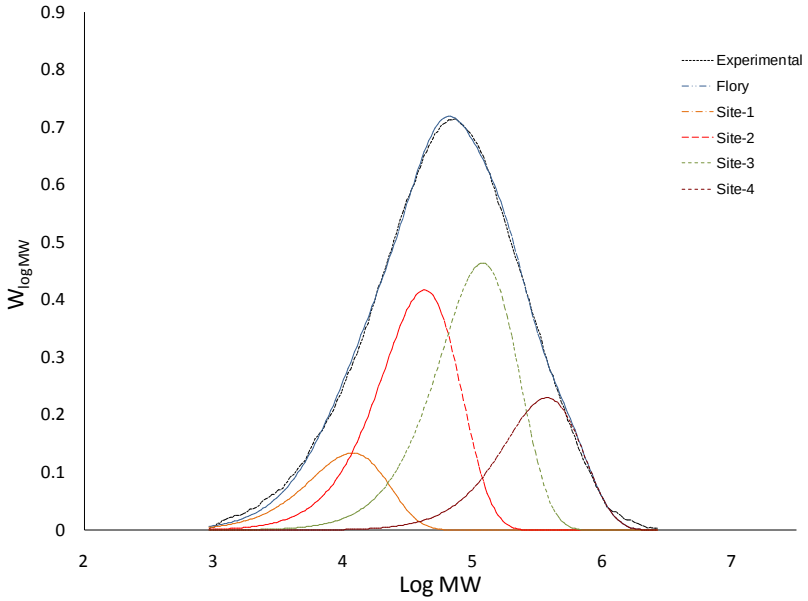

Figure C.7 MWD deconvolution for EBH-7 (χ^2= 0.0297).

Table C.7 Parameter estimates from MWD deconvolution for EBH-7.

Site type	*w*	M_n	M_w	*PDI*
1	0.108	6 000	12 000	2.00
2	0.335	21 000	42 000	2.00
3	0.373	59 000	119 000	2.00
4	0.185	186 000	371 000	2.00
All	1.000	24 000	128 000	5.31

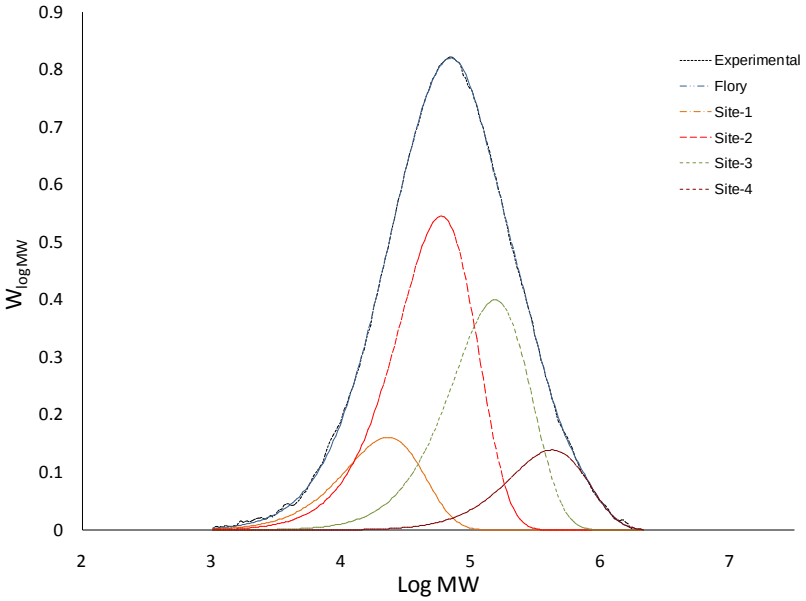

Figure C.8 MWD deconvolution for EBH-8 (χ^2= 0.0071).

Table C.8 Parameter estimates from MWD deconvolution for EBH-8.

Site type	*w*	M_n	M_w	*PDI*
1	0.130	12 000	23 000	2.00
2	0.438	29 000	59 000	2.00
3	0.321	77 000	154 000	2.00
4	0.112	212 000	424 000	2.00
All	1.000	32 000	125 000	3.87

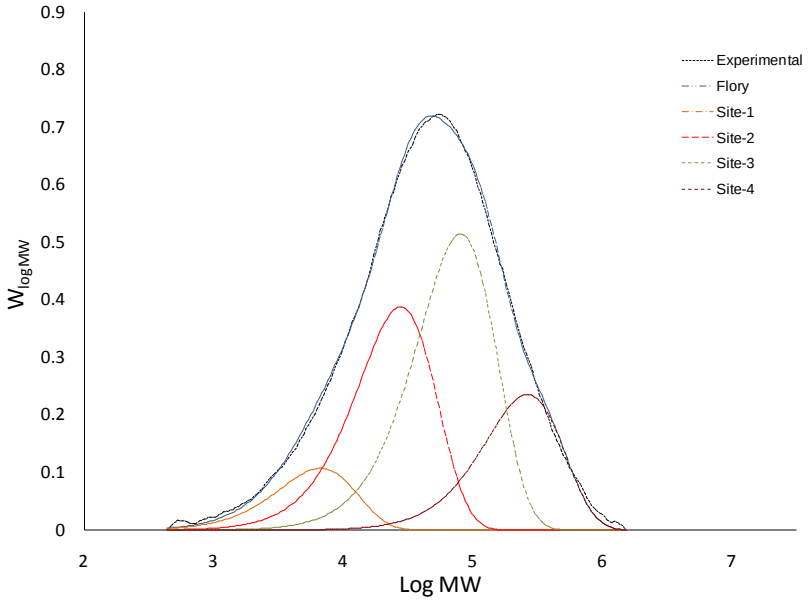

Figure C.9 MWD deconvolution for EBH-9 (χ^2= 0.0305).

Table C.9 Parameter estimates from MWD deconvolution for EBH-9.

Site type	*w*	M_n	M_w	*PDI*
1	0.086	3 000	7 000	2.00
2	0.311	14 000	28 000	2.00
3	0.413	40 000	80 000	2.00
4	0.189	132 000	264 000	2.00
All	1.000	17 000	92 000	5.54

C.2 MWD Deconvolution of EB Samples

Experimental MWDs measured by GPC and their MWD deconvolutions for EB-1 to EB-9 are shown along with their MWD deconvolution parameter estimates.

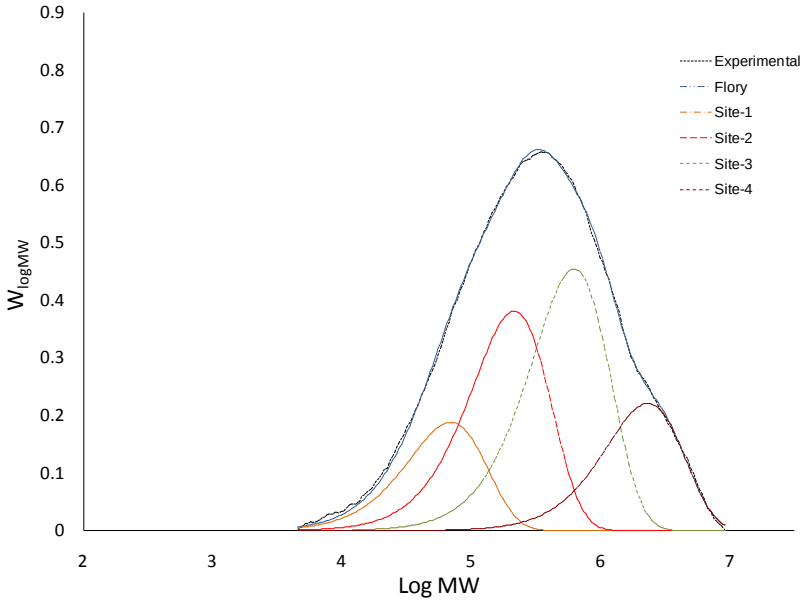

Figure C.10 MWD deconvolution for EB-1 (χ^2=0.0157).

Table C.10 Parameter estimates from MWD deconvolution for EB-1.

Site type	w	M_n	M_w	PDI
1	0.151	35 000	69 000	2.00
2	0.306	107 000	214 000	2.00
3	0.365	310 000	621 000	2.00
4	0.178	1 154 000	2 307 000	2.00
All	1.000	117 000	712 000	6.11

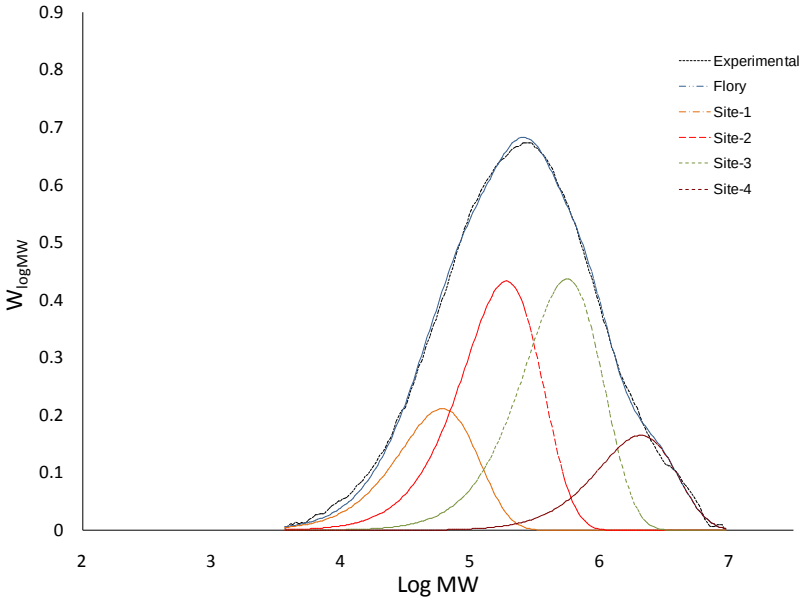

Figure C.11 MWD deconvolution for EB-2 (χ^2=0.0328).

Table C.11 Parameter estimates from MWD deconvolution for EB-2.

Site type	*w*	M_n	M_w	*PDI*
1	0.170	30 000	61 000	2.00
2	0.348	95 000	189 000	2.00
3	0.350	279 000	558 000	2.00
4	0.133	1 036 000	2 073 000	2.00
All	1.000	94 000	546 000	5.82

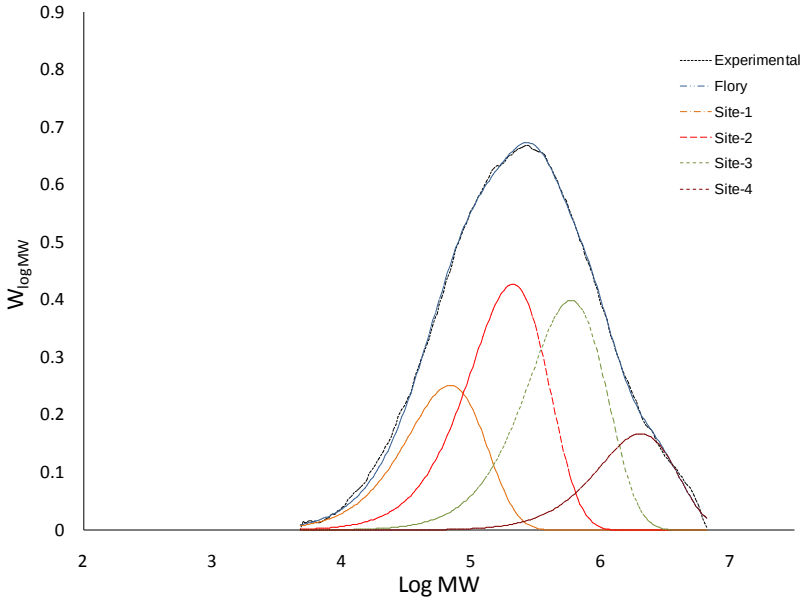

Figure C.12 MWD deconvolution for EB-3 (χ^2=0.0294).

Table C.12 Parameter estimates from MWD deconvolution for EB-3.

Site type	*w*	M_n	M_w	*PDI*
1	0.202	34 000	68 000	2.00
2	0.343	104 000	209 000	2.00
3	0.321	294 000	588 000	2.00
4	0.134	1 020 000	2 039 000	2.00
All	1.000	96 000	548 000	5.71

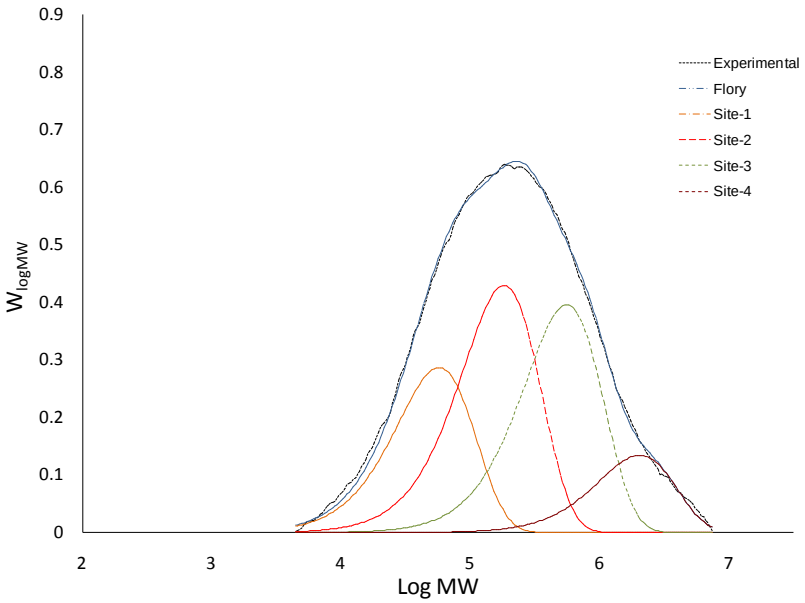

Figure C.13 MWD deconvolution for EB-4 (χ^2=0.0403).

Table C.13 Parameter estimates from MWD deconvolution for EB-4.

Site type	w	M_n	M_w	PDI
1	0.230	29 000	57 000	2.00
2	0.345	91 000	182 000	2.00
3	0.318	277 000	554 000	2.00
4	0.108	1 014 000	2 027 000	2.00
All	1.000	76 000	470 000	6.16

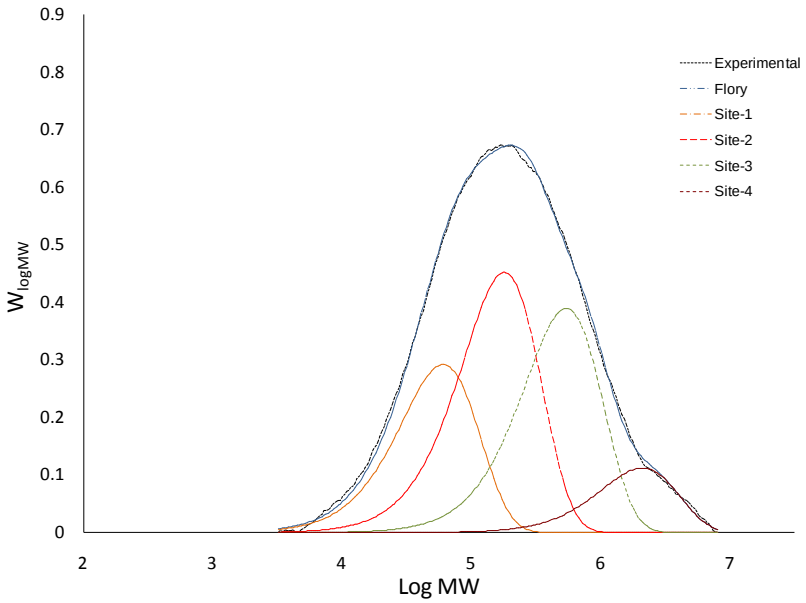

Figure C.14 MWD deconvolution for EB-5 (χ^2=0.0337).

Table C.14 Parameter estimates from MWD deconvolution for EB-5.

Site type	*w*	M_n	M_w	*PDI*
1	0.234	30 000	60 000	2.00
2	0.363	90 000	179 000	2.00
3	0.313	270 000	540 000	2.00
4	0.090	1 043 000	2 086 000	2.00
All	1.000	77 000	436 000	5.69

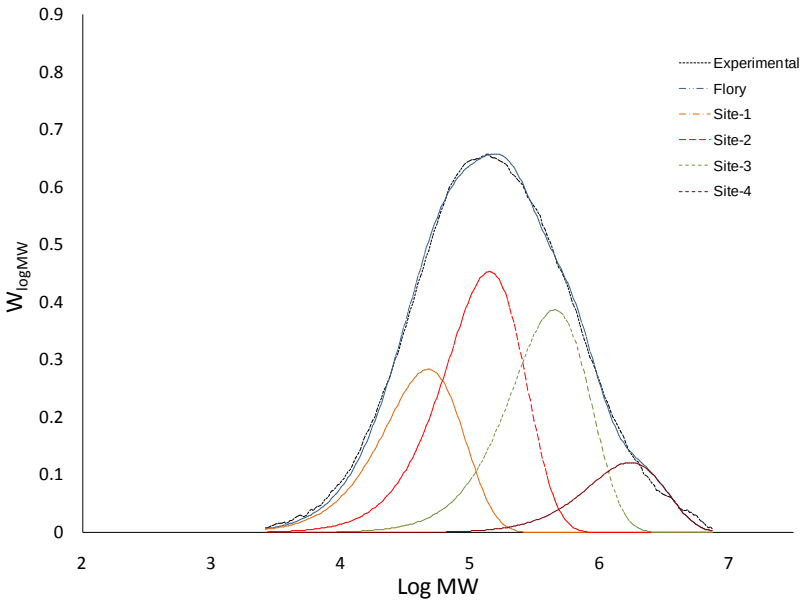

Figure C.15 MWD deconvolution for EB-6 (χ^2=0.0384).

Table C.15 Parameter estimates from MWD deconvolution for EB-6.

Site type	w	M_n	M_w	PDI
1	0.228	24 000	47 000	2.00
2	0.364	70 000	140 000	2.00
3	0.311	224 000	447 000	2.00
4	0.098	858 000	1 715 000	2.00
All	1.000	61 000	368 000	6.03

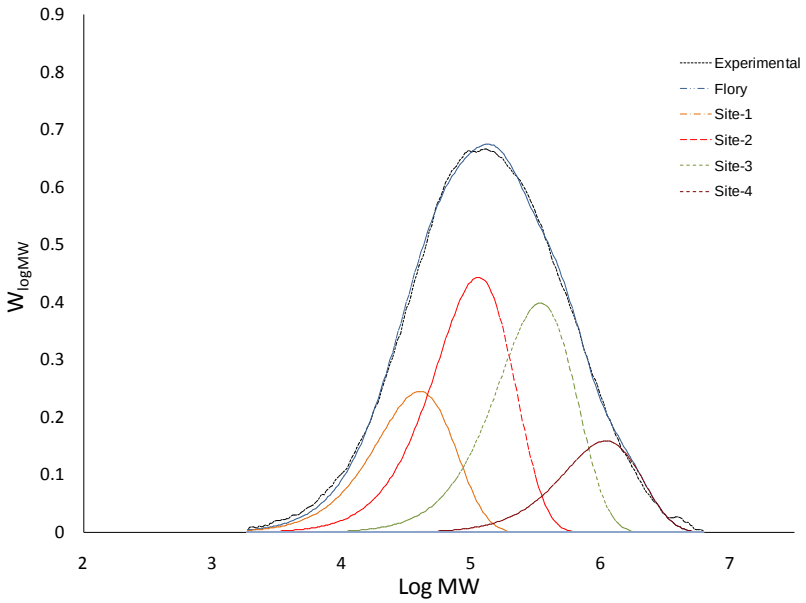

Figure C.16 MWD deconvolution for EB-7 (χ^2=0.0353).

Table C.16 Parameter estimates from MWD deconvolution for EB-7.

Site type	w	M_n	M_w	PDI
1	0.197	20 000	40 000	2.00
2	0.356	56 000	113 000	2.00
3	0.320	171 000	342 000	2.00
4	0.128	546 000	1 092 000	2.00
All	1.000	55 000	297 000	5.43

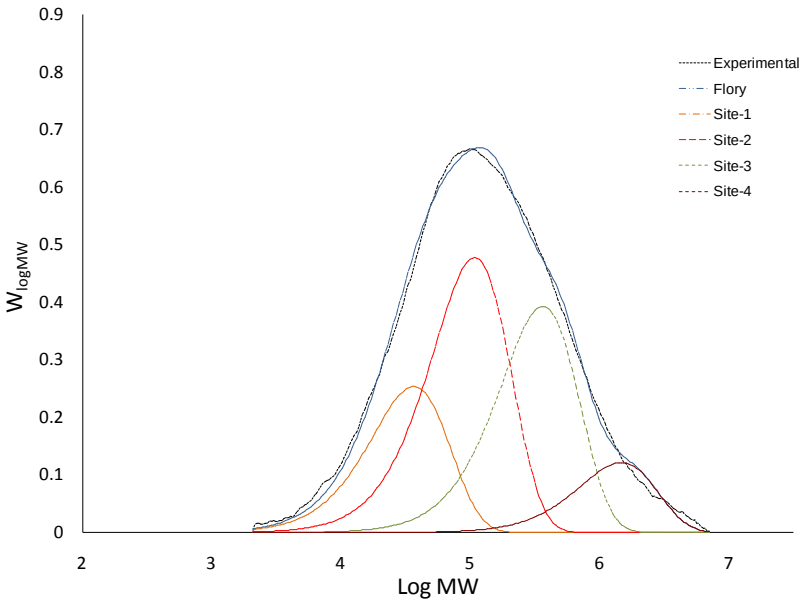

Figure C.17 MWD deconvolution for EB-8 (χ^2=0.0668).

Table C.17 Parameter estimates from MWD deconvolution for EB-8.

Site type	w	M_n	M_w	PDI
1	0.204	18 000	36 000	2.00
2	0.383	54 000	108 000	2.00
3	0.316	181 000	362 000	2.00
4	0.098	730 000	1 460 000	2.00
All	1.000	50 000	305 000	6.17

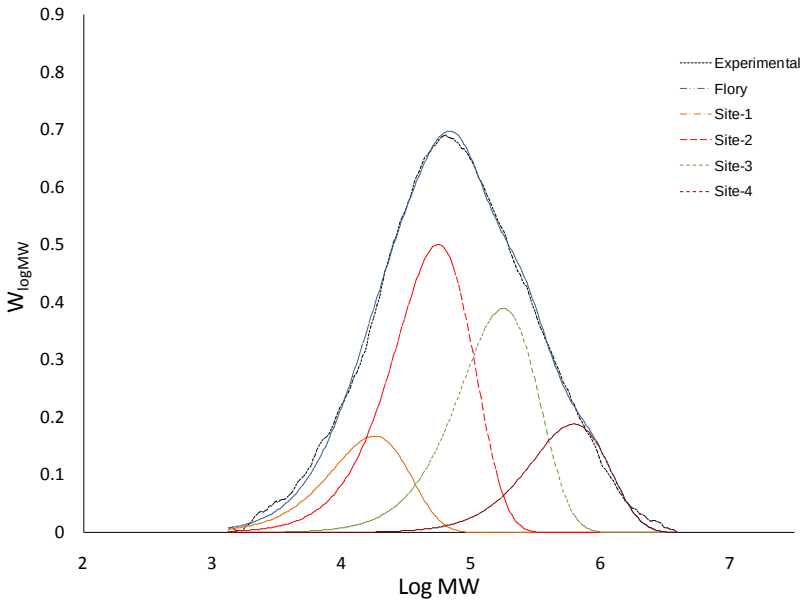

Figure C.18 MWD deconvolution for EB-9 (χ^2=0.0538).

Table C.18 Parameter estimates from MWD deconvolution for EB-9.

Site type	w	M_n	M_w	PDI
1	0.135	9 000	18 000	2.00
2	0.402	28 000	55 000	2.00
3	0.312	88 000	176 000	2.00
4	0.151	308 000	616 000	2.00
All	1.000	30 000	173 000	5.83

Appendix D

D.1 ^{13}C NMR spectra of EBH Samples

^{13}C NMR spectra of ethylene-*co*-1-butene copolymer samples (EBH-1 to EBH-9) made with different comonomer fractions.

Table D.1 ^{13}C NMR spectra normalized peak intensities for samples (EBH-1 to EBH-9)

Region	Range (ppm)	Carbon assignment	EBH-1	EBH-2	EBH-3	EBH-4	EBH-5	EBH-6	EBH-7	EBH-8	EBH-9
A	37-40	αα Methylene, $(Methine)_{EBE}$	0.51	0.73	1.06	1.21	1.84	2.38	2.59	3.47	4.42
B	37.4	$(Methine)_{EBB+BBE}$	0.03	0.07	0.11	0.15	0.36	0.36	0.42	0.62	0.88
C	33.5-35.5	αγ, $\alpha\delta^+$, $(Methine)_{BBB}$	0.96	1.40	2.10	2.40	3.71	4.64	4.76	6.92	8.30
D	29.5-31.5	γγ, γ δ^+, δ^+ δ^+	100	100	100	100	100	100	100	100	100
E	26-28	β δ^+, $2B_2$	1.29	2.39	3.26	3.42	5.22	6.36	6.42	9.30	11.19
F	24-25	ββ	0.06	0.08	0.04	0.06	0.16	0.28	0.34	0.42	0.68
G	10.5-11.5	Methyl	0.59	1.05	1.52	1.74	2.50	3.49	3.93	5.33	6.31

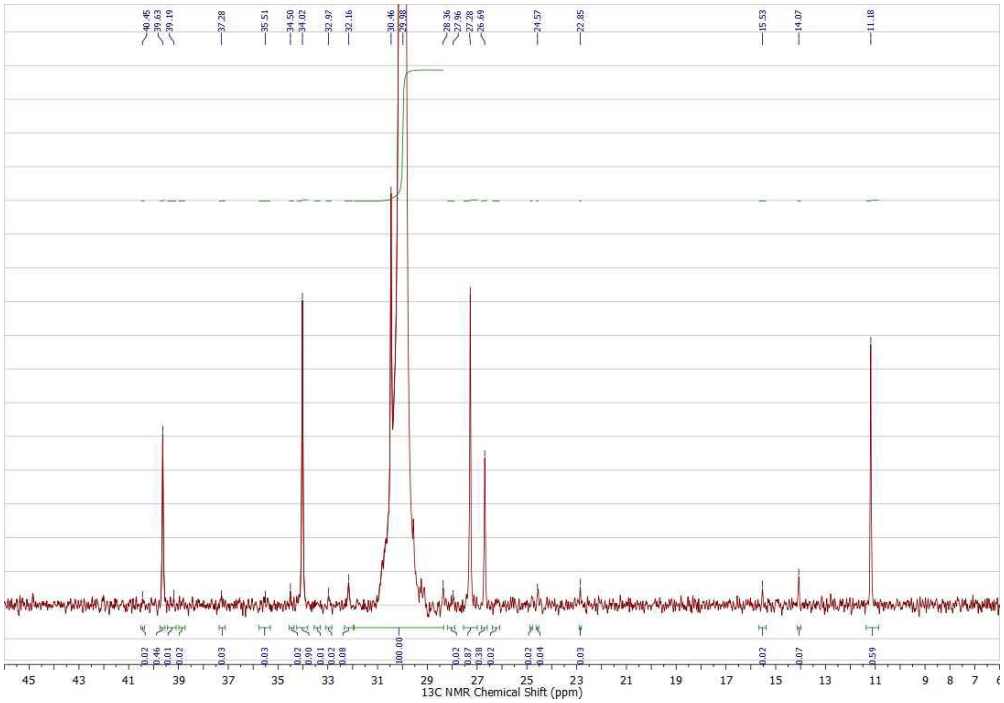

Figure D.1 ^{13}C NMR spectra of poly(ethylene-*co*-1-butene), containing 1.0% 1-butene, EBH-1.

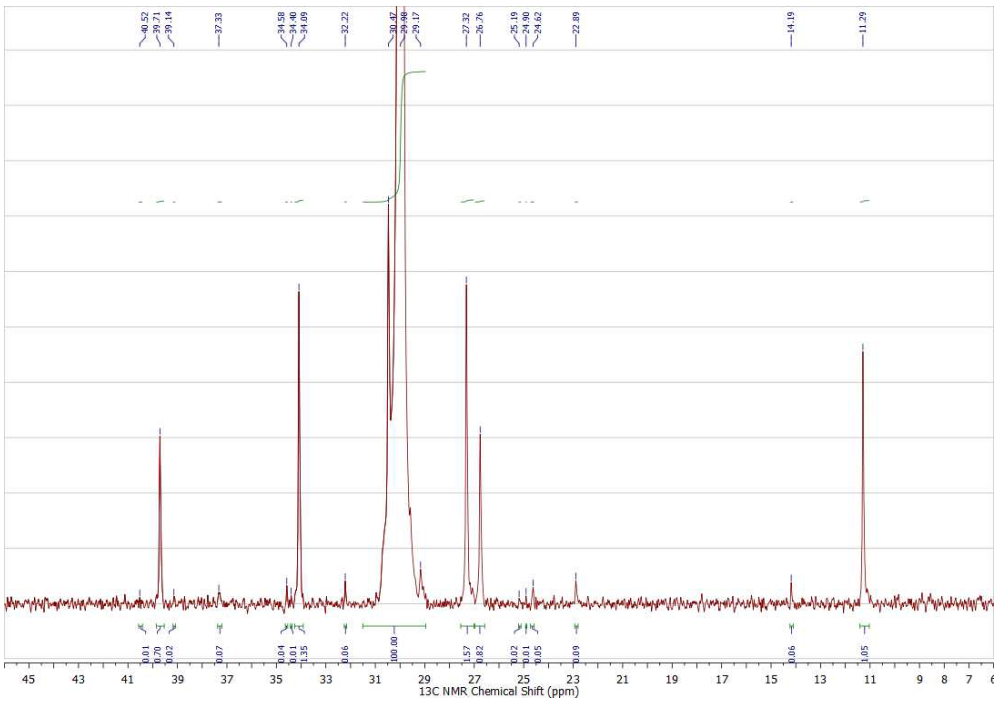

Figure D.2 ^{13}C NMR spectra of poly(ethylene-*co*-1-butene), containing 1.6% 1-butene, EBH-2.

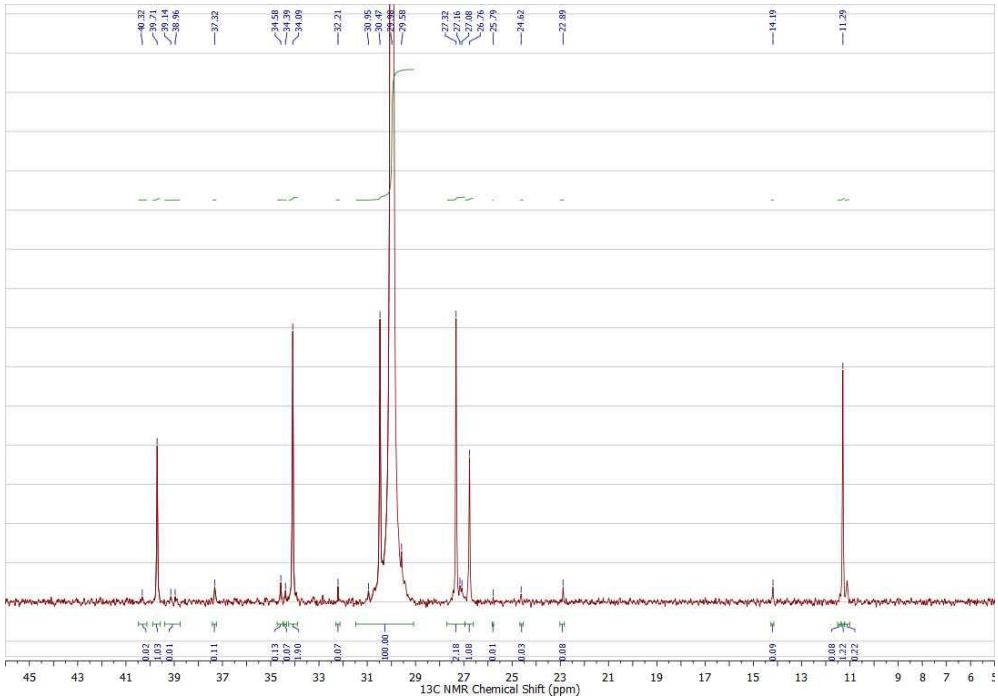

Figure D.3 ^{13}C NMR spectra of poly(ethylene-*co*-1-butene), containing 2.0% 1-butene, EBH-3.

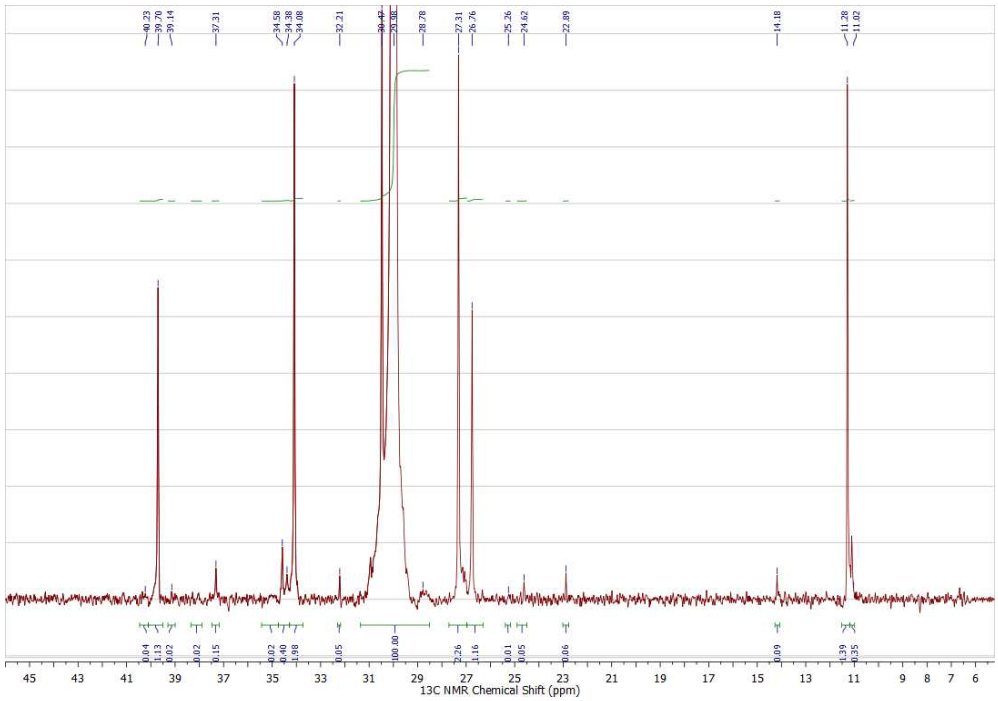

Figure D.4 ^{13}C NMR spectra of poly(ethylene-*co*-1-butene), containing 2.5% 1-butene, EBH-4.

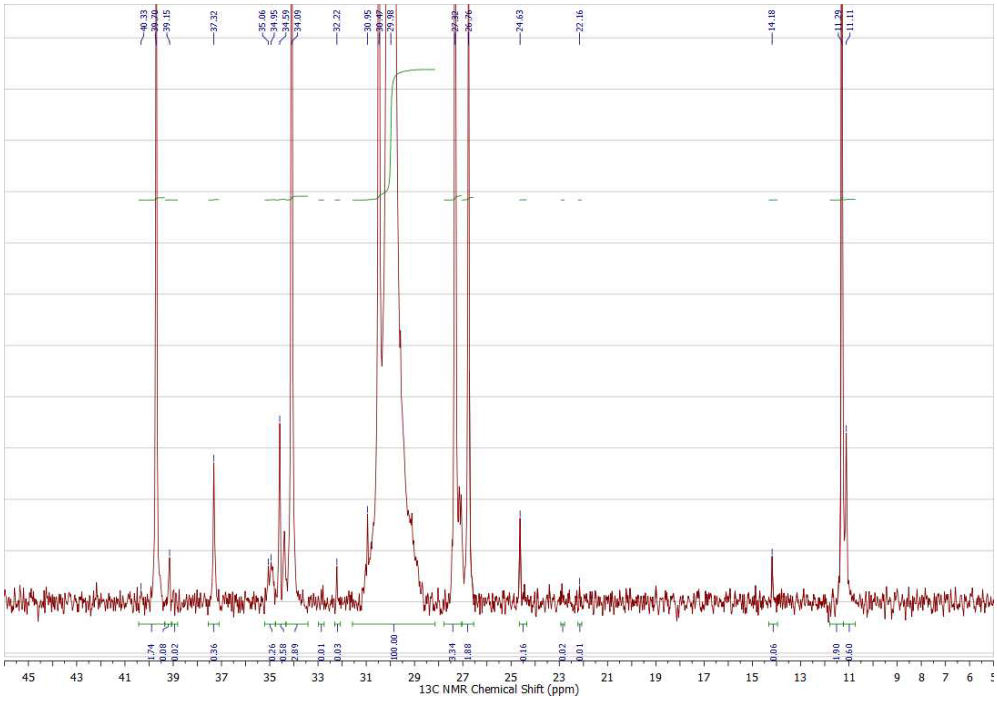

Figure D.5 ^{13}C NMR spectra of poly(ethylene-*co*-1-butene), containing 3.8% 1-butene, EBH-5.

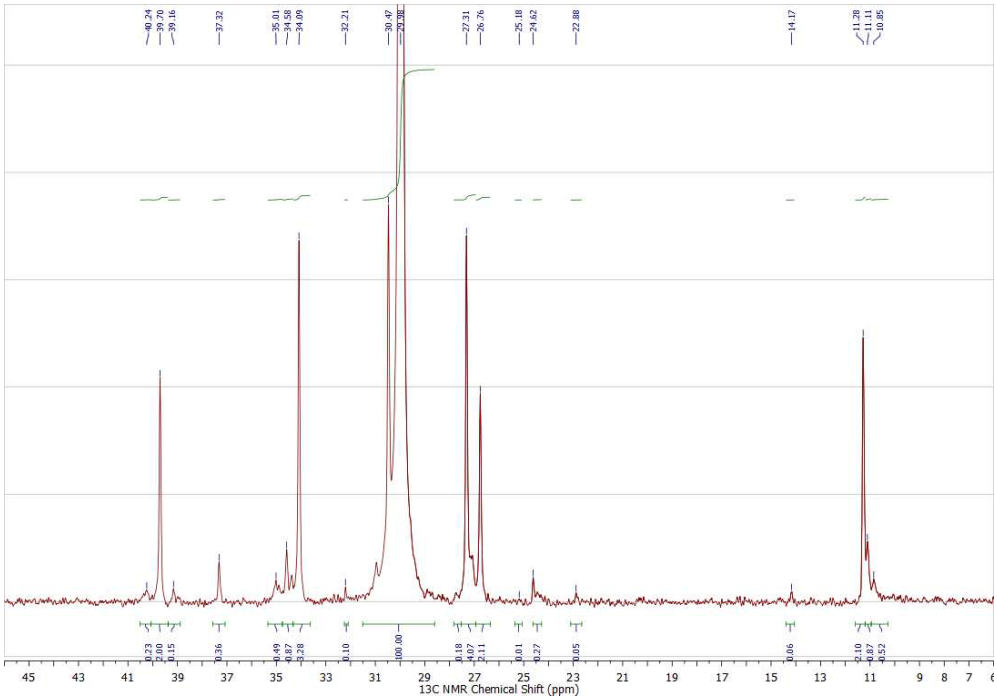

Figure D.6 ^{13}C NMR spectra of poly(ethylene-*co*-1-butene), containing 4.6% 1-butene, EBH-6.

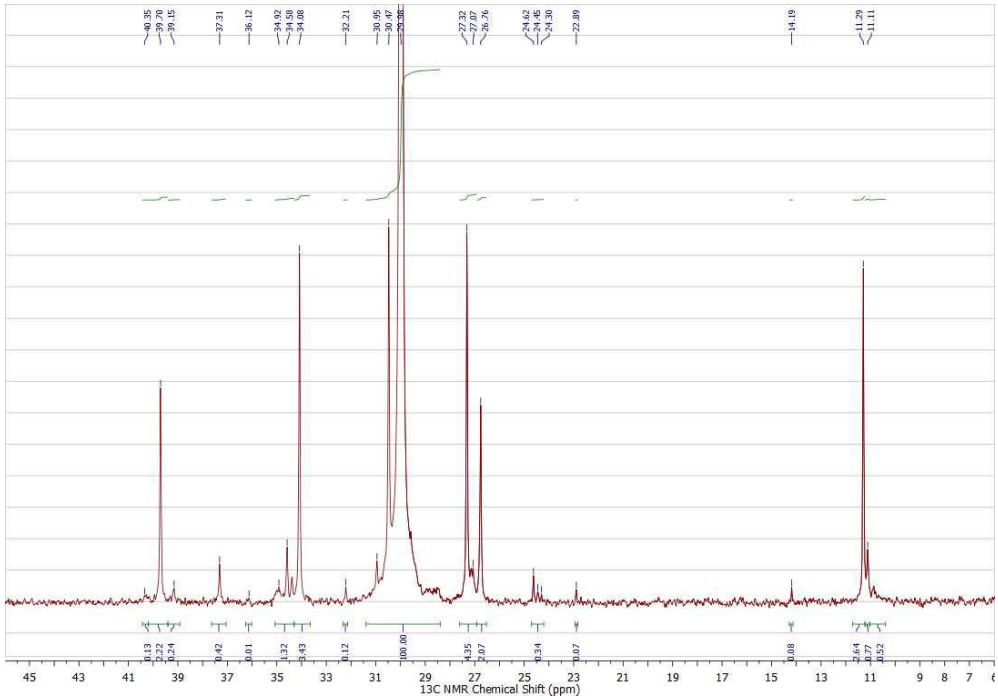

Figure D.7 ^{13}C NMR spectra of poly(ethylene-*co*-1-butene), containing 5.0% 1-butene, EBH-7.

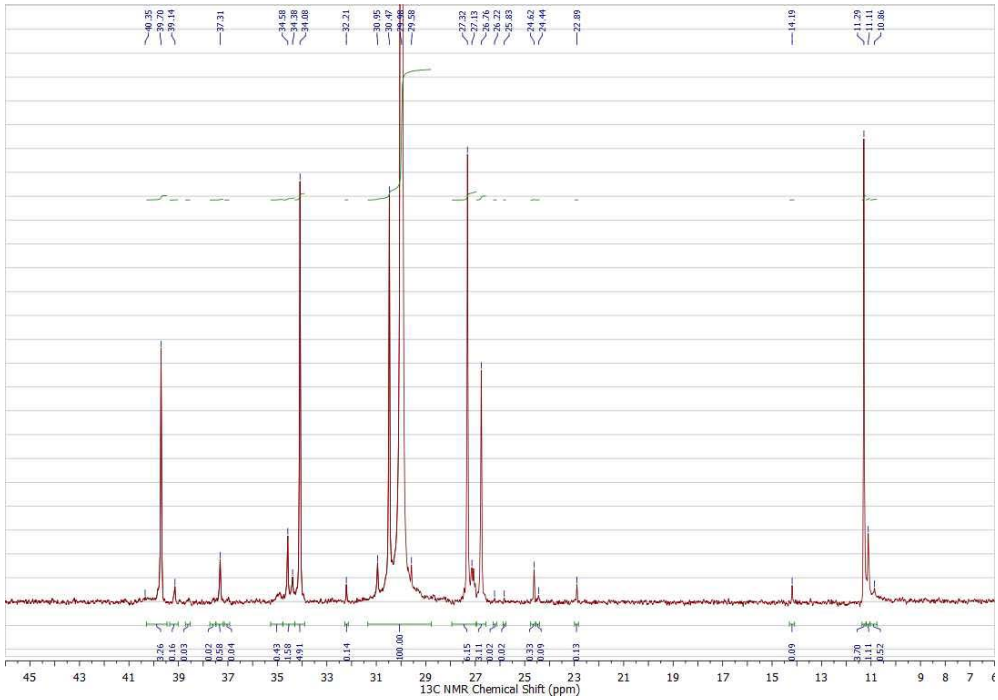

Figure D.8 ^{13}C NMR spectra of poly(ethylene-*co*-1-butene), containing 6.7% 1-butene, EBH-8.

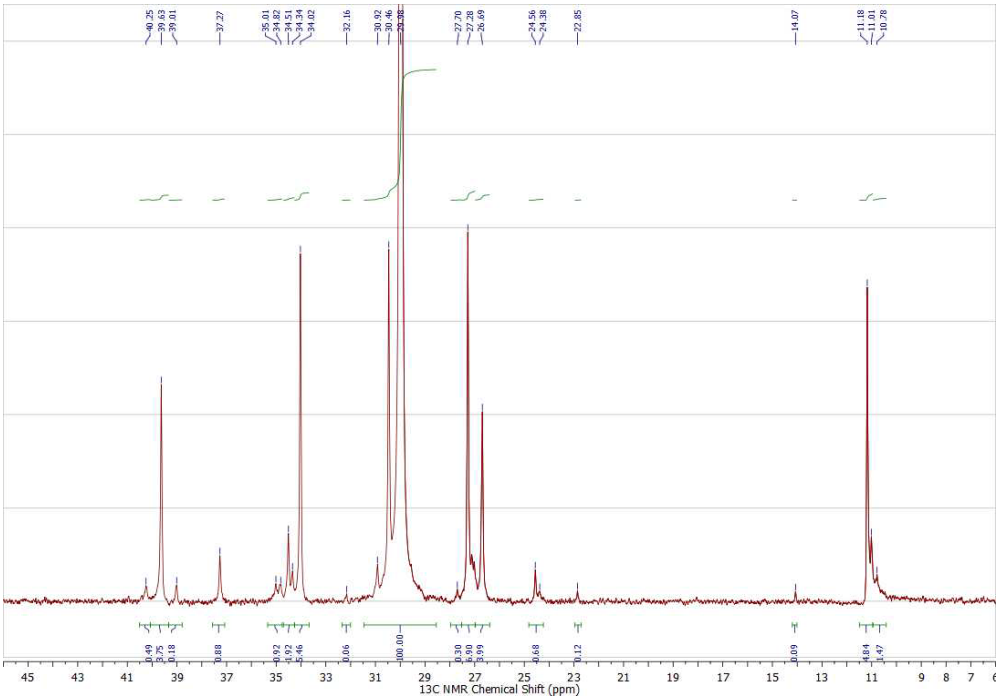

Figure D.9 ^{13}C NMR spectra of poly(ethylene-*co*-1-butene), containing 8.1% 1-butene, EBH-9.

D.2 CEF of EBH Samples

Following CEF analysis of the ethylene-*co*-1-butene copolymer samples (EBH-1 to EBH-9) made with different comonomer fractions.

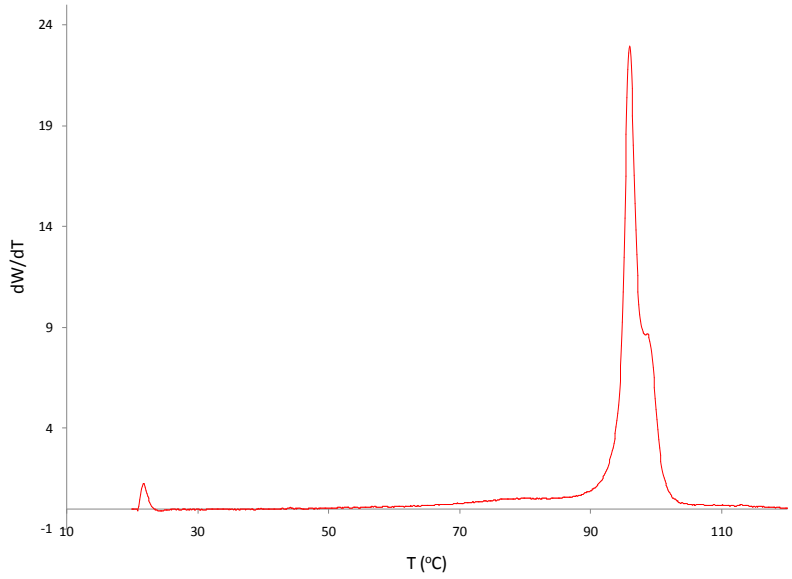

Figure D.10 CEF analysis of poly(ethylene-*co*-1-butene), containing 1.0% 1-butene, EBH-1.

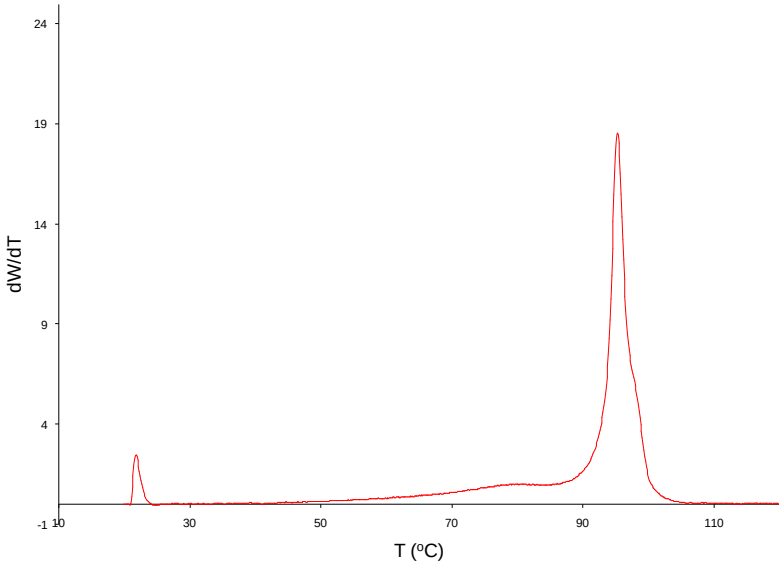

Figure D.11 CEF analysis of poly(ethylene-*co*-1-butene), containing 1.6% 1-butene, EBH-2.

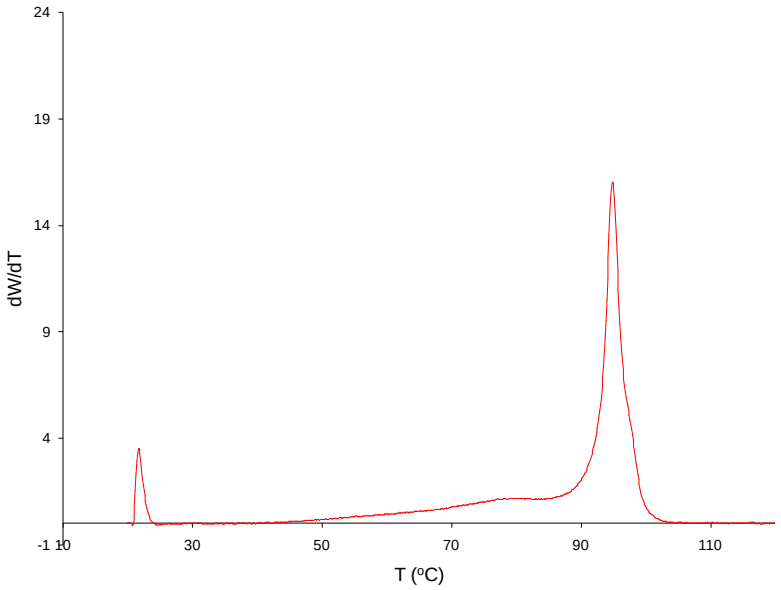

Figure D.12 CEF analysis of poly(ethylene-*co*-1-butene), containing 2.0% 1-butene, EBH-3.

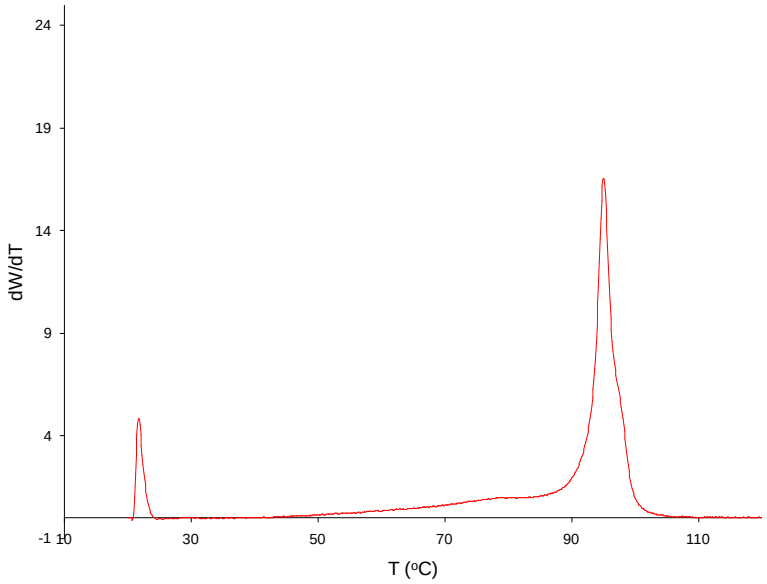

Figure D.13 CEF analysis of poly(ethylene-*co*-1-butene), containing 2.5% 1-butene, EBH-4.

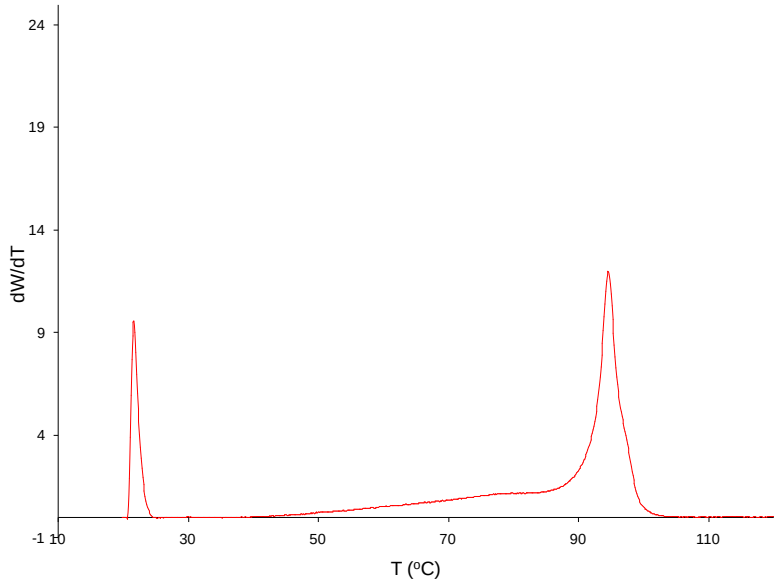

Figure D.14 CEF analysis of poly(ethylene-*co*-1-butene), containing 3.8% 1-butene, EBH-5.

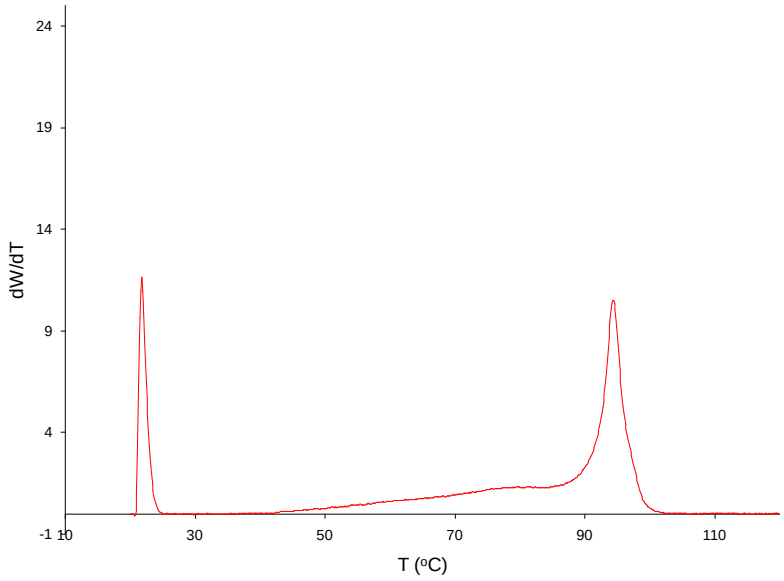

Figure D.15 CEF analysis of poly(ethylene-*co*-1-butene), containing 4.6% 1-butene, EBH-6.

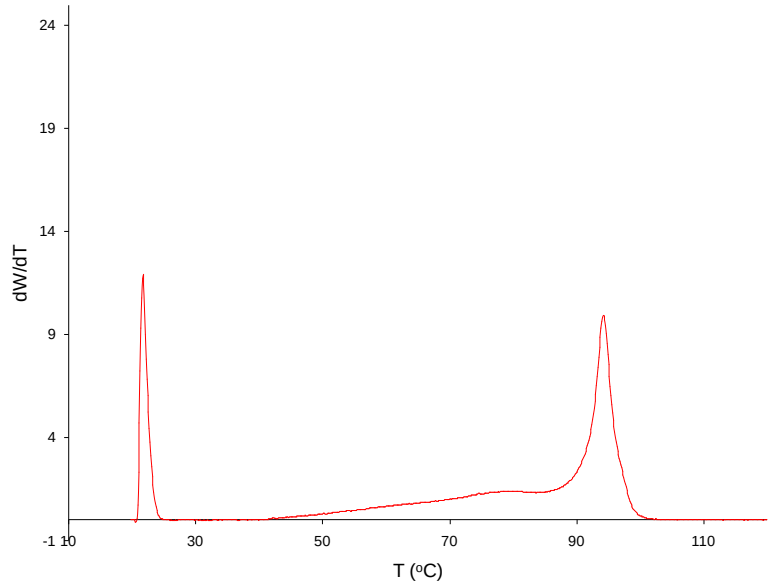

Figure D.16 CEF analysis of poly(ethylene-*co*-1-butene), containing 5.0% 1-butene, EBH-7.

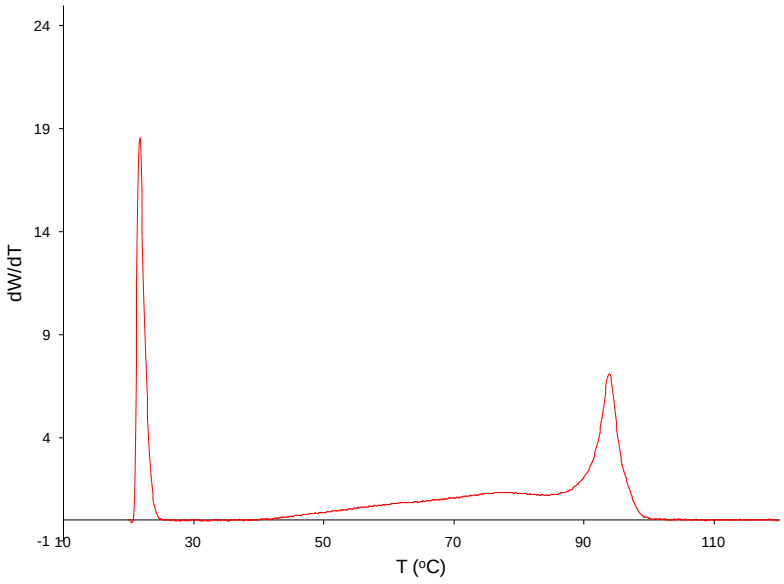

Figure D.17 CEF analysis of poly(ethylene-*co*-1-butene), containing 6.7% 1-butene, EBH-8.

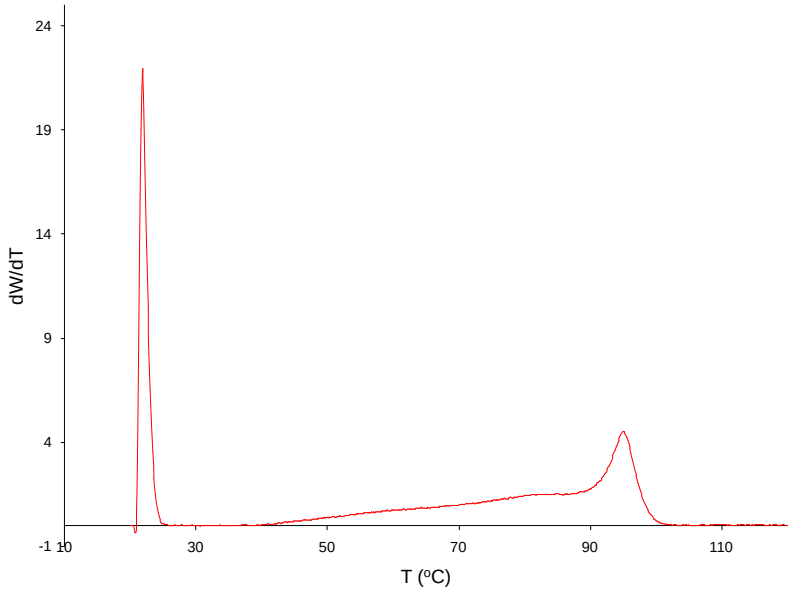

Figure D.18 CEF analysis of poly(ethylene-*co*-1-butene), containing 8.1% 1-butene, EBH-9.

D.3 ^{13}C NMR spectra of EB Samples

^{13}C NMR spectra of ethylene-*co*-1-butene copolymer samples (EB-1 to EB-9) made with different comonomer fractions.

Table D.2 ^{13}C NMR spectra normalized peak intensities for samples (EB-1 to EB-9).

Region	Range (ppm)	Carbon assignment	EB-1	EB-2	EB-3	EB-4	EB-5	EB-6	EB-7	EB-8	EB-9
A	37-40	αα Methylene, $(Methine)_{EBE}$	0.67	0.88	1.11	1.8	2.6	3.29	4.59	5.76	8.41
B	37.4	$(Methine)_{EBB+BBE}$	0.03	0.04	0.03	0.42	0.43	0.6	1.01	1.17	2.67
C	33.5-35.5	αγ, $\alpha\delta^+$, $(Methine)_{BBB}$	1.25	1.52	1.74	2.94	4.35	6.34	7.58	9.92	14.74
D	29.5-31.5	γγ, γ δ^+, δ^+ δ^+	108.36	106.22	103.42	110.04	110.69	111.81	112.94	113.98	117.11
E	26-28	β δ^+, $2B_2$	1.96	2.62	2.8	3.27	5.41	7.97	8.6	12.25	18.12
F	24-25	ββ	0.02	0.15	0.13	0.16	0.33	0.33	0.48	0.75	1.41
G	10.5-11.5	Methyl	0.93	0.14	0.54	1.59	2.76	4.73	5.18	6.81	10.55

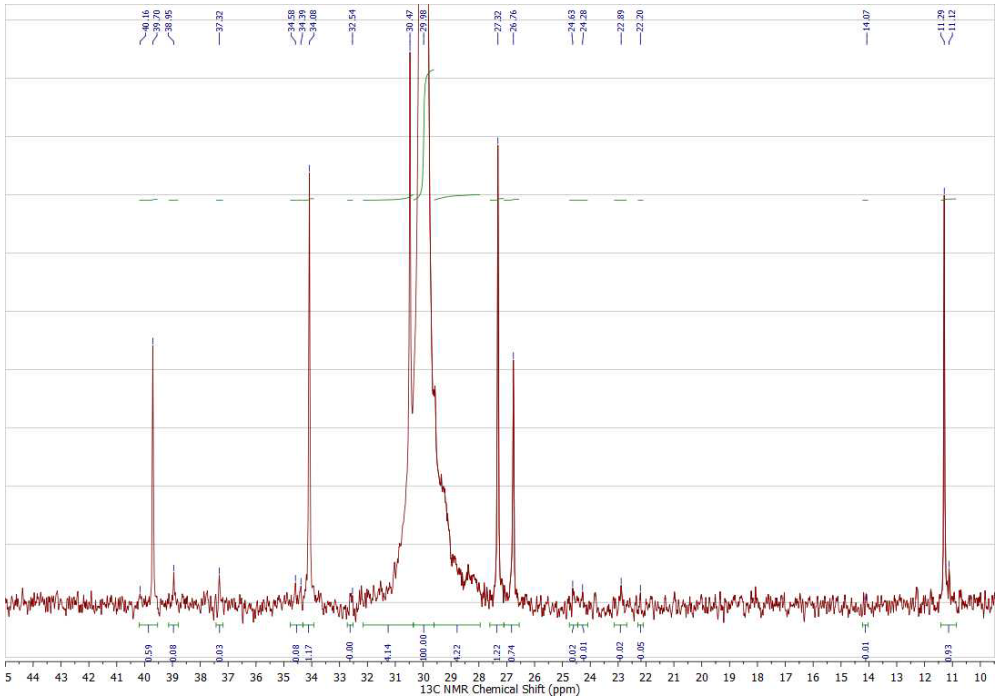

Figure D.19 ^{13}C NMR spectra of poly(ethylene-*co*-1-butene), containing 1.5% 1-butene, EB-1.

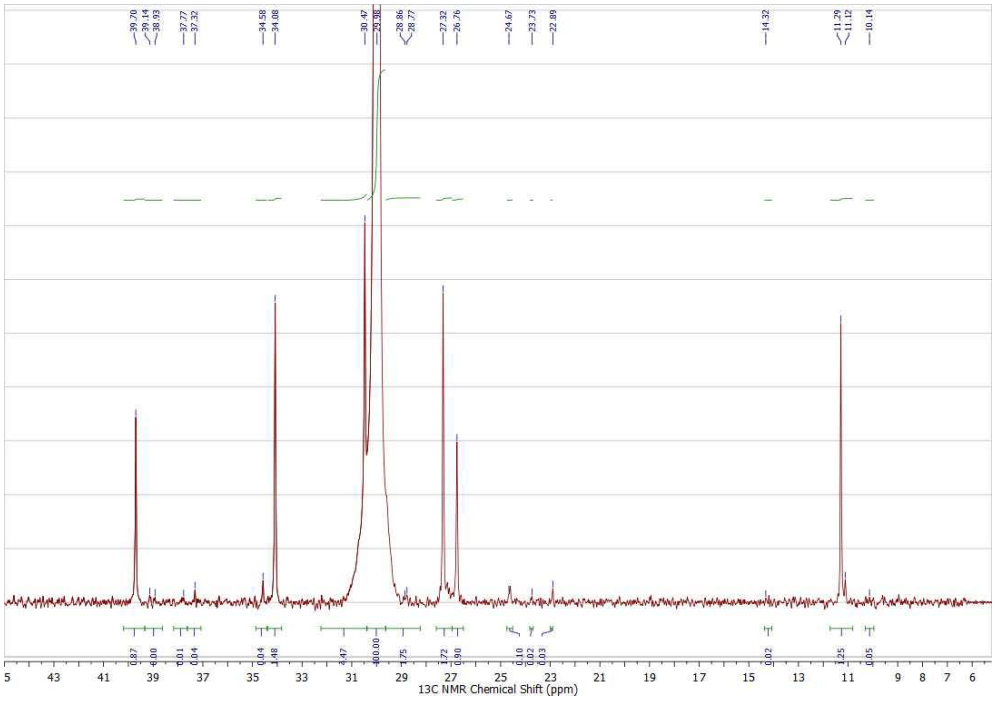

Figure D.20 ^{13}C NMR spectra of poly(ethylene-*co*-1-butene), containing 3.1% 1-butene, EB-2.

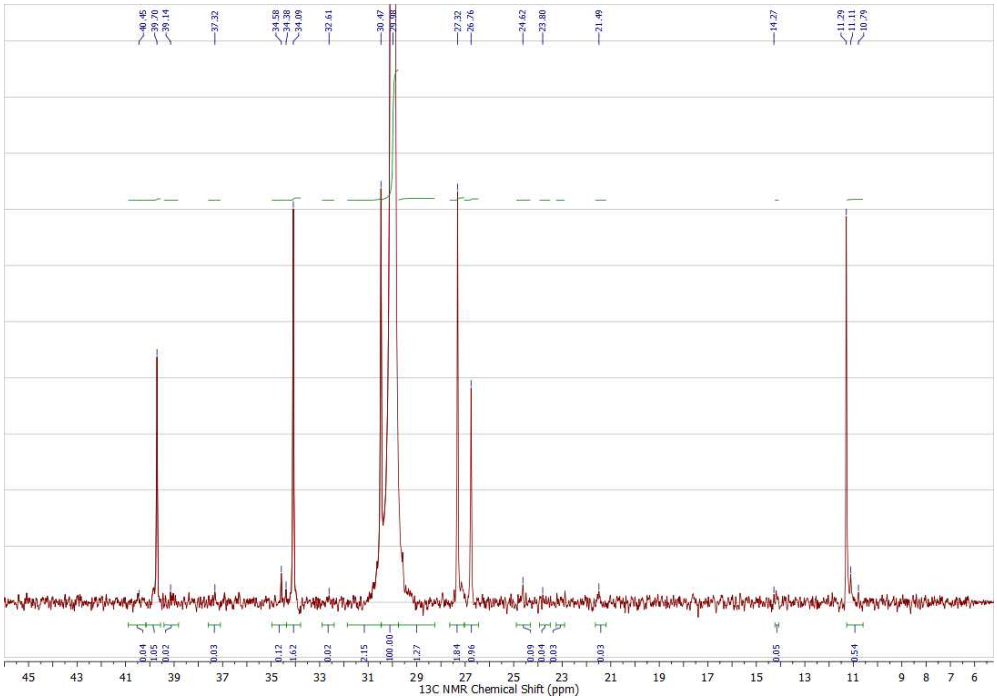

Figure D.21 ^{13}C NMR spectra of poly(ethylene-*co*-1-butene), containing 3.8% 1-butene, EB-3.

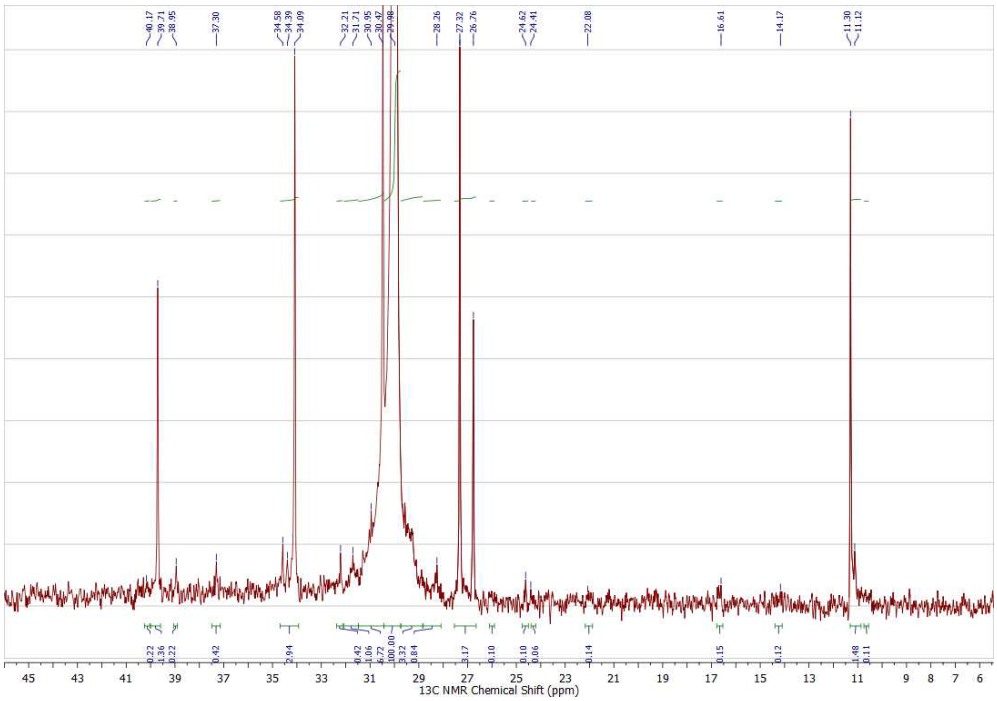

Figure D.22 ^{13}C NMR spectra of poly(ethylene-*co*-1-butene), containing 4.5% 1-butene, EB-4.

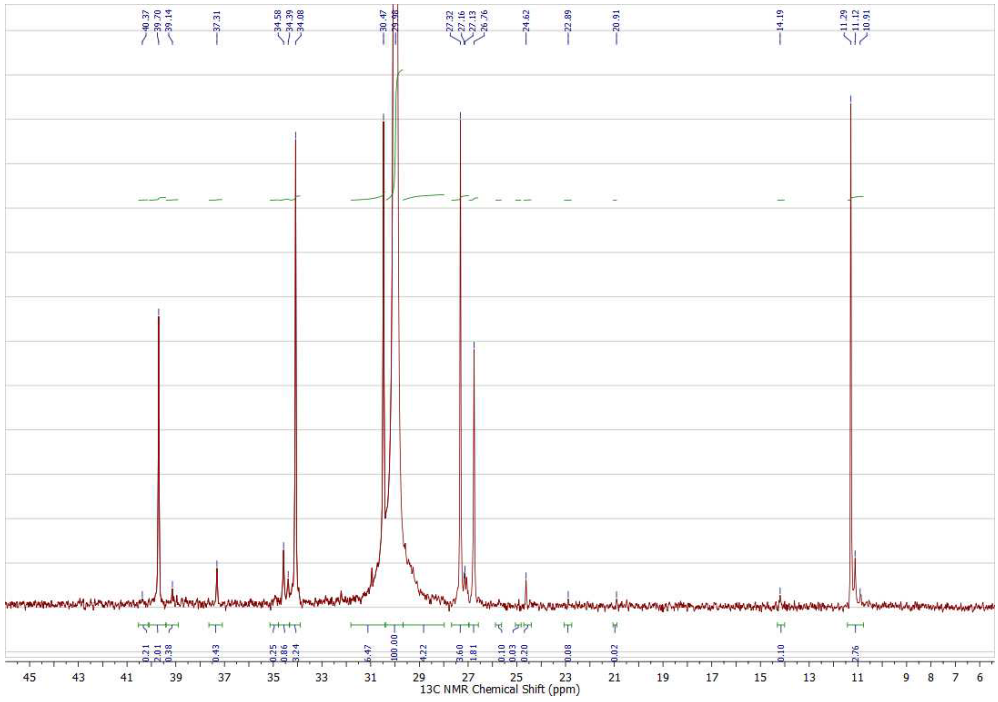

Figure D.23 ^{13}C NMR spectra of poly(ethylene-*co*-1-butene), containing 4.8% 1-butene, EB-5.

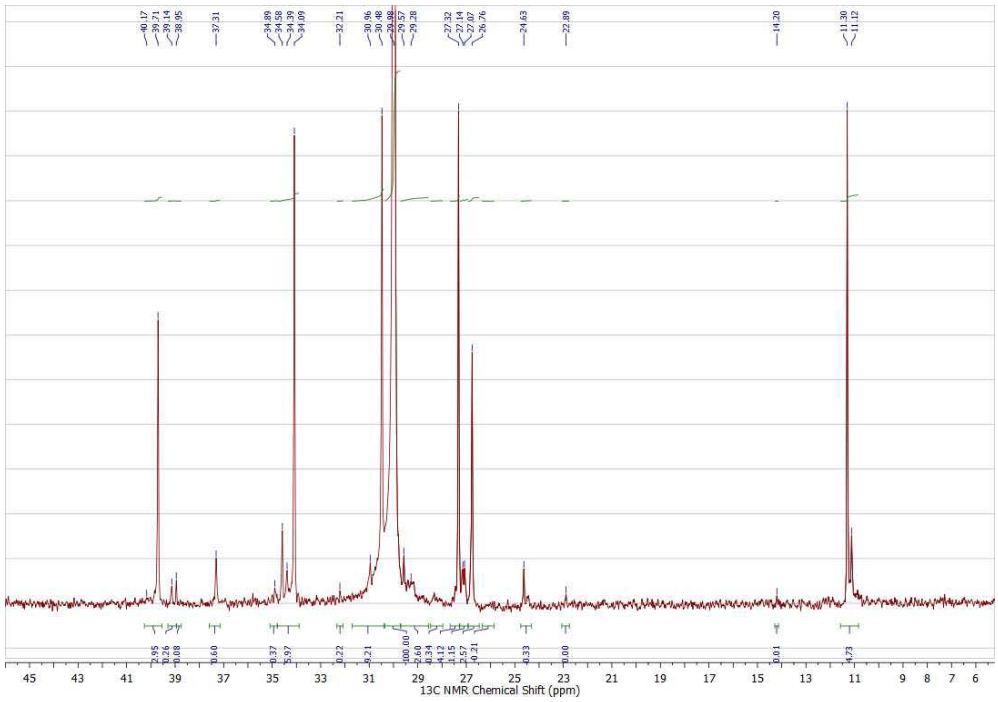

Figure D.24 ^{13}C NMR spectra of poly(ethylene-*co*-1-butene), containing 7.2% 1-butene, EB-6.

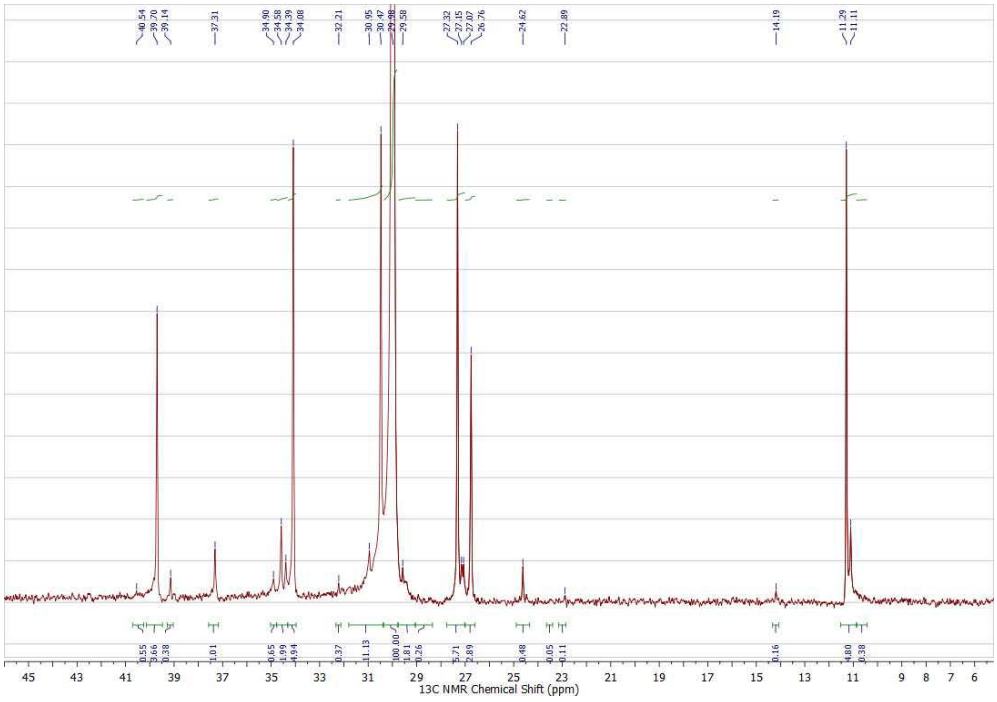

Figure D.25 ^{13}C NMR spectra of poly(ethylene-*co*-1-butene), containing 8.4% 1-butene, EB-7.

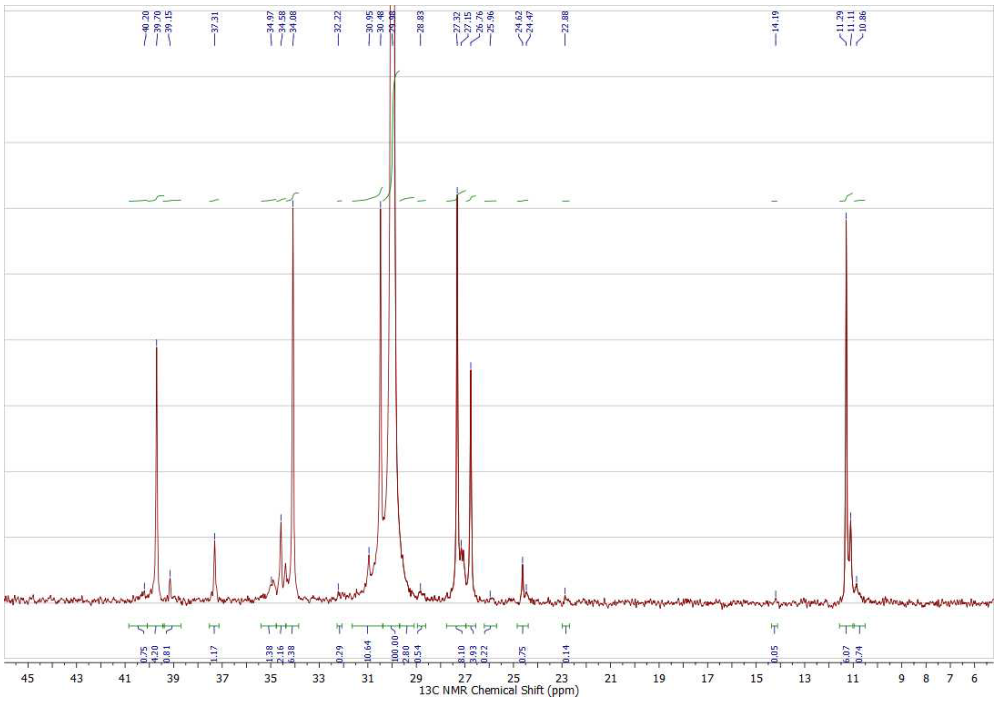

Figure D.26 ^{13}C NMR spectra of poly(ethylene-*co*-1-butene), containing 9.1% 1-butene, EB-8.

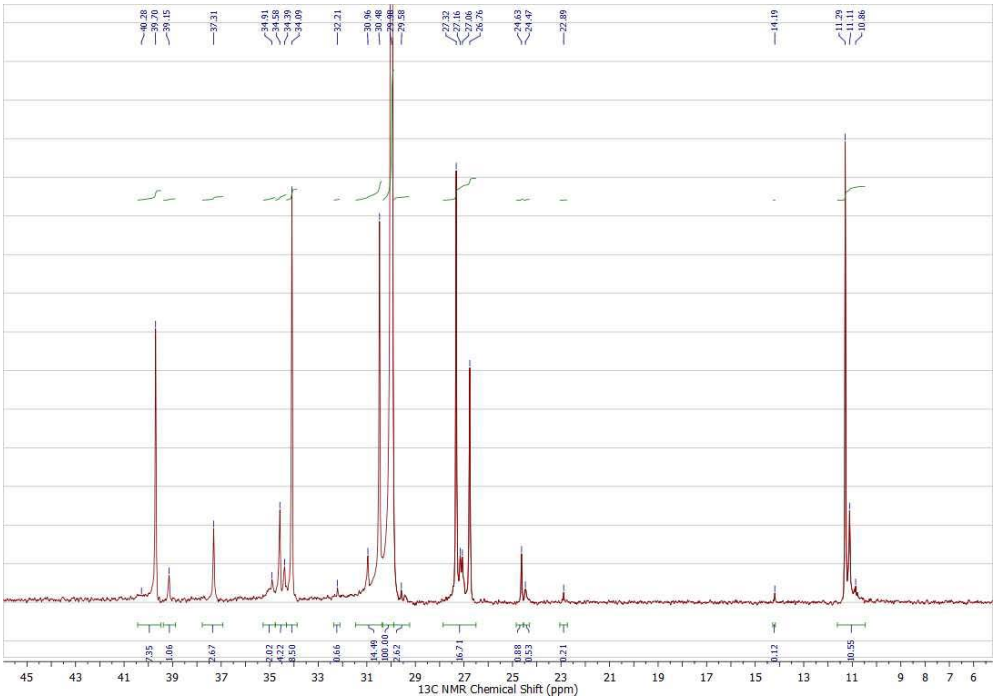

Figure D.27 ^{13}C NMR spectra of poly(ethylene-*co*-1-butene), containing 13.9% 1-butene, EB-9.

Appendix E

E.1 Triads and Tetrads Percentage Absolute Deviations for EBH

Table E.1 Percentage absolute deviations between predicted and EBH sample triad values when all triads are used.

Sample	ΔBBB%	ΔBBA%	ΔABA%	ΔBAB%	ΔAAB%	ΔAAA%
EBH-1	98.2	43.0	41.5	80.0	66.7	1.2
EBH-2	88.0	121.5	81.9	45.3	77.5	3.1
EBH-3	38.4	99.4	38.8	56.3	62.5	3.2
EBH-4	82.6	141.2	75.5	72.8	70.0	4.8
EBH-5	85.1	6.4	23.8	30.8	18.8	1.6
EBH-6	84.3	42.6	8.9	46.7	15.7	1.1
EBH-7	88.2	37.5	14.6	50.2	28.2	1.8
EBH-8	75.0	83.4	19.5	19.4	20.9	3.5
EBH-9	67.0	55.0	0.0	39.1	14.4	1.5
Average	78.5	70.0	33.8	48.9	41.6	2.4

Table E.2 Percentage absolute deviations between predicted and EBH sample triad values when 4 triads are used.

Sample	ΔBBB%	ΔBBA%	ΔABA%	ΔBAB%	ΔAAB%	ΔAAA%
EBH-1	99.2	34.4	3.4	93.2	13.6	0.1
EBH-2	94.8	2.2	22.9	81.4	19.6	0.6
EBH-3	73.0	6.8	5.1	46.1	10.8	0.2
EBH-4	92.8	9.8	16.5	42.8	12.6	0.6
EBH-5	93.1	48.4	13.7	75.3	17.3	2.5
EBH-6	92.9	31.1	24.0	81.0	19.4	3.7
EBH-7	94.5	32.0	18.0	81.7	8.5	3.1
EBH-8	87.6	6.1	15.6	70.1	14.5	4.2
EBH-9	81.8	13.8	22.2	74.3	11.3	5.4
Average	90.0	20.5	15.7	71.8	14.2	2.3

Table E.3 Percentage absolute deviations between predicted and EBH sample triad values when all triads are used, $r_{B,4} = 0$.

Sample	ΔBBB%	ΔBBA%	ΔABA%	ΔBAB%	ΔAAB%	ΔAAA%
EBH-1	98.6	25.6	40.1	84.3	65.0	1.1
EBH-2	90.7	93.7	75.2	58.2	71.2	2.8
EBH-3	51.9	75.1	34.7	20.6	58.1	2.9
EBH-4	86.8	106.7	65.1	28.1	60.4	4.0
EBH-5	88.1	5.1	20.8	45.8	16.3	1.2
EBH-6	87.6	26.4	5.8	58.6	12.8	0.6
EBH-7	90.5	23.4	13.8	60.2	27.5	1.5
EBH-8	79.5	65.6	13.6	37.6	16.2	2.2
EBH-9	71.2	47.3	3.2	47.3	18.4	1.9
Average	82.8	52.1	30.3	49.0	38.4	2.0

Table E.4 Percentage absolute deviations between predicted and EBH sample triad values when 4 triads are used, $r_{B,4} = 0$.

Sample	ΔBBB%	ΔBBA%	ΔABA%	ΔBAB%	ΔAAB%	ΔAAA%
EBH-1	99.2	2.4	38.9	93.4	62.8	1.1
EBH-2	95.2	57.4	75.7	82.0	70.0	2.7
EBH-3	75.1	42.8	34.6	47.9	56.2	2.7
EBH-4	93.4	67.0	62.5	45.3	56.0	3.6
EBH-5	93.6	22.2	21.0	76.1	14.8	0.9
EBH-6	93.4	4.1	6.6	81.7	11.8	0.3
EBH-7	94.9	2.7	15.0	82.3	26.7	1.3
EBH-8	88.5	35.5	14.0	71.2	14.0	1.4
EBH-9	83.1	27.5	8.5	74.9	21.0	2.2
Average	90.7	29.1	30.7	72.8	37.0	1.8

Table E.5 Percentage absolute deviations between predicted and EBH sample 6 triads and 3 tetrads.

Sample	ΔBBB%	ΔBBA%	ΔABA%	ΔBAB%	ΔAAB%	ΔAAA%	ΔABBA%	ΔABAA%	ΔBAAB%
EBH-1	98.2	43.8	44.2	79.1	69.7	1.2	106.4	64.1	79.8
EBH-2	88.3	121.8	83.4	43.1	78.6	3.2	137.4	76.5	7.4
EBH-3	40.0	99.7	40.2	62.5	63.9	3.3	98.9	52.4	32.3
EBH-4	83.1	141.3	76.0	82.2	70.0	4.8	219.9	67.4	58.1
EBH-5	85.5	6.3	24.3	29.3	19.1	1.6	68.0	23.7	35.1
EBH-6	84.8	42.7	9.9	44.8	16.5	1.2	38.3	21.2	75.9
EBH-7	88.5	38.1	16.8	48.3	30.2	2.0	36.9	24.3	76.1
EBH-8	75.7	81.2	16.8	20.4	18.3	3.0	128.5	21.0	51.3
EBH-9	67.6	56.6	3.5	37.8	18.0	2.2	92.7	17.0	56.9
Average	79.1	70.2	35.0	49.7	42.7	2.5	103.0	40.8	52.5

Table E.6 Percentage absolute deviations between predicted and EBH sample 4 triads and 3 tetrads.

Sample	ΔBBB%	ΔBBA%	ΔABA%	ΔBAB%	ΔAAB%	ΔAAA%	ΔABBA%	ΔABAA%	ΔBAAB%
EBH-1	99.4	3.6	20.1	93.1	41.5	0.6	39.0	37.8	89.7
EBH-2	96.0	48.6	48.7	81.4	45.5	1.7	60.6	45.3	47.2
EBH-3	79.5	34.5	14.9	46.2	35.0	1.6	35.4	27.1	65.9
EBH-4	94.3	56.3	38.4	43.8	34.8	2.2	110.6	34.8	80.7
EBH-5	94.8	25.8	3.9	75.3	0.2	0.6	18.8	5.6	65.2
EBH-6	94.5	2.3	9.3	81.1	3.1	1.6	3.9	2.5	87.4
EBH-7	95.8	4.6	1.4	81.7	10.6	0.7	3.9	7.6	86.9
EBH-8	90.6	33.4	2.3	70.4	0.7	1.1	70.9	4.5	72.7
EBH-9	86.6	16.8	7.8	73.8	5.8	1.3	45.1	7.3	71.8
Average	92.4	25.1	16.3	71.9	19.7	1.3	43.1	19.1	74.2

Table E.7 Percentage absolute deviations between predicted and EBH sample triad values when all triads are used, four site type model with 4th site is homopolymer.

Sample	ΔBBB%	ΔBBA%	ΔABA%	ΔBAB%	ΔAAB%	ΔAAA%
EBH-1	98.9	9.2	27.9	88.1	50.9	0.8
EBH-2	92.9	62.0	58.1	69.2	54.7	2.1
EBH-3	63.0	48.3	22.0	10.4	43.4	2.0
EBH-4	90.5	65.9	45.5	10.5	41.6	2.6
EBH-5	90.9	20.3	9.2	60.0	5.3	0.1
EBH-6	90.6	6.1	4.1	69.4	2.4	0.8
EBH-7	92.6	6.3	4.5	69.8	17.5	0.2
EBH-8	84.4	36.2	1.4	55.1	4.0	0.5
EBH-9	76.2	32.2	2.2	57.0	12.8	0.3
Average	86.7	31.8	19.4	54.4	25.8	1.0

Table E.8 Percentage absolute deviations between predicted and EBH sample triad values when 4 triads are used, four site type model with 4th site is homopolymer.

Sample	ΔBBB%	ΔBBA%	ΔABA%	ΔBAB%	ΔAAB%	ΔAAA%
EBH-1	99.3	41.4	59.1	91.2	87.3	1.6
EBH-2	95.6	107.0	91.9	77.7	87.3	3.5
EBH-3	76.6	88.9	47.7	34.6	73.3	3.7
EBH-4	93.8	108.4	70.9	34.2	66.3	4.4
EBH-5	94.1	0.7	31.7	70.1	26.6	2.2
EBH-6	93.9	33.8	14.7	77.4	22.2	1.7
EBH-7	95.2	34.8	26.4	77.6	41.4	3.2
EBH-8	90.0	66.3	16.8	66.2	19.6	2.7
EBH-9	84.4	67.6	18.9	68.1	35.5	5.8
Average	91.4	61.0	42.0	66.3	51.1	3.2

Table E.9 Percentage absolute deviations between predicted and EBH sample triad values when only triad deconvolution model is used, 4 triads.

Sample	ΔBBB%	ΔBBA%	ΔABA%	ΔBAB%	ΔAAB%	ΔAAA%
EBH-1	89.9	620.6	297.9	35.0	372.0	8.5
EBH-2	37.4	804.7	349.0	190.8	341.6	15.0
EBH-3	52.5	605.4	250.6	643.4	306.1	17.7
EBH-4	42.4	685.7	283.7	612.7	273.0	20.1
EBH-5	39.6	277.5	213.8	272.8	194.6	21.8
EBH-6	44.1	339.2	152.5	154.5	162.5	21.6
EBH-7	65.7	387.5	178.1	153.5	205.0	26.0
EBH-8	61.8	483.7	132.0	226.1	137.4	30.7
EBH-9	10.5	451.9	118.0	207.3	143.4	38.9
Average	49.3	517.4	219.5	277.4	237.3	22.2

Table E.10 Percentage absolute deviations between predicted and EBH sample triad values with simultaneous IDEM, 4 triads.

Sample	ΔBBB%	ΔBBA%	ΔABA%	ΔBAB%	ΔAAB%	ΔAAA%
EBH-1	99.5	33.4	3.0	92.8	14.1	0.1
EBH-2	96.9	7.5	18.9	82.4	15.4	0.4
EBH-3	83.5	14.9	8.0	48.7	7.1	0.0
EBH-4	96.1	10.7	8.4	51.2	4.0	0.0
EBH-5	95.8	52.9	16.1	76.4	20.0	2.8
EBH-6	95.3	34.2	24.8	81.4	20.5	3.8
EBH-7	95.3	22.1	14.2	79.1	3.9	2.5
EBH-8	92.0	11.8	16.8	71.0	16.1	4.6
EBH-9	83.0	8.3	16.7	68.0	3.5	3.5
Average	93.0	21.8	14.1	72.3	11.6	2.0

E.2 Triads Percentage Absolute Deviations, EB

Table E.11 Percentage absolute deviations between predicted and EB sample triad values when 3 triads are used.

Sample	ΔBBB%	ΔBBA%	ΔABA%	ΔBAB%	ΔAAB%	ΔAAA%
EB-1	4.7	1504.1	25.1	13.8	80.6	2.6
EB-2	15.5	1918.4	40.1	79.1	0.9	1.7
EB-3	45.0	3136.8	50.6	69.6	21.4	2.8
EB-4	42.3	198.0	13.9	66.9	94.3	4.0
EB-5	40.0	252.9	24.6	79.9	39.6	2.1
EB-6	49.5	198.6	25.5	75.5	5.3	0.7
EB-7	41.5	119.7	45.0	77.9	38.6	0.7
EB-8	12.7	145.7	57.4	80.6	3.5	1.7
EB-9	2.5	42.0	64.7	85.4	8.7	6.9
Average	28.2	835.1	38.5	69.9	32.5	2.6

Table E.12 Percentage absolute deviations between predicted and EB sample triad values when 3 triads and F_A are used.

Sample	ΔBBB%	ΔBBA%	ΔABA%	ΔBAB%	ΔAAB%	ΔAAA%
EB-1	1.1	1586.9	30.7	5.8	88.8	2.9
EB-2	13.1	2001.7	45.4	77.4	4.7	2.0
EB-3	43.6	3263.3	56.3	67.3	26.0	3.2
EB-4	41.4	206.9	17.6	64.8	100.2	4.3
EB-5	39.2	262.4	22.3	78.7	43.5	2.5
EB-6	48.7	207.5	23.2	73.9	2.5	0.2
EB-7	40.0	128.3	43.1	76.3	43.4	1.3
EB-8	10.9	153.8	56.0	79.2	6.7	1.1
EB-9	7.2	49.6	63.3	84.0	4.8	5.7
Average	27.2	873.4	39.8	67.5	35.6	2.6

Appendix F

The percentage absolute deviations for the EBH and EB samples using triad distributions predicted by Dow Chemical Company are presented in this appendix.

Table F.1 Percentage absolute deviations between predicted and EBH sample triad values when all triads are used.

Sample	ΔBBA%	ΔABA%	ΔAAB%	ΔAAA%
EBH-1	43.2	113.9	102.5	3.0
EBH-2	95.8	110.9	104.5	5.7
EBH-3	81.4	88.3	83.9	6.4
EBH-4	75.8	126.7	102.8	8.8
EBH-5	1.3	41.8	50.5	5.3
EBH-6	16.8	42.8	54.8	6.6
EBH-7	9.8	42.7	55.6	7.2
EBH-8	129.1	60.1	68.9	12.2
EBH-9	34.6	34.9	49.8	11.2
Average	54.2	73.6	74.8	7.4

Table F.2 Percentage absolute deviations between predicted and EBH sample triads using 4 triads.

Sample	ΔBBA%	ΔABA%	ΔAAB%	ΔAAA%
EBH-1	54.9	32.3	27.8	0.8
EBH-2	59.1	37.5	38.1	2.0
EBH-3	48.1	22.2	24.5	1.9
EBH-4	41.2	53.2	44.2	3.7
EBH-5	16.0	6.0	5.3	0.4
EBH-6	2.2	5.5	8.9	0.0
EBH-7	8.3	8.2	7.0	0.4
EBH-8	111.7	16.8	33.7	5.5
EBH-9	17.5	15.3	4.0	1.0
Average	39.9	21.9	21.5	1.7

Table F.3 Percentage absolute deviations between predicted and EB sample triad values when all triads are used.

Sample	ΔBBA%	ΔABA%	ΔAAB%	ΔAAA%
EB-1	104.9	88.0	84.3	3.6
EB-2	143.2	79.2	83.6	5.0
EB-3	382.6	63.3	72.4	5.4
EB-4	206.4	76.5	89.9	6.6
EB-5	142.2	24.1	30.9	4.2
EB-6	64.4	14.6	4.2	0.2
EB-7	28.7	11.4	5.2	0.4
EB-8	35.1	24.6	0.5	1.7
EB-9	7.0	33.0	11.8	7.9
Average	123.8	46.1	42.5	3.9

Table F.4 Percentage absolute deviations between predicted and EB sample triad values using 4 triads.

Sample	ΔBBA%	ΔABA%	ΔAAB%	ΔAAA%
EB-1	7.7	62.6	54.8	2.3
EB-2	28.7	61.0	57.9	3.4
EB-3	171.5	49.4	50.2	3.7
EB-4	79.3	62.5	65.8	4.7
EB-5	40.5	16.3	15.4	2.1
EB-6	6.6	19.2	7.8	2.2
EB-7	32.4	15.2	7.0	2.5
EB-8	30.0	25.7	10.9	5.0
EB-9	61.6	31.2	19.7	11.9
Average	50.9	38.1	32.2	4.2

Table F.5 Percentage absolute deviations between predicted and EB sample triad values when 3 triads are used (BBA are calculated from estimated reactivity ratios).

Sample	ΔBBA%	ΔABA%	ΔAAB%	ΔAAA%
EB-1	6.95	34.43	29.89	1.23
EB-2	27.50	33.23	33.25	2.01
EB-3	169.15	24.00	27.56	2.16
EB-4	77.88	35.69	42.06	3.09
EB-5	39.33	2.96	0.97	0.22
EB-6	7.46	32.68	20.94	4.27
EB-7	33.10	29.74	20.55	5.04
EB-8	30.76	38.40	23.56	7.91
EB-9	62.36	43.61	32.07	15.92
Average	50.5	30.5	25.6	4.6

Appendix G

G.1 Hierarchical Experiment Calculations

The hierarchical experiment calculations are presented in this appendix. First table describes the weight-average molecular weight results. The triad and tetrad distribution results are shown in Table G.2 to G.10.

Table G.6 Weight-average molecular weight results measured by GPC in 4 × 2 × 3.

Poly (p)	Sample (s)	Test (t)	y_{pst}	Avg y_{ps}	Avg y_p	Avg y	$(\text{Avg } y_{ps} - \text{Avg } y_p)^2$	$(y_{pst}-\text{Avg } y)^2$
A	1	1	76563	72964	76959	79682	15960025	9727381
		2	72367					53507396
		3	69962					94475970
	2	1	75982	80954			15960025	13689075
		2	70371					86692393
		3	96509					283152136
B	1	1	63726	80198	85776		31106647	254589947
		2	90295					112638422
		3	86574					47501387
	2	1	91826	91353			31106647	147479772
		2	93044					178546385
		3	89189					90385426
C	1	1	67975	71422	72727		1702155	137050922
		2	72456					52213270
		3	73836					34174255
	2	1	68909	74032			1702155	116054836
		2	82919					10478978
		3	70267					88639871
D	1	1	74273	80012	83266		10587431	29255929
		2	80941					1585396
		3	84822					26420885
	2	1	83343	86520			10587431	13403836
		2	87699					64274293
		3	88517					78059434
			1912365				*118712517*	*2023997595*

Table G.7 BBB results measured by ^{13}C NMR in 4 × 2 × 3.

Poly (p)	Sample (s)	Test (t)	y_{pst}	Avg y_{ps}	Avg y_p	Avg y	(Avg y_{ps} - Avg y_p)^2	(y_{pst}-Avg y)^2
A	1	1	2.40	2.88	2.33	2.19	0.30	0.05
		2	3.38					1.41
		3	2.85					0.44
	2	1	2.10	1.79			0.30	0.01
		2	1.03					1.35
		3	2.24					0.00
B	1	1	2.86	2.50	2.79		0.08	0.45
		2	2.48					0.08
		3	2.17					0.00
	2	1	2.33	3.07			0.08	0.02
		2	3.79					2.55
		3	3.10					0.82
C	1	1	1.12	1.17	1.67		0.25	1.15
		2	0.98					1.47
		3	1.42					0.59
	2	1	2.17	2.17			0.25	0.00
		2	1.25					0.87
		3	3.08					0.80
D	1	1	1.69	2.68	1.97		0.50	0.25
		2	2.89					0.49
		3	3.45					1.59
	2	1	1.40	1.26			0.50	0.62
		2	1.21					0.96
		3	1.16					1.06
			52.53				*2.26*	*17.03*

Table G.8 ABB results measured by ^{13}C NMR in 4 × 2 × 3.

Poly (p)	Sample (s)	Test (t)	y_{pst}	Avg y_{ps}	Avg y_p	Avg y	(Avg y_{ps} - Avg y_p)^2	(y_{pst}-Avg y)^2
A	1	1	2.66	2.66	2.50	2.51	0.02	0.02
		2	2.70					0.04
		3	2.61					0.01
	2	1	2.26	2.34			0.02	0.07
		2	2.42					0.01
		3	2.36					0.02
B	1	1	2.23	2.17	2.13		0.00	0.08
		2	2.12					0.15
		3	2.16					0.13
	2	1	2.03	2.10			0.00	0.23
		2	2.13					0.15
		3	2.14					0.14
C	1	1	2.08	2.28	2.49		0.04	0.19
		2	2.23					0.08
		3	2.54					0.00
	2	1	2.63	2.70			0.04	0.01
		2	2.60					0.01
		3	2.87					0.13
D	1	1	2.65	2.71	2.93		0.05	0.02
		2	2.83					0.10
		3	2.66					0.02
	2	1	3.15	3.15			0.05	0.41
		2	2.97					0.20
		3	3.33					0.66
			60.33				*0.23*	*2.88*

Table G.9 ABA results measured by ^{13}C NMR in 4 × 2 × 3.

Poly (p)	Sample (s)	Test (t)	y_{pst}	Avg y_{ps}	Avg y_p	Avg y	$(\text{Avg } y_{ps} - \text{Avg } y_p)^2$	$(y_{pst}-\text{Avg } y)^2$
A	1	1	7.14	6.82	7.04	7.14	0.05	0.00
		2	6.65					0.24
		3	6.68					0.21
	2	1	6.62	7.26			0.05	0.27
		2	8.43					1.67
		3	6.73					0.17
B	1	1	5.75	6.16	5.85		0.09	1.92
		2	6.30					0.70
		3	6.41					0.53
	2	1	6.22	5.54			0.09	0.84
		2	5.27					3.49
		3	5.14					4.00
C	1	1	7.53	7.90	7.74		0.03	0.15
		2	8.28					1.29
		3	7.90					0.58
	2	1	7.72	7.58			0.03	0.34
		2	8.51					1.89
		3	6.49					0.42
D	1	1	8.57	6.99	7.93		0.87	2.03
		2	6.45					0.48
		3	5.97					1.37
	2	1	8.51	8.86			0.87	1.88
		2	9.32					4.74
		3	8.75					2.61
			171.34				*2.07*	*31.82*

Table G.10 BAB results measured by ^{13}C NMR in 4 × 2 × 3.

Poly (p)	Sample (s)	Test (t)	y_{pst}	Avg y_{ps}	Avg y_p	Avg y	$(\text{Avg } y_{ps} - \text{Avg } y_p)^2$	$(y_{pst}-\text{Avg } y)^2$
A	1	1	2.05	2.06	2.00	1.91	0.00	0.02
		2	2.12					0.04
		3	2.01					0.01
	2	1	1.86	1.95			0.00	0.00
		2	2.18					0.07
		3	1.81					0.01
B	1	1	1.54	1.57	1.47		0.01	0.13
		2	1.57					0.11
		3	1.58					0.11
	2	1	1.50	1.36			0.01	0.17
		2	1.33					0.34
		3	1.26					0.42
C	1	1	1.63	1.89	1.96		0.00	0.08
		2	2.09					0.03
		3	1.96					0.00
	2	1	2.03	2.03			0.00	0.02
		2	2.08					0.03
		3	1.97					0.00
D	1	1	2.41	2.01	2.21		0.04	0.25
		2	1.89					0.00
		3	1.71					0.04
	2	1	2.33	2.41			0.04	0.18
		2	2.38					0.22
		3	2.52					0.37
			45.81				*0.12*	*2.65*

Table G.11 BAA results measured by ^{13}C NMR in 4 × 2 × 3.

Poly (p)	Sample (s)	Test (t)	y_{pst}	Avg y_{ps}	Avg y_p	Avg y	(Avg y_{ps} - Avg y_p)^2	(y_{pst}-Avg y)^2
A	1	1	14.82	14.23	14.02	14.26	0.04	0.32
		2	13.45					0.65
		3	14.41					0.02
	2	1	13.17	13.81			0.04	1.18
		2	14.58					0.10
		3	13.68					0.33
B	1	1	12.84	13.00	12.90		0.01	2.00
		2	12.74					2.31
		3	13.41					0.73
	2	1	13.01	12.81			0.01	1.57
		2	12.37					3.56
		3	13.05					1.47
C	1	1	15.00	14.85	14.74		0.01	0.55
		2	14.18					0.01
		3	15.38					1.25
	2	1	14.34	14.63			0.01	0.01
		2	15.18					0.85
		3	14.38					0.01
D	1	1	14.28	14.46	15.37		0.84	0.00
		2	14.41					0.02
		3	14.67					0.17
	2	1	16.34	16.29			0.84	4.32
		2	16.17					3.66
		3	16.35					4.36
			342.21				*1.80*	*29.47*

Table G.12 AAA results measured by ^{13}C NMR in 4 × 2 × 3.

Poly (p)	Sample (s)	Test (t)	y_{pst}	Avg y_{ps}	Avg y_p	Avg y	(Avg y_{ps} - Avg y_p)^2	(y_{pst}-Avg y)^2
A	1	1	70.93	71.36	72.11	71.99	0.56	1.11
		2	71.70					0.08
		3	71.44					0.30
	2	1	74.00	72.85			0.56	4.03
		2	71.37					0.38
		3	73.19					1.43
B	1	1	74.77	74.61	74.86		0.06	7.71
		2	74.78					7.81
		3	74.27					5.22
	2	1	74.91	75.12			0.06	8.52
		2	75.11					9.76
		3	75.32					11.11
C	1	1	72.64	71.90	71.40		0.25	0.42
		2	72.25					0.06
		3	70.81					1.39
	2	1	71.11	70.90			0.25	0.78
		2	70.38					2.61
		3	71.20					0.62
D	1	1	70.40	71.15	69.60		2.42	2.54
		2	71.54					0.21
		3	71.53					0.21
	2	1	68.27	68.04			2.42	13.87
		2	67.96					16.25
		3	67.90					16.77
			1727.78				*6.60*	*113.20*

Table G.13 ABBA results measured by ^{13}C NMR in 4 × 2 × 3.

Poly (p)	Sample (s)	Test (t)	y_{pst}	Avg y_{ps}	Avg y_p	Avg y	(Avg y_{ps} - Avg y_p)^2	(y_{pst}-Avg y)^2
A	1	1	1.03	1.05	1.00	0.96	0.00	0.01
		2	1.03					0.00
		3	1.08					0.02
	2	1	0.84	0.96			0.00	0.01
		2	1.07					0.01
		3	0.96					0.00
B	1	1	0.80	0.79	0.78		0.00	0.02
		2	0.82					0.02
		3	0.75					0.04
	2	1	0.71	0.76			0.00	0.06
		2	0.82					0.02
		3	0.76					0.04
C	1	1	0.82	0.80	0.92		0.01	0.02
		2	0.76					0.04
		3	0.83					0.02
	2	1	1.15	1.04			0.01	0.04
		2	1.01					0.00
		3	0.98					0.00
D	1	1	1.05	1.06	1.13		0.00	0.01
		2	0.96					0.00
		3	1.15					0.04
	2	1	1.12	1.20			0.00	0.03
		2	1.18					0.05
		3	1.28					0.10
			22.99				*0.04*	*0.60*

Table G.14 ABAA results measured by ^{13}C NMR in 4 × 2 × 3.

Poly (p)	Sample (s)	Test (t)	y_{pst}	Avg y_{ps}	Avg y_p	Avg y	(Avg y_{ps} - Avg y_p)^2	(y_{pst}-Avg y)^2
A	1	1	12.62	12.56	12.19	12.12	0.14	0.25
		2	12.36					0.06
		3	12.71					0.34
	2	1	11.44	11.82			0.14	0.47
		2	12.57					0.20
		3	11.45					0.45
B	1	1	11.28	11.46	10.95		0.26	0.71
		2	11.38					0.55
		3	11.72					0.16
	2	1	10.95	10.44			0.26	1.37
		2	10.40					2.95
		3	9.95					4.72
C	1	1	12.31	12.32	12.51		0.04	0.03
		2	12.55					0.18
		3	12.11					0.00
	2	1	12.63	12.71			0.04	0.26
		2	12.94					0.67
		3	12.55					0.18
D	1	1	12.51	12.10	12.84		0.55	0.15
		2	12.05					0.00
		3	11.72					0.16
	2	1	13.26	13.58			0.55	1.29
		2	13.94					3.32
		3	13.52					1.97
			290.92				*1.97*	*20.44*

Table G.15 BAAB results measured by ^{13}C NMR in 4 × 2 × 3.

Poly (p)	Sample (s)	Test (t)	y_{pst}	Avg y_{ps}	Avg y_p	Avg y	(Avg y_{ps} - Avg y_p)^2	(y_{pst}-Avg y)^2
A	1	1	2.03	2.03	1.82	1.98	0.05	0.00
		2	1.92					0.00
		3	2.15					0.03
	2	1	1.64	1.61			0.05	0.11
		2	1.50					0.23
		3	1.67					0.09
B	1	1	1.93	1.95	2.06		0.01	0.00
		2	2.12					0.02
		3	1.80					0.03
	2	1	2.19	2.17			0.01	0.04
		2	2.44					0.21
		3	1.87					0.01
C	1	1	1.84	1.73	1.95		0.04	0.02
		2	1.69					0.09
		3	1.68					0.09
	2	1	1.94	2.16			0.04	0.00
		2	2.09					0.01
		3	2.44					0.21
D	1	1	2.15	2.07	2.09		0.00	0.03
		2	1.94					0.00
		3	2.11					0.02
	2	1	2.31	2.11			0.00	0.11
		2	2.08					0.01
		3	1.95					0.00
			47.50				*0.20*	*1.38*

G.2 ^{13}C NMR spectra of Replicate Samples

In Appendix G.2 we present the ^{13}C NMR spectra of the (ethylene-*co*-1-butene) copolymer samples.

Table G.16 ^{13}C NMR spectra normalized peak intensities for the replicates of sample 1.

Region	Range (ppm)	A.1.1	A.1.2	A.1.3	B.1.1	B.1.2	B.1.3	C.1.1	C.1.2	C.1.3	D.1.1	D.1.2	D.1.3
A	37-40	7.28	7.58	7.22	6.24	6.31	6.22	6.34	6.84	7.09	7.83	7.15	7.15
B	37.4	1.78	1.8	1.74	1.43	1.36	1.39	1.36	1.47	1.7	1.79	1.88	1.77
C	33.5-35.5	14.28	14.03	14.18	12.05	11.78	12.07	12.69	12.76	13.87	14.06	14.03	14.33
D	29.5-31.5	100	100	100	100	100	100	100	100	100	100	100	100
E	26-28	18.1	17.44	17.69	15.19	15.16	15.55	16.84	16.93	18.24	18.38	17.68	17.79
F	24-25	1.37	1.41	1.34	0.99	1.01	1.02	1.07	1.38	1.31	1.63	1.26	1.14
G	10.5-11.5	11.57	11.86	11.25	9.81	9.4	9.9	10.25	10.84	11.31	11.57	11.61	11.32

Table G.17 ^{13}C NMR spectra normalized peak intensities for the replicates of sample 2.

Region	Range (ppm)	A.2.1	A.2.2	A.2.3	B.2.1	B.2.2	B.2.3	C.2.1	C.2.2	C.2.3	D.2.1	D.2.2	D.2.3
A	37-40	6.37	7.11	6.62	6.12	6.47	5.92	7.5	7.46	7.36	7.94	8.34	8.00
B	37.4	1.46	1.61	1.54	1.3	1.36	1.36	1.76	1.75	1.92	2.18	2.06	2.29
C	33.5-35.5	12.28	13.3	12.75	11.73	12.03	11.87	13.77	13.88	14.31	15.48	15.37	15.58
D	29.5-31.5	100	100	100	100	100	100	100	100	100	100	100	100
E	26-28	15.62	17.63	16.32	15.09	15.06	14.9	17.98	18.57	17.93	20.32	20.6	20.47
F	24-25	1.2	1.45	1.18	0.96	0.85	0.8	1.36	1.4	1.32	1.61	1.65	1.73
G	10.5-11.5	10.25	11.36	10.25	9.43	9.48	9.71	11.22	11.59	12.05	12.43	12.81	12.84

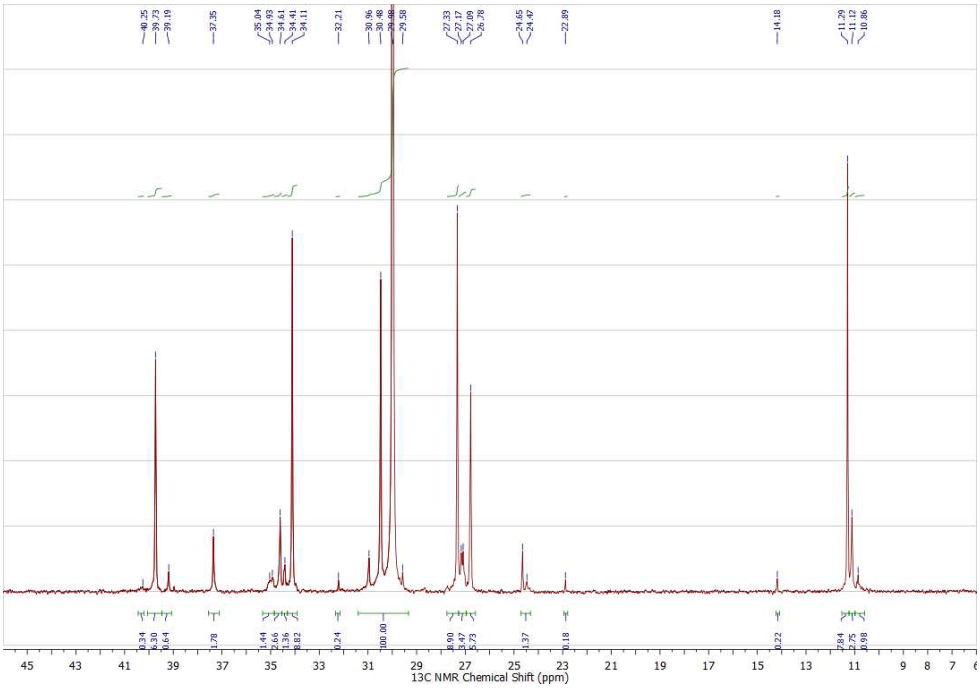

Figure G.1 ^{13}C NMR spectrum of poly(ethylene-*co*-1-butene) replicate sample A.1.1.

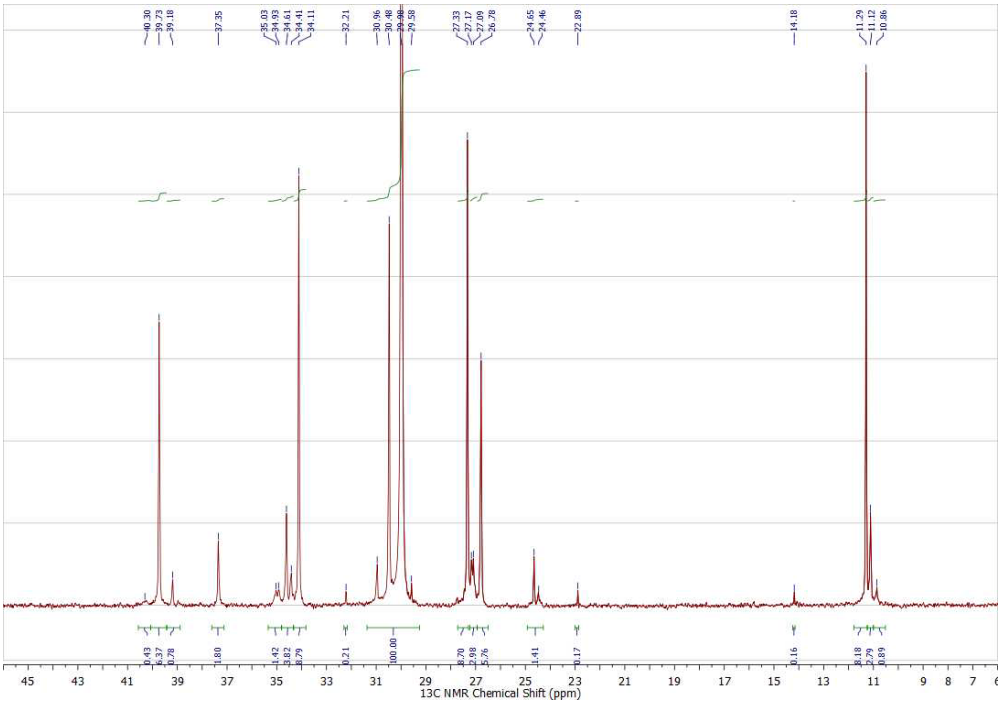

Figure G.2 ^{13}C NMR spectrum of poly(ethylene-*co*-1-butene) replicate sample A.1.2.

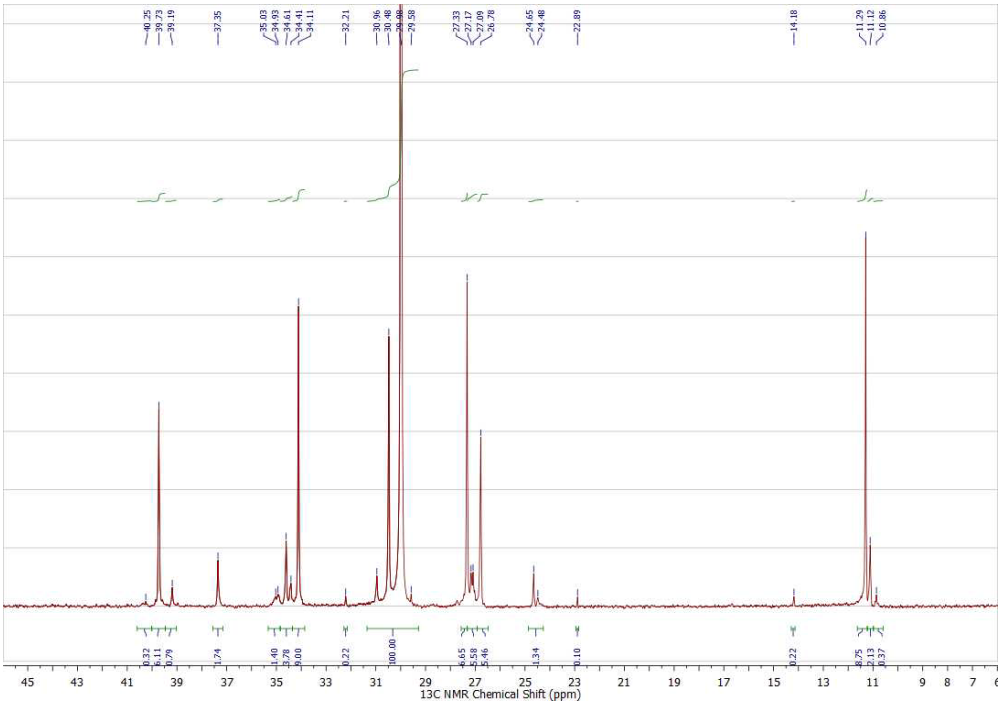

Figure G.3 ^{13}C NMR spectrum of poly(ethylene-*co*-1-butene) replicate sample A.1.3.

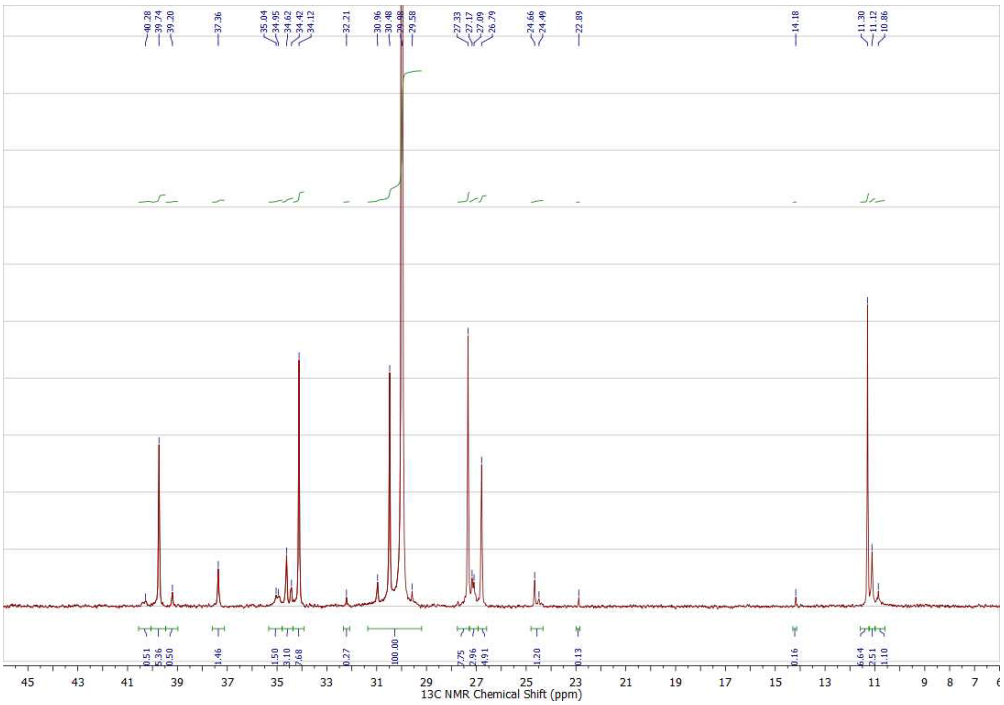

Figure G.4 ^{13}C NMR spectrum of poly(ethylene-*co*-1-butene) replicate sample A.2.1.

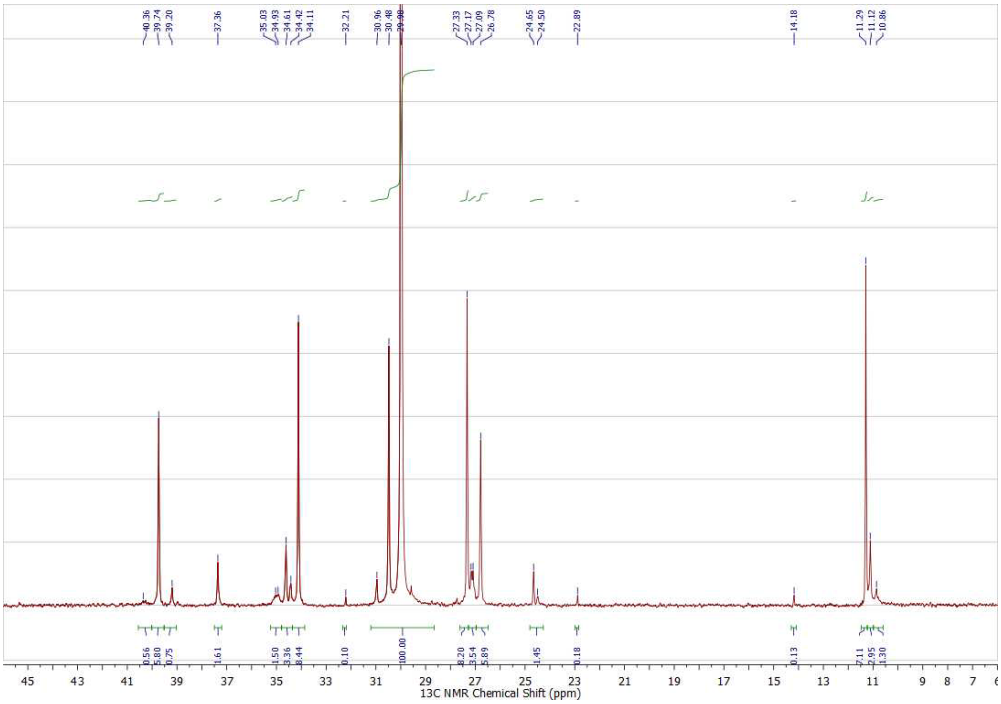

Figure G.5 ^{13}C NMR spectrum of poly(ethylene-*co*-1-butene) replicate sample A.2.2.

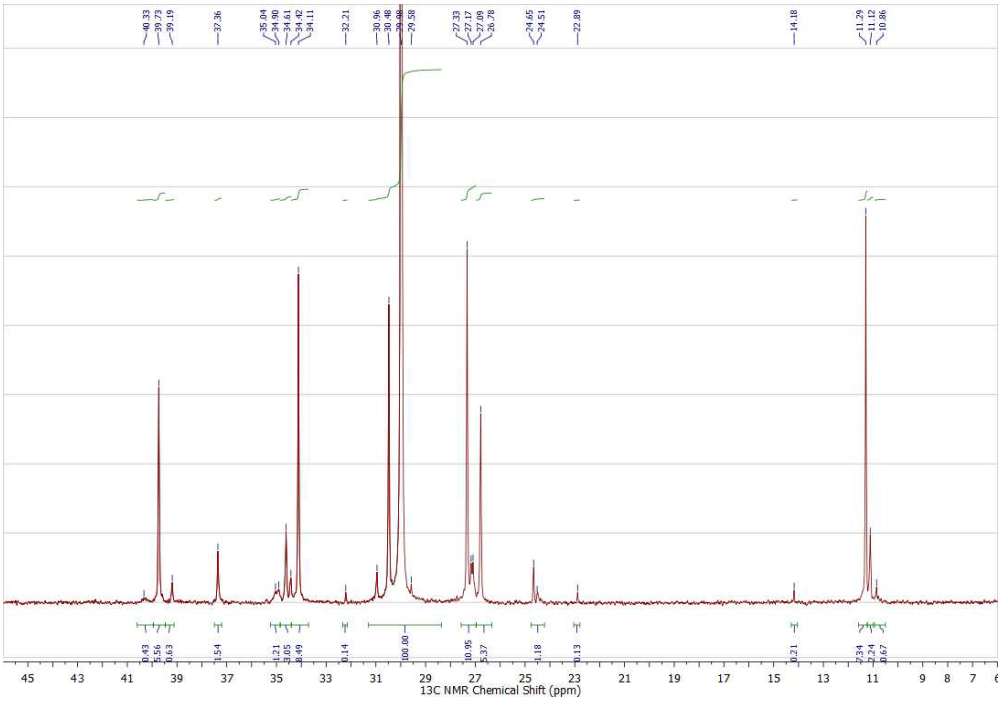

Figure G.6 ^{13}C NMR spectrum of poly(ethylene-*co*-1-butene) replicate sample A.2.3.

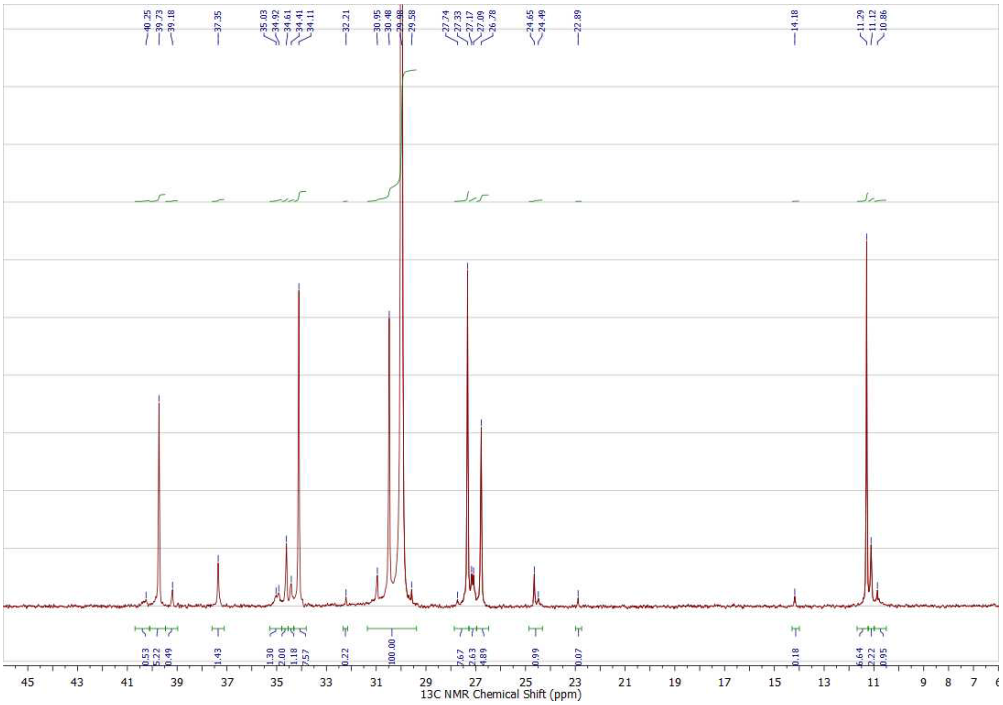

Figure G.7 ^{13}C NMR spectrum of poly(ethylene-*co*-1-butene) replicate sample B.1.1.

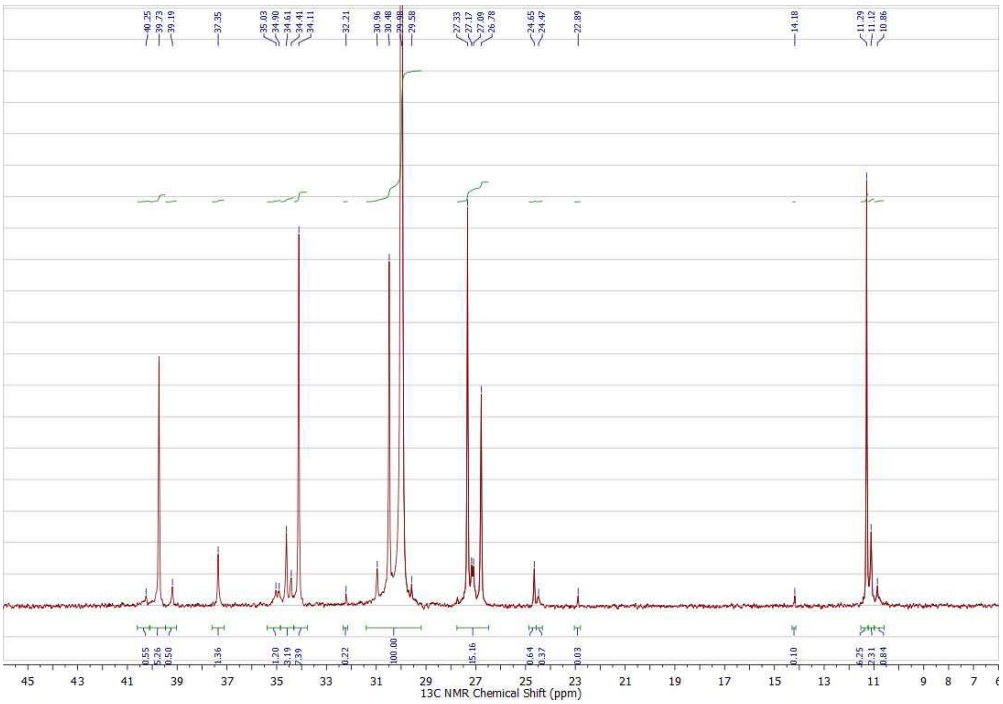

Figure G.8 ^{13}C NMR spectrum of poly(ethylene-*co*-1-butene) replicate sample B.1.2.

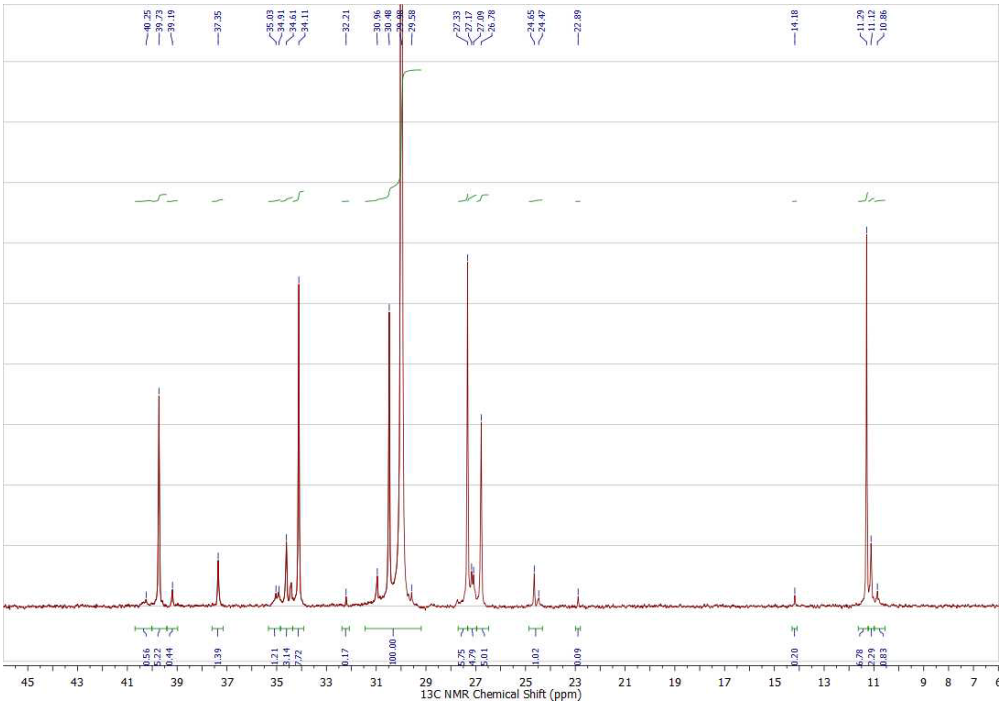

Figure G.9 ^{13}C NMR spectrum of poly(ethylene-*co*-1-butene) replicate sample B.1.3.

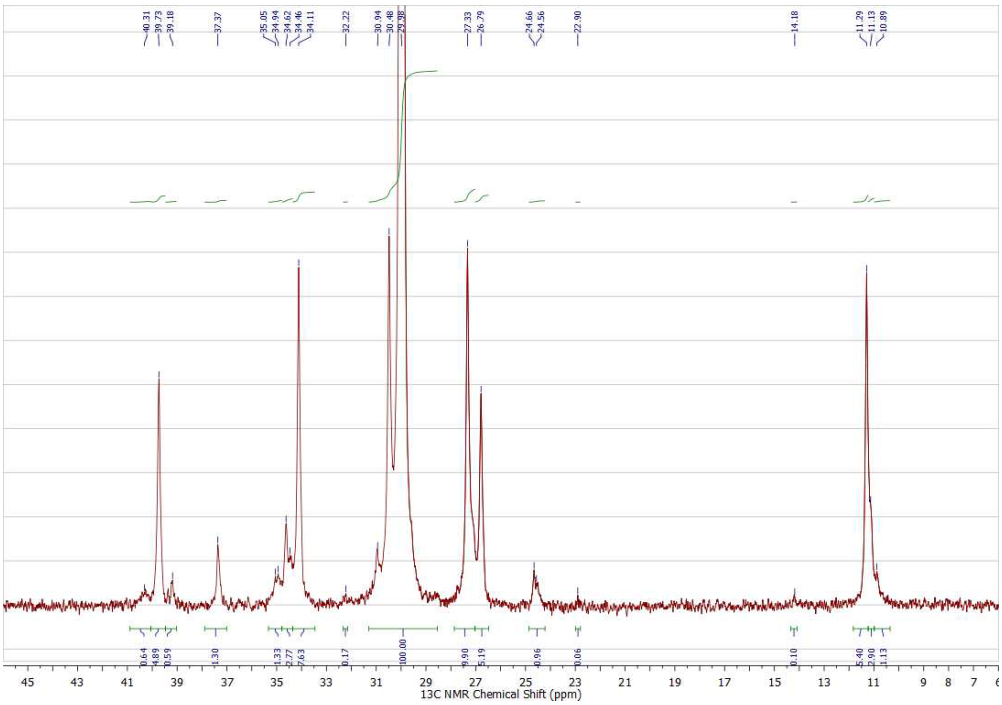

Figure G.10 ^{13}C NMR spectrum of poly(ethylene-*co*-1-butene) replicate sample B.2.1.

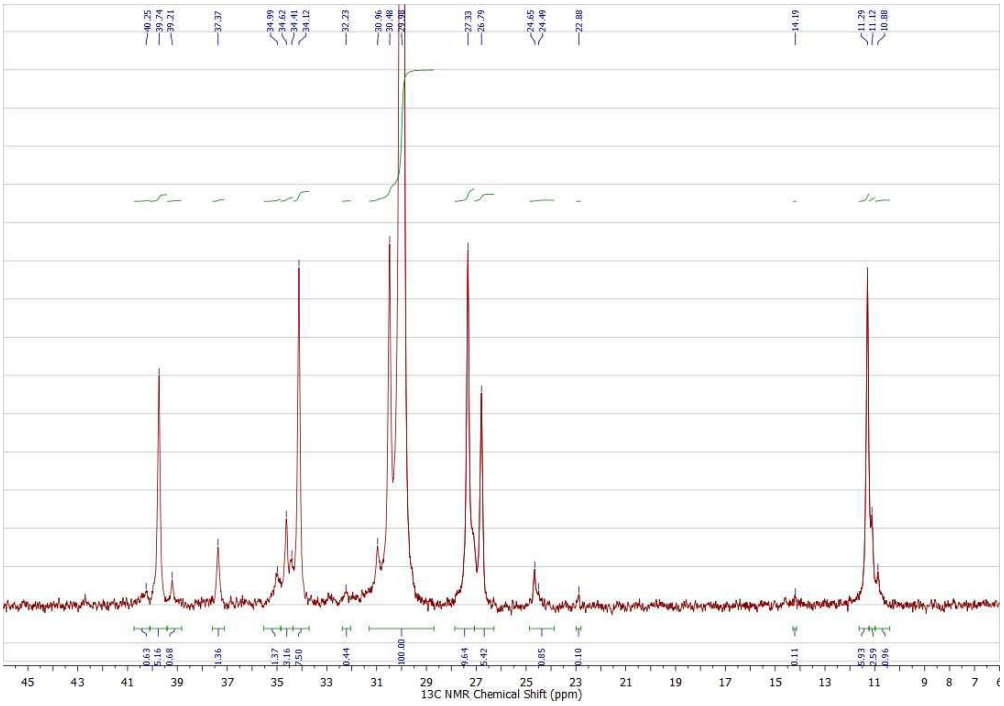

Figure G.11 ^{13}C NMR spectrum of poly(ethylene-*co*-1-butene) replicate sample B.2.2.

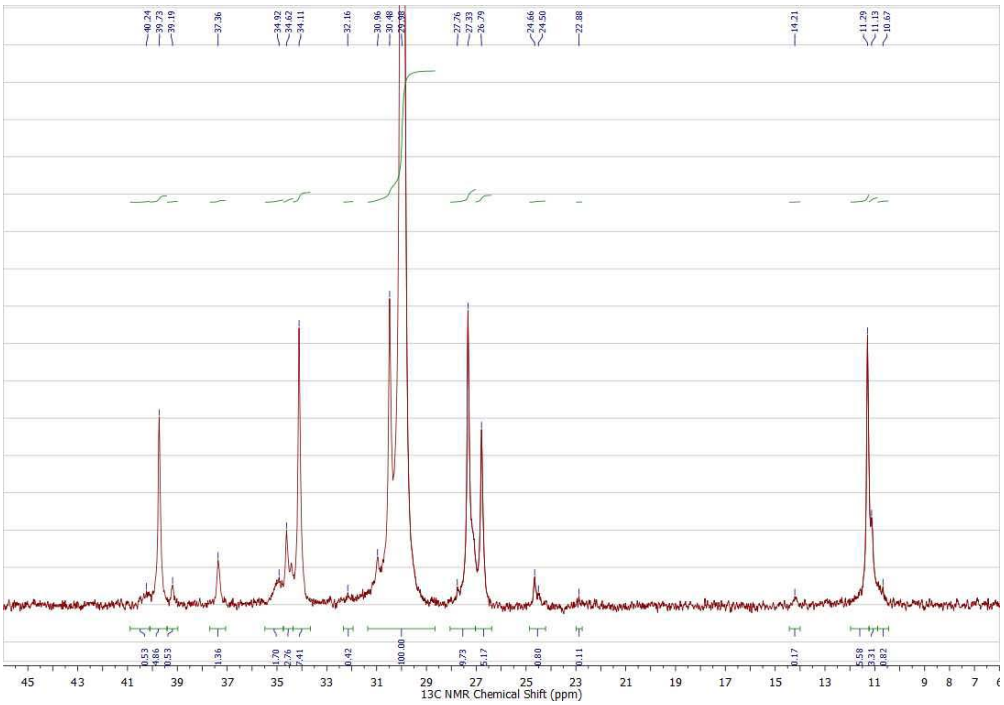

Figure G.12 ^{13}C NMR spectrum of poly(ethylene-*co*-1-butene) replicate sample B.2.3.

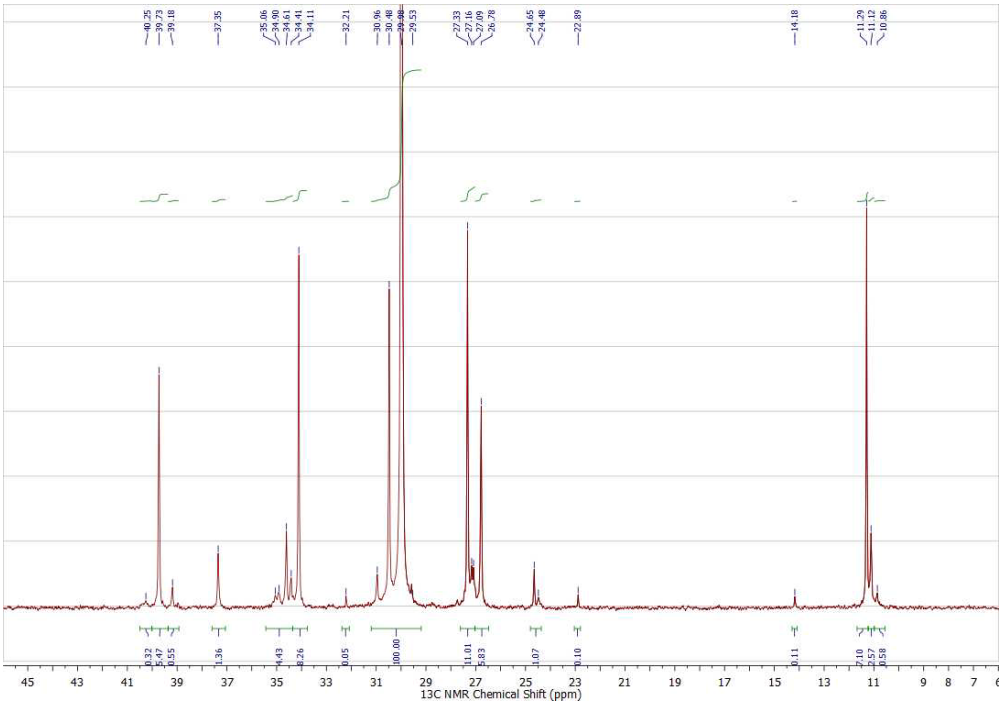

Figure G.13 ^{13}C NMR spectrum of poly(ethylene-*co*-1-butene) replicate sample C.1.1.

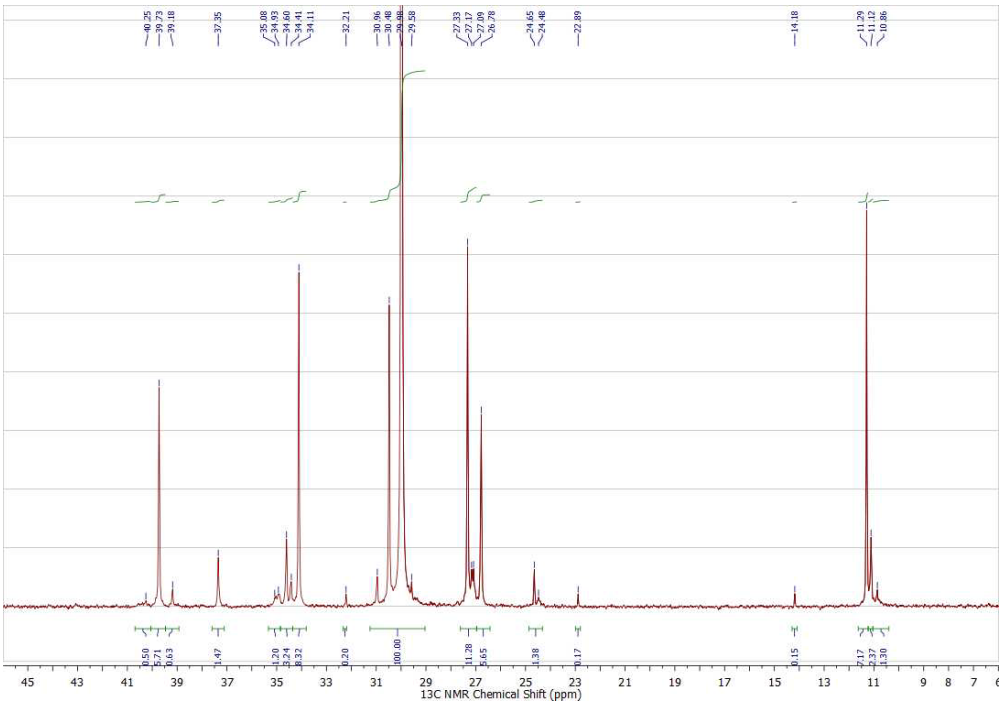

Figure G.14 ^{13}C NMR spectrum of poly(ethylene-*co*-1-butene) replicate sample C.1.2.

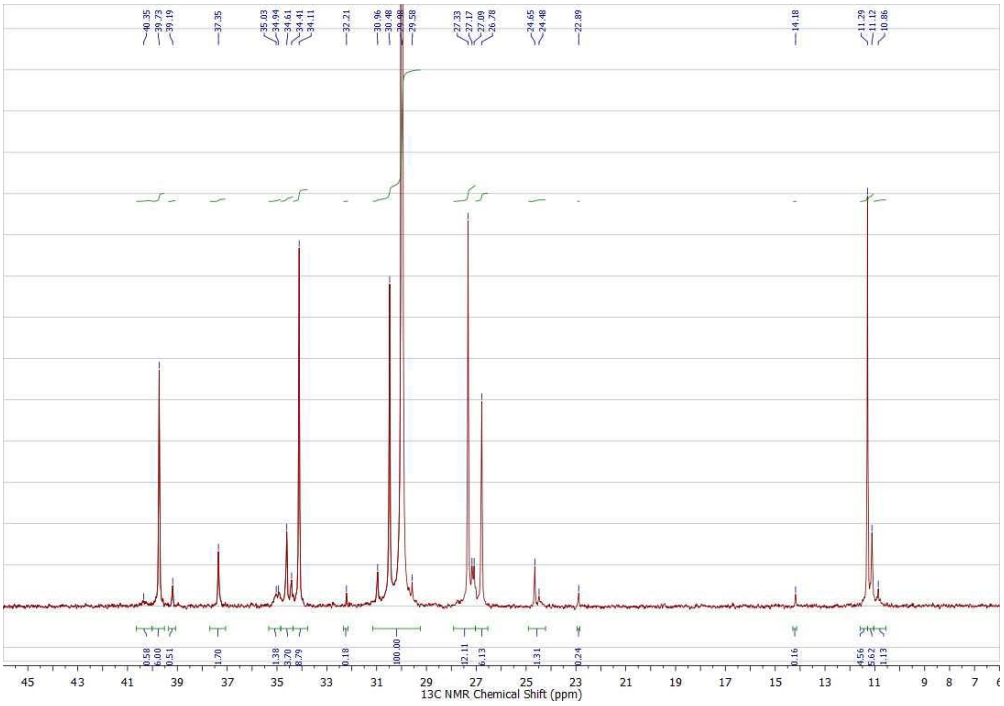

Figure G.15 ^{13}C NMR spectrum of poly(ethylene-*co*-1-butene) replicate sample C.1.3.

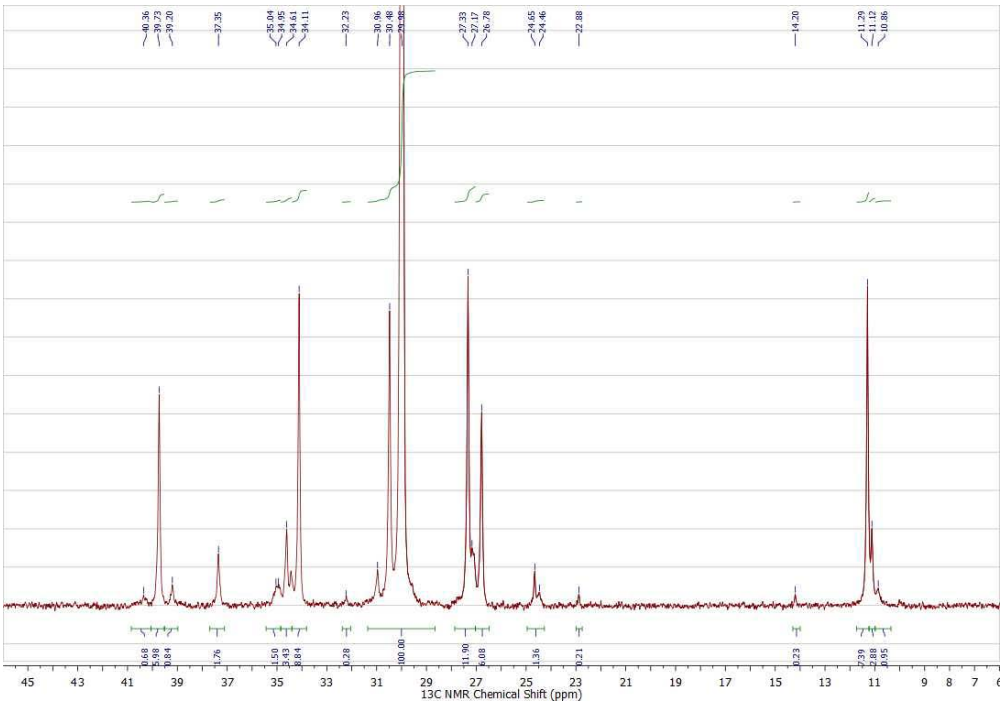

Figure G.16 ^{13}C NMR spectrum of poly(ethylene-*co*-1-butene) replicate sample C.2.1.

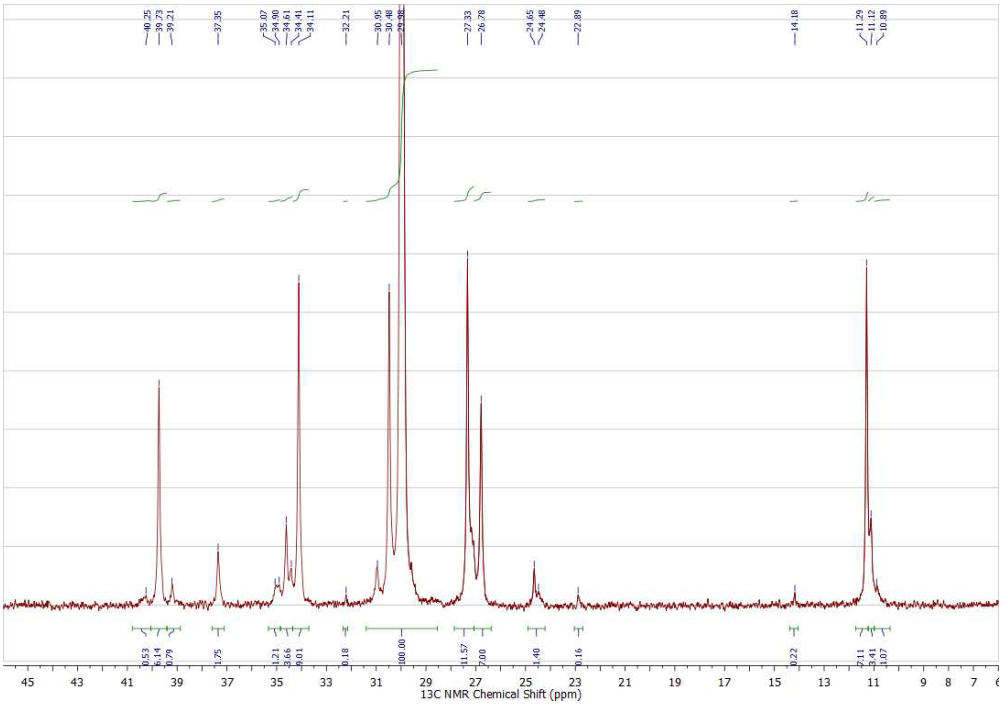

Figure G.17 ^{13}C NMR spectrum of poly(ethylene-*co*-1-butene) replicate sample C.2.2.

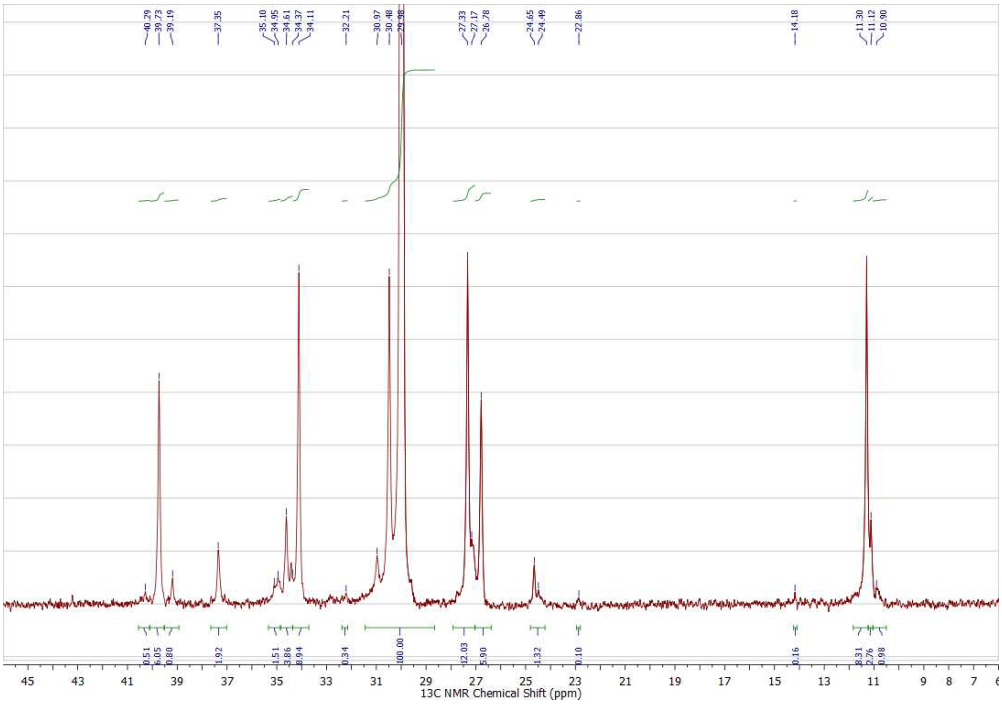

Figure G.18 ^{13}C NMR spectrum of poly(ethylene-*co*-1-butene) replicate sample C.2.3.

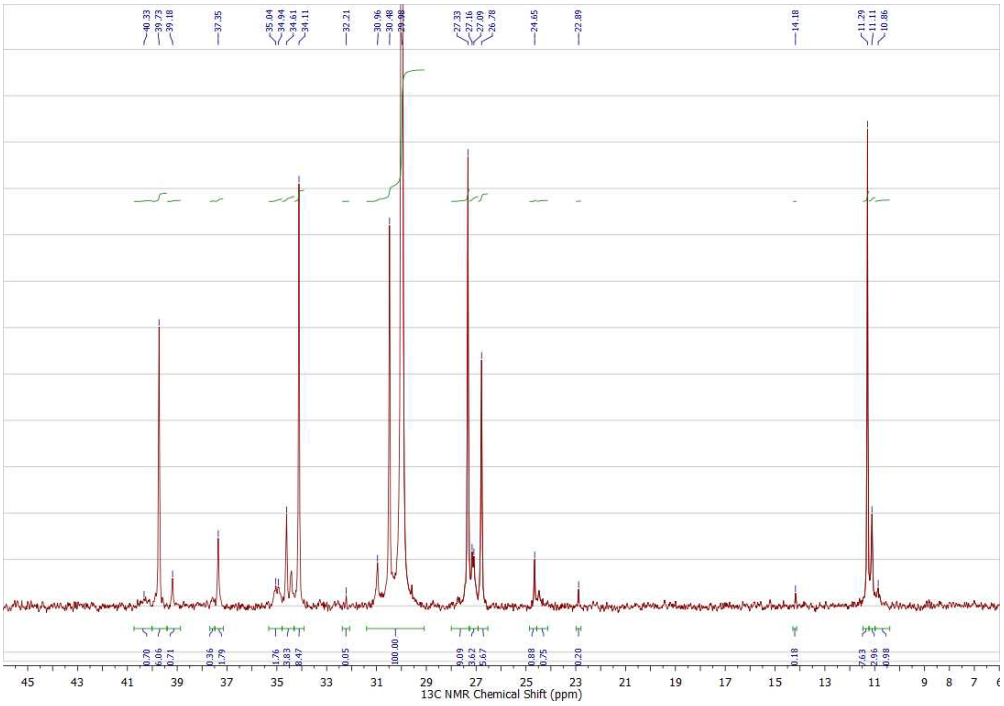

Figure G.19 ^{13}C NMR spectrum of poly(ethylene-*co*-1-butene) replicate sample D.1.1.

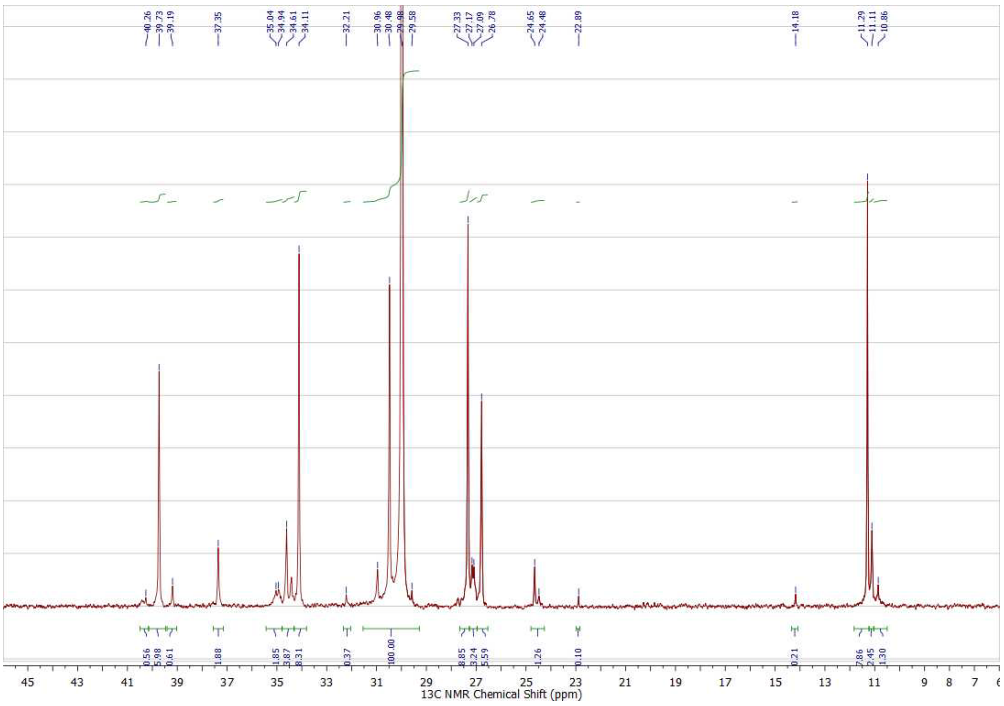

Figure G.20 ^{13}C NMR spectrum of poly(ethylene-*co*-1-butene) replicate sample D.1.2.

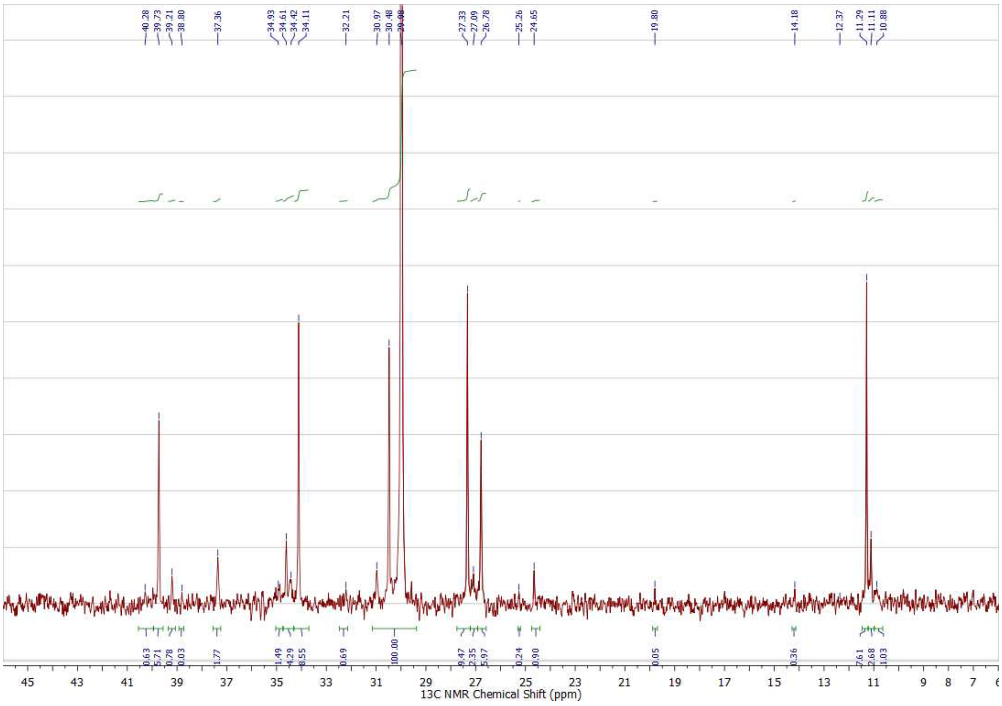

Figure G.21 ^{13}C NMR spectrum of poly(ethylene-*co*-1-butene) replicate sample D.1.3.

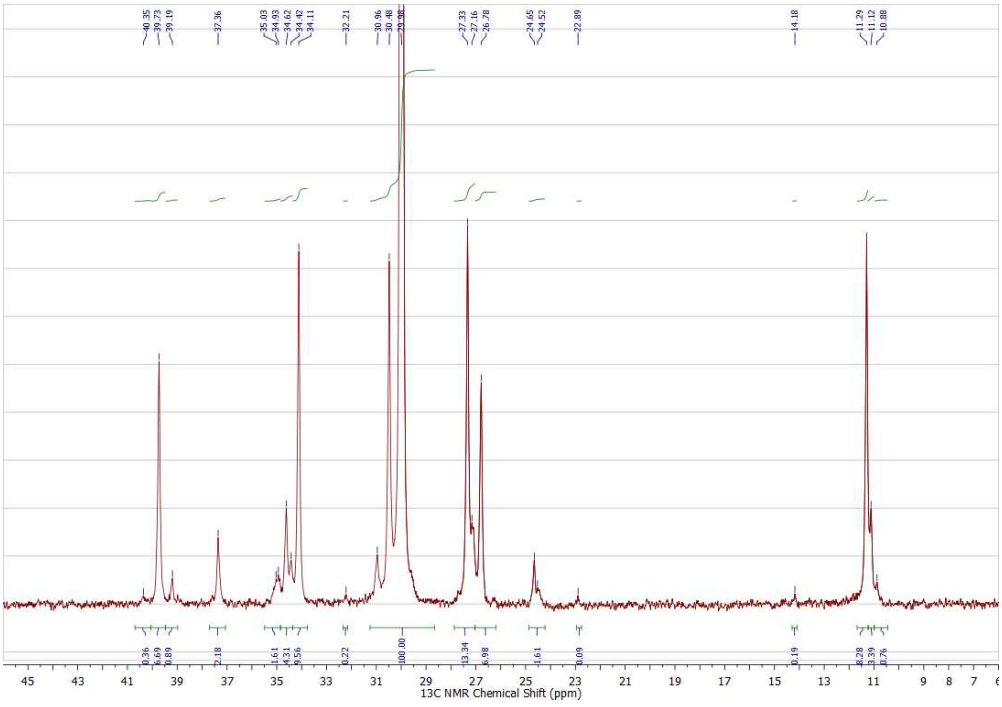

Figure G.22 ^{13}C NMR spectrum of poly(ethylene-*co*-1-butene) replicate sample D.2.1.

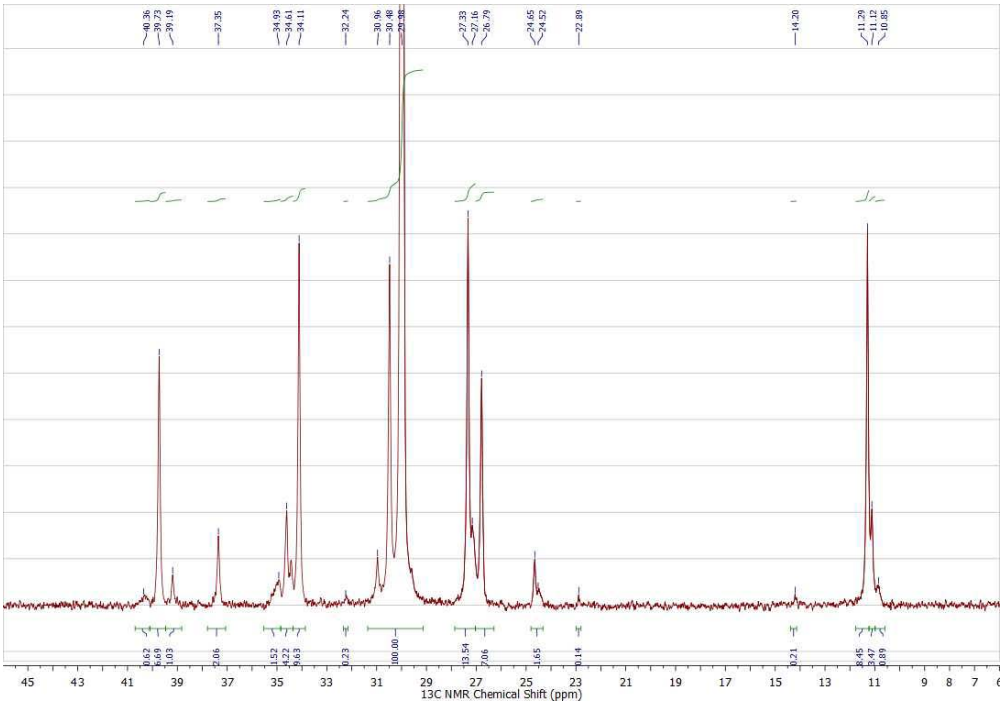

Figure G.23 ^{13}C NMR spectrum of poly(ethylene-*co*-1-butene) replicate sample D.2.2.

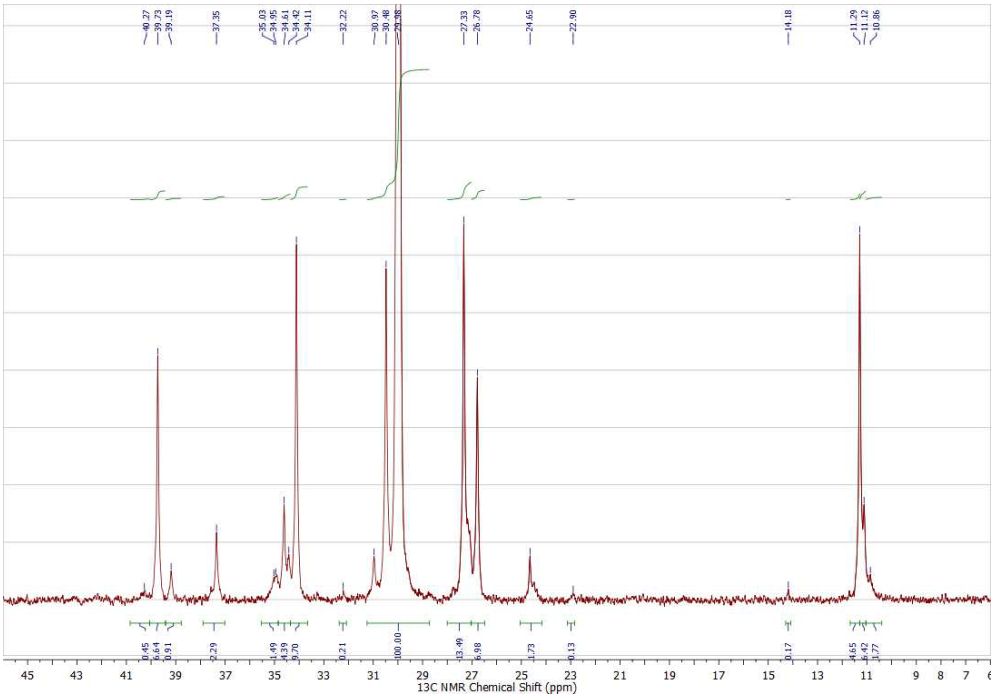

Figure G.24 ^{13}C NMR spectrum of poly(ethylene-*co*-1-butene) replicate sample D.2.3.

Nomenclature

Abbreviations

A – Monomer A (ethylene).

ANOVA – analysis of variance.

B – Comonomer B (α-olefin).

^{13}C NMR – carbon-13 nuclear magnetic resonance spectroscopy.

CCD – Chemical Composition Distribution.

CEF – Crystallization Elution Fractionation.

CSLD – Comonomer Sequence Length Distribution.

df – degrees of freedom.

E(MS)– expected values of mean squares.

EB – ethylene-*co*-1-butene copolymers synthesized without hydrogen.

EBH – ethylene-*co*-1-butene copolymers synthesized with hydrogen.

GPC – Gel Permeation Chromatography.

HDPE – High-density polyethylene.

IDEM – Integrated Deconvolution Estimation Model.

LDPE – Low-density polyethylene.

LLDPE – Linear low-density polyethylene.

MS – mean squares.

MW – molecular weight of polymer chain.

MWD – molecular weight distribution.

NLLS – Nonlinear Least Squares.

P – highest level of the experiment, polymerization.

PDI – polydispersity index.

S – second level of the experiment, sampling.

SS – sum of squares.

T – Third level of experiment, test or analytical.

TCB – trichlorobenzene.

TREF – Temperature Rising Elution Fractionation.

Equations

A – transition metal (most commonly, Ti or Zr).

L – ligand.

X – halogen atom (commonly Cl).

AlR_3 – alkylaluminum cocatalyst.

R – alkyl group (methyl, ethyl).

M_n – number average molecular weight.

M_w – weight average molecular weight.

f_A – monomer molar fraction in the reactor.

w_i – weight fraction of polymer made on site i.

N – total number of site types in the catalyst.

$W_{\log MW}^{GPC}$ – MWD measured by GPC.

n_{GPC} – number of sampling points taken by GPC.

$F_{A\text{-}chain}$ – fraction of monomer type A in a given copolymer chain.

F_A – the average fraction of monomer type A in the whole copolymer sample.

r_A – ethylene, monomer (A) reactivity ratio.

r_B – 1-butene, comonomer (B) reactivity ratio.

m – number of responses.

n – number of trials.

x_i – molar fractions of monomer A (f_A) – and comonomer B (f_B) – in the reactor.

f_j – model function for the jth.

y_{ij} – measured value of the jth response for the ith case.

Y_{ij} – measured value of the jth response for the ith case, the matrix of triads, and or tetrads.

P_{xy} – propagation probability for a copolymer ending with monomer x and propagating with monomer y.

N – number of site types.

α – Confidence interval (95%, α = 0.05).

$\underline{\theta}$ – $p \times 1$ vector of unknown parameters $(\theta_1, \theta_2, ..., \theta_p)$.

θ – estimated reactivity ratios.

ε_{ij} – residual.

z_{ij} – random error associated with the measured value of the *j*th response for the *i*th case.

τ_{MW} – the reciprocal of the number average molecular weight.

s_s^2 – estimate of the variance attributed to different sampling.

s_p^2 – estimate of the variance attributed to different polymerization reaction.

χ^2 – objective function of the MWD deconvolution.

$\phi(\underline{\theta})$ – objective function of the MWD deconvolution and the CSLD deconvolution.

σ – Standard deviation.

σ^2 – variance.

Bibliography

Alghyamah, Abdulaziz A.; Soares, Joao B.P., 2009, Simultaneous Deconvolution of the Molecular Weight and Chemical Composition Distribution of Polyolefins Made with Ziegler-Natta Catalysts, Macromol. Symp. 2009, 285, 81-89.

Al-Harthi, Mamdouh; Sardashti, Amirpouyan; Soares, Joao B.P.; Simon, Leonardo C., 2007, Atom transfer radical polymerization (ATRP) of styrene and acrylonitrile with monofunctional and bifunctional initiators, Polymer, 48, 1954-1961.

Anantawaraskul, Siripon; Soares, Joao B.P.; Wood-Adams, Paula M., 2005, Fractionation of Semicrystalline Polymers by Crystallization Analysis Fractionation and Temperature Rising Elution Fractionation, Adv Polym Sci., 182, 1-54.

Askeland, D.; Phule, P., 2003, The Science and Engineering of Materials, Fourth Edition, Brooks/Cole, Thomson Learning Inc.

Atta-ur-Rahman; Choudhary, Muhammad Iqbal, 1996, Solving Problems with NMR Spectroscopy, First Edition, Academic Press Inc.

Barlow, A.; Wild, L.; Ranganath, R., 1977, Gel Permeation Chromatography of Polyethylene, I. Calibration, Journal of Applied Polymer Science, 21, 3319-3329.

Bates, Douglas M.; Watts, Donald G., 2007, Nonlinear Regression Analysis and Its Applications, Wiley Series in Probability and Statistics, John Wiley & Sons, Inc.

Beigzadeh, Daryoosh; Soares, Joao B.P., Duever, Thomas A., 2004, Effect of Cocatalyst on the Chain Microstructure of Polyethylene Made with CGC-Ti/MAO/B(C_6F_5)$_3$, Journal of Polymer Science: Part A: Polymer Chemistry, 42, 3055-3061.

Bergstra, Michiel F., 2004, Catalytic Ethylene Polymerization Novel Reactors for Kinetics in Gas, Slurry and Solution Processes, Thesis Dissertation, Enschede, The Netherlands.

Bubeck, R., 2002, Structure–Property Relationships in Metallocene Polyethylenes, Materials Science and Engineering, R 39, 1-28.

Burke, Annette L.; Duever, Thomas A.; Penlidis, Alexander, 1994, Model Discrimination via Designed Experiments: Discriminating Between the Terminal and Penultimate Models Based on Triad Fraction Data, Macromol. Theory Simul., 3, 1005-1031.

Burke, A.L.; Duever, T.A.; Penlidis, A., 1996, An Experimental Verification of Statistical Discrimination between the Terminal and Penultimate Copolymerization Models, Journal of Polymer Science: Part A: Polymer Chemistry, 34, 2665-2678.

Blumich, Bernhard, 2005, Essential NMR: for Scientists and Engineers, First Edition, Springer-Verlag Berlin Heidelberg.

Box, George E.P.; Draper, Norman R., 1965, The Bayesian Estimation of Common Parameters from Several Responses, Biometrika, 52, 3 and 4, 355.

Box, G.E.P.; Hunter, W.G.; MacGregor, J.E.; Erjavec, J., 1973, Some Problems Associated with the Analysis of Multiresponse Data, Technometrics, 15, 1, 33.

Box, George E. P.; Hunter, J. Stuart; Hunter, William G., 2005, Statistics for Experimenters: Design, Innovation and Discovery, Second Edition, Wiley & Sons Inc.

Box, George E.P.; Tiao, George C., 1973, Bayesian Inference in Statistical Analysis, Addison-Wesley.

Bovey, Frank A.; Mirau, Peter A., 1996, NMR of Polymers, Academic Press Inc.

Cerruti, L., 1999, Historical and Philosophical Remarks on Ziegler-Natta Catalysts, HYLE-International Journal for Philosophy of Chemistry, 5 (1), 3-41.

Cheng, H.N., 1989, ^{13}C-NMR Analysis of Multicomponent Polymer Systems, American Chemical Society, Computer Applications in Applied Polymer Science II, Chapter 17, 174-188.

Cheng, H.N., 1990, Analysis of NMR Triad Distribution in Ethylene/1-Butene Copolymer, Polymer Bulletin, 23, 589-596.

Cheng, N.H., 1991, Comonomer Sequence Distribution in Ethylene/1-Hexene Copolymers, Polymer Bulletin, 26, 325-332.

Cheng, N.H., 1993, Statistical Propagation Models for Ziegler-Natta Polymerization, New Advances in Polyolefins, Plenum Press, New York, 15-30.

D'Agnillo, Luigi; Soares, Joao B.P.; Penlidis, Alexander, 1999, A Hierachrical Data Analysis of Replicate Experiment in Polyethylene Synthesis with High-Temperature Gel Pearmation Chromatography, Polymer Reaction Engineering, 7, 2, 259-281.

Draper, Norman; Smith, Harry, 1998, Applied Regression Analysis, Third Edition, Wiley Series in Probability and Statistics, John Wiley & Sons, Inc.

Dube, March A.; Penlidis, Alexander, 1996, Hierarchical Data Analysis of a Replicate Experiment in Emulsion Terpolymerization, AIChE Journal, 42, 7, 1985-1994.

Epacher, E.; Krohnke, C.; Pukanszky, B., 2000, Effect of Catalyst Residues on the Chain Structure and Properties of a Phillips Type Polyethylene, Polymer Engineering and Science, 40, 6, 1458-1468.

Hamielec, Archie E.; Soares, Joao B. P., 1996, Polymerization Reaction Engineering Metallocene Catalysts, Prog. Polym. Sci., Vol. 21, 651-706.

Hsieh, Eric T.; Randall, James C., 1982, Ethylene-1-Butene Copolymers. 1. Comonomer Sequence Distribution, Macromolecules, 15, 353-360.

Kaminsky, Walter; Hoff, Matthias; Derlin, Stefanie, 2007, Tailored Branched Polyolefins by Metallocene Catalysis, Macromol. Chem. Phys., 208, 1341-1348.

Kashiwa, N., 2004, The Discovery and Progress of $MgCl_2$-Supported $TiCl_4$ Catalysts, Journal of Polymer Science: Part A: Polymer Chemistry, 42, 1-8.

Kim, J. D., 1998, Synthesis of Polyolefins with Controlled Distributions of Molecular Weight and Chemical Composition by Selective Combination of Supported Metallocene / MAO Catalysts." PhD Thesis Chemical Engineering, University of Waterloo.

Kim, J. D.; Soares, J.B.P.; Rempel, G. L., 1999, Synthesis of Tailor-Made Polyethylene Through the Control of Polymerization Conditions Using Selectively Combined Metallocene Catalysts in Supported Systems. Journal of Polymer Science: Part A: Polymer Chemistry, 37, 331-339.

Kim, Kee Jeong; Choi, Kyu Yong, 1991, Continuous Olefin Copolymerization with Soluble Ziegler-Natta Catalysts, AIChE Journal, 37, 8, 1255-1260.

Kou, Bo; McAuley, Kim B;. Hsu, James C. C.; Bacon; David W., 2005, Mathematical Model and Parameter Estimation for Gas-Phase Ethylene/Hexene Copolymerization with Metallocene Catalyst, Macromol. Mater. Eng., 290, 537-557.

Kuroda, N.; Nishikitani, Y.; Matsuura, K.; Miyoshi, M., 1987, Sequence and Branching Distribution of Ethylene/1-Butene Copolymers Prepared with a Heterogeneous Ziegler Catalyst, Makromol. Chem., 188, 1897-1907.

Liu, Boping ; Nitta, Takashi; Nakatani, Hisayuki; Terano, Minoru, 2003, Stereospecific Nature of Active Sites on $TiCl_4/MgCl_2$ Ziegler-Natta Catalyst in the Presence of an Internal Electron Donor, Macromol. Chem. Phys., 204, 395-402.

Liu, Weixia; Rinaldi, Peter L.; McIntosh, Lester H.; Quirk, Roderic P., 2001, Poly(ethylene-co-1-octene) Characterization by High-Temperature Multidimensional NMR at 750 MHz, Macromolecules, 34,14, 4757-4767.

Manson, Robert L.; Gunst, Richard F.; Hess, James L., 2003, Statistical Design and Analysis of Experiments: with Applications to Engineering and Science, Second Edition, Wiley & Sons Inc.

Montgomery, Douglas C., 2001, Design and Analysis of Experiments, 5th Edition, John Wiley & Sons, Inc.

Monrabal, B.; Sancho-Tello, J.; Mayo, N.; Romero, L., 2007, Crystallization Elution Fractionation, A New Separation Process for Polyolefin Resins., Macromol. Symp., 257, 71-79.

Monrabal, B.; Romero, L.; Mayo, N.; Sancho-Tello, J., 2009, Advances in Crystallization Elution Fractionation, Macromol. Symp., 282, 14-24.

Monwar, Masud; Sahoo, Sangrama K.; Rinaldi, Peter L.; McCord, Elizabeth F.; Marshall, Donald R., Buback, Michael; Latz, Henning, 2003, A 3D-NMR Method for Studying Hydrocarbon-Based Polymer Structures, Macromolecules 2003, 36, 6695-6697.

Ohshima, M.; Tanigaki, M., 2000, Quality Control of Polymer Production Processes, Journal of Process Control, 10,135-148.

Peng, Ding-Yu; Robinson, Donald B., 1976, A New Two-Constant Equation of State, Ind. Eng. Chem. Fundam., 15, 1, 59-64

Polic, A. Loui; Lona, Liliane M. F.; Duever, Thomas A.; Penlidis, Alexander, 2004, A Protocol for the Estimation of Parameters in Process Models: Case Studies with Polymerization Scenarios, Macromol. Theory Simul., 13, 115-132.

Pooter, M. De; Smith P. B.; Dohrer, K. K.; Bennett, K. F.; Meadows, M. D.; Smith, C. G.; Schouwenaars, H. P; Gerrads, R. A., 1991, Determination of the Composition of Common linear low Density Polyethylene Copolymers by ^{13}C-NMR Spectroscopy, Journal of Applied Polymer Science, Vol., 42, 399-408.

Randall, J., 1989, A Review of High Resolution Liquid ^{13}Carbon Nuclear Magnetic Resonance Characterization of Ethylene-Based Polymers, Macromolecular: Chemistry and Physics, C29 (2-3), 201-317.

Randall, James C., 1977, Polymer Sequence Determination Carbon-13 NMR Method, Academic Press, 71-92.

Rinaldi, Peter L., 2003, Polymer Characterization by 3D NMR, NMR Spectroscopy of Polymers in Solution and in Solid State, ACS Symposium Series, 834, 94-122.

Rudin, Alfred, 1999, The Elements of Polymer Science and Engineering, Second Edition, Academic Press, 103-112.

Sahoo, Sangrama K.; Zhang, Tong; Reddy, D. Venkat; Rinaldi, Peter L.; McIntosh, Laster H.; Quirk, Roderick P., 2003, Multidimensional NMR Studies of Poly(ethylene-*co*-1-butene) Microstructures, Macromolecules, 36, 4017-4028.

Salzer, S., 1999, Nomenclature of Organometallic Compounds of the Transition Elements, Pure Applied Chemistry, 71 (8), 1557-1585.

Sarzotti, Deborah M.; Narayan, Abhishek; Whitney, Philip M.; Simon, Leonardo C.; Soares, Joao B.P., 2005, Microstructural Characterization of Molecular Weight Fractions of Ethylene/1,7-Octadiene Copolymers Made with a Constrained Geometry Catalyst, Macromol. Mater. Eng., 290, 584-591.

Schmidt-Rohr, K.; Spiess, H. W., 1994, Multidimensional Solid-State NMR and Polymers, Academic Press Limited.

Seger, M.; Maciel, G., 2004, Quantitative ^{13}C NMR Analysis of Sequence Distributions in Poly(ethylene-co-1-hexene), Analytical Chemistry, 76 (19), 5734-5747.

Shin, Sang-Young A.; Simon, Leonardo C.; Soares, Joao B.P., 2004, Copolymerization of olefin and nitrile monomers, PMSE Preprints, 91, 100-101.

Soares, Joao B.P., 2007, An Overview of Important Microstructural Distributions for Polyolefin Analysis, Macromol. Symp., 257, 1-12.

Soares, Joao B.P.; Anantawaraskul, Siripon, 2005, Crystallization Analysis Fractionation, Journal of Polymer Science: Part B: Polymer Physics, 43, 1557-1570.

Soares, J.B.P.; McKenna, T.F.; Cheng, C.P., 2007, Coordination polymerization. In Polymer Reaction Engineering, Chapter 2, Asua J.M. (Ed.), Blackwell Publishing, 29-115.

Soares, J.B.P., 2004, Fractionation. In Encyclopedia of Polymer Science and Technology, 3rd Edition, Wiley-VCH, Weinheim, 75-131.

Soares, Joao B.P., 2001, Mathematical Modelling of the Microstructure of Polyolefins Made by Coordination Polymerization: a Review, Chemical Engineering Science, 56, 4131-4153.

Soares, J.B.P.; Willis, J. N.; Liu, X., 1996, A New Methodology for Studying Multiple-Site-Type Catalysts for the Copolymerization of Olefins, Macromol. Chem. Phys., 197, 3383-3396.

Stockmayer, W.H., 1945, Distribution of Chain Lengths and Compositions in Copolymers, The Journal of Chemical Physics, 13, 6, 199-207.

Thompson, Duncan E.; McAuley, Kim B.; McLellan, P. James, 2007, Exploring Reaction Kinetics of a Multi-Site Ziegler-Natta Catalyst Using Deconvolution of Molecular Weight Distributions for Ethylene-Hexene Copolymers, Macromol. React. Eng., 1, 264-274.

Tidwell, Paul W.; Mortimer, George A., 1970, Science of Determining Copolymerization Reactivity Ratios, J. Macromol. Sci. Revs. Macromol. Chem., C4 (2), 281-312.

Whiteley, K.S., 2002, Polyolefins - Polyethylene. Ullmann's Encyclopedia of Industrial Chemistry, InterScience Wiley-VCH.

Wild, Leslie, 1990, Temperature Rising Elution Fractionation, Advances in Polymer Science 98, Spfingor-Verlag Berlin Heidelberg.

Yao, K. Zhen; Shaw, Benjamin M.; Kou, Bo; McAuley, Kim B.; Bacon, D. W., 2003, Modeling Ethylene/Butene Copolymerization with Multi-site Catalysts: Parameter Estimability and Experimental Design, Polymer Reaction Engineering, Vol. 11, No.3, 563-588.

Zhou, Zhe; Kummerle, Rainer; Stevens, C. James; Redwine, David; He, Yiyong; Qiu, Xiaohua; Cong, Rongjuan; Klosin, Jerzy; Montanez, Nikki; Roof, Gordon, 2009, ^{13}C NMR of polyolefins with a new high temperature 10 mm cryoprobe, Journal of Magnetic Resonance, 200, 328-333.